UNIVERSITY OF LIVERPOOL

Preparation and characterisation of maraviroc loaded SLNs stabilised with branched branched copolymers

By

Mona K. Omir

A thesis

Submitted to

The University of Liverpool

In fulfilment of the requirements
for the degree of

PhD in Chemistry

September 2017

Dedicated to my lovely mum

Declaration

I hereby declare that this thesis is my original work and it has been written by me in its entirety. I have been duly acknowledged all the sources of information, which has been used in this thesis

This thesis has not been previously accepted in substance for any degree

_____

Mona Kab Omir, September 2017

Abbreviations

AIDS	Acquired Immune Deficiency Syndrome
ART	Antiretroviral Therapy
API	Active Pharmaceutical Ingredients
ATP	Adenosine triphosphate
ATRP	Atom Transfer Radical Polymerisation
AZT	Azidothymidine
bbb	Blood Brain Barrier
bpy	2,2'-bipyridyl
CCR5	C-C chemokine Receptor type 5
CMC	Critical Micelle Concentration
CNS	Central Nervous System
CD4	Cluster of differentiation 4
CD	Cyclodextrin
CS	Chitosan
CXCR4	Chemokine Receptor Type 4
DBiB	Dodecyl-2-bromoisobutyrate
DCM	Dichloromethane
DCR	Derived Count Rate
DLS	Dynamic Light Scattering
DMF	Dimethyl Formamide
DNA	Deoxyribonucleic Acid
DOSY	Diffusion-ordered spectroscopy
DP_n	Degree of polymerisation
DRV	Darunavir
DSC	Differential Scanning Calorimetry
D_z	Z- average diameter
EE	Encapsulation Efficiency
EGDMA	Ethylene Glycol Dimethacrylate
ES-MS	Electrospray Mass spectrometry
FDA	Food and Drug Administration
GALT	Gut Associated Lymphoid Tissue
GMS	Glycerol Monostearate
GI	Gastrointestinal
gp	Glycoprotein
GRAS	Generally recognised as safe
HAART	Highly Active Antiretroviral Therapy
HAP	Hydroxyapatite
HDL	High Density Lipoprotein

HIV	Human Immunodeficiency Virus
HPH	High Pressure Homogenisation
HPMA	N-(2-Hydroxypropyl)-methyl acrylamide
Hz	Herz
IE	Initiator Efficacy
IPA	Isopropanol
IV	Intravenous
kcps	kilo counts per minute
kDa	kilo Dalton
LALS	Low-angle light scattering
LCST	Lower Critical Solution Temperature
LDL	Low-density lipoprotein
LPV	Lopinavir
LUV	Large unilamellar vesicle
M	Monomer conversion
MHz	Mega hertz
mV	milivolt
MVC	Maraviroc
MWCO	Molecular weight cut-off
MLV	Multilamellar Vesicle
MRP	Multidrug resistance-associated protein
NLC	Nano Lipid Carrier
NMP	Nitroxide mediated polymerisation
nm	nano meter
NRTI	Nucleoside reverse transcriptase inhibitor
NNRTI	Non-nucleoside reverse transcriptase inhibitor
NMR	Nuclear Magnetic Resonance
OEGMA	Oligo Ethylene Glycol Methacrylate
OMRP	Organometallic-mediated polymerisations
O/W	Oil in water
Panc-1	Pancreatic adenocarcinoma cells
PBS	Phosphate buffer saline
PCL	Poly(caprolactone)
PDI	Polydispersity index
PEG	Polyethylene Glycol
PEGDMA	Poly Ethylene Glycol Dimethacrylate
PEO	Polyethylene oxide
PI	Protease inhibitor
PIT	Phase inversion temperature
PLA	Poly(lactic acid)

PVP	Polyvinylpyrrolidone
PK	Pharmacokinetic
PLGA	Poly Lactic-*co*-Glycolic Acid
PMMA	Poly(methyl methacrylate)
PPI	Polypropylene imine
PPO	Poly(propylene oxide)
ppm	parts per million
RAFT	Reversible Addition-Fragmentation Chain Transfer
RALS	Right-angle light scattering
RDRP	Reversible-deactivation radical polymerisation
RES	Reticuloendothelial system
RI	Refractive Index
RIF	Rifampicin
RNA	Ribonucleic Acid
SCF	Supercritical Fluid
SDS	Sodium dodecyl sulphate
SEM	Scanning electron microscopy
SLS	Sodium lauryl sulphate
SLN	Solid Lipid Nanoparticle
SLM	Solid Lipid Microparticle
SUV	Small unilamellar liposome vesicle
TBHF	Tetrabutyl hexaflourophosphate
TEA	Triethyl Amine
TEM	Transmission electron microscopy
TNF	Tenofovir
VFS	Simulated varginal fluid
WHO	World Health Organisation
UV	Ultraviolet
ZP	Zeta potential

Acknowledgements

This PhD thesis is written at the Department of Chemistry at the University of Liverpool in September 2017 under supervision of Professor Steve Rannard and Doctor Tom McDonald. The report is a final summary of my research within the group of Nanomedicine. The aim of this thesis was to design a SLN stabilised by a branched OEGMA based polymer and show that it can encapsulate maraviroc.

It has been a pleasure to join the group of Professor Steve Rannard and Doctor Tom McDonald. I would like to express my sincere gratitude to my supervisor Professor PhD Steve Rannard for allowing me to join his research group in the middle of my PhD and for our discussions from which I benefitted greatly. I would also like to extend my gratitude to Dr Tom McDonald for his contribution, and for discussions that inspired me during the project. I would further like to thank Dr Pierre Chambon and Dr Andrew Dwyer for their unwavering interest, motivation and supervision in the meetings and laboratory during this period as well as for their support of my experimental ideas. I would also like to thank Dr Helen Cauldbeck and Dr Alison Savage for performing ^{3}H labelled MVC studies on MVC-SLN formulations. I also like to thank Dr Lee Tatham for performing *in vivo* mouse studies from Department of Pharmacology. I also like to extend my gratitude to Dr Konstantin Luzyanin for his help and effort of running ^{19}F NMR of my samples and the Mass Spectrometry Laboratory at the University of Liverpool to run electrospray mass spectrometry data (ES-MS) of my samples. Moreover, I would like to thank Dr James Hobson for his help and interesting scientific discussions in the laboratory. Additionally, I owe many thanks to Samantha Ashcroft and Stephanie Edwards for constantly supplying me with tea throughout my PhD and the department of Chemistry for all their help and support with the machines and equipments, for having a great sense of humour and creating an excellent working environment. I would like to thank my mum and dad for always supporting me. Finally, I would like to thank my fiancé Dr Frederik Romer for being very supportive, being there for me during my hard times of life and always believing in me.

Abstract

Oligo (ethylene glycol) methacrylate (OEGMA) based copolymers were branched with ethylene glycol dimethacrylate (EGDMA) and poly(ethylene glycol) dimethacrylate (PEGDMA) using ATRP and characterised using ^{1}H-NMR and GPC. The stabilising properties of synthesised DBiB-p(OEGMA) based homo- and copolymers were assessed using a model oil in water emulsion study with *n*-dodecane. The polymer chosen for evaluation as a stabiliser for SLNs was DBiB-p(OEGMA)$_{10}$-*co*-(EGDMA)$_{0.6}$. This polymer was tested its ability to assist lipids in forming drug free SLN through such processes as hot high shear homogenisation, hot probe sonication and solvent injection. In all cases Compritol ATO 888 was used as the solid lipid excipient. In our study, the best technique to process DBiB-p(OEGMA)$_{10}$-co-(EGDMA)$_{0.6}$ stabilised drug-free SLNs was an optimised solvent injection method. The conditions under which the solvent injection method was shown to give successful results were a w/w ratio of 1:3 DBiB-p(OEGMA)$_{10}$-*co*-(EGDMA)$_{0.6}$ to Compritol 888 ATO and a total solid content (DBiB-p(OEGMA)$_{10}$-*co*-(EGDMA)$_{0.6}$ and Compritol ATO 888) of 1.2 mg/mL in deionised water. The solvent were removed by dialysis and DLS stability studies showed that the drug-free SLN dispersions were stable up to 39 days. MVC was then encapsulated into SLNs and the drug loading was quantified using ^{19}F-NMR. However, it was shown that most of the drug was lost upon dialysis. On that basis another method was used to remove IPA which was to freeze dry the MVC-SLN formulation and redispersed it using ultrasonication. A formulation was developed with 80 wt. % MVC relative to lipid encapsulation in MVC-SLN formulation. The sample was tested *in vitro* and *in vivo* as a ^{3}H-labelled drug. Overall the *in vitro* and in vivo tests showed slow release and improved bioavailability. Moreover, tissue analysis of oral administration of MVC-SLNs in rats showed increased concentration of MVC in the intestine and liver when compared to unformulated oral administered MVC.

Table of contents

Chapter 1 Literature background 11
1.1 Introduction to Human Immunodeficiency (HIV) 12
1.1.1 HIV/AIDS lifecycle and current treatment to attack lifecycle 13
1.1.2 Drug delivery challenges 14
1.1.3 Maraviroc (MVC) 15
1.2 State of the Art Oral delivery 18
1.2.1 Nanocarriers 18
1.3 Solid lipid nanoparticles (SLNs) for encapsulation of hydrophobic drugs 26
1.3.1 Methods to prepare SLNs 26
1.3.2 Lipids used for SLN production 28
1.3.3 Surfactants for SLNs 30
1.4 Synthesis and application of branched amphiphilic copolymers 32
1.4.1 Reversible deactivation radical polymerisation (RDRP) 32
1.4.2 Atom transfer radical polymerisation (ATRP) 33
1.5 Nanomedicine administration 35
1.5.1 Oral administration of drugs 35
1.5.2 Lipids in oral administration 36
1.5.3 SLNs for oral administration 38
1.6 Objectives of the research 39
Chapter 2. Synthesis and characterisation of branched oligo ethylene glycol methacrylate (OEGMA) based polymers utilizing ATRP used in *n*-dodecane model oil studies 43
2.1 Introduction 44
2.2 Results and discussion 49
2.2.1 Synthesis of DBiB initiator 49
2.2.2 Kinetic studies of polymerisation of linear DBiB-p(OEGMA)$_{50}$ 52
2.2.3 Synthesis of p(OEGMA) based copolymers utilising ATRP 56
2.2.4. Synthesis and characterisation of DBiB-p(OEGMA)$_{10\text{-}50}$ branched with EGDMA 59
2.2.5. Synthesis and characterisation of DBiB-p(OEGMA)10-50 branched with PEGDMA 68
2.2.6 *n*-dodecane emulsion studies of linear and branched DBiB-p(OEGMA)$_{10\text{-}50}$ 75
2.2.7 Surface tension measurements 93
2.2.8 Thermo responsive behaviour of DBiB-p(OEGMA)$_{10}$-*co*-(EGDMA)$_{0.6}$ 94
2.3 Conclusion 98

Chapter 3 Synthesis, optimisation and stability studies of OEGMA based polymer stabilised SLNs 100
3.1 Introduction 101
3.2 Results and discussion 104
3.2.1. Synthesis of p(OEGMA) based polymer stabilised drug-free SLNs using homogenisation approach 104
3.2.2 Synthesis of p(OEGMA) based polymer stabilised drug-free SLNs using sonication 106
3.2.3 Synthesis of p(OEGMA) based polymer stabilised SLNs using solvent injection 107
3.2.4 Optimisation of solvent injection method 111
3.2.5 Polymer to lipid ratio optimisation experiment 114
3.2.6 Stability studies of dialysed versus non-dialysed empty SLN dispersions 120
3.2.7 Temperature stability studies of dialysed versus non-dialysed empty SLN dispersions 125
3.3 Conclusion 127
Chapter 4. Synthesis, optimisation and stability studies of OEGMA based polymer stabilised maraviroc loaded SLNs 129
4.1 Introduction 130
4.2. Optimisation of methodology and synthesis of drug loaded MVC in SLNs 133
4.2.1. DLS measurements of MVC encapsulation SLNs after dialysis 136
4.2.2 Stability studies of MVC encapsulation SLNs after dialysis 138
4.2.3 Stability studies of MVC loaded SLNs after dialysis in PBS 142
4.2.4 ^{1}H NMR studies of MVC encapsulation SLNs after dialysis 145
4.2.5 ^{19}F NMR studies of MVC encapsulation SLNs after dialysis and freeze drying .. 149
4.2.6. Differential scanning calorimetry (DSC) of MVC-SLNs 160
4.3 Conclusion 162
Chapter 5. Optimisation of freeze dried MVC loaded SLNs for *in vitro* and *in vivo* studies 163
5.1 Introduction 164
5.2 Results and discussion 165
5.2.1 Freeze drying of MVC loaded SLNs using sugars as cryoprotection 165
5.2.2. Freeze drying of MVC loaded SLNs with PEGs as cryoprotant *versus* no cryoprotectant 166
5.2.3 Role of MVC, Compritol ATO 888 and DBiB-p(OEGMA)$_{10}$-co-(EGDMA)$_{0.6}$ in MVC-SLNs 171
5.2.4 Stability studies of freeze dried MVC-SLNs with 80 wt. % MVC loading 176
5.2.5. Synthesis of Radiolabelled MVC loaded SLNs and biological evaluation 179
5.2.6. *In vivo* evaluation of ^{3}H-labelled MVC loaded SLNs 184

5.3. Conclusion 187
Chapter 6. Overall conclusions and future work 189
6.1 Overall conclusions 190
6.2 Future work 192
6.2.1 Synthesis of DRV loaded SLNs using solvent injection 192
6.2.2 Synthesis and characterisation of gemini surfactants for use as stabilisers in MVC-SLNs 193
6.2.3 Characterisation of size and structure of SLNs using ^{1}H NMR 194
Chapter 7 Experimental section 196
7.1 Materials and methods – Chapter 2 197
7.1.1 Materials 197
7.1.2 Synthesis of DBiB-p(OEGMA) based copolymers 197
7.1.3 Characterisation of p(OEGMA) based copolymers 202
7.2 Materials and methods – Chapter 3 204
7.2.1 Materials 204
7.2.2 Synthesis of empty SLNs by hot high shear homogenisation 205
7.2.3 Synthesis of empty SLNs by hot probe sonication 205
7.2.4 Synthesis of drug-free SLNs by solvent injection methods 206
7.3 Materials and methods – Chapter 4 208
7.3.1. Materials 208
7.3.2 Synthesis of MVC loaded SLN dispersion by optimised solvent injection method 208
7.3.3 Dialysis of MVC loaded SLN dispersion by optimised solvent injection method. 210
7.3.4 Freeze drying of MVC loaded SLN dispersion by optimised solvent injection method 210
7.3.5 Quantification of MVC in MVC loaded SLNs 211
7.4 Materials and methods – Chapter 5 213
7.4.1 Freeze drying of MVC loaded SLNs using cryoprotection 214
7.4.2 Freeze drying of MVC loaded SLNs without cryoprotection 215
7.4.3. Synthesis of ^{3}H-labelled MVC loaded SLNs 215
Bibliography 218
Appendix 240

Chapter 1 Literature background

1.1 Introduction to Human Immunodeficiency (HIV)

Human immunodeficiency virus (HIV) is a lentivirus that infects the body's immune system by damaging the cells responsible for its defence. The virus is transmitted through body fluid contact such as unprotected sex, needle sharing, blood borne infection or from mother to child during pregancy.[1,2] It is estimated by the WHO, that over 37 million people were infected and live with HIV/AIDS worldwide in 2015[3] among those only 17 million receive anti-HIV therapy Fig.1.1. Most of the HIV infected populations are in the third world and in Africa there are 23 – 28.4 million victims.[3]

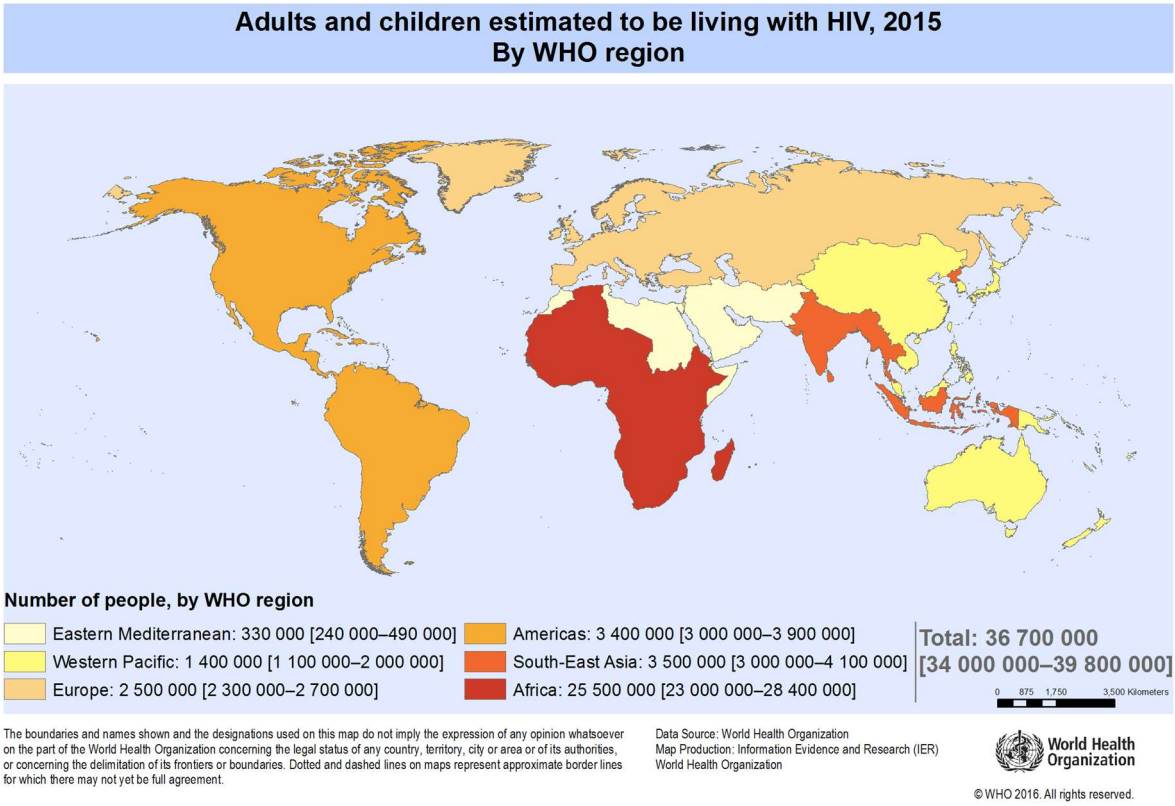

Fig. 1.1. Estimated numbers of HIV infected people in World Health Organization (WHO). From AIDS epidemic update, August 2016[3]

HIV is a life threatening disease as if left untreated it results in immunodeficiency syndrome known as acquired immunodeficiency syndrome (AIDS); a severely damaged immune system open to other infections and diseases.[1]

1.1.1 HIV/AIDS lifecycle and current treatment to attack lifecycle

HIV is a 100 nm virus particle that comprises an outer envelope and an inner capsid. Its outer surface envelope is functionalised with glycoproteins, known as gp120 and gp41.[1] The HIV capsid encompasses a positive sense developed ribonucleic acid (RNA), protease, integrase and reverse transcriptase enzymes. The virus proliferates by using immune cells as host cells and these include T cells, macrophages and the dendritic cells.[1,4–6] The life cycle of HIV which results in pathogenesis is divided into seven stages and described briefly, Fig.1.2A.

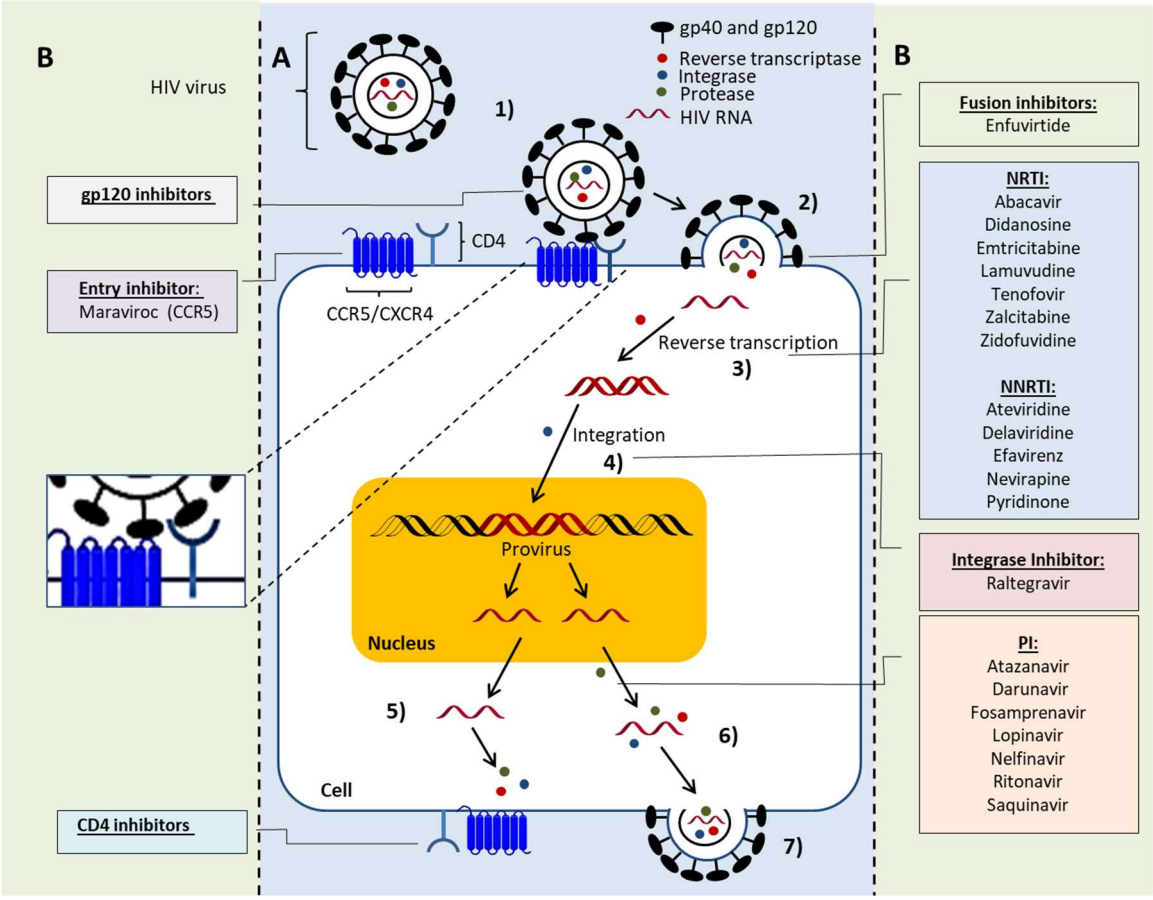

Fig. 1.2. **A)** HIV lifecycle and **B)** antiretroviral drugs that act at different stages of the virus lifecycle. **1)** Binding of the virus gp120 and gp41 to host cell receptor, CD4, CCR5 or CXCR4. **2)** Viral fusion. **3)** Reverse transcription of positive sense RNA catalysed by reverse transcriptase. **4)** Integration of viral DNA into chromosome in nucleus. **5)** Replication and integration of viral proteins. **6)** Viral particle assembly. **7)** Budding of mature virions from the host cell. NNRTI: non-nucleoside protease inhibitor; NRTI: nucleoside protease inhibitor; PI: protease inhibitor.

In stage **1)** the glycoproteins on the surface of the virus, gp120 and gp41, bind to a receptor, cluster differentiation 4 (CD4), C-C chemokine receptor (CCR5) or C-X-C chemokine receptor type 4 (CXCR4), on the surface of the host cell.[4] Stage **2)** comprises viral cell entry via endocytosis which allows the surface of the viral envelope to fuse with the surface of the target cell and subsequently release the positive sense RNA and corresponding enzymes into the host cell[7,8] Stage **3)** starts with reverse transcription of the positive RNA followed by integration of the viral DNA into the chromosome of the host cell in stage **4)**.[4] During stage **5)**, the replication and translation of viral proteins take place followed by viral particle assembly at the cell membrane to produce progeny immature virions during stage **6)**.[4] During the last stage of the cycle, stage **7)**, the mature virions will be budding from the host cell and continue spreading the infection through other host cells.[9] A more detailed description of the mechanism of the infection is described in the literature.[4,10]

1.1.2 Drug delivery challenges

Antiretroviral drugs work by inhibiting different stages of the HIV lifecycle as shown in Fig. 1.2B. These drugs were introduced in 1987 and since then more than 26 antiretroviral drugs became available for treatment of HIV.[1] The first known approved anti-HIV drug was a cancer drug and classified as a nucleoside reverse transcriptase inhibitor (NRTI) and named zidovudine (AZT).[11] Later other drugs were introduced to the market inhibiting other stages of the HIV life cycle. The commercial anti-HIV drugs are divided into categories based on their activities on the stages of HIV cycle mentioned in the lifecycle. These included entry inhibitors, fusion inhibitors, reverse transcriptase inhibitors that can be classified as NRTI or non- nucleoside reverse transcriptase inhibitors (NNRTI), integrase inhibitors and protease inhibitors (PI), Fig.1.2B.

The treatment and monitoring of HIV is challenging as the use of a single category of anti-HIV drug alone is not efficient in terms of managing the virus, as this results in the development of resistance of the virus to the therapy.[2] A typical treatment of HIV requires a

combination regimens that have three drugs as a minimum from two categories.[1,6] The administration of a cocktail of anti-HIV drugs or combinations referred to as highly effective antiretroviral therapy (HAART) and was introduced in 1996.[12] This therapy approach was demonstrated to inhibit the HIV lifecycle more aggressively and significantly reduces the probability of the virus developing resistance so that the treatment can continue to work safely.[1,2] The treatment is lifelong and its purpose is to effectively suppress the plasma viral load to an undetectable level resulting in maintenance or partial recovery of CD4+ T cell numbers and function in the blood.[9,13] Despite the great benefits of the therapeutic combinations of anti-HIV drugs from different categories, HAART therapy is considered as a challenge due to several factors which include; the multiple resistant strains of the virus, dormant cells with integrated HIV DNA which activate in later stages, increased side effects toxicity due to high/frequent dosing and the high cost of the drugs.[6] Another considerable challenge with HAART therapy is its inability to access the reservoir sites of HIV that serve as viral sanctuaries thereby preventing the opportunity for the HIV infection to be eradicated in sequestered anatomically privileged sites.[1] The anatomically privileged sites in question are the central nervous system (CNS),[1,14] lymphatic system, testes, gut, vaginal epithelium and lungs.[1,15] Combined anti-HIV drug oral administration can also require very high daily dosing due to some of the drugs' low bioavailabilities.[16] However, frequent (daily) administration and high dosages are crucial in the treatment of HIV infection.[16] To overcome some of these problems novel drug delivery systems have been introduced to the area of HIV treatment, the aim of this research is to improve the treatment of HIV/AIDS and to overcome some of the abovementioned challenges of current drugs available in the market.[1,6,17]

1.1.3 Maraviroc (MVC)

Entry inhibitors are among the categories mentioned earlier of which maraviroc (MVC) Fig. 1.3, was the first approved for treatment of HIV through targeting the host cell.[18] In the

absence of MVC the HIV virus uses its envelope to enter the host cell through interactions with the CD4 receptor.[19] This mechanism was discovered in 1986[4], and in 1996 a chemokine receptor named CCR5 receptor was demonstrated to be essential for HIV entry.[20] Later on that year, another publication demonstrated a second chemokine co-receptor that was identified as CXCR4.[21] Since 1996 the understanding of the viral entry into host cells has been redefined and viruses are characterised based on their affinity for the coreceptors; R5 uses CCR5 as a coreceptor, X4 uses CXCR4 as a coreceptor and R5X4 that uses both of the coreceptors.[22]

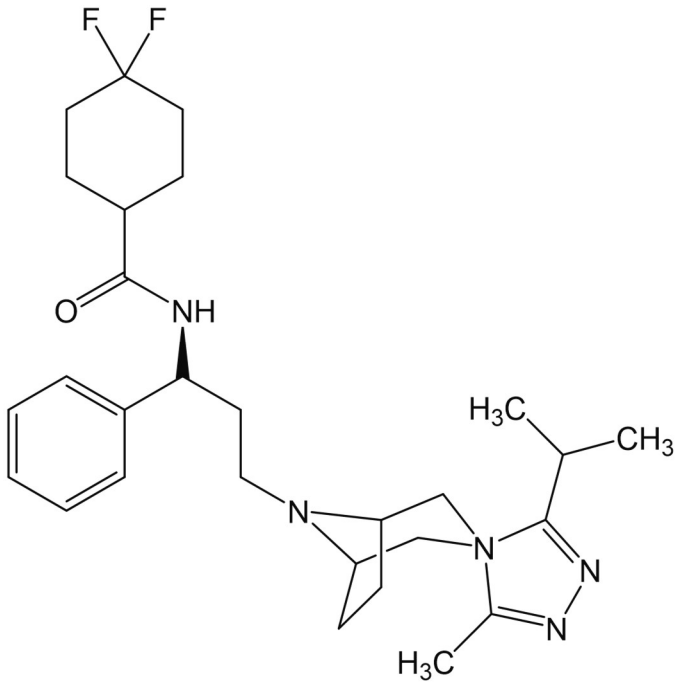

Fig. 1.3 Structure of CCR5 antagonist maraviroc, MVC.[23]

The targeting of chemokine receptors for treatment of HIV has both been characterised as being promising and challenging.[24] As mentioned earlier, MVC only inhibits the CCR5 receptor and can result in resistance when administered as a drug alone.[22] CXCR4 coreceptor inhibitors such as AMD3100/plerixafor have not been approved by the food and drug administration (FDA) for treatment of HIV/AIDS, this was due to unwanted side effects

in clinical trials such as cardiac disturbances and lack of oral bioavailability.[25] However, despite plerixafor not receiving FDA approval as an anti-HIV drug, it has been approved as an immunostimulant to mobilise hemapoetic stem cells in cancer patients.[26]

MVC is currently the only FDA approved drug in the market that targets the host cell on the CCR5 receptor.[27,28] MVC was developed after the role of CCR5 coreceptors in the HIV life cycle was established.[29,30] The story behind the discovery of MVC started when a research group, de Roda Husman *et al*, demonstrated that the lack of CCR5 receptor in some patient populations resulted in HIV-1 resistance.[31] The lack of CCR5 receptors was due to a mutation in the CCR5 coreceptor gene that resulted in a translation of a truncated and thereby a non-functional CCR5 coreceptor.[30] This mutation is referred to as CCR5Δ32. [22,32] These findings motivated pharmaceutical companies to perform high throughput screening of existing compound libraries to find a suitable candidates to inhibit the CCR5 coreceptors on the host cell.[22] The pharmaceutical giant, Pfizer, successfully obtained FDA approved its use of MVC as an anti-HIV therapy after a successful phase III clinical trial.[18]

MVC is typically administered in standard doses of 300 mg twice daily[33], but depending on the drug combination used to treat HIV/AIDS MVC can be adjusted between 150 mg to 600 mg twice daily.[34] However, use of MVC is limited due to adverse side effects including hepato-toxicity.[18,35] Other challenges with administration of MVC are its pharmacokinetic and pharmacological properties, the oral bioavailability of 100 mg MVC was shown to be between 23 % and 33 % for 300 mg doses.[35] The oral bioavailability of MVC is controlled by many factors such as the hydrophobicity of the drug, the first passage metabolism, cytochrome CYP P450 enzymes and drug interactions.[18] The CYP P450 system consists of liver enzymes that metabolise toxins and nutrients that are delivered through the hepatic portal system from the duodenum after digestion of food or a drug. When MVC is administered orally it has been reported to interact with two different enzymes in the liver called CYP3A4[36,18] and CYP3A5.[18,37] MVC's interaction with these enzymes has been shown to result in additional negative side effects when other common drugs are administered simultaneously.[35] In an attempt to overcome the low bioavailability of MVC the use of drug

delivery platforms have been considered. The different types of drug delivery platforms investigated for MVC is discussed in the next section.

1.2 State of the Art Oral delivery

1.2.1 Nanocarriers

Drug encapsulation into nanocarriers is done to improve a drug's low bioavailability, which can be caused by the drugs hydrophilicity or hydrophobicity among other factors. Interest in drug-loaded nanoparticles began in the early 1960s when novel nanocarrier systems for drug delivery were first synthesised and characterised.[38] A wide range of nanocarriers have been developed (Fig 1.4a-l), of which polymeric drug conjugates[73940] (Fig 1.4e) and liposomes[8] (Fig 1.4a) were the start of what is today called nanomedicine. These nanocarriers were originally conceived as carrier platforms for vaccines and anticancer drugs in 1970s.[38]

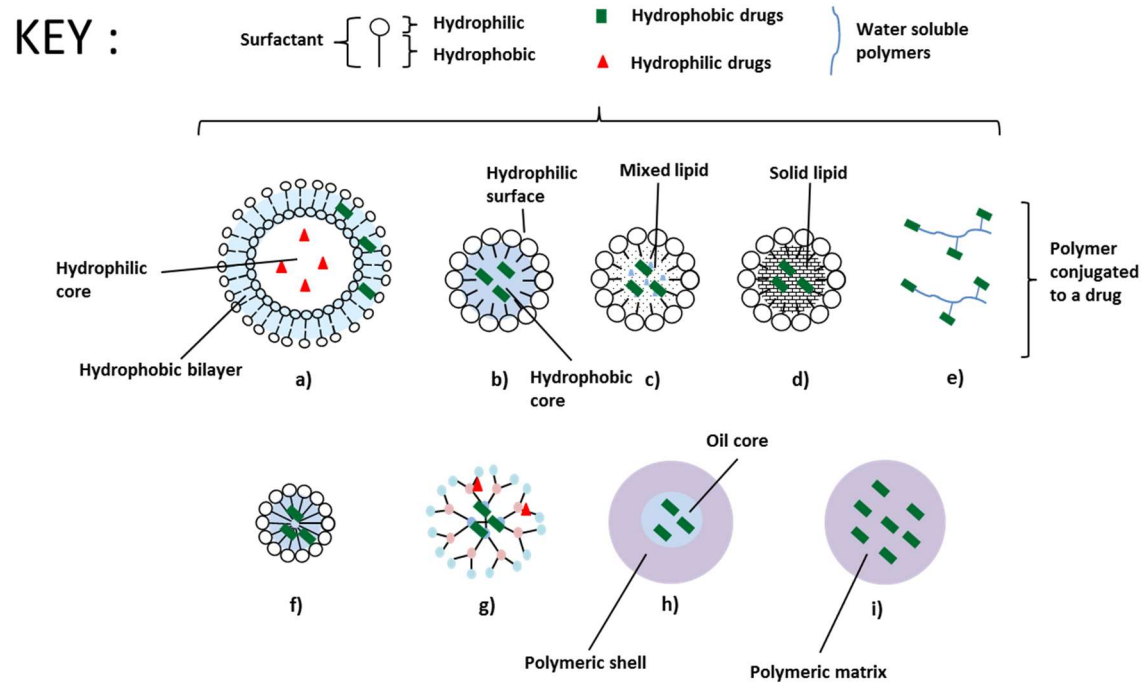

Fig. 1.4 Overview of different particles and their characteristic features. **a)** Liposome, **b)** lipid nanoparticle; LN, **c)** nanolipid carrier; NLC, **d)** solid lipid nanoparticles; SLN, **e)** polymeric drug conjugate, **f)** polymeric micelles, **g)** dendrimeric particles, **h)** nanocapsule and **i)** nanosphere.

Since then, these early examples have been used as an inspiration to develop a broader range of nanoparticle carrier platforms for encapsulation of a wide variety of drugs used for treatment of various diseases including HIV/AIDS[12] , cancer[41,42], diabetes[43] and Alzheimer's disease.[44,45]

Nanocarrier platforms are categorised based on their constituent materials and will be summarised in this section. Liposomes have a single type of additive, which is a lipid, for example a phospholipid that then forms bilayers, Fig. 1.4a. Nanocarrier systems can also be made from a lipid excipient and an amphiphilic stabiliser such as a surfactant or polymer. Examples of this includes oil-in-water (O/W) emulsions and oil droplets, Fig. 1.4b, nano lipid carriers (NLC), Fig. 1.4c, and solid lipid nanoparticle (SLNs), Fig. 1.4d. Another approach is to use amphiphilic polymers as the additive, these polymers then can self-assemble into particles with a hydrophobic core and a hydrophilic surface in an aqueous environment, examples include, micelles, Fig.1.4f, dendrimers, Fig. 1.4g, and polymeric nanospheres. The abovementioned nanocarriers are designed to both provide targeting and address bioavailability issues that comes with free drug administration.[2] The nanocarrier systems are thought to offer prolonged circulation time of the drug, controlled drug release and loading, increased stability, enhanced bioavailability, decreased side effect and targeted drug delivery.[1,6] Each of the different nanocarrier systems will be discussed in detail in the subsequent sections.

1.2.1.1 Micelles

Amphiphilic polymers or surfactants spontaneously aggregate to form micelles after reaching a critical micelle concentration (CMC) Fig. 1.5a-c.[46]

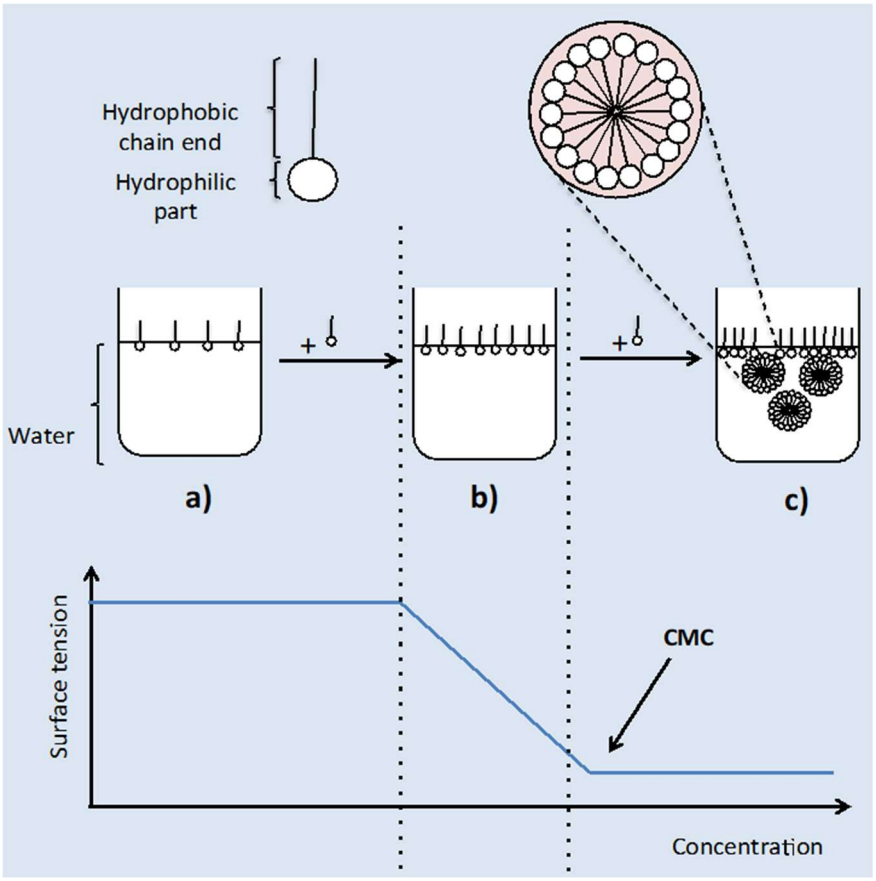

Fig. 1.5 a) Amphiphilic polymers in water, **b)** concentration of amphiphilic polymers below CMC, **c)** concentration of amphiphilic polymers above CMC. The relationship between the concentration of the surfactant and surface tension Adapted from Singh *et al*.[47]

The structure of a micelle in aqueous solvents typically consists of amphiphilic surfactants that point their hydrophilic heads outwards and hydrophobic tails are organised in a core which then forms spherical, lamellar or worm like structures. The hydrophobic core can entrap lipophilic drugs and the size of the nanoparticle is typically in the range of 10-100 nm.[48] Some amphiphilic polymers or surfactants a high CMC which limits the use of micelles in drug delivery.[49] Surfactants with high CMC may be diluted below the CMC upon dilution in the bloodstream or in other biological fluids leading to the micelle dissociation and expel the drug.[46] However, to overcome this problem, amphiphilic polymers or surfactants with lower CMC concentrations have been designed by tuning the properties of amphiphilic polymers with variety of monomeric building blocks and chain end functionalities.[50,51,52,53,54,55]

1.2.1.2 Polymeric conjugates

Polymeric drug conjugates are systems that consist of hydrophilic polymers such as polyethylene glycol (PEG) and *N*-(2-Hydroxypropyl) methacrylamide (HPMA) that are covalently attached to a drug, Fig. 1.4e. One of the purposes of conjugation has been to extend the residence time in the circulatory system.[56] An additional advantage of attaching water-soluble polymers to a drug with poor bioavailability was to deliver the drug across physiological barriers in the gut and intestine.[57] This research dates back to 1950 and was pioneered by Jatzkewitz[58] who conjugated a mescaline to poly(vinyl pyrrolidone) (PVP) through a dipeptide spacer.[57] Since then many polymer-drug conjugation methods have been reported including PEGylation,[59] attachment of water-soluble dendrimers[60] to drugs and branched polymers.[61] The technology of polymer-drug conjugates gained prominence in the scientific community after the first polymer-drug conjugate entered clinical trial in 1994.[62,63] In these clinical trials, cancer drugs such as methoxy morpholino-doxorubicin and paclitaxel were successfully attached to HPMA through a peptidyl linker and the research concluded that polymers could provide an ideal platform for delivery of a range of antitumor compounds reducing their toxicities.[63] In addition, conjugates can be prepared so that they bear both therapeutic and diagnostic agents with the potential to both “see and treat” patients.[56] Despite these promising developments there are several challenges in terms of final approval for polymeric drug conjugates in the market. For example, polymeric drug conjugates based on PEG or HPMA progressed to clinical development, but were not approved to progress to market due to the non-biodegradable nature of the polymers. Additionally, conjugates with low molecular weight were evaluated, but unable to take the full benefits of long blood circulation times.[56] Due to this, many research groups are working towards designing more biodegradable polymers for future development of polymeric drug conjugates. Another challenge described in the literature reports is that polymeric drug conjugates offer insufficient drug loading due to the polymer to drug ratio which remains as an aspect constraining their clinical applications.[1]

1.2.1.3 Dendrimers

The term dendrimer is a term derived from *dendri* [branched] and *mer* [part of][64] and was first time described by Tomalia *et al* [65] and Buhleier *et al.*[66] discovered that by reacting polymers with amines on dendritic arms they could grow the dendrimer and isolate a macromolecule with large molecular cavities.[6768] This work inspired other research groups to develop dendrimers with various properties. Application of dendrimers in nanomedicine is attractive owing their tuneable features, their size and the possibility of encapsulating drugs in the hydrophobic core. Dendrimers can be prepared with amphiphilic character; with hydrophobic cores and branched hydrophilic surfaces. Dendrimers also offer advantages of both 'void spaces' and conjugation. The most commonly reported dendrimers are derived from polyamidoamine, polyester, polypropyleneimiine, carbosilane and polylysine chemistry.[69] This high surface functionality allows possible conjugation or functionalisation with targeted moieties that allow the drug to be delivered to physiological barriers such as the blood brain barrier (BBB).[70] However, some dendrimers are reported to be toxic.[71] To decrease the toxicity of dendrimers it has been attempted to conjugate the surface either with targeted moieties such as PEGs. [70,72] The first nanomedicine product based on dendrimers went into the human clinical trials but still awaits approval to get into the market.[73]

1.2.1.4 Polymeric nanoparticles

In addition to dendrimers, typically, polymer nanoparticles are made from linear polymers and copolymers. Polymer nanoparticles offer advantage for drug delivery in literature such as size control,[74] biodegradablebility [75], control of release rate.[76] Encapsulation of drugs in various forms such as nanocapsules, Fig. 1.4h, and nanospheres, Fig. 1.4i.[75,77] Polymer nanoparticles have been used to encapsulate several drugs used in treating diseases such as cancer, AIDS, diabetes, malaria, prion disease and tuberculosis.[75]

Polymeric nanoparticles can be made out of natural, synthetic and semisynthetic polymers.

The use of synthetic and semisynthetic polymers offers several desirable features including promising reproducibility, stability and sustained drug release. Various monomers have been used as building blocks to synthesise different types of polymers such as poly(lactic acid) (PLA), poly(lactic-co-glycolic acid) (PLGA), poly(alkyl)-cyanoacrylates, poly(ethylene glycol-co-(lactic–glycolic acid)), poly(caprolactone), and poly(methyl) methacrylate.[1,76] Variation in monomer chemistry can be used to tune the properties of the polymers and help to tailor the encapsulation of drugs with different degrees of hydrophobicity or hydrophilicity depending on the properties of the drugs. Tailored polymers for drug encapsulation can have sustainable release capabilities over several weeks.[74,76] In addition, depending on the structure of the polymer backbone, biodegradability of polymers is possible.[75]

1.2.1.5 Liposomes

Liposomes were originally derived from intravenous nutrient emulsions that were later developed into drug delivery systems.[78] They were first introduced in the early 1960s and the first successful PEGylated liposome nanoparticle received FDA approval in 1995 followed by 20 different clinical investigations.[43] Liposomes are known as one of the first drug nanocarrier systems published in 1976[79] with the aim to protect labile drugs from denaturation by the acidic environment of the digestive system.[80,81,82]

The structure of liposomes is characterised as phospholipid bilayers formed from phospholipids with hydrophobic tails and a hydrophilic core, Fig. 1.4a. The amphiphilic phospholipids form either one or more bilayers. Liposomes are spherical vesicles with a broad particle size range from 30 nm to several microns[83] and are classified as three main types which include the small unilamellar vesicles (SUV), large unilamellar vesicles (LUV) and multilamellar vesicles (MLV).[84,85] Liposomes can encapsulate both hydrophilic drugs in the hydrophilic core and/or hydrophobic drugs in the bilayers,[85] and encapsulated drugs used for treatment of cancer,[86,87,88] ocular diseases,[89] Alzheimer's disease,[44] Parkinson's disease,[90] HIV[1,91] and skin disorders. Liposomes are considered as a promising delivery

system that improves biocompatibility but there remains challenges associated with drug leakage and a short shelf life as a result of instability upon storage.[92] Other disadvantages reported in the literature include low encapsulation efficacy, rapid removal by reticuloendothelial system (RES), cell interactions or adsorption and intermembrane transfer.[93]

1.2.1.6 Oil in water (O/W) emulsions and solid lipid nanoparticles

Lipids are water insoluble biodegradable organic molecules and some of them function as energy storage in our body or as building blocks with different physiological and biological roles in the cell membranes. Lipids can pass through biological membranes and be digested by enzymes. Lipids have been used in variety of formulations in the pharmaceutical industry and examples include formulations such as emulsions, pellets, ointments and suppositories [94,95] The advantage of using a lipid matrix as a colloidal carrier system is that the excipient is composed of physiological components are typically selected from materials that have a generally recognised as safe (GRAS) status.[96] Lipids used for the preparation of nanoparticles can either have a melting point below or close to body temperature or a melting point above the temperature of the body. If the lipids are solid at body temperature these nanocarriers are described as solid lipid nanoparticles (SLNs). A wide range of different of lipids have been used for SLNs in the literature, including fatty acids, free fatty alcohols, glycerol esters of fatty acids and waxes.[97] However, lipids with a high melting point used in nanoparticles formation have disadvantages such as crystallisation and low drug loading when used in drug delivery.[94] If the melting point of the lipid used for the drug delivery system is below body temperature the liquid lipids are referred to as ‘oil-in-water’ (O/W) emulsions or nanoemulsions. The common feature that the low and high melting point lipids share in a drug delivery system is that they can encapsulate poorly water-soluble hydrophobic drugs. The O/W emulsions are known to be used in variety of administration routes such as parenteral, oral and ocular delivery.[98] O/W emulsions comprise a biphasic

dispersion of oil dispersed in water, which are thermodynamically unstable and will ultimately separate into two layers over time. In the presence of an emulsifier the liquid oil droplets can be given a high degree of kinetic stabilisation and the length of time for which the oil droplet will stay well dispersed is dependent on the emulsifiers stabilising properties.[99] Nanoemulsions can made with liquid lipids such as castor oil, corn oil, coconut oil, evening primrose oil and olive oil.[99] Liquid lipid nanoparticles emerged as a potential drug carrier to improve the gastrointestinal (GI) absorption and oral bioavailability of lipophilic drug.[95] Lipid droplets in nanoemulsions or nanoparticles in dispersions can vary in size below 1000 nm.[100]The process used to make O/W emulsions often involves applying mechanical energy in various forms (e.g. high-pressure homogenisation) to an immiscible two-component liquid system to break the oil phase into droplets.

Replacing liquid lipid core in liquid lipid emulsion with lipids that are solid at body temperature allow the drug mobility to be lower .[101,102] These lipids refer to as solid lipids and examples of those are triglycerides, partial glycerides, fatty acids, steroids and waxes.[103] Solid lipid nanoparticles may be prepared using similar techniques used to process O/W emulsions, however, heat is also regularly used to melt the lipids during processing followed by cooling steps to form the solid lipid dispersion. Examples of processes that requires heat to produce SLNs are hot high shear homogenisation.[104] In this example by Alex *et* al,[104] the hydrophobic drug is added to a lipid and melted to 80 ºC. Then a hot aqueous surfactant solution is added to hot lipid phase and homogenised with high-speed homogeniser.[104,105] After cooling the mixture result in a SLN dispersion. SLNs (Fig. 1.4d) are described as having a solid sphere and an amorphous and lipophilic surface.[95] They can be prepared with different forms of lipids, surfactants and processing methods and have been investigated to encapsulate different drugs.. The next section summarises the features of SLNs by highlighting the preparation techniques, use of excipients, surfactants and design and synthesis of biodegradable macromolecular surfactants.

1.3 Solid lipid nanoparticles (SLNs) for encapsulation of hydrophobic drugs

1.3.1 Methods to prepare SLNs

SLNs can be prepared by many different techniques and can be divided into experiments that either requires high energy or low energy during the processing and these techniques are summarised in Table 1.1. Once SLNs have been produced a dry product can be produced using a number of different methods for removing the aqueous phase such as freeze-drying, evaporation or dialysis. [95,101]

Table 1.1. Methods for preparation of SLNs.

Method	
High energy	High pressure homogenisation[106,107,108] High shear homogenisation[104,105,109] Ultrasonication[109,110] Probe sonication[111]
Low energy	Microemulsion method[112,113] Membrane contactor[114] Phase inversion temperature (PIT) method[115,116] Coacervation method[117,118] Double emulsion method[119,120,121]
Organic solvent	Emulsification-solvent evaporation[122] Emulsification solvent diffusion[123] Solvent injection[124,125] Supercritical fluid (SCF) technique[126]

One of the most frequently used SLN production techniques is homogenisation which can be performed by either high shear mixing or high pressure and the two different methods are discussed and illustrated in Fig. 1.6.

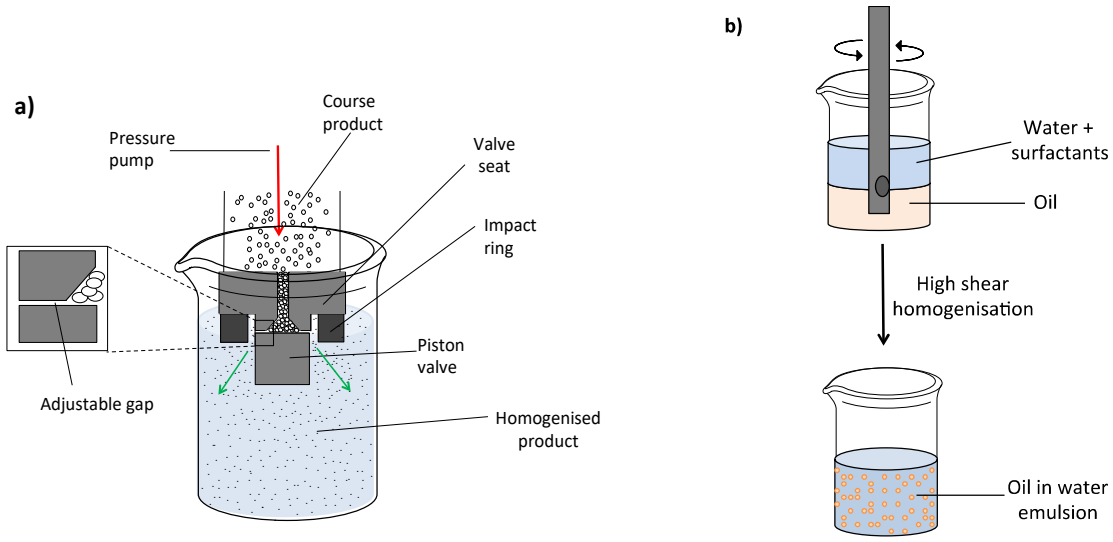

Fig. 1.6. Two different high-energy procedures used to prepare SLNs **a)** high pressure homogenisation *versus* **b)** high shear homogenisation.

The preparation of solid lipid nanoparticles by high pressure homogenisation (HPH), Fig. 1.6a, and this process was described in the literature.[101] This method is favourable in commercial large-scale production and very cost effective. Using this technique, a coarse emulsion is forced at a high pressure (100-2000 bar) through a narrow submicron sized gap. The high shear stress and cavitation forces at the adjustable gap between the valve seat and the piston valve is used to decrease the particle size.[101] The resulting dispersion is generally obtained with a narrow size distribution. Another typical method to prepare SLNs used in research is high shear speed homogenisation, Fig. 1.6b. A typical procedure for SLN preparation involves using the high shear obtained by using homogenisation while heating the sample.[104127] A research group, Olbrich *et al*,[128] investigated and optimised the homogenisation process by considering variables and parameters such as time, stirring rate, cooling conditions and zeta potential that might have an impact on the particle sizes. They managed to optimise the homogenisation procedure and concluded that a faster stirring speed could result in a narrow and smaller size of resulting SLNs when analysed by dynamic light scattering (DLS). In addition to that the addition of more surfactants to the composition result in producing a narrow size distribution for the resulting SLNs.[101]

1.3.2 Lipids used for SLN production

The pharmaceutical properties of the drug that is encapsulated in SLNs can be adjusted by the use of the lipid matrix as it forms the structure that stores, transports and releases the drug from the nanocarrier. The lipid core of SLNs has physical stability and is generally highly biocompatible.[103] It can incorporate a lipophilic drug by the emulsification of a molten matrix lipid followed by cooling the mixture down.[94,103129] Solid lipids used for the preparation of SLNs usually require temperatures above 50 °C to melt before they can be mechanically incorporated into a SLN structure.[95,103,130] The different solid lipids used for preparation of SLNs have been summarised in a review by Mehnert and Mäder[103] and a table of lipids is listed in Table 1.2

Table 1.2. Lipids with high melting points used for preparation of SLNs. [101, 103]

Lipid class	Examples
Triglycerides	Dynasan 114[131,132], 116[132] and 118[133,134] (monoacid triglyceride)
Mono, di and triglycerides mixture	Witeposol bases[135], Glyceryl Monosterate (Inwitor 900)[136], Glyceryl behenate (Compritol ATO 888)[105,137] and Glyceryl Palmitostearate (Precirol ATO 5)[135,138]
Waxes	Beewax[139], Cetyl palmitate[140]
Hard fats	Stearic acid[141,142,143], Palmitic acid[118,144] arachidic acid[143], behenic acid[117], Myristic acid[117]
Other lipids	Miglyol 812 [133], Miglyol 840[133] (triglycerides with fatty acids C8 and C10) and Paraffin[145]

Glyceryl dibehenate, also known as Compritol ATO 888, is a lipid frequently used in SLN formulations due to its properties including controlled and sustainable drug release.[94] However, a significant disadvantage of using Compritol ATO 888 as an excipient for drug delivery in SLNs has also been highlighted [94,94] suggesting that Compritol ATO 888 can undergo polymorphic transition that leads to drug expulsion upon storage.[95,146] Compritol

ATO 888 based SLNs have also been shown to have relatively poor drug loading. The poor drug loading has been linked to crystallographic transitions of pure lipids upon storage. The stability has been investigated by differential scanning calorimetry (DSC) to detect the polymorphic transitions of lipids in SLNs and it is based on monitoring changes in melting points.[94] The polymorphic transition happens over time upon storage and involves various crystal forms of the lipid such as α, β and β'.[147] The α form is the most thermodynamically unstable while the β forms are thermodynamically stable.[147,148] Dynamic light scattering (DLS) is another technique which has been used to investigate if a lipid in SLN formulation crystallises over time due to changes in the observed size distribution.[149] In order to avoid the polymorphic transition additional liquid or solid lipids are often blended into the formulation, and this nanocarrier system is referred to as a nanolipid carrier (NLC).[150,151] SLNs and NLCs has been compared to each other in terms of their structural properties, Fig. 1.7. SLNs can form highly ordered crystalline structures, sometimes depicted in a 'brick wall' arrangement, known as a perfect crystal arrangement. This leaves no holes in which drugs can reside and consequently this lead to expulsion. This happens when a highly ordered crystalline structure undergoes a polymorphic transition from α to β' in the brick wall arrangement as seen on Fig.1.7. NLCs utilise the co-formulation of a second lipid to form a less ordered structure to form a lipid matrix that is less susceptible to crystallisation and able to accommodate drug compounds in a more stable form.[152]

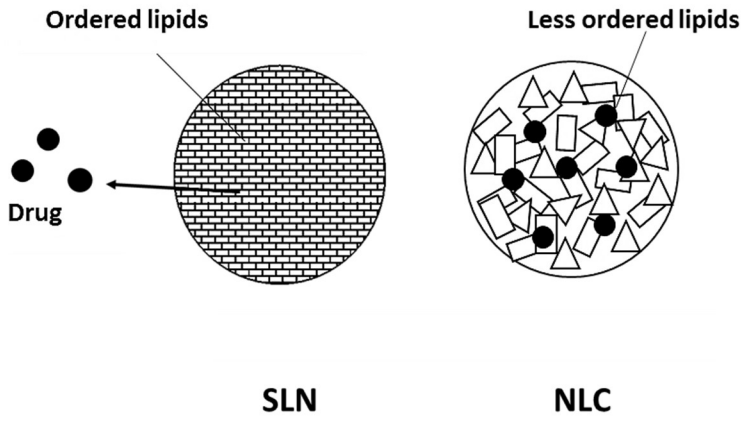

Fig. 1.7. Illustration of SLN (ordered structure) and NLC (less ordered structure). Adapted from Beloqui *et al*.[146]

1.3.3 Surfactants for SLNs

Surfactants are used to stabilise liquid and solid colloids. In general, when oil droplets are formed or particles are dispersed in another liquid, an interfacial boundary between the two immiscible phases is created with a corresponding interfacial energy that depends on the surface area and the interfacial tension (Δp) as given by the following equation.[97]

$$\Delta p = P_{in} - P_{out} = 2\gamma/r \qquad \textbf{(1.1)}$$

Where P_{in} is the pressure inside the lipid droplet/particle and P_{out} is the pressure outside the droplet/or particle, γ is the surface tension and r is the radius of the spherical droplet/particle.[97] The radius r of the droplet is inversely proportional to the pressure, so decreasing the droplet size results in an increase in the pressure difference across the droplet and also leads to a higher interfacial tension. Therefore, a nanoscale dispersion may require a lot of energy to form small droplets/particles dispersed in water. In order to create smaller droplets while minimising the interfacial tension the surface tension needs to be lowered by a surfactant.[97] However, it is common for a limit of surface tension stabilisation to be present within the chosen system. In order to further decrease the surface tension a co-surfactant can be added to the system. The structure of the surfactant can influence the particle size obtained from the production process, the physical long-term stability during storage, the drug release profile and the enzymatic degradation rate.[153]

Other types of stabilisers mentioned in literature, which include Pickering stabilisers, Fig. 1.8. Pickering stabilisers, sometimes called Ramsden stabilisers, are used to make Pickering emulsions were introduced by the pioneering work of Ramsden *et al* in 1903 and Pickering in 1907.[154,155]Pickering emulsions are stabilised by solid particles within a size range of several nanometers to microns[154] These particles are absorbed into liquid-liquid interfaces and provide emulsion stability.[154]This happens by interfacial absorption of the particle into the

surface of the colloid.[156] Pickering emulsions opened a new avenue of emulsion stabilisation and practical applications, such as biomedicine, food, fine chemical synthesis and cosmetics.[154] This can be done by tuning the types and properties of solid emulsifiers.[157] They showed that solid particle stabilisers result in a very stable emulsion and that it is energetically unfavourable for the solid particle multi attachment stabilising ends on the surface of the emulsion to exist freely in solution.[155,157] Examples of solid particles that stabilise Pickering emulsions include hydroxyapatite (HAP) silica, clay, magnetic nanoparticles, chitosan, cyclodextrin, nanotube, and food-grade stabilisers such as protein based particles.[157] Another type of polymer that resembles the character of Pickering emulsions are branched copolymers. There are many examples of types of building blocks in literature that can be used to synthesise branched copolymers such as vinyl and divinyl functional monomers.[158,159,160–162]

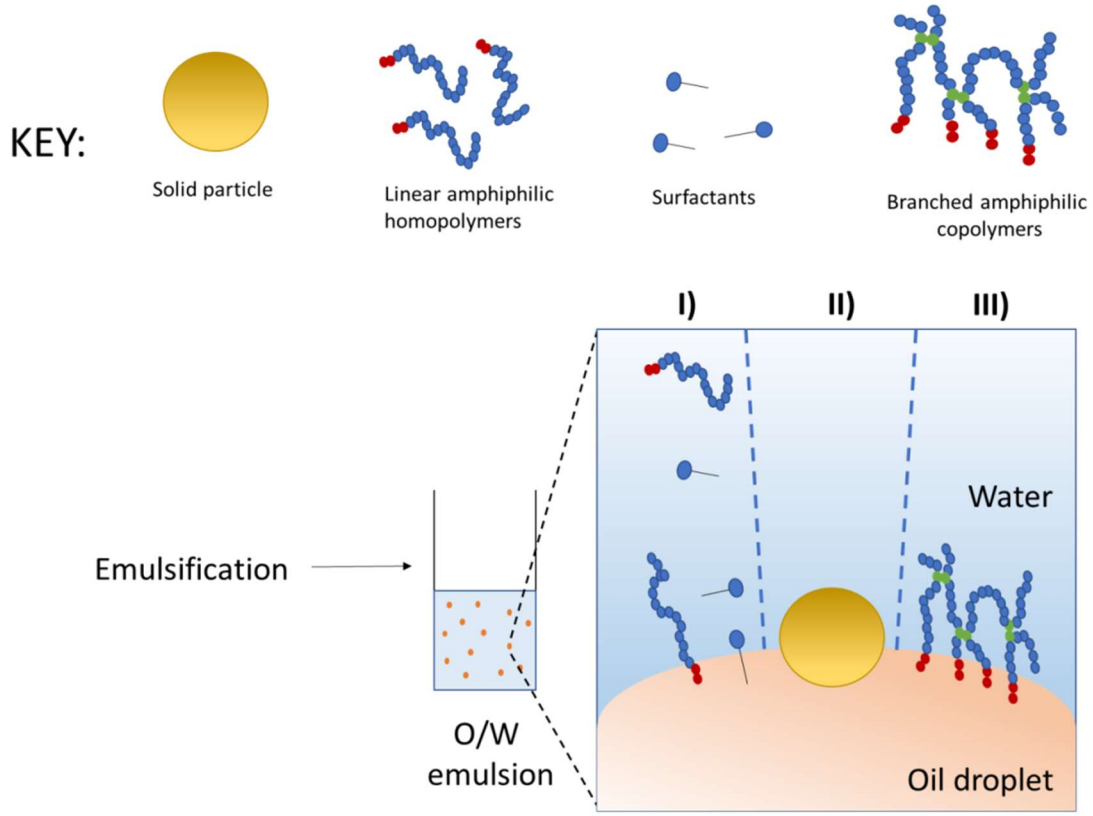

Fig. 1.8. Schematic illustration of synthesis of emulsions that result in O/W emulsion with the use of three different types of stabilisers described in the key as **I)** Surfactant or amphiphilic polymers, **II)** Pickering stabilisers and emulsion stabilised by solid particles absorbed on the surface of an oil droplet and **III)** branched polymers on the surface of an oil droplet.

1.4 Synthesis and application of branched amphiphilic copolymers

1.4.1 Reversible deactivation radical polymerisation (RDRP)

Linear and branched grafted polymers can be synthesised by variety of methods that are collectively known as conventional free radical polymerisations.[163] These approaches are considered to be cost effective, versatile and scalable approaches for industry manufacturing.[159,164] Another advantage of conventional free radical polymerisation is that it requires facile reaction conditions and can use a broad range of monomers in order to synthesise a customised polymer.[160,161,165] Conventional free radical polymerisations reactions may be controlled by a range of techniques collectively known as reversible-deactivation radical polymerisation (RDRP).[166] There are many different RDRP methods presented in literature.[166] The methods are divided into nitroxide mediated polymerisation (NMP),[167,168,169] reversible addition fragmentation chain transfer (RAFT) polymerisation[170,171,172] variations of organometallic-mediated polymerizations (OMRP)[173] and atom transfer radical polymerisation (ATRP),[174–176] NMP and ATRP follow a very similar mechanistic strategy which is based on the dynamics of equilibrium between the majority of dormant species and a few active species and this result in a low radical concentration, Scheme 1.1. [177,178]

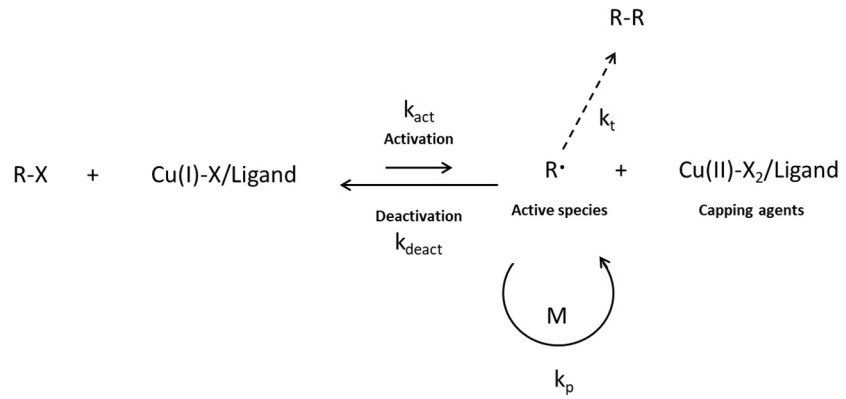

Scheme 1.1 General mechanism of ATRP X; halide Br, Cl. k_{act}; activity rate, k_{deact} ;deactivation rate, k_t; termination rate, k_p is the propagation rate. Modified from literature. [179,175]

The mechanism of RAFT polymerisation is different in terms of it being controlled by a reversible chain transfer.[172]

1.4.2 Atom transfer radical polymerisation (ATRP)

ATRP is a reversible-deactivation radical polymerisation technique that has been thoroughly investigated since its discovery and development.[175,179] Its typical conditions require a copper (Cu) catalyst and a ligand which is often 2,2'-bipyridyl (bpy), Scheme 1.1.[180,181, 182] Cu is by far the most widely used metal catalyst due to its versatility in ATRP and relatively low cost. The bpy ligand controls the redox chemistry of the final metal complex in the reaction media through selective steric and electronic effects, additionally the redox equilibrium leads to the maintenance of a low radical concentration as demonstrated on Scheme 1.[180,181,182] The controllability of ATRP can be used to synthesise brushed and graft copolymers with different initiators such as for example macroinitiators or bromoisobutyrate initiators and monovinyl or divinyl monomers such as methacrylates and other acrylates.[183,184,185,186,187] Moreover, ATRP offers several advantages such as varying parameters that result in different polymer architectures.[186,187,185,188,189,190] Our group has used ATRP to synthesise branched amphiphilic polymers often with methacrylate and acrylate building blocks.[186,187] In a study by He *et al*,[186] poly(*n*-butyl methacrylate) (poly(*n*BuMA)) branched copolymers were synthesised using monovinyl and divinyl monomer, ethylene glycol dimethacrylate (EGDMA), as a branching agent. They synthesised various polymer architectures to demonstrate self-assembled nanomaterials.[186] Similar materials synthesised with methacrylate polymers have been demonstrated to stabilise oil emulsions.[191] This research demonstrated that the individual emulsion droplets retained their structural integrity and no de-emulsification was observed after disassembly. Moreover, the engineered emulsions have far-reaching potential in applications where encapsulation and controlled delivery of large payloads is desirable.[191] Additionally, the branched architecture ensures that each stabiliser molecule contains multiple potential points of attachment to the droplet surface and

dodecane chain ends were chosen to mimic the oil phase which in this case is the dodecane.[191] Weaver *et al*, used another approach to synthesis the branched polymer architecture which is the 'Stratchclyde route' in which the reaction is controlled by a chain transfer agent (CTA). The function of this approach is to control the reaction and inhibit gelation.[161] However, the amphiphilic branched copolymers can be synthesised by other controlled free radical approaches such as ATRP and RAFT among those the ATRP is widely studied in our group as mentioned earlier.

To demonstrate the controllability of ATRP for a given reaction samples can be collected at the beginning of the reaction and monitored throughout the reaction from the time a copper catalyst has been added to the reaction. There are two different methodologies that can be used to control ATRP reaction which ^{1}H NMR and gel permeation chromatography (GPC). This has already been demonstrated in studies performed in our group.[185,186,192] In the work by Dwyer *et al*[193], analysis was carried out by ^{1}H NMR in $CDCl_3$ and the monomer conversion was determined by using crude samples of the reaction medium.[193] The integrals of the vinyl protons of the unreacted monomer were compared against integration of an internal reference which in this case was the CH_2 signal adjacent to an ester group of the formed polymer repeat units and the monomer. This could be used to determine the conversion of the polymer in the reaction mixture.[193] GPC is another method that can be used to confirm the controllability of the ATRP. In this case crude samples can be analysed at different time points during throughout the reaction. The parameters obtained from GPC is the number average molecular weight (M_n) and weight average molecular weight (M_w) and can be plotted as M_w or M_n against % of converstion to give a straight line in case of controlled radical polymerisation.[163,175] In the event that the reaction is not controlled (such as a free radical polymerisation) this line is not straight. Lack of controllability can be due to rapid termination or if the concentration of dormant species is far less than the concentration of the radical and thereby that the equilibrium has been shifted towards the radicals as shown on Scheme 1.1.[175,177]

These methods will be used to create a range of highly branched polymers which may be able to envelop the SLNs imitating the effect of a Pickering emulsion which confers additional stability to the SLNs. The criteria which will be used to determine which polymer is best suited to stabilise SLNs. The use of suitable polymer can be evaluated by designing a model oil study designed by earlier mentioned research group.[191] This allows the assessment of the stabilising effect of different synthesised polymer architectures when comparing different features.

1.5 Nanomedicine administration

1.5.1 Oral administration of drugs

When drugs/active compounds are orally administered into the body their therapeutic goals are fulfilled through absorption, distribution, metabolism and elimination or excretion.[194]

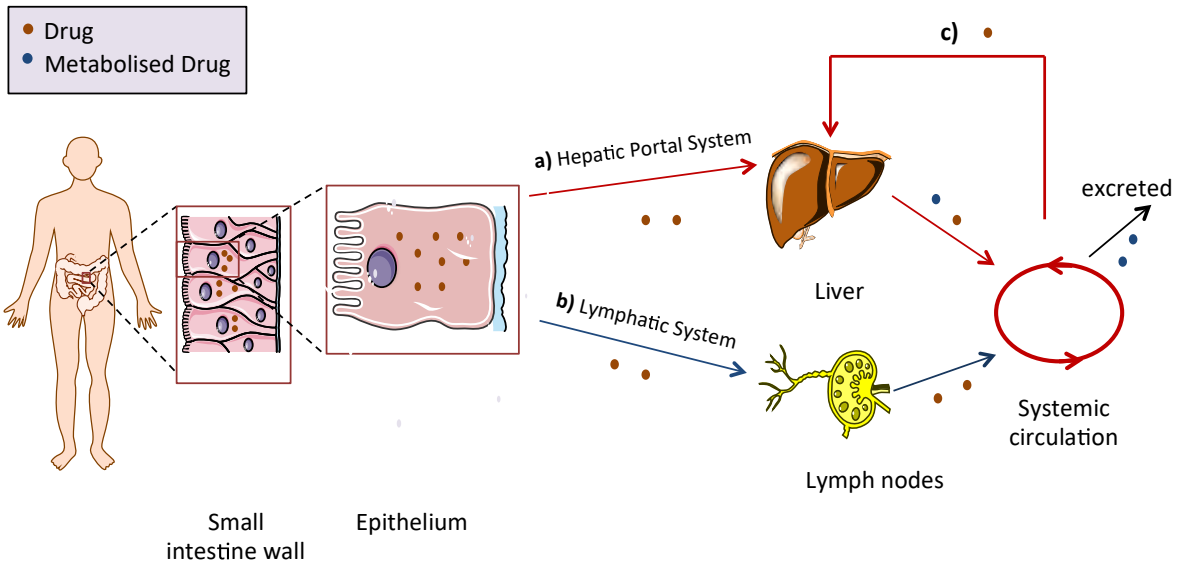

Fig. 1.9. Examples of two oral delivery routes **a)** hepatic portal system and first passage metabolism and the **b)** lymphatic system. **c)** other liver metabolisms that results in clearance.

In the first process, absorption, the drug is administered orally and transported into the blood through the digestive system. There are three well-known pathways that the drug can use to reach the circulatory system after traversing mucus barrier within the gut, the two main

routes are the hepatic portal system (Fig. 1.9a) and the lymphatic system (Fig. 1.9b). When the drug is administered orally, it is absorbed from duodenum which lead to the drug entering the hepatic portal vein and undergo a first round of metabolism (first passage metabolism).[195] As a result the CYP450 enzymes oxidise, hydrolyse or reduce which chemically modify the drug and this may lead to toxic or non-toxic metabolites that may be excreted through the kidney.[196] First passage metabolism of an orally administered free drug can cause several common issues. Firstly, if a high level of metabolism occurs during the first pass this will result in less delivery of active drug into the circulatory system as most of the drug has been metabolised and excreted by the kidneys.[194] Secondly, the active free drug can be metabolised by other wild type CYP450 enzymes depending on the genetics of the subject that might result in side effects and toxicity. Thirdly, drug interactions with CYP450 enzymes that either induce or inhibits the enzymes can be an issue.[197] The concentration of active drug is measured by pharmacokinetic studies in which a subject takes a drug and the concentration of metabolites and the drugs are measured in the blood throughout time after the drug was orally administered.[198,199] After the active free drug has undergone the first round of metabolism it is distributed to different compartments of the body by the circulatory system in a process which involves transport proteins etc. The drug undergoes several rounds of metabolism before it gets cleared from the body as illustrated in Fig. 1.9.

1.5.2 Lipids in oral administration

Lipids delivered by oral administration have been shown to enhance the bioavailability of poorly bioavailable drugs.[96] The use of lipids has been shown to decrease the effect of cytochrome CYP450 on drug when the lipid is administered with a drug.[200] Moreover lipids have an impact on the uptake of poorly water soluble drugs through the intestine.[201]A nanocarrier formed by lipids can be compared to chylomicron particles (Fig. 1.11) synthesised by the body in the endocytes[202] of the small intestine and secreted to the

lymphatic vessel through to the circulatory system. The function of the chylomicron is to deliver water insoluble long chained fatty acids to supply the tissues with fats absorbed from the diet bypassing the portal system of the liver. This behaviour means that lipids containing nanoparticles may be adsorbed by the lymphatic route, avoiding the first-passage metabolism and acting as a bypass route for compounds with lower bioavailability.[203]

1.5.2.1 Influence of uptake in the epithelial barrier and intracellular drug delivery

The uptake mechanism through the intestinal barrier of an orally administered nanoparticle depends on the specific characteristic features of the particle used, Fig. 1.10.

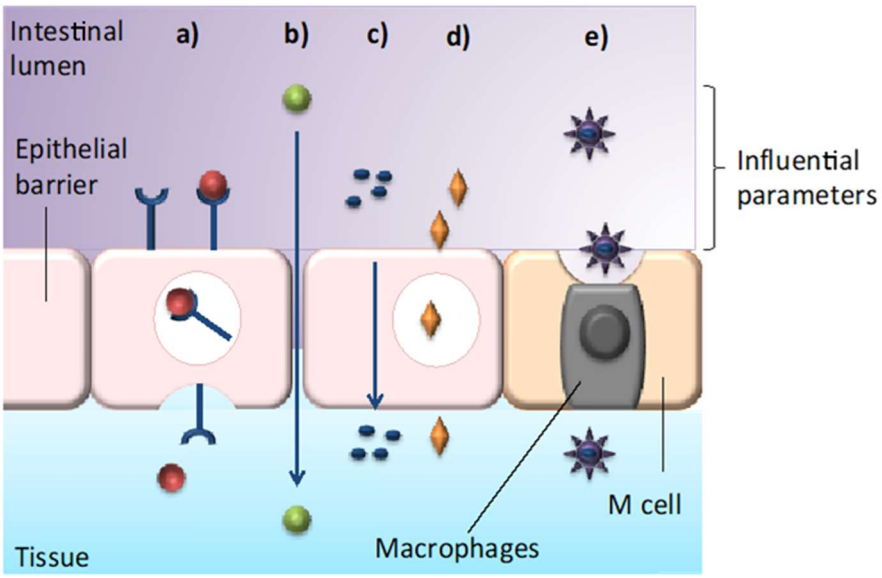

Fig. 1.10. Mechanisms of uptake of nanoparticles that reach the epithelial barrier from intestinal lumen. Transport mechanisms **a)** receptor mediated transcytosis, **b)** paracellular diffusion, **c)** transcellular diffusion, **d)** absorption mediated transcytosis **e)** M cell antigen sampling. Adapted from Yu *et al*. [204]

First, a particle may pass through the intestinal barrier using the mechanism of transcytosis, Fig. 1.10a, which is the passage of material from one side of the cell called the epithelial barrier through the other with subsequent release on the other side of the cell. Second, a particle can use paracellular diffusion, Fig. 1.10b, which is facilitated by particles that are coated with polymers or the size of the particle that is small enough to penetrate the narrow

junction between the cells.[204] Third, particles can use transcellular diffusion, Fig. 1.10c, through the intestinal barrier, which depends on the lipophilicity of the nanoparticles. Additionally, there are two ways that nanoparticles can be absorbed through the epithelial barrier due to its surface charges that facilitates either absorption mediated transcytosis, Fig. 1.10d and/or antigen recognition that facilitate M-cell antigen sampling, Fig 1.10e. [205,204] The mechanism by which SLNs get absorbed when orally delivered to the body has not yet been investigated in detailed literature reports. Since SLNs share similarities with chylomicron particles it is possible that they may also benefit from a degree of absorption via the lymphatic system. Some articles have shown this by studies performed in rats. [104,206] Cho *et al*[206] compared two drugs, docetaxel and taxotere, encapsulated in SLNs. They[206] concluded that SLNs injected into the intestine of rats showed enhanced intestinal absorption, lymphatic uptake, and relative oral bioavailability of docetaxel compared with taxotere.[206] Based on this the similarities between SLNs and chylomicron is interesting to consider as both type of particles share characteristic features in terms of size, absorption and encapsulation of hydrophobic moieties which will be outlined in the next section.

1.5.3 SLNs for oral administration

The structure of SLNs, Fig. 1.11a, resembles the structure of a physiological chylomicron particle which is a nanoparticle synthesised naturally by the endosomes using long chained fats in the body.[202] Chylomicrons, Fig. 1.11b, are a good example of natural lipid carriers that are produced in the gut.[96] and the structure of chylomicrons is characterised as having a lipid core. The aforementioned property of chylomicrons is very similar to the behaviour observed from SLNs in many aspects. SLNs are composed of biodegradable and physiological solid lipids such as high melting point fat and cholesterols. These lipids give the particle the property of sustainable and controlling release a hydrophobic drug into a system. [94, 207, 208,209]

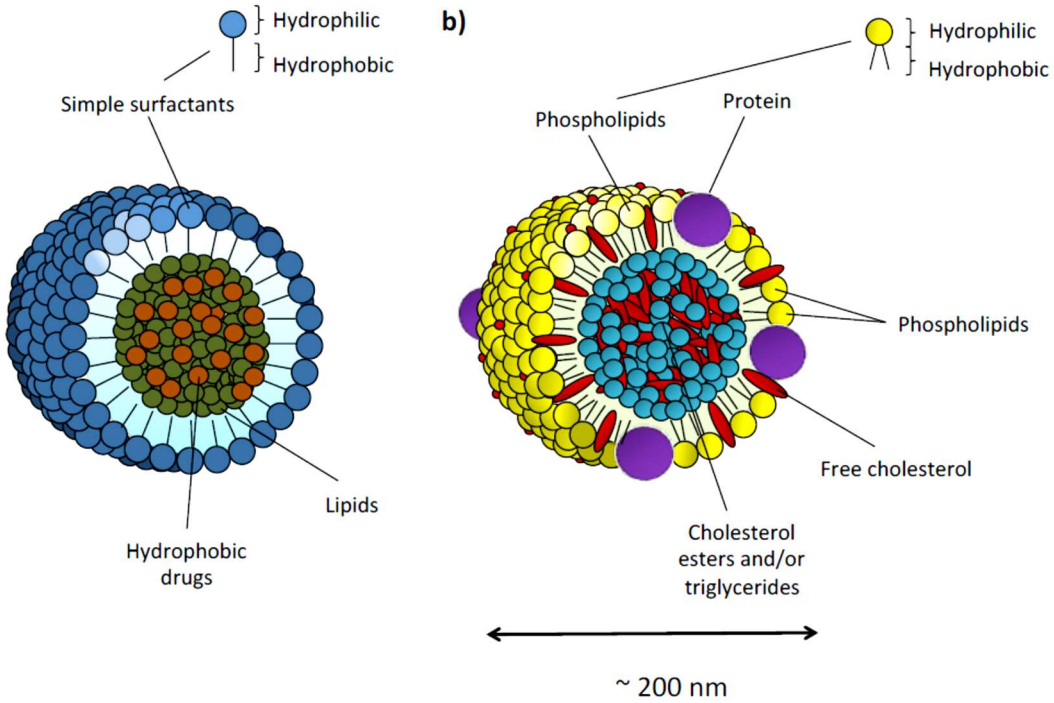

Fig. 1.11. Comparison of solid lipid nanoparticles and chylomicron nanoparticles. **a)** Synthesised solid lipid nanoparticles stabilised with simple surfactants with a hydrophobic core comprising of lipid and hydrophobic drug and **b)** chylomicron nanoparticles stabilised with proteins, phospholipids and free cholesterol with a hydrophobic core comprising of cholesterol esters and/or triglycerides.

1.6 Objectives of the research

MVC is the only drug in its category of CCR5 receptor inhibitor of anti-HIV drug that targets the binding of the virus to a host cell in the beginning of the HIV life cycle, but MVC has limitations due to low bioavailability and complications with its commercial formulation. The complications with the commercial formulation is due to the drug hydrophobicity. In order to increase the bioavailability of the drugs a different formulation approach needs to be considered. It is hypothesised that encapsulation of MVC in a delivery platform is likely to improve its bioavailability. Our group has already demonstrated improved delivery of anti HIV drugs using other types of delivery systems including solid drug nanoparticle (SDN) delivery of lopinavir[210] and efavirenz.[211]

Various drug delivery platforms have been considered for MVC and those examples include PLGA nanoparticles[212] and nanolipogels.[213] It has been demonstrated that such nanocarrier platforms provide sustained release and that there is a possibility to extend the dosage interval in different delivery compartments of the body. This is based on body

mimicking *in vitro* studies.[212,213] However, the understanding of how a combination of a lipid and a polymer in MVC loaded nanoparticles impacts the release of drug *in vitro* has not yet been demonstrated in the literature. Solid lipids are known to also delay release of a drug in tablets and other formulation forms.[94] It is our objective to provide a framework for making MVC more bioavailable and for this we chose SLNs. SLNs are a good choice to achieve such a release due to the fact that MVC is a hydrophobic drug and compatible with encapsulation in a hydrophobic core using a biocompatible and biodegradable lipid excipient.[101] Other hydrophobic anti-HIV drugs have already been encapsulated in SLNs in a number of previous reports,[104,214,215] however no anti-HIV drugs has been encapsulated SLNs in our group. Anti-HIV drugs in our groups has been encapsulated in related nanoparticles such as SDNs.[210,211] Those encapsulation studies successfully showed an improvement in bioavailability of lopinavir[210] and efavirenz.[211] In other research groups, anti-HIV drugs including examples such as lopinavir,[104] darunavir,[215,216] tenofovir[217] and efavirenz[214] have been encapsulated in SLNs. Alex *et al*, [104] synthesised SLNs lopinavir using the lipid Compritol ATO 888 as a hydrophobic excipient. The study showed an encapsulation efficiency (EE) of above 99 %.[104] This study showed that oral SLN formulation of lopinavir *in vivo* improved the bioavailability in Wistar male rats.[104] Other research groups, Bhalekar *et al*,[216] demonstrated that encapsulated darunavir relative to lipid (GMS) in the processing of DRV- increased the bioavailability of DRV and lymphatic uptake in Wistar male rats.[216] The same was demonstrated by Gaur *et al*[214] that encapsulated efavirenz into a SLN containing GMS as a lipid excipient. In conclusion all of these pharmacokinetic researches by Alex *et al*, [104] Bhalekar *et al*,[216] and Gaur *et al*[214] demonstrated that the oral bioavailability of i*n vivo* SLN formulation increased when compared against the conventional formulation of the investigated anti-HIV drugs administered orally to Wistar rats.

The stability of SLNs has often been reported to be a challenge due to low drug loading and crystallisation of particularly the lipid excipient in the core. The stabilisers used to make SLNs usually small molecular surfactants. However, the use of large amphiphilic polymer structures as stabilisers in SLN system has not been demonstrated. Large amphiphilic

polymer structures may potentially imitate the behaviour of Pickering stabilisers. We hypothesise that branched polymers can be used to stabilise a SLN system via a mechanism that imitates the use of Pickering stabilisers. This hypothesis is based on the idea that bigger stabilisers with multiple chain ends such as branched polymers can form a stronger attachment to the surface of a given droplet. In order to maximise the stability of the SLNs we will identify important parameters that determine the branched copolymeric architecture. These architectures can be varied using ATRP as a synthesis route. The stabilising properties of the branched copolymers can be tested using a model oil study that is inspired by an early a research group Weaver *et al*[191] This study can be used to compare different parameters in the obtained polymer library such as chain length, molecular weight, degree of branching and linear vs. branched polymers as a stabiliser. It can be hypothesised that these comparisons can help us to assess the stabilising properties of the branched polymers in a simple oil emulsion study that can be translated to a more complicated study using solid lipids.

Since optimisation of SLNs with large amphiphilic and branched copolymers has not yet been described in the literature many general processing procedures will be tested. Hot high shear hot homogenisation which is the common methodology for processing of SLNs will be tested. In this methodology experimental parameters such as stirring speed, heat, composition and solvents will be varied. Moreover, other methodologies in literature will also be considered such as sonication[134] and solvent injection.[124] Probe sonication uses high energy in the system to make SLNs. With the use of this methodology we can speculate if the high energy is the important parameter to vary. The synthesis of SLNs by a solvent solvent injection method will also be assessed, this is an approach that imitates nanoprecipitation method that has been used in our group with similar types of branched copolymers.[185,188,192] This methodology involves the injection of a water miscible solvent containing the lipid and the polymer into a stirred solution of water containing the polymer. The use of this approach for synthesis of SLNs is relatively obscure and requires more optimisation than former mentioned hot high shear homogenisation methodology. This

methodology for synthesis of branched copolymer stabilised SLNs is used as it is hypothesised that the variation of parameters in those platforms can be used to optimise a SLN system with maximum MVC loading and increased stability over time. The final aim is to find a suitable and reproducible processing methodology of SLNs that can be used to encapsulate hydrophobic drugs such as MVC.

Chapter 2. Synthesis and characterisation of branched oligo ethylene glycol methacrylate (OEGMA) based polymers utilizing ATRP used in *n*-dodecane model oil studies

2.1 Introduction

SLN platforms for anti-HIV treatments have been developed with the aim of encapsulating drugs with poor water solubility and bioavailability.[104,202,214,215] Encapsulating drugs in the matrix of SLNs has been shown to allow drugs to slowly be released into target tissue including brain and intestine.[104,215,218]

In order for SLNs to display colloidal stability surfactants (also called stabilisers) are used to stabilise the interface between the colloidal surface and its surroundings.[219,220,221] The stabilisers are categorised into different types based on their physical properties such as being anionic, cationic, amphoteric and non-ionic[222] as was described in Chapter 1 section 1.6.3. This chapter is focused on the design of new non-ionic stabilisers and comparisons with commercial materials, specifically poloxamers, Fig. 2.1, used to stabilise SLN systems, in order to determine specific benefits; poloxamers exhibit low toxicity which is attributed to their non-charged nature.[223] Examples of the use of non-ionic stabilisers have been reported in various SLN systems in the literature.[224,225,226]

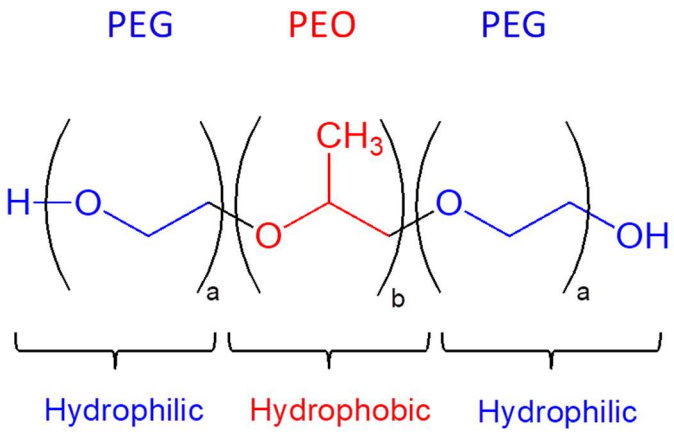

Fig. 2.1. General structure of poloxamers modified from Shubhra *et al.*[227] EO: ethylene oxide; PO; propylene oxide; a: repeats of EO forming PEG; b: repeats of PO forming PPO.

One of the most commonly used polymers for stabilising SLN formulations is poloxamer 188 (Pluronic® F-68)[228–230] which is a non-ionic amphiphilic copolymer[231] consisting of hydrophilic poly(ethylene oxide) (PEO) and hydrophobic poly(propylene oxide) (PPO) blocks that are arranged in A-B-A tri-block structure: PEO-PPO-PEO, see Fig. 2.1.[227,232] Poloxamer 188 has

a nominal molecular weight of 8.4 kDa, which makes it a high molecular weight surfactant in comparison to for example sodium dodecyl sulphate (SDS), which has a molecular weight of 288 Da. Another parameter of interest is the critical micelle concentration (CMC) for poloxamer 188 which has been determined to be 4.8 x 10^{-4} M.[233]

Some problems have been found to be inherent in the use of poloxamers as an excipient or surfactant for drug delivery systems. A study by Lee *et al*.[234] demonstrated that poloxamer in a dose dependent manner could result in cellular necrosis as it is capable of sealing electroporated and radio permeabilised cells which prevented rapid exhaustion of high-energy cellular compounds.[234] There is also evidence that poloxamers may cause other cytotoxicity issues including inhibition of multidrug resistance, P-glycoprotein (Pgp), the modulation of the membrane fluidity, and the impairment of adenosine triphosphate (ATP) synthesis.[233] Examples of inhibition of multidrug resistance was demonstrated by a study of different poloxamers carried out in the group of Miller *et al*.[235] They used monolayers of human pancreatic adenocarcinoma cells (Panc-1) to express the multidrug resistance-associated protein (MRP) to investigate the effects of poloxamer block copolymers on the functional activity of MRP.[235] The study concluded that poloxamer block copolymers could inhibit multidrug resistance-associated protein (MRP), however was found to be dependent on the poloxamer molecular structure, specifically, the lengths of hydrophilic PEO and hydrophobic PPO.[235] The effects of Pluronic block copolymers on MRP have been compared to P-glycoprotein drug efflux systems and it was demonstrated that there is a single unifying mechanism which may explain the inhibition of both mechanisms.[235] However, poloxamer also results in cytoprotection by enhancing the drug delivery of anti-cancer, -fungi, and -bacterial drugs which can be further studied in given references.[231,232,233]

Poloxamers are promising stabilisers, excipients and binding agents used in the pharmaceutical industry. Their chemical structures are comparable particularly to PEO/PEG based copolymers synthesised by research groups using simple and well-known radical polymerisation methods.[184,185] Recent development of graft (comb) copolymer surfactants for specific applications in dispersions are already demonstrated and examples include

commercial structures with meth)acrylate backbones and numerous PEO side chains, such as materials sold under the name of poly(methyl) methacrylate.[223] It is sold under the name Hypermer CG6 and known to have excellent stabilising properties for concentrated dispersions of hydrophobic particles in water.[223]

PEO/PEG based synthetic polymers have already been used in a variety of drug delivery systems[51,236,50,237] and a range of polymers containing PEO have been made within academic studies using a well-known synthetic route called atom transfer radical polymerisation (ATRP) which are described in Chapter 1 section 1.7.3.1. This method is useful because it offers a numbers of advantages such as facile, versatile reaction conditions and possible scalability.[161] Additional advantages offered include the ability to vary different parameters during synthesis of the polymer e.g. the number average degree of polymerisation and the targeted brancher to initiator ratio when designing branched copolymers.[160–162,165,188] This can be used to synthesise a library of polymers.[160] ATRP is described as a controlled radical polymerization technique and has been widely used in our group to synthesis similar polymer architectures. [185,187,193]Amphiphilic branched copolymers with hydrophobic chain-end chemistry have been shown to provide excellent stabilisation of oil in water emulsions and in the literature reports branched copolymers have stabilised oils such as *n*-dodecane,[191,238] dicaprylyl carbonate, propyl-heptyl caprylate, silicone oil, and isooctyl palmitate.[239] These studies have demonstrated that the stabilising mechanism is related to the degree of branching of the polymers, which also relates to the number of chain-ends within each polymer structure.[191,238,239] In addition, the studies have shown that an increase in the targeted degree of branching increases the stability of an oil droplet and decreases the particle agglomeration. Weaver *et al*,[191] have shown that a variety of branched oligo(ethylene glycol) methyl ether methacrylate (OEGMA) based polymers polymerised with a long chained hydrophobic initiator can stabilise oil-in-water emulsions using *n*-dodecane as an oil. The authors have proposed that the enhanced stability of the emulsions is due to the increased degree of branching which provides multiple sites for the hydrophobic initiator group to anchor onto the hydrophobic surface thereby increasing the

stabilising efficiency when compared to their linear analogue.[191,238] Furthermore, it has been demonstrated that varying the hydrophilic part of an A-B-A block copolymer can have an impact on the CMC and the molecular weight.[240,241,233] This can be done by either changing the degree of polymerisation or by using a different brancher. In conclusion the CMC and molecular weight parameters have all been shown to be important when designing branched copolymer stabilisers. This chapter focuses on the synthesis and characterisation of a library of linear OEGMA based homopolymers and branched OEGMA based copolymers polymerised with either EGDMA or PEGDMA to act as stabilisers for SLN manufacture. Methods to synthesise PEG based polymers are well-established using ATRP and will be described below.[179,175,176] The building blocks chosen for the synthesis of stabilisers for SLNs resembles the hydrophilic PEG structure in poloxamer 188 which is a typical conventional stabiliser reported to stabilise SLN[202,230,242] The structure of OEGMA, and the bifunctional monomers ethylene glycol dimethacrylate (EGDMA) and poly(ethylene glycol) dimethacrylate (PEGDMA) are shown in Fig. 2.2.

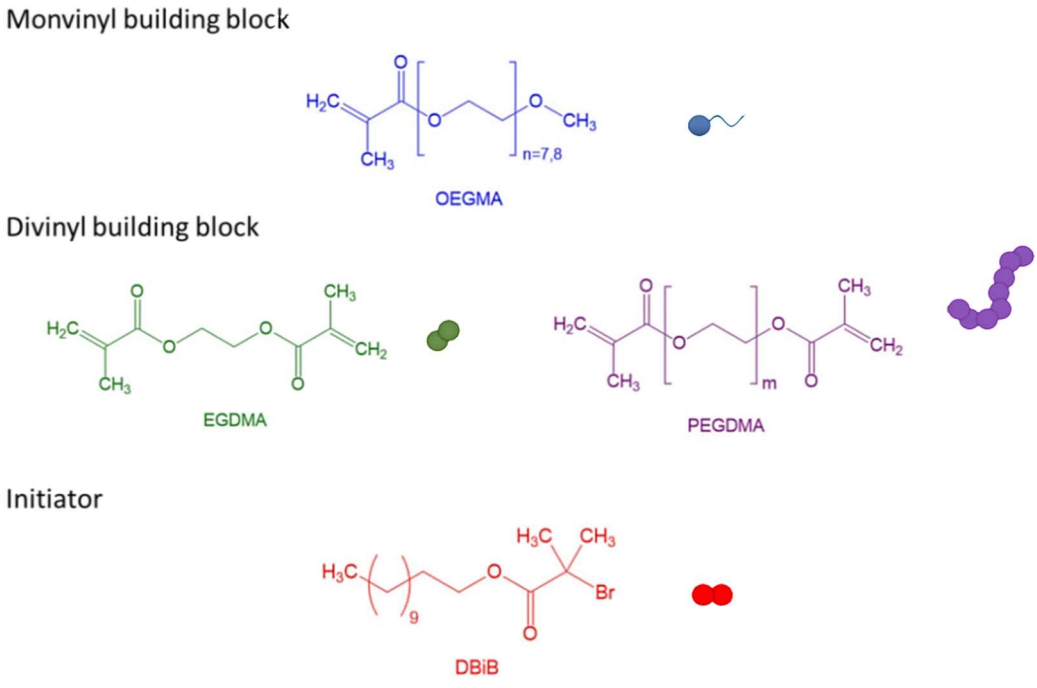

Fig. 2.2. Monovinylic; oligo(ethylene glycol) methacrylate (OEGMA) and divinylic; ethylene glycol dimethacrylate (EGDMA) and poly(ethylene glycol) dimethacrylate (PEGDMA) building blocks, DBiB; dodecyl-2-bromoisobutyrate chosen for the study.

These building blocks are used to synthesise highly branched copolymers. The molar ratios of the branching agents are varied relative to the initiator. This was done with the purpose of investigating how the stabilisation changes depending on the architecture of these stabilisers in SLN dispersions. The chain end functionality is chosen to be a long C_{12} dodecyl chain, dodecyl-2-bromoisobutyrate (DBiB), Fig. 2.2. The initiator chosen for the synthesis of the polymer is DBiB. The influence of the hydrophobic chain ends on the amphiphilic branched copolymer's properties is interesting to compare against the chain end functionality of polymers such as poloxamer 188 and Tween 80 which are typical polymers used to stabilise SLNs in literature reports.[110,202,214] A library of polymers will be synthesised with different degrees of polymerisation with the hydrophilic OEGMA monomer and lipophilic, dodecyl-bromoisobutyrate (DBiB), initiator by varying the monomer to initiator ratio as shown in Fig. 2.3.

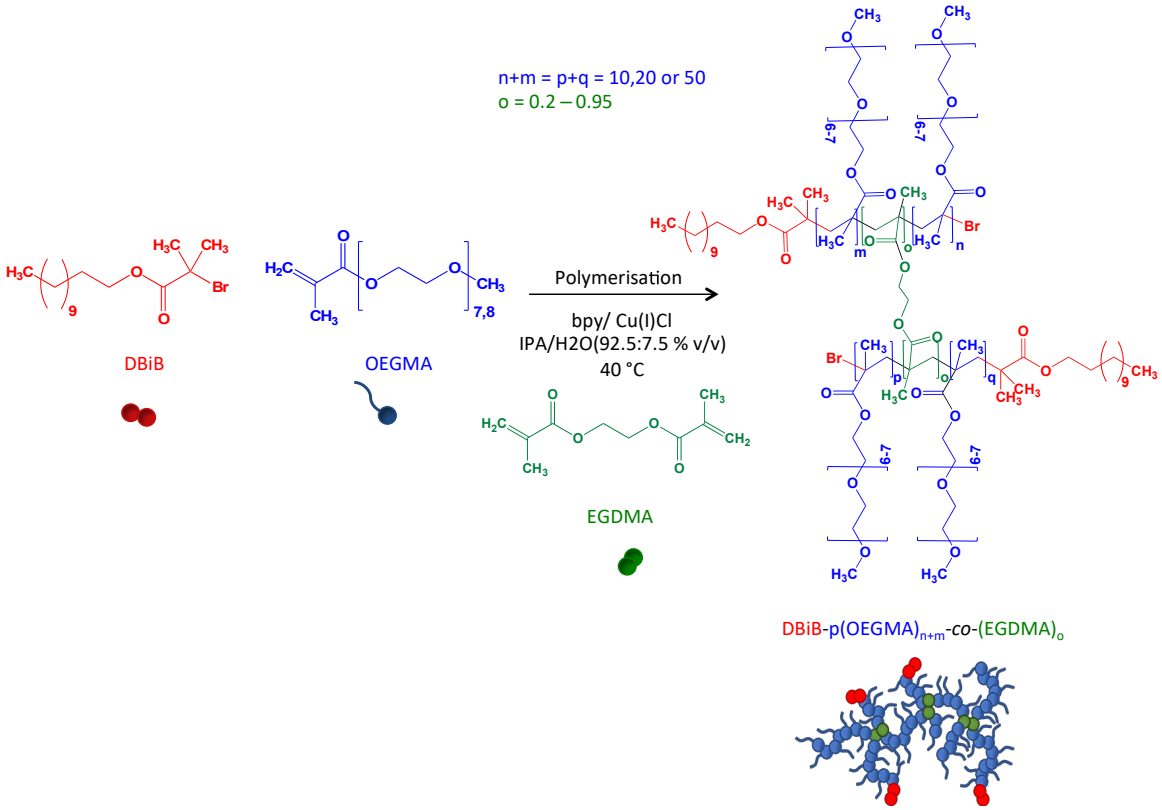

Fig. 2.3. Polymerisation conditions that are proposed to be used for the synthesis of OEGMA based copolymers using EGDMA as the branching agent. Following conditions are considered: Cu(I)Cl, bpy, IPA/H_2O (92.5,7.5 v/v) at 40˚C with modification from Auty *et al* [183] and He *et al.*[186,187]

In order to probe the influence of the brancher on the architecture and physical properties of branched polymer macromolecules, the two different branching agents will be used, EGDMA and PEGDMA, the molar ratios of the brancher to the initiator will be varied between 0.2 - 0.95:1 in order to investigate how to obtain high molecular weight copolymers. By varying the size of the polymer with different number average degrees of polymerisation (DP_n) of OEGMA and tuning the degree of branching with EGDMA or PEGDMA we hypothesise that a longer branching agent will results in more flexibility and greater distance between the primary chains, while smaller branching agents will result in less flexibility and closer distance between the primary chains, Fig. 2.3. These two different characteristic features of amphiphilic polymers are interesting to investigate and compare in an SLN stabilised systems. Subsequently, the aim of this study is to assess the polymeric architectures from the library using model oil in water emulsion studies and choose the best candidate for future studies of branched polymers as stabilisers in an SLN system. The structural architecture could lead to a potential impact in drug delivery systems where the highly branched copolymer stabilises emulsions or other nanoparticles as already seen in case of polymeric nanoparticles and micelles mentioned in Chapter 1.

2.2 Results and discussion

2.2.1 Synthesis of DBiB initiator

DBiB initiator was synthesised by an esterification reaction between the hydroxyl groups of dodecyl alcohol and 2-bromoisobutyryl bromide using a well-known procedure[243] and the synthesis method is described in the experimental section in chapter 7 section 7.1. DBiB was characterised by ^{1}H, ^{13}C NMR and ESI mass spectra and the results are given in Fig. 2.4-2.6.

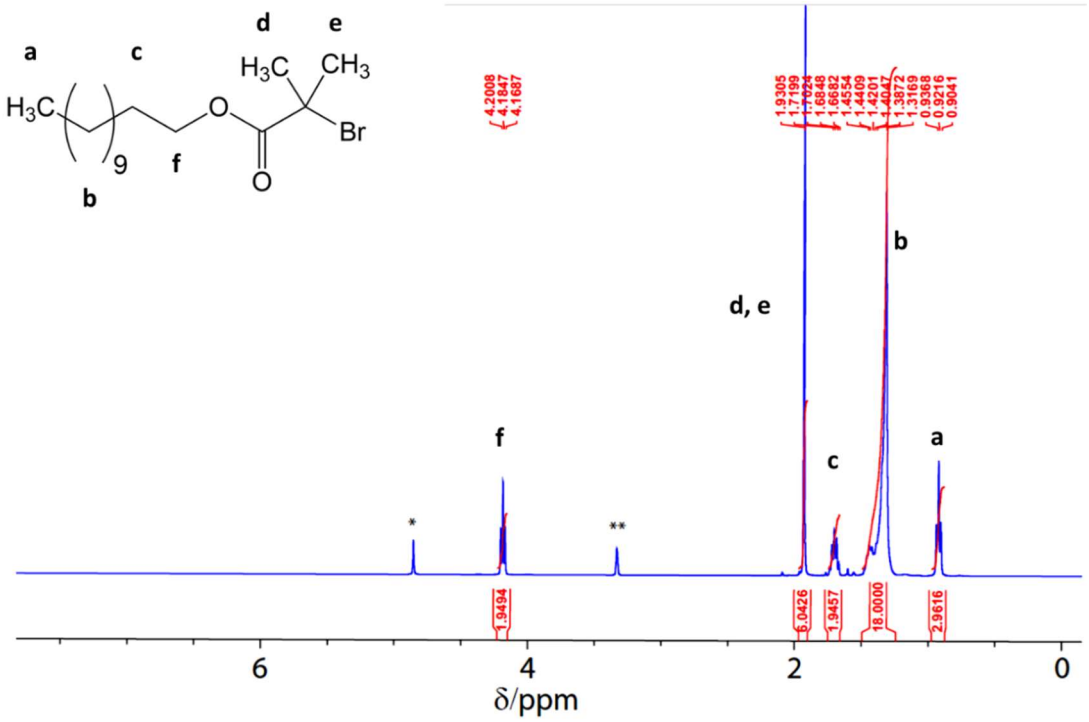

Fig. 2.4. ^{1}H NMR (400 MHz, MeOD-d_4) of 2-dodecyl-2-bromoisobutyrate (DBiB); **1**. **solvent residual peak at 3.31 ppm and *H_2O at 4.87 ppm

In the ^{1}H and ^{13}C NMR spectra the proton and carbons located at the ends of DBiB can be identified unambiguously while the protons and carbons on the long alkane chain has chemical shifts which are too similar to be distinguished and therefore lumped together. The full assignment can be seen on Fig. 2.4-2.5 and Chapter 7 section 7.1.

Moreover the mass of $C_{16}H_{31}BrO_2$ found by ESI-MS is given on Fig. 2.6 and is $[M+Na]^+$ = 357.1 Da. This is comparable to the theoretical calculated mass M^+ of DBiB, which is 335.32 Da.

In conclusion the ^{1}H-, ^{13}C and ESI-MS results showed that DBiB was successfully synthesised and purified.

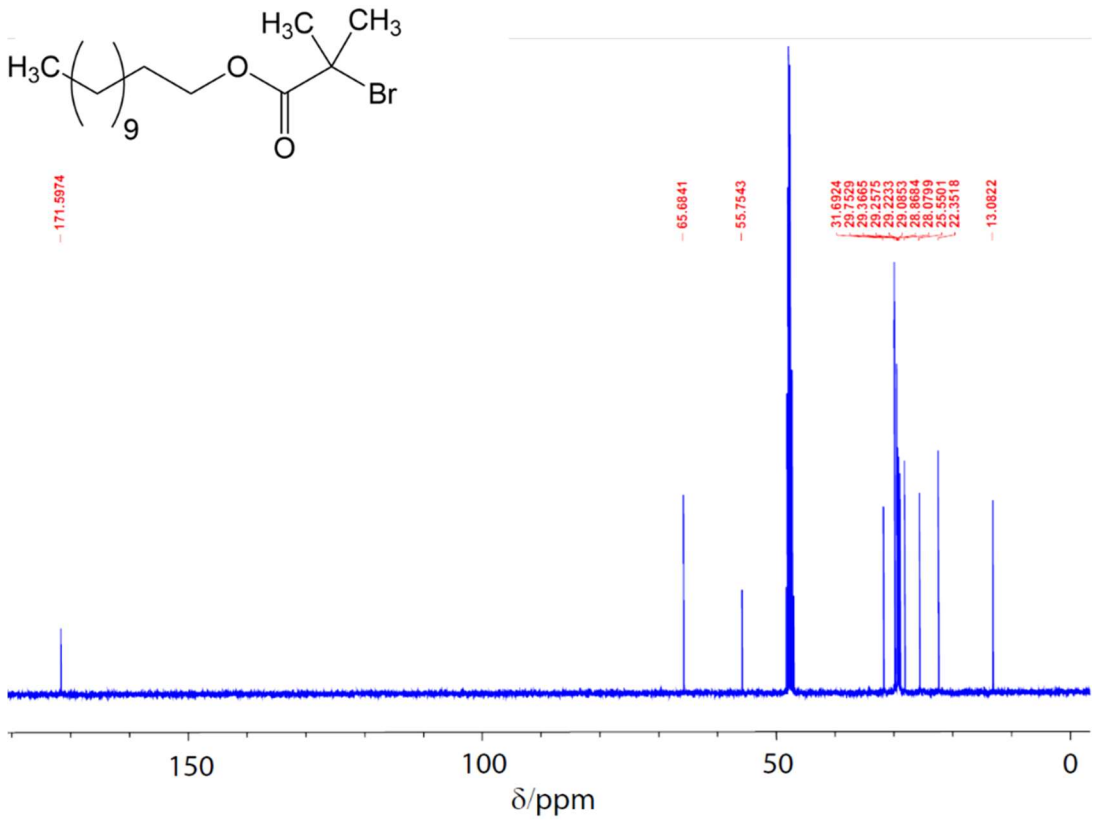

Fig. 2.5. ^{13}C NMR (100.61 MHz, MeOD-d_4) of 2-dodecyl-2-bromoisobutyrate (DBiB)

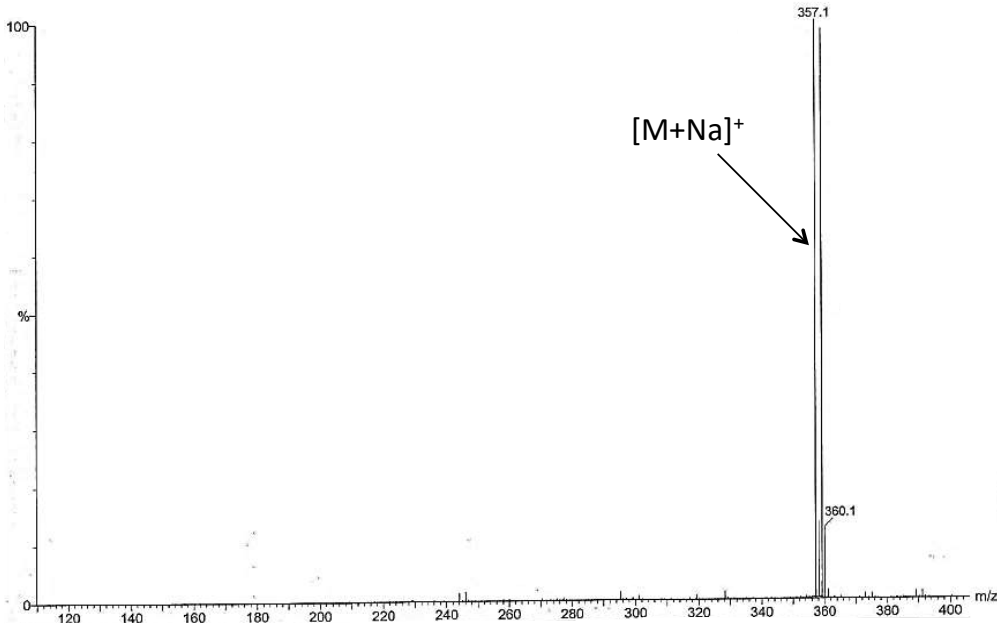

Fig. 2.6. ESI-MS (MeOH) of 2-dodecyl-2-bromoisobutyrate (DBiB).

2.2.2 Kinetic studies of polymerisation of linear DBiB-p(OEGMA)$_{50}$

The controllability of the ATRP polymerisaion reaction was investigated by a kinetic study targeting a DP$_n$ of 50 monomer unit with the linear homopolymer. In this study, the main focus was to show that the reaction was controlled and provided a polymer with a specific number average molecular weight (M_n) and low dispersity index (M_w/M_n). Two different measurements, ^{1}H NMR as well as gel permeation chromatography (GPC) were used to characterise the polymers that were formed. It was expected that an ATRP reaction would follow a first order kinetic relationship. The data from these studies were therefore plotted on a semi-logarithmic graph showing Ln ($[M]_0/[M]_n$) against the timepoints.[176,179] The ATRP reaction was monitored by observing vinyl ^{1}H chemical shifts of resonances from the OEGMA structure and ^{1}H δ resonances from the internal reference, mesitylene. Examples of such spectra are shown in Fig. 2.7.

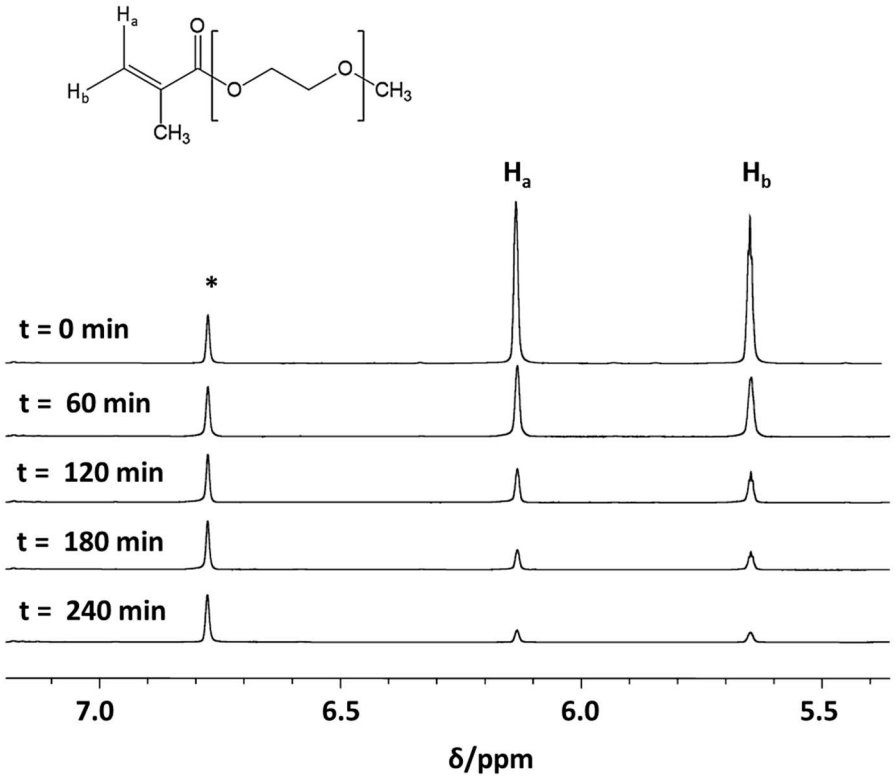

Fig. 2.7. Zoomed in overlay of ^{1}H NMR spectra (MeOD-d$_4$) selected sample points t= 0- 240 min of kinetic studies for synthesis of DP$_{50}$. Signals of two vinyl protons H$_a$ and H$_b$ was integrated against an internal reference -CH- signal of mesitylene.*

A few drops of the internal reference, mesitylene, was added to the reaction mixture while it was degassed with a nitrogen inlet. The concentration of mesitylene remains constant throughout the polymerisation and within all timepoint samples taken during the reaction copper (I) chloride (CuCl) was added to the reaction at the timepoint t = 0 min. The reaction was then monitored by analysing sample points at times t = 15, 30, 45, 60, 90, 120, 180, 240 minutes. The samples for ^{1}H NMR were prepared as described in Chapter 7, section 7.1. The monomer conversions were assessed by ^{1}H NMR spectroscopy in MeOD-d_4, Fig. 2.7, and the polymer conversions were calculated by integrating the ^{1}H resonances of the vinyl groups on the monomer relative to the internal reference ^{1}H resonance of mesitylene.

The NMR resonance of mesitylene –CH group with a chemical shift of ^{1}H δ = 6.8 ppm was integrated to 1 and compared against the vinyl chemical shifts of the OEGMA monomer in the range between ^{1}H δ= 5.6 and 6.1 ppm, Fig. 2.7. At t = 0 the monomeric conversion was given by $[M]_0$ and at timepoints t = 15, 30, 45, 60, 90, 120, 180, 240 minutes as $[M]_n$. A first order kinetic semilogaritmic plot of $Ln[M]_0/[M]_n$ *versus* time gave a straight line, Fig 2.8a. The straight line of the ^{1}H NMR studies indicated that the reaction followed a first order kinetic model and that the radical polymerisation was controlled in agreement with examples in the literature.[175,176] The ultimate monomer conversion was 94 ± 2%. In addition to ^{1}H NMR the molecular weight distributions of DP_n 50 at timepoints t = 15, 30, 45, 60, 90, 120, 180, 240 minutes was assessed by GPC. The samples were taken at the same time points as for ^{1}H-NMR samples mentioned earlier in this section. The preparation of GPC samples is described in Chapter 7, section 7.1.

The GPC results at t = 15, 30, 45, 60, 90, 120 and 240 min, Fig. 2.8b, showed a linear increase in the number average molecular weight (M_n) as a result of the increase in conversion from monomer to polymer. This demonstrated that M_n was controlled throughout the experiment. This was in agreement with the increase in molecular weight, M_n, calculated using ^{1}H NMR. The M_w/M_n distribution of the GPC traces remained constant throughout the reactions, Fig 2.8b.

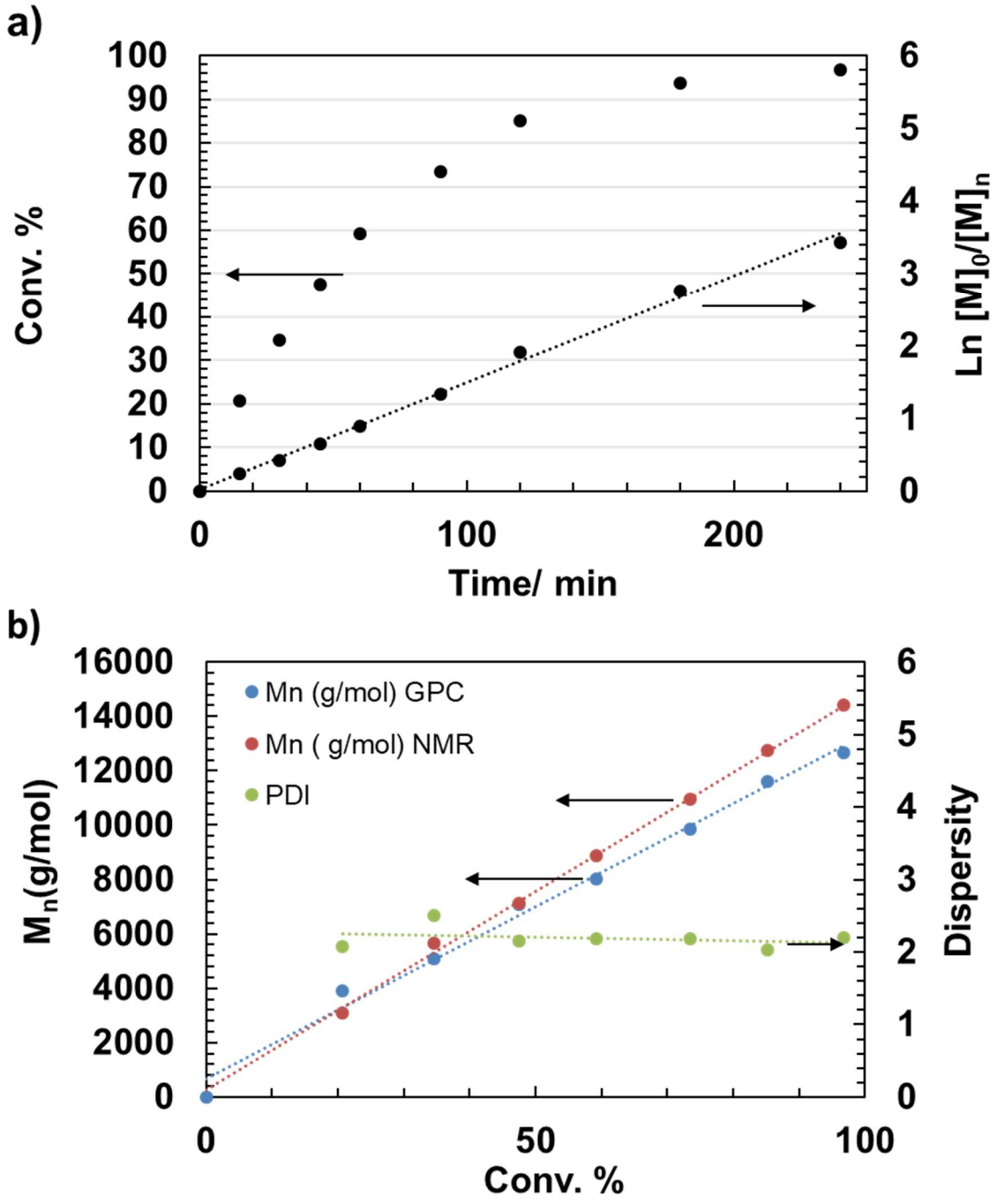

Fig. 2.8. a) ^{1}H NMR kinetics of DBiB-p(OEGMA)$_{50}$ kinetics and **b)** number average molecular weight M_n of DBiB-p(OEGMA)$_{50}$ kinetic experiment calculated from GPC traces recorded in DMF (blue and red) and ^{1}H NMR spectroscopy (black) at timepoints t = 0, 15, 30, 45, 60, 90, 120, 180, 240 minutes. PDI distribution (green) of GPC traces. Conv.; Conversion. PDI; polydispersity.

The GPC traces of the kinetic points are shown in Fig. 2.9. The overlay of the traces over the time points given demonstrated that the retention volume decreased as the chain size increased in the reaction mixture. The polydispersity and retention time of the polymer were estimated by a plot of retention volume in mL against the IR signal, see Fig. 2.9. This

estimate is sufficient for our purposes rather than an accurate molecular weight distribution plot of logM versus dw/dlogM was not deemed nessesary. These observations are supported by the M_n increasing as observed in the ^{1}H-NMR studies, Fig. 2.8a and are comparable to examples of kinetic studies mentioned in the literature.[184]

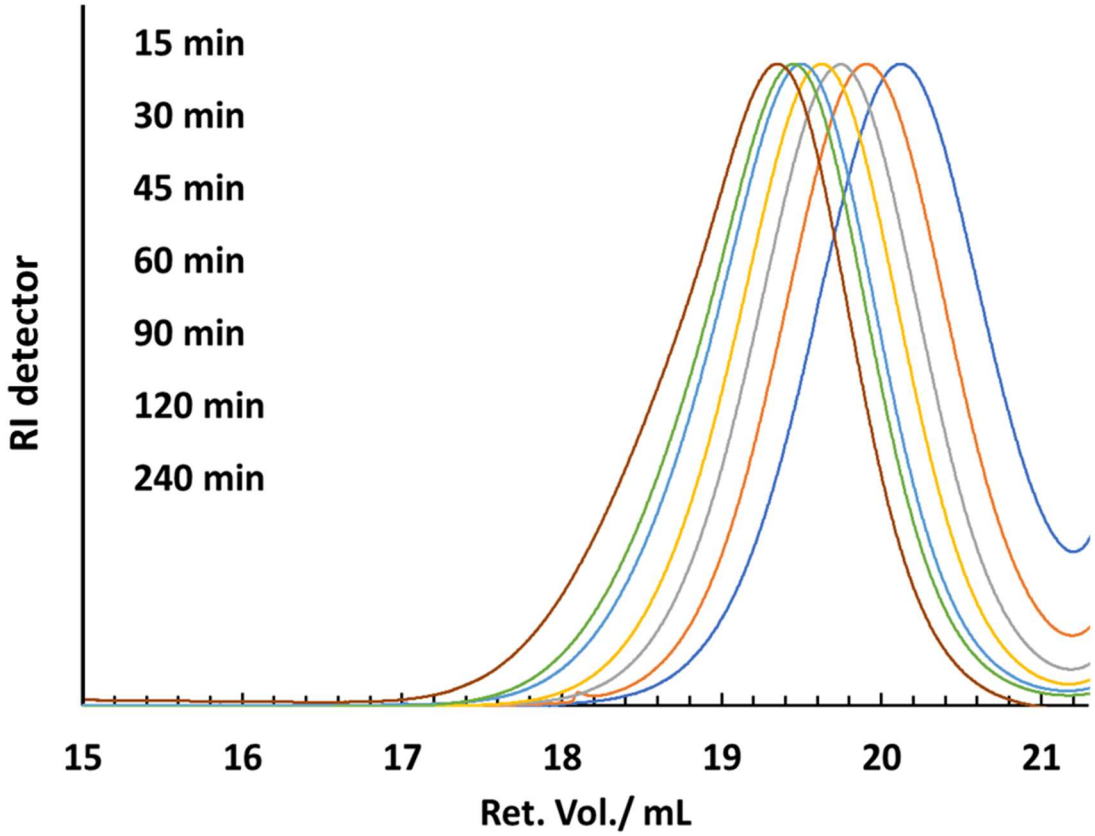

Fig. 2.9. Raw RI data of GPC chromatograms of DP_n of 50 kinetics. Traces at time points t = 15-120 and 240 min taking during kinetics of $p(OEGMA)_{50}$ are normalised with the intensity of the highest trace signal. The retention volume is given in mL. Analysis performed by GPC with mobile phase of DMF (+ 0.01M) at 1mL/min 60 ˚C. Traces were normalised to the highest peak. Ret.; retention. Vol.; volume.

In conclusion, it was demonstrated that the synthesis of DBiB-$p(OEGMA)_{50}$ by the ATRP conditions given in Chapter 7, section 7.1 was controlled. This condition will be used to synthesis a polymer library of $DP_{10\text{-}50}$ of both linear homopolymers and branched copolymers.

2.2.3 Synthesis of p(OEGMA) based copolymers utilising ATRP

Controlled radical polymerisation, ATRP was used to synthesise a library of p(OEGMA) based homo- and copolymers using procedures described in Chapter 7 section 7.1 while targeting the degree of polymerisation (DP_n) of 10, 20 and 50 monomer units. The branchers used in the experiments were short chained EGDMA; M_w= 198.9 $gmol^{-1}$ and long chained PEGDMA; M_w = 875 $gmol^{-1}$. Their proportions were varied relative to initiator DBiB for each of the targeted polymerisations. Reactions were left until 93-99 % conversion and were assessed using ^{1}H-NMR spectroscopy in MeOD-d_4. After precipitation of the polymer into petroleum ether, the final pure OEGMA based polymer product was dried in the vacuum oven at 40 °C to ensure that all of the solvent was evaporated. The final polymer products were characterised by ^{1}H NMR and GPC to assess the polymer architecture in terms of dispersity (Đ) and molecular weights (M_n and M_w). The library of OEGMA based homo- and copolymers are discussed in the next subsections.

2.2.3.1 ^{1}H NMR Characterisation of linear DBiB-p(OEGMA)$_{10-50}$

A characterised ^{1}H NMR spectrum of a selected ^{1}H-NMR spectra of linear DBiB-p(OEGMA)$_{50}$ is shown in Fig. 2.10. The protons at ^{1}H δ = 0.9 ppm were assigned to the –CH_3 group on the initiator chain end and the –CH_2- group on the backbone of the DBiB-p(OEGMA)$_{50}$ polymer. The integral of the resonance at δ = 0.9-1.1 ppm is 153, which indicates that there are 3 protons in the terminating –CH_3 and 150 protons from the –CH_3 on the polymer backbone. The CH_3 from the backbone are in different chemical environments and therefore appear at a different chemical shift depending on whether it's nearer to a C-Br or a C-CH_2 on the polymer backbone. Therefore, the –CH_3 nearer to the C-CH_2 have a chemical shift of 1.1 ppm and the –CH_3 nearer to C-Br have a higher chemical shift in the range of 1.5-1.9 ppm due to the higher electronegativity of Br compared to C.

The increase depends on how close the CH_2 is to C-Br on the backbone of DBiB-p(OEGMA)$_{50}$. The signal at ^{1}H δ = 1.3 ppm was integrated to 18 protons and assigned to the –CH_2- groups on the initiator part of the polymer. The signals between ^{1}H δ = 1.5 -1.9 ppm were assigned to the –CH_2- group and the two –CH_3 groups on the initiator part of the polymer. The signal at ^{1}H δ = 3.4 ppm were integrated to 150 H and was assigned to the –CH_3 group at the end of the OEGMA chain of the resulting polymer. The peaks from 3.5-4.1 ppm were assigned to the PEG protons from the –CH_2- in the PEG part of the polymer.

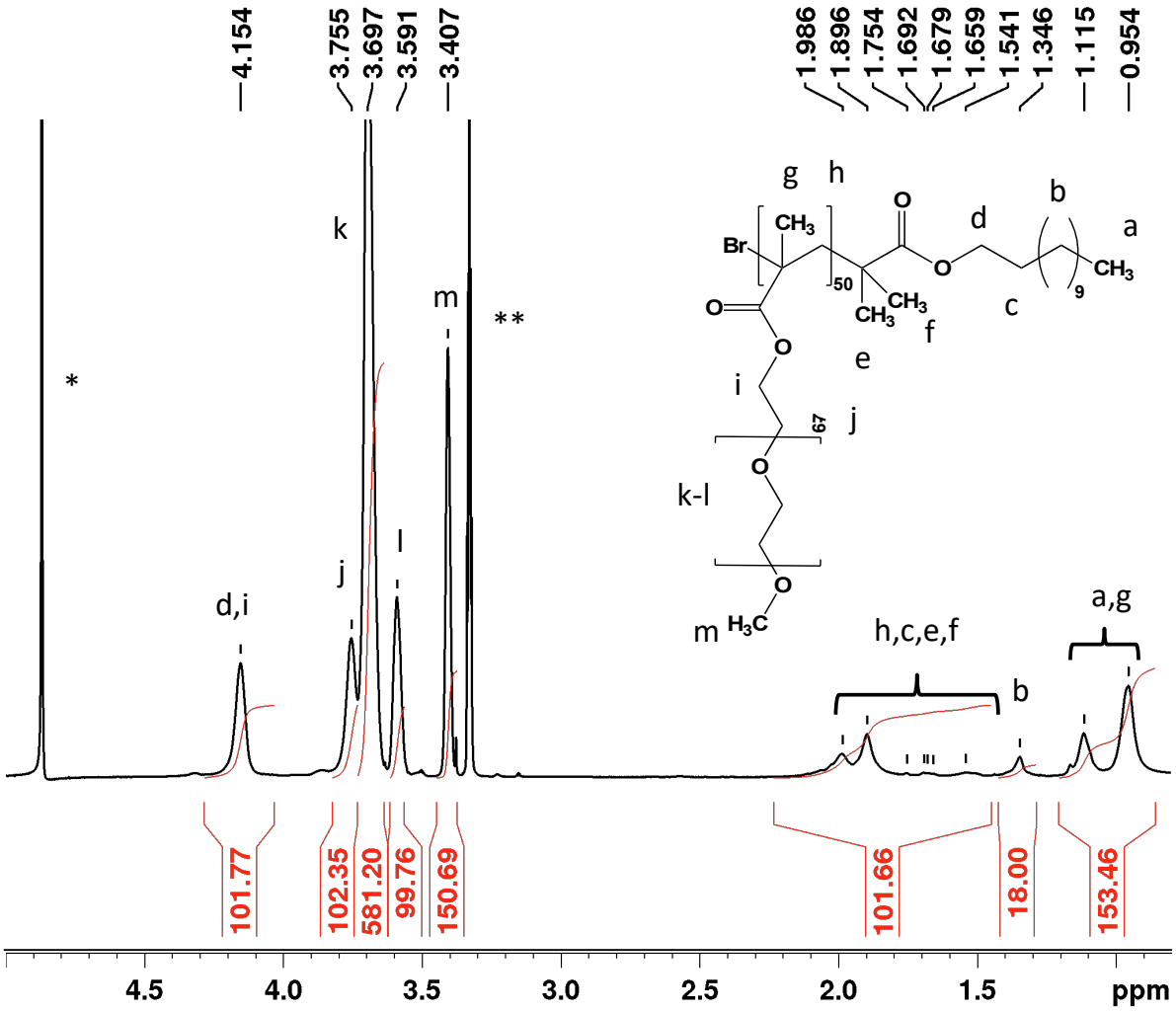

Fig. 2.10. Characterised ^{1}H NMR spectra of DP$_{50}$ OEGMA homopolymer. **Solvent residual peak at 3.33 ppm and *H_2O at 4.88 ppm.

ATRP was used to synthesise homopolymers of OEGMA with a M_W = 300 $gmol^{-1}$ and with a degree of polymerisation DP_n of 10, 20 and 50. The reactions were left for 2-8 hours to reach completion depending on the degree of polymerisation based upon the starting composition. The % conversion of linear DBiB-p(OEGMA)$_{10}$, DBiB-p(OEGMA)$_{20}$ and DBiB-p(OEGMA)$_{50}$ were calculated through ratio of pendant vinyl groups by integrating the signal of vinyl protons ^{1}H δ = 5.6 and 6.1 ppm with chemical shift of against an internal reference from the mesitylene (=CH- group) with a chemical shift of ^{1}H δ = 6.8 ppm. DP_n and the initiator efficiency was calculated by integrating the chemical shift ^{1}H δ = 1.3 ppm and 3.4 ppm. DP_n and IE calculated by integrating ^{1}H resonances of the –(C$\underline{H}_2$)$_9$- group (Fig. 2.8**b**) from reacted initiator at ^{1}H δ =1.35 ppm (18 H) with –C$\underline{H}_3$ of reacted OEGMA peak at δ = 3.40 ppm ^{1}H signal assigned to m see Fig. 2.10 and the $DP_{n,exp}$ is calculated by the value of the integral X divided by 3 H of the –CH_3 group of the initiator assigned to m see Fig 2.9**m**. The calculated parameters are given in the Table 2.1.

Table 2.1. ^{1}H NMR of DBiB-p(OEGMA)$_{10\text{-}50}$. DP_n; degree of polymerisation. IE; initiator efficiency. Analysis performed in MeOD-d_4 and the residual solvent and water peaks were assigned with respect to literature.[244]

Polymer	$M_{n,theo}$ $gmol^{-1}$	$DP_{n,theo}$	$M_{n,exp}$ $gmol^{-1}$	$DP_{n,exp}$	IE %	Conv.%
DBiB-p(OEGMA)$_{10}$	3,335	10	3,635	11	91	98
DBiB-p(OEGMA)$_{20}$	6,335	20	6,635	21	95	99
DBiB-p(OEGMA)$_{50}$	15,335	50	15,335	50	96	>99

The experimentally calculated DP_n was used to calculate $M_{n,exp}$ of the resulting homopolymer. The experimentally calculated $M_{n,exp}$ for DBiB-p(OEGMA)$_{10}$, DBiB-p(OEGMA)$_{20}$ and DBiB-p(OEGMA)$_{50}$ where in agreement with the theoretically calculated $M_{n,theo.}$ The IE for the homopolymers were 91 % for DBiB-p(OEGMA)$_{10}$, 95 % for DBiB-p(OEGMA)$_{20}$ and 96 % for DBiB-p(OEGMA)$_{50}$. IE was calculated to be above 91 % for the homopolymers which is a high value. IE is the efficiency of an initiator to initiate and rapidly establish the dormant and active equilibrium. The IE is calculated using ^{1}H NMR by the

comparison of DP_n targeted and DP_n achieved as measured by NMR. Any unreacted initiator will interfere with the signals if the sample is not rigorously purified and purification can fractionate the polymer sample.

2.2.3.2. Characterisation of DBiB-p(OEGMA)$_{10}$, DBiB-p(OEGMA)$_{20}$ and DBiB-p(OEGMA)$_{50}$ by GPC

Samples DBiB-p(OEGMA)$_{10}$, DBiB-p(OEGMA)$_{20}$ and DBiB-p(OEGMA)$_{50}$ were purified and vacuum dried at 40 °C. They were then dissolved in DMF (+0.01 M LiBr) and analysed using GPC. GPC results of M_n, M_w and dispersity (Đ) are given on Table 2.2. The results showed that M_n increased from 3,230 $gmol^{-1}$ to 15,700 $gmol^{-1}$ as the degree of polymerisation increases from DP_n of 10 to 50. A similar trend was observed for M_w. However, it was also observed that the Đ of DBiB-p(OEGMA)$_{10}$ was 2.1 while the Đ of DBiB-p(OEGMA)$_{20}$ and DBiB-p(OEGMA)$_{50}$ were 1.4. This indicates that the size distribution of for DBiB-p(OEGMA)$_{10}$ is broader than those of the other polymers.

Table 2.2. Calculated M_n, M_w and Đ for GPC data obtained for DBiB-p(OEGMA)$_{10}$, DBiB-p(OEGMA)$_{20}$ and DBiB-p(OEGMA)$_{50}$ recorded in DMF (+0.01 M LiBr)

Polymer	M_n ($gmol^{-1}$)	M_w($gmol^{-1}$)	Đ
DBiB-p(OEGMA)$_{10}$	3,230	6,920	2.1
DBiB-p(OEGMA)$_{20}$	9,390	13,060	1.4
DBiB-p(OEGMA)$_{50}$	15,700	22,450	1.4

2.2.4. Synthesis and characterisation of DBiB-p(OEGMA)$_{10-50}$ branched with EGDMA

2.2.4.1. ^{1}H NMR characterisation of DBiB-p(OEGMA)$_{10-50}$ branched with EGDMA

EGDMA was used to synthesis branched p(OEGMA)$_{10-50}$ copolymers with the aim to create a library of high molecular weight branched polymers. This was done by using ATRP.[161,245] DBiB was used an initiator in the reaction. The molar ratio of the brancher was varied relative to the initiator. The ratios used were in the range between 0.2:1 and 0.8:1. A higher

brancher to initiator molar ratio was initially used to investigate how much the molar ratio could be increased before reaching the gel point. The gel point is the point in which occurrence of gelation in polymerisation can be observed visually and a polymerisation mixture loses its fluidity and becomes insoluble in all solvents. [246] The formed gel corresponds to the formation of an infinite network in which the polymer molecules have been crosslinked to each other to form macroscopic molecule. [246] The reactions of DBiB-p(OEGMA)$_{10\text{-}50}$ branched with EGDMA were left 2-8 hours to reach completion and monitored with ^{1}H NMR. The ^{1}H-NMR results obtained for EGDMA branched DBiB-p(OEGMA)$_{10}$, DBiB-p(OEGMA)$_{20}$ and DBiB-p(OEGMA)$_{50}$ were calculated using the methods mentioned earlier and are shown on Table 2.3-2.5.

Table 2.3. ^{1}H NMR of EGDMA branched DBiB-p(OEGMA)$_{10}$. DP_n; degree of polymerisation. IE; initiator efficiency. Analysis performed in MeOD-d_4 and the residual solvent and water peaks were assigned with respect to literature.[244]

Polymer	brancher to initiator molar ratio	DP_n	IE %	Conv.%
DBiB-p(OEGMA)$_{10}$-co-(EGDMA)$_{0.2}$	0.2:1	10	>99	94
DBiB-p(OEGMA)$_{10}$-co-(EGDMA)$_{0.5}$	0.5:1	10	>99	>99
DBiB-p(OEGMA)$_{10}$-co-(EGDMA)$_{0.6}$	0.6:1	11	91	>99
DBiB-p(OEGMA)$_{10}$-co-(EGDMA)$_{0.7}$	0.7:1	11	91	>99
DBiB-p(OEGMA)$_{10}$-co-(EGDMA)$_{0.8}$	0.8:1	10	>99	>99

EGDMA branched DBiB-p(OEGMA)$_{10}$ were branched with molar brancher to initiator ratios of 0.2:1-0.8:1. All of the reactions reached a high conversions of 94 - >99 % according to ^{1}H-Using NMR spectra analysis at time points t = 0 and t = 2-8 hours. DP_n were calculated to be 10-11 and the IE values were relatively high. Overall the ^{1}H NMR data of EGDMA branched DBiB-p(OEGMA)$_{10}$ showed that it was possible to increase the molar brancher to initiator ratio to 0.8:1 without experiencing gelation. EGDMA branched DBiB-p(OEGMA)$_{20}$ were branched with molar brancher to initiator ratios of 0.2:1-0.8:1. All of the reactions reached a

high conversions of 99 % according to ^{1}H-NMR spectra analysis at time points t = 0 and t = 7-8 hours. DP_n were calculated to be 20-23 and the IE values were high. Overall the ^{1}H NMR data of EGDMA branched DBiB-p(OEGMA)$_{20}$ showed that it was possible to increase the molar brancher to initiator ratio to 0.8:1 without experiencing gelation.

Table 2.4. ^{1}H NMR of EGDMA branched DBiB-p(OEGMA)$_{20}$. DP_n; degree of polymerisation. IE; initiator efficiency. Analysis performed in MeOD-d_4 and the residual solvent and water peaks were assigned with respect to literature.[244]

Polymer	brancher to initiator molar ratio	DP_n	IE %	Conv.%
DBiB-p(OEGMA)$_{20}$-co-(EGDMA)$_{0.2}$	0.2:1	21	80	99
DBiB-p(OEGMA)$_{20}$-co-(EGDMA)$_{0.5}$	0.5:1	22	91	>99
DBiB-p(OEGMA)$_{20}$-co-(EGDMA)$_{0.8}$	0.8:1	23	87	>99

DBiB-p(OEGMA)$_{50}$ were branched with EGDMA using molar brancher to initiator ratios of 0.2:1 to 0.95:1, Table 2.5. All of the reactions reached a high conversion rate of 97 - >99 % according to ^{1}H-NMR spectra analysis at time points t = 0 and t = 8-13 hours. DP_n were calculated to be 50-52 and the corresponding IE values were calculated to be 94-99 %.

Table 2.5. ^{1}H NMR of EGDMA branched DBiB-p(OEGMA)$_{50}$. DP_n; degree of polymerisation. IE; initiator efficiency. Analysis performed in MeOD-d_4 and the residual solvent and water peaks were assigned with respect to literature.[244]

Polymer	brancher to initiator molar ratio	DP_n	IE %	Conv.%
DBiB-p(OEGMA)$_{50}$-co-(EGDMA)$_{0.2}$	0.2:1	52	96	98
DBiB-p(OEGMA)$_{50}$-co-(EGDMA)$_{0.5}$	0.5:1	50	94	>99
DBiB-p(OEGMA)$_{50}$-co-(EGDMA)$_{0.6}$	0.6:1	51	98	99
DBiB-p(OEGMA)$_{50}$-co-(EGDMA)$_{0.7}$	0.7:1	50	>99	97
DBiB-p(OEGMA)$_{50}$-co-(EGDMA)$_{0.8}$	0.8:1	50	>99	98
DBiB-p(OEGMA)$_{50}$-co-(EGDMA)$_{0.9}$	0.9:1	50	>99	>99
DBiB-p(OEGMA)$_{50}$-co-(EGDMA)$_{0.95}$	0.95:1	51	98	>99

Overall the ^{1}H NMR data of EGDMA branched DBiB-p(OEGMA)$_{50}$ showed that it was possible to increase the molar brancher to initiator ratio to 0.95:1 without experiencing gelation.

2.2.4.3. GPC characterisation of DBiB-p(OEGMA)$_{10\text{-}50}$ branched with EGDMA

In the previous section we described the synthesis and characterisation of DBiB-p(OEGMA)$_{10\text{-}50}$ that were branched with EGDMA using ^{1}H-NMR spectroscopy. The molar ratios between brancher and initiator were varied with the aim to obtain highly branched polymer architectures. The resulting purified and vacuum dried EGDMA branched DBiB-p(OEGMA)$_{10,}$ DBiB-p(OEGMA)$_{20}$ and DBiB-p(OEGMA)$_{50}$ were analysed using GPC.
Parameters obtained by GPC were M_w, M_n and Đ given on Table 2.6-2.8. These parameters can be used to assess the branched polymer architecture e.g to calculate other parameters such as the numbers of conjoined chains, the average number of primary chains per branched polymers, denoted WA #, was determined. This parameter was calculated by an equation given by the equation (2.1):

$$WA\ \# = \frac{M_w(branched\ copolymer)}{M_w(primary\ chain)} \qquad \textbf{(2.1)}$$

Where M_w (branched copolymer) is given in Table 2.6-8 and M_w (primary chain) is given in Table 2.1. The obtained M_w, $M_{n,}$ Đ and WA # for EGDMA branched DBiB-p(OEGMA)$_{10}$ are given on Table 2.6.

Table 2.6. Calculated M_n, M_w, Đ and WA # for GPC data obtained for DBiB-p(OEGMA)$_{10}$ polymers branched with EGDMA recorded in DMF (+0.01 M LiBr).

Polymer	M_n (gmol^{-1})	M_w(gmol^{-1})	Đ	WA #
DBiB-p(OEGMA)$_{10}$-co-(EGDMA)$_{0.2}$	7,610	11,840	1.6	2
DBiB-p(OEGMA)$_{10}$-co-(EGDMA)$_{0.5}$	11,490	23,660	2.1	3
DBiB-p(OEGMA)$_{10}$-co-(EGDMA)$_{0.6}$	14,800	38,440	2.6	6
DBiB-p(OEGMA)$_{10}$-co-(EGDMA)$_{0.7}$	14,950	46,730	3.1	7
DBiB-p(OEGMA)$_{10}$-co-(EGDMA)$_{0.8}$	15,240	48,670	3.2	7

The results showed that M_n increased from 7,610 gmol^{-1} to 15,240 gmol^{-1} when the molar ratio of brancher to initiator was increased from 0.2:1 to 0.8:1. Moreover, the Mw values increased from 11,840 gmol^{-1} to 48,670 gmol^{-1} when the molar ratio of brancher to initiator was increased from 0.2:1 to 0.8:1. In addition to that Đ of the resulting polymer increased from 1.6 to 3.2. These observations suggest that the EGDMA branched DBiB-p(OEGMA)$_{10}$ became more disperse as the molar ratio of brancher to initiator increased from 0.2:1 to 0.8:1. It was also observed that the maximum number of conjoined chains pr. branched polymer WA # were calculated to be 7 for DBiB-p(OEGMA)$_{10}$-co-(EGDMA)$_{0.8}$.

GPC chromatograms of linear DBiB-p(OEGMA)$_{10}$ overlaid with two selected branched copolymers, DBiB-p(OEGMA)$_{10}$-co-(EGDMA)$_{0.5}$ and DBiB-p(OEGMA)$_{10}$-co-(EGDMA)$_{0.8}$, were shown in Fig. 2.11 and appendix Fig. A1-A3. As mentioned earlier this estimate is sufficient for our purposes throughout this chapter rather than an accurate molecular weight distribution plot of logM versus dw/dlogM was not deemed nessesary. The results showed that the linear DBiB-p(OEGMA)$_{10}$ has a narrower distribution while the branched copolymers DBiB-p(OEGMA)$_{10}$-*co*-(EGDMA)$_{0.5}$ and DBiB-p(OEGMA)$_{10}$-*co*-(EGDMA)$_{0.8}$ had much broader distributions due to branching.

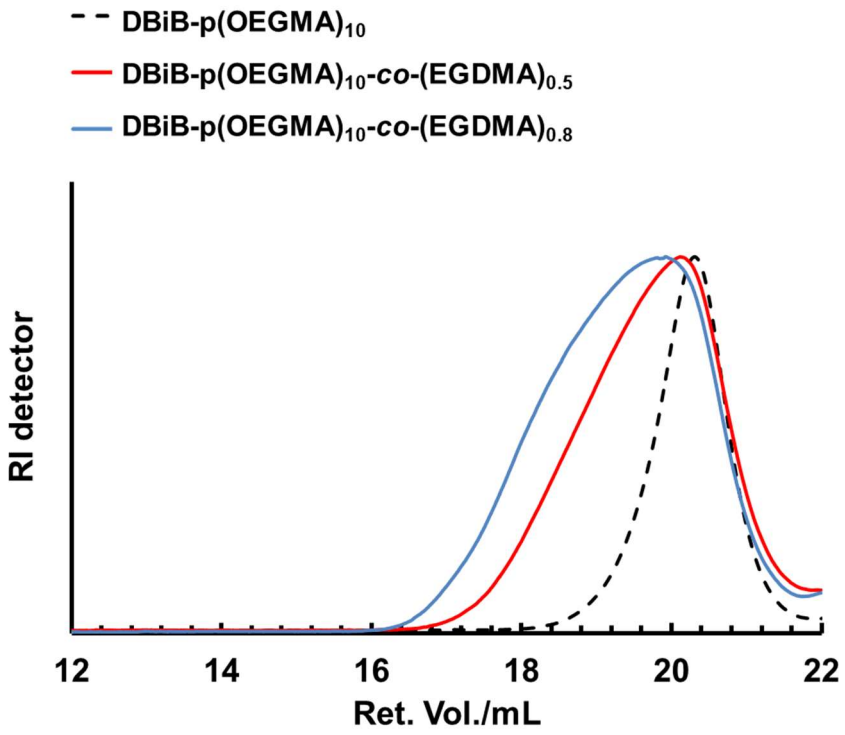

Fig. 2.11. Selected raw GPC chromatograms obtained with RI detector in mV. Selected chromatograms of linear DBiB-p(OEGMA)$_{10}$, DBiB-p(OEGMA)$_{10}$-*co*-(EGDMA)$_{0.5}$, DBiB-p(OEGMA)$_{10}$-*co*-(EGDMA)$_{0.8}$. Analysis performed by GPC with mobile phase of DMF (+ 0.01M) at 1mL/min 60 ˚C. All of the RI traces were normalised. Ret.; retention. Vol.; volume.

The obtained M_w, M_n, Đ and WA # for EGDMA branched DBiB-p(OEGMA)$_{20}$ are given on Table 2.7.

Table 2.7. Calculated M_n, M_w, Đ and WA # for GPC data obtained for DBiB-p(OEGMA)$_{20}$ copolymers branched with EGDMA recorded in DMF (+0.01 M LiBr)

Polymer	M_n (gmol^{-1})	M_w(gmol^{-1})	Đ	WA #
DBiB-p(OEGMA)$_{20}$-co-(EGDMA)$_{0.2}$	16,230	34,930	2.1	3
DBiB-p(OEGMA)$_{20}$-co-(EGDMA)$_{0.5}$	20,020	114,870	5.7	9
DBiB-p(OEGMA)$_{20}$-co-(EGDMA)$_{0.8}$	102,950	1,430630	13.7	109

The results showed that M_n increased from 16,230 gmol^{-1} to 102,950 gmol^{-1} when the molar ratio of brancher to initiator was increased from 0.2:1 to 0.8:1. Moreover, the Mw values increased from 34,930 gmol^{-1} to 1,430,630 gmol^{-1} when the molar ratio of brancher to initiator was increased from 0.2:1 to 0.8:1. In addition, the Đ of the resulting polymer

increased from 2.1 to a significantly broader Đ of 13.7. This indicated that DBiB-p(OEGMA)$_{20}$-co-(EGDMA)$_{0.8}$ was highly branched. These observations showed that the EGDMA branched DBiB-p(OEGMA)$_{10}$ became more disperse as the molar ratio of brancher to initiator increased from 0.2:1 to 0.8:1. It was also noted that the maximum number of conjoined chains pr. branched polymer, WA #, were calculated to be 109 for DBiB-p(OEGMA)$_{20}$-co-(EGDMA)$_{0.8}$.

GPC chromatograms of linear DBiB-p(OEGMA)$_{20}$ was overlaid against branched DBiB-p(OEGMA)$_{20}$-co-(EGDMA)$_{0.5}$ and DBiB-p(OEGMA)$_{20}$-co-(EGDMA)$_{0.8}$ and shown in Fig. 2.12 and Appendix Fig. A4-A6 The results showed that the linear DBiB-(OEGMA)$_{20}$ has a narrow distribution than the branched polymers DBiB-p(OEGMA)$_{20}$-co-(EGDMA)$_{0.5}$ and DBiB-p(OEGMA)$_{20}$-co-(EGDMA)$_{0.8}$. This indicated that DBiB-p(OEGMA)$_{20}$-co-(EGDMA)$_{0.5}$ and DBiB-p(OEGMA)$_{20}$-co-(EGDMA)$_{0.8}$ was highly branched.

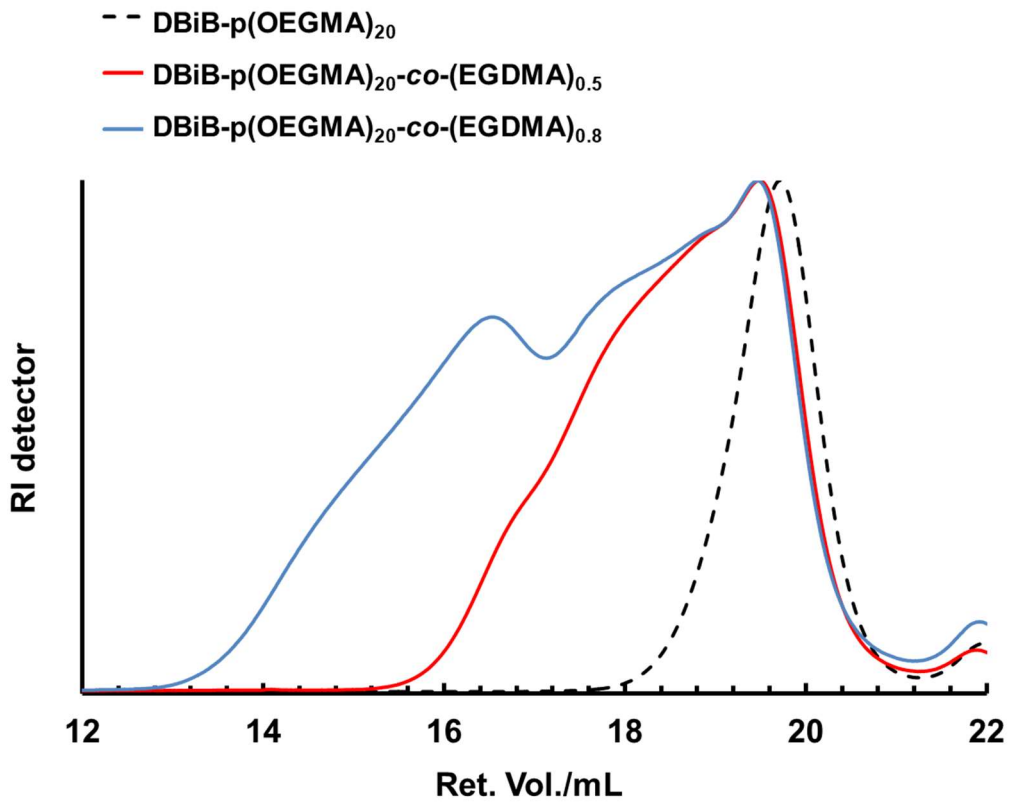

Fig. 2.12. Selected raw GPC chromatograms obtained with RI detector. Selected chromatograms of Linear DBiB-p(OEGMA)$_{20}$, DBiB-p(OEGMA)$_{20}$-*co*-(EGDMA)$_{0.5}$, DBiB-p(OEGMA)$_{20}$-*co*-(EGDMA)$_{0.8}$. Analysis performed by GPC with mobile phase of DMF (+ 0.01M) at 1mL/min 60 ˚C. All of the RI traces were normalised. Ret.; retention. Vol.; volume.

The obtained M_w, M_n, Đ and WA # for EGDMA branched DBiB-p(OEGMA)$_{20}$ are given on Table 2.8.

Table 2.8. Calculated M_n, M_w, Đ and WA # for GPC data obtained for DBiB-p(OEGMA)$_{50}$ copolymers branched with EGDMA recorded in DMF (+0.01 M LiBr)

Polymer	M_n (gmol^{-1})	M_w(gmol^{-1})	Đ	WA #
DBiB-p(OEGMA)$_{50}$-co-(EGDMA)$_{0.2}$	23,460	35,590	1.5	2
DBiB-p(OEGMA)$_{50}$-co-(EGDMA)$_{0.5}$	26,940	57,980	2.1	3
DBiB-p(OEGMA)$_{50}$-co-(EGDMA)$_{0.6}$	28,200	58,130	2.1	3
DBiB-p(OEGMA)$_{50}$-co-(EGDMA)$_{0.7}$	29,920	63,620	2.1	3
DBiB-p(OEGMA)$_{50}$-co-(EGDMA)$_{0.8}$	33,870	90,880	2.7	4
DBiB-p(OEGMA)$_{50}$-co-(EGDMA)$_{0.9}$	34,100	92,080	2.7	4
DBiB-p(OEGMA)$_{50}$-co-(EGDMA)$_{0.95}$	41,500	136,090	3.3	6

The results showed that M_n increased from 23,460 gmol^{-1} to 41,500 gmol^{-1} when the molar ratio of brancher to initiator was increased from 0.2:1 to 0.95:1. Additionally, the Mw values increased from 35,590 gmol^{-1} to 136,090 gmol^{-1} when the molar ratio of brancher to initiator was increased from 0.2:1 to 0.8:1. In addition, the Đ of the resulting polymer increased slightly from 1.5 to 3.3 as the molar ratio of brancher to initiator from 0.2:1 to 0.95:1 for polymers DBiB-p(OEGMA)$_{50}$-*co*-(EGDMA)$_{0.2}$ and DBiB-p(OEGMA)$_{50}$-co-(EGDMA)$_{0.95}$. This indicated that the increase in molar ratio of brancher to initiator from 0.2:1 to 0.95:1 only resulted in slight increase in Đ. These observations showed that the EGDMA branched DBiB-p(OEGMA)$_{10}$ became 2 fold more disperse as the molar ratio of brancher to initiator increased from 0.2:1 to 0.95:1. It was also observed that the numbers of conjoined chains pr. branched polymers WA # were calculated to be 6 for DBiB-p(OEGMA)$_{50}$-co-(EGDMA)$_{0.95}$. Chromatograms of linear DBiB-p(OEGMA)$_{50}$ was overlaid against selected branched DBiB-p(OEGMA)$_{50}$-co-(EGDMA)$_{0.5}$ and DBiB-p(OEGMA)$_{50}$-co-(EGDMA)$_{0.95}$ and shown in Fig. 2.13 and Appendix Fig. A7- A9.

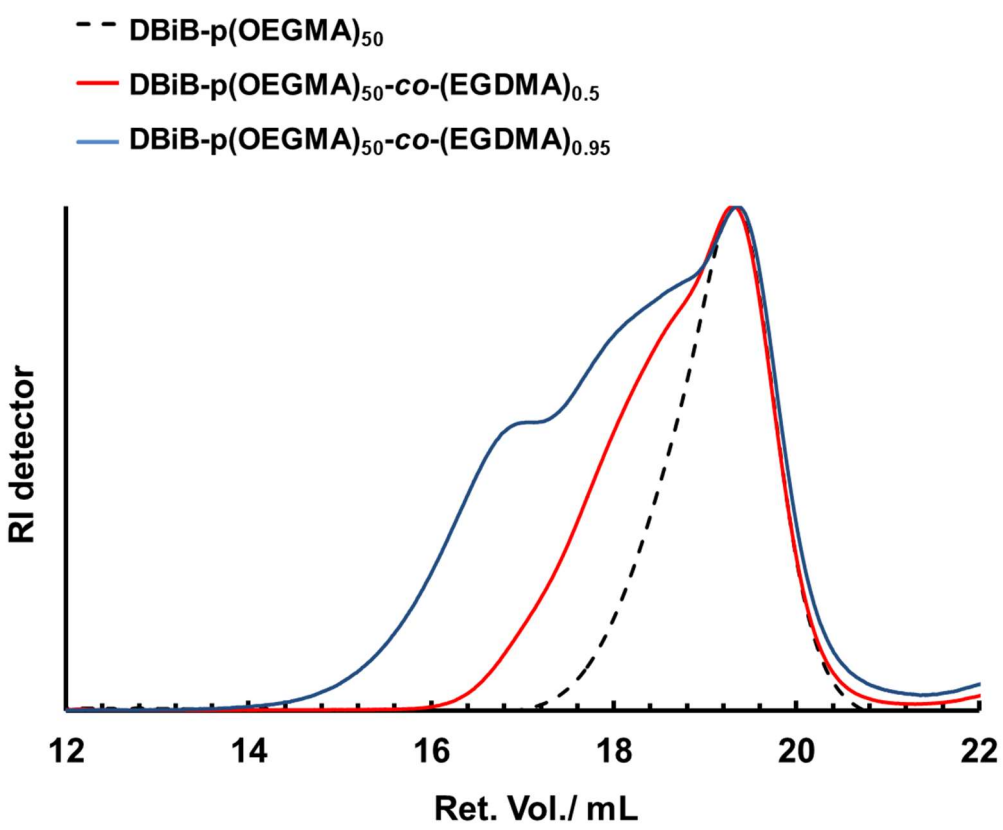

Fig. 2.13. Selected raw GPC chromatograms obtained with RI detector in mV. Selected chromatograms of linear DBiB-p(OEGMA)$_{50}$, DBiB-p(OEGMA)$_{50}$-*co*-(EGDMA)$_{0.5}$ and DBiB-p(OEGMA)$_{50}$-*co*-(EGDMA)$_{0.95}$ were overlaid. Analysis performed by GPC with mobile phase of DMF (+ 0.01M) at 1mL/min 60 ˚C. All of the RI traces were normalised. Ret.; retention. Vol.; volume

The results showed that the linear DBiB-(OEGMA)$_{50}$ has a narrow distribution than the branched polymers DBiB-p(OEGMA)$_{50}$-co-(EGDMA)$_{0.5}$ and DBiB-p(OEGMA)$_{50}$-co-(EGDMA)$_{0.95}$. This indicated that DBiB-p(OEGMA)$_{50}$-co-(EGDMA)$_{0.5}$ and DBiB-p(OEGMA)$_{50}$-co-(EGDMA)$_{0.95}$ was highly branched.

Overall the results obtained for the chromatograms of EGDMA branched of DBiB-p(OEGMA)$_{10\text{-}50}$ copolymers indicated that the increase of monomer units per initiator from 10 to 50 has an impact on the branching of the copolymer system. This has been demonstrated in literature by Bannister *et al.*[245] The highly branched copolymers composed of a broad distribution of molecular weights and architectural variations and this was well studied in literature.[188] Another approach was used to investigate at which point the reaction gelled when increasing EGDMA to DBiB ratio. Using this approach, it was concluded that it was possible to increase the EGDMA to DBiB ratio up to 0.95 without the reaction gelling. However, it was

observed that the chromatogramsof DBiB-p(OEGMA)$_{10\text{-}20}$ branched with EGDMA with a brancher to initiator ratio above 0.8:1 was not changed relative to 0.95:1. This trend was only observed for DBiB-p(OEGMA)$_{10\text{-}20}$ while DBiB-p(OEGMA)$_{50}$ branched with EGDMA above 0.95:1 brancher to initiator ratio showed a a broad Đ.

2.2.5. Synthesis and characterisation of DBiB-p(OEGMA)10-50 branched with PEGDMA

2.2.5.1 ^{1}H-NMR characterisation of PEGDMA branched DBiB-p(OEGMA)$_{10\text{-}50}$ copolymers

PEGDMA which is a longer chained brancher with a molecular weight of M_w= 875 gmol^{-1} was used to synthesis branched DBiB-p(OEGMA)$_{10\text{-}50}$ copolymers. PEGDMA was used in this study as the length of the PEGDMA in comparison to earlier used brancher, EGDMA, may be sterically easier to branch if the brancher is longer. The aim of this study was to investigate how the length of a brancher can change the polymer architecture of library of high molecular weight branched polymers. Same method as described earlier was used to synthesise the PEGDMA branched DBiB-p(OEGMA)$_{10\text{-}50}$ copolymers. DBiB was again used as an initiator in the reaction and the molar ratio of the brancher was varied relative to the initiator with the same compositions as described for EGDMA branched copolymers earlier. The ratios used were in the range between 0.2:1 and 0.8:1. The reactions of DBiB-p(OEGMA)$_{10\text{-}50}$ branched with PEGDMA were left 3-8 hours to reach completion and samples were withdrawn and analysed by with ^{1}H NMR. The ^{1}H-NMR results obtained for PEGDMA branched DBiB-p(OEGMA)$_{10}$, DBiB-p(OEGMA)$_{20}$ and DBiB-p(OEGMA)$_{50}$ were calculated using methods from earlier and are shown on Table 2.9-2.11.

Table 2.9. ^{1}H NMR of PEGDMA branched DBiB-p(OEGMA)$_{10}$. DP_n; degree of polymerisation. IE; initiator efficiency. Analysis performed in MeOD-d_4 and the residual solvent and water peaks were assigned with respect to literature.[244]

Polymer	brancher to initiator molar ratio	DP_n	IE %	Conv.%
DBiB-p(OEGMA)$_{10}$-co-(PEGDMA)$_{0.2}$	0.2:1	13	77	>99
DBiB-p(OEGMA)$_{10}$-co-(PEGDMA)$_{0.5}$	0.5:1	11	91	>99
DBiB-p(OEGMA)$_{10}$-co-(PEGDMA)$_{0.7}$	0.7:1	Gel	Gel	Gel

PEGDMA branched DBiB-p(OEGMA)$_{10}$ were branched with molar brancher to initiator ratios of 0.2:1-0.7:1. However, it was observed that the molar brancher to initiator ratio 0.7:1 resulted in the reaction to gel. The reactions with the other molar brancher to initiator ratio resulted in high conversions of 99 % according to ^{1}H-NMR spectra analysis at time points t = 0 and t = 3-4 hours. DP_n were calculated to be 13 and 11 and the corresponding IE values were calculated to be 77 and 91 %. Overall the ^{1}H NMR data of PEGDMA branched DBiB-p(OEGMA)$_{10}$ showed that it was possible to increase the molar brancher to initiator ratio to 0.8:1 without experiencing gelation.

PEGDMA branched DBiB-p(OEGMA)$_{20}$ were branched with molar brancher to initiator ratios of 0.2:1-0.8:1 and the results were summarised in Table 2.10. PEGDMA branched DBiB-p(OEGMA)$_{20}$ were branched with molar brancher to initiator ratios of 0.8:1 resulted in the reaction to gel. The reactions with the other molar brancher to initiator ratio resulted in high conversions of 97-99 % according to ^{1}H-NMR spectra analysis DP_n were calculated to be 21-23 and the corresponding IE values were calculated to be 87-95%.

Table 2.10. ^{1}H NMR of PEGDMA branched DBiB-p(OEGMA)$_{20}$. DP_n; degree of polymerisation. IE; initiator efficiency. Analysis performed in MeOD-d_4 and the residual solvent and water peaks were assigned with respect to literature.[244]

Polymer	brancher to initiator molar ratio	DP_n	IE %	Conv.%
DBiB-p(OEGMA)$_{20}$-co-(PEGDMA)$_{0.2}$	0.2:1	22	91	97
DBiB-p(OEGMA)$_{20}$-co-(PEGDMA)$_{0.5}$	0.5:1	23	87	99
DBiB-p(OEGMA)$_{20}$-co-(PEGDMA)$_{0.7}$	0.7:1	21	95	96
DBiB-p(OEGMA)$_{20}$-co-(PEGDMA)$_{0.8}$	0.8:1	Gel	Gel	Gel

Overall the ^{1}H NMR data of PEGDMA branched DBiB-p(OEGMA)$_{20}$ showed that it was possible to increase the molar brancher to initiator ratio to 0.7:1 without experiencing gelation. However, when the molar brancher to initiator increased to 0.8:1 the reaction started gelling.

Finally, PEGDMA branched DBiB-p(OEGMA)$_{50}$ were branched with molar brancher to initiator ratios of 0.2:1-0.7:1 and the results were summarised in Table 2.11.

Table 2.11. ^{1}H NMR of PEGDMA branched DBiB-p(OEGMA)$_{50}$. DP_n; degree of polymerisation. IE; initiator efficiency. Analysis performed in MeOD-d_4 and the residual solvent and water peaks were assigned with respect to literature.[244]

Polymer	brancher to initiator molar ratio	DP_n	IE %	Conv.%
DBiB-p(OEGMA)$_{50}$-co-(PEGDMA)$_{0.2}$	0.2:1	50	>99	>99
DBiB-p(OEGMA)$_{50}$-co-(PEGDMA)$_{0.5}$	0.5:1	51	98	>99
DBiB-p(OEGMA)$_{50}$-co-(PEGDMA)$_{0.7}$	0.7:1	Gel	Gel	Gel

PEGDMA branched DBiB-p(OEGMA)$_{50}$ branched with molar brancher to initiator ratios of 0.7:1 resulted in the reaction to gel. The reactions with the other molar brancher to initiator ratios resulted in high conversions of >99 % and a soluble product. DP_n were calculated to be 50-51 and the corresponding IE values were calculated to be 98- >99%. Overall the ^{1}H NMR data of PEGDMA branched DBiB-p(OEGMA)$_{50}$ showed that it was possible to increase the molar brancher to initiator ratio to 0.5:1 without experiencing gelation.

2.2.5.2 GPC characterisation of PEGDMA branched DBiB-p(OEGMA)$_{10\text{-}50}$ copolymers

The obtained M_w, M_n, Đ and WA # for EGDMA branched DBiB-p(OEGMA)$_{20}$ are given on Table 2.12.

Table 2.12. Calculated M_n, M_w, Đ and WA # for GPC data obtained for DBiB-p(OEGMA)$_{10}$ copolymers branched with PEGDMA recorded in DMF (+0.01 M LiBr)

Polymer	M_n (gmol^{-1})	M_w(gmol^{-1})	Đ	WA #
DBiB-p(OEGMA)$_{10}$-co-(PEGDMA)$_{0.2}$	10,620	21,730	2.0	3
DBiB-p(OEGMA)$_{10}$-co-(PEGDMA)$_{0.5}$	21,150	154,540	7.3	22

The results showed that M_n increased from 10,620 gmol^{-1} to 21,150 gmol^{-1} when the molar ratio of brancher to initiator was increased from 0.2:1 to 0.5:1. M_w values increased from 21,730 gmol^{-1} to 154,540 gmol^{-1}, respectively. In addition, the Đ of the resulting polymer increased significantly from 2 to 7.3 as the molar ratio of brancher to initiator from 0.2:1 to 0.5:1 for polymers DBiB-p(OEGMA)$_{10}$-*co*-(PEGDMA)$_{0.2}$ and DBiB-p(OEGMA)$_{10}$-co-(PEGDMA)$_{0.5}$. This indicated that the increase in molar ratio of brancher to initiator from 0.2:1 to 0.5:1 only resulted in slight increase in Đ. It was also observed that the numbers of conjoined chains pr. branched polymers WA # were calculated to be up to 22 for DBiB-p(OEGMA)$_{10}$-co-(PEGDMA)$_{0.5}$.

Chromatograms of linear DBiB-p(OEGMA)$_{10}$ was overlaid against selected branched DBiB-p(OEGMA)$_{10}$-co-(PEGDMA)$_{0.5}$ and DBiB-p(OEGMA)$_{10}$-co-(PEGDMA)$_{0.95}$ and shown in Fig. 2.14 and Appendix Fig. A1, A10-A11. The results showed that the linear DBiB-(OEGMA)$_{10}$ has a narrow distribution than the branched polymers DBiB-p(OEGMA)$_{10}$-co-(PEGDMA)$_{0.2}$ and DBiB-p(OEGMA)$_{10}$-co-(PEGDMA)$_{0.5}$ which indicated that DBiB-p(OEGMA)$_{10}$-co-(PEGDMA)$_{0.2}$ and DBiB-p(OEGMA)$_{10}$-co-(PEGDMA)$_{0.5}$ was highly branched. In addition to that and DBiB- more disperse than DBiB-p(OEGMA)$_{10}$-co-(PEGDMA)$_{0.2.}$

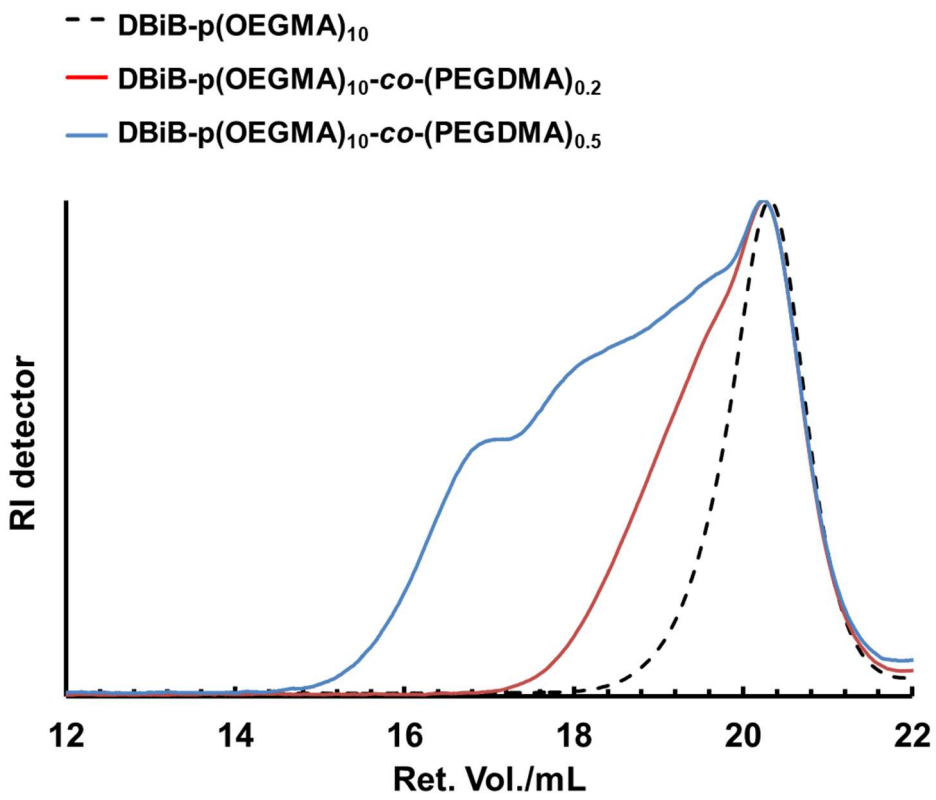

Fig. 2.14. Selected raw GPC chromatograms obtained with RI detector in mV. Selected chromatograms of linear DBiB-p(OEGMA)$_{10}$ and copolymers DBiB-p(OEGMA)$_{10}$-*co*-(PEGDMA)$_{0.2}$ and DBiB-p(OEGMA)$_{10}$-*co*-(PEGDMA)$_{0.5}$. Analysis performed by GPC with mobile phase of DMF (+ 0.01M) at 1mL/min 60 ˚C. All of the RI traces were normalised. Ret.; retention. Vol.; volume

The obtained M_w, M_n, Đ and WA # for EGDMA branched DBiB-p(OEGMA)$_{20}$ are given on Table 2.13.

Table 2.13. Calculated M_n, M_w, Đ and WA # for GPC data obtained for DBiB-p(OEGMA)$_{20}$ copolymers branched with PEGDMA recorded in DMF (+0.01 M LiBr)

Polymer	M_n (gmol^{-1})	M_w(gmol^{-1})	Đ	WA #
DBiB-p(OEGMA)$_{20}$-co-(PEGDMA)$_{0.2}$	16,080	26,520	1.6	2
DBiB-p(OEGMA)$_{20}$-co-(PEGDMA)$_{0.3}$	15,590	38,880	2.5	3
DBiB-p(OEGMA)$_{20}$-co-(PEGDMA)$_{0.4}$	12,260	48,450	3.9	4
DBiB-p(OEGMA)$_{20}$-co-(PEGDMA)$_{0.5}$	20,980	106,500	5.1	8
DBiB-p(OEGMA)$_{20}$-co-(PEGDMA)$_{0.6}$	15,120	148,200	9.8	11
DBiB-p(OEGMA)$_{20}$-co-(PEGDMA)$_{0.7}$	335,450	3,060000	9.1	234

GPC chromatograms of linear DBiB-p(OEGMA)$_{20}$ were overlaid against selected branched DBiB-p(OEGMA)$_{20}$-co-(PEGDMA)$_{0.5}$ and DBiB-p(OEGMA)$_{20}$-co-(PEGDMA)$_{0.7}$ and shown in Fig. 2.15 and Appendix A4, A12-A13.

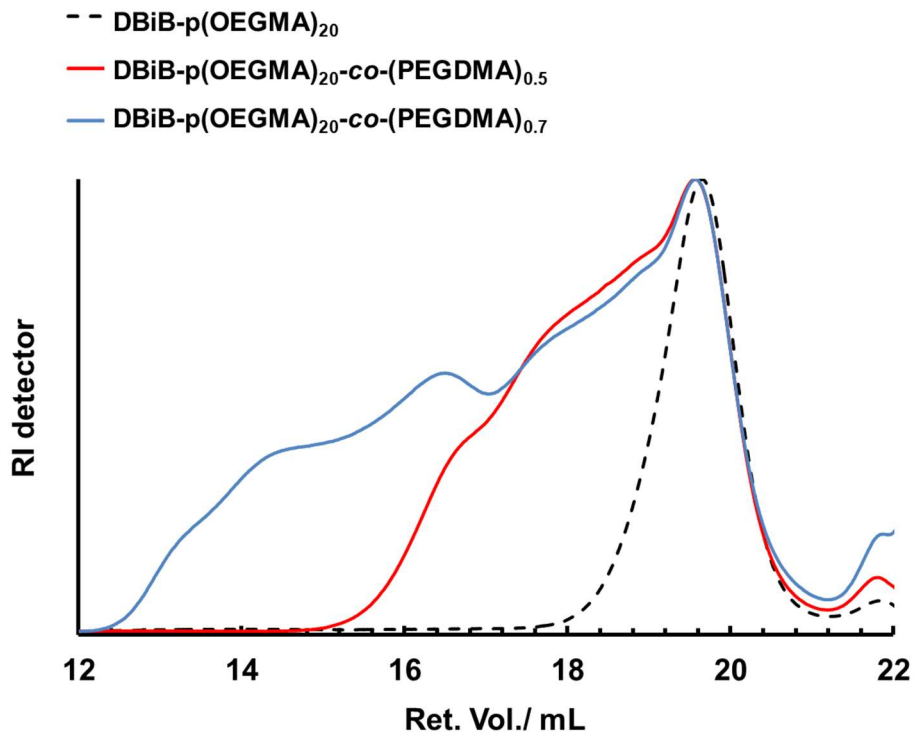

Fig. 2.15. Selected raw GPC chromatograms obtained with RI detector. Selected chromatograms of Linear DBiB-p(OEGMA)$_{20}$, DBiB-p(OEGMA)$_{20}$-*co*-(PEGDMA)$_{0.5}$ and DBiB-p(OEGMA)$_{20}$-*co*-(PEGDMA)$_{0.7}$. Analysis performed by GPC with mobile phase of DMF (+ 0.01M) at 1mL/min 60 ˚C. All of the RI traces were normalised. Ret.; retention. Vol.; volume

The results showed that the linear DBiB-(OEGMA)$_{20}$ has a narrow distribution than the branched polymers DBiB-p(OEGMA)$_{20}$-co-(PEGDMA)$_{0.5}$ and DBiB-p(OEGMA)$_{10}$-co-(PEGDMA)$_{0.7}$. This indicated that DBiB-p(OEGMA)$_{20}$-co-(PEGDMA)$_{0.5}$ and DBiB-p(OEGMA)$_{20}$-co-(EGDMA)$_{0.7}$ was highly branched when PEGMA was introduced into the polymerisation.

The obtained M_w, M_n, Đ and WA # for EGDMA branched DBiB-p(OEGMA)$_{50}$ are given on Table 2.14.

Table 2.14. Calculated M_n, M_w, Đ and WA # for GPC data obtained for DBiB-p(OEGMA)$_{50}$ copolymers branched with PEGDMA recorded in DMF (+0.01 M LiBr)

Polymer	M_n (gmol^{-1})	M_w(gmol^{-1})	Đ	WA #
DBiB-p(OEGMA)$_{50}$-co-(PEGDMA)$_{0.2}$	15,170	27,850	1.8	1
DBiB-p(OEGMA)$_{50}$-co-(PEGDMA)$_{0.5}$	23,200	88,010	3.8	4

The results showed that M_n increased from 15,170 gmol^{-1} to 23,200 gmol^{-1} when the molar ratio of brancher to initiator was increased from 0.2:1 to 0.5:1. M_w values increased from 27,850 gmol^{-1} to 88,010 gmol^{-1}, respectively. In addition, the Đ of the resulting polymer increased significantly from 1.8 to 3.8 as the molar ratio of brancher to initiator from 0.2:1 to 0.5:1 for polymers DBiB-p(OEGMA)$_{50}$-*co*-(EGDMA)$_{0.2}$ and DBiB-p(OEGMA)$_{50}$-co-(EGDMA)$_{0.5}$. This indicated that the increase in molar ratio of brancher to initiator from 0.2:1 to 0.5:1 only resulted in slight increase in Đ. It was also observed that the numbers of conjoined chains pr. branched polymers WA # were calculated to be up to 4 for DBiB-p(OEGMA)$_{10}$-co-(EGDMA)$_{0.5}$.

Selected GPC chromatograms of linear DBiB-p(OEGMA)$_{50}$ was overlaid against selected branched DBiB-p(OEGMA)$_{50}$-co-(PEGDMA)$_{0.2}$ and DBiB-p(OEGMA)$_{50}$-co-(PEGDMA)$_{0.5}$ and shown in Fig. 2.16 and Appendix Fig. A7, A14-A15. The results showed that the linear DBiB-(OEGMA)$_{50}$ has a narrow distribution than the branched polymers DBiB-p(OEGMA)$_{50}$-co-(PEGDMA)$_{0.2}$ and DBiB-p(OEGMA)$_{50}$-co-(PEGDMA)$_{0.5}$. This indicated that DBiB-p(OEGMA)$_{50}$-co-(PEGDMA)$_{0.2}$ and DBiB-p(OEGMA)$_{50}$-co-(PEGDMA)$_{0.5}$ was highly branched when PEGMA was introduced into the polymerisation.

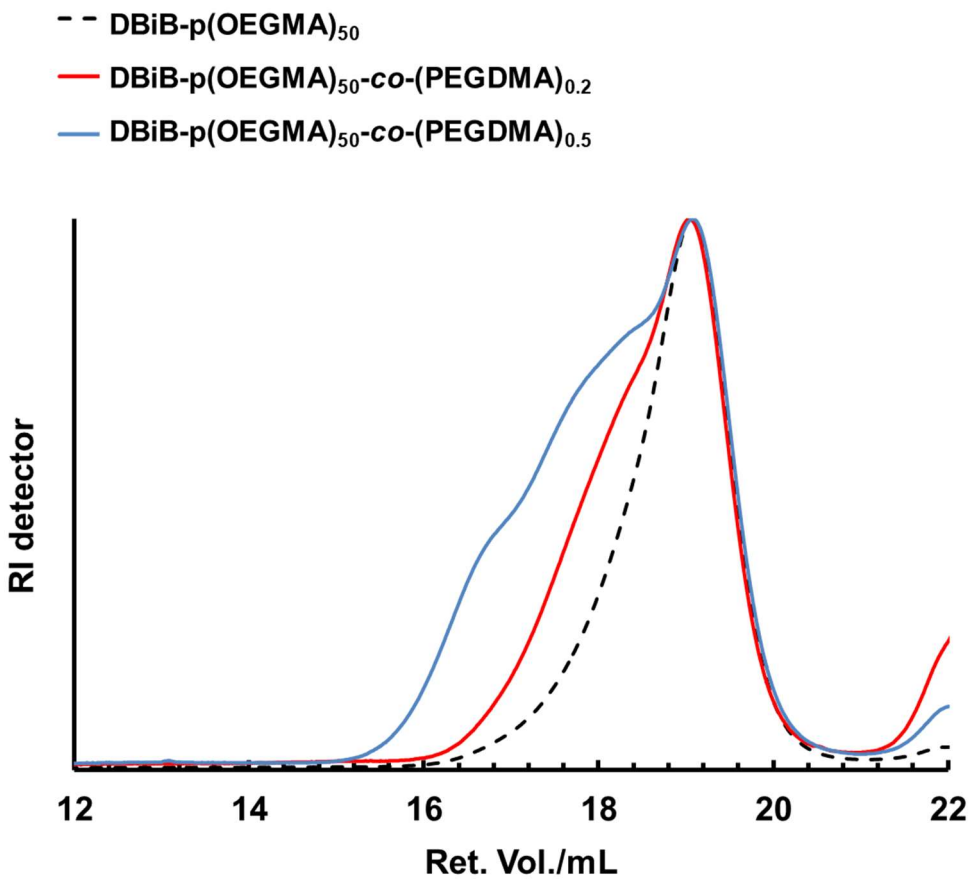

Fig. 2.16. Selected raw GPC chromatograms obtained with RI detector. Selected chromatograms of linear DBiB-p(OEGMA)$_{50}$, DBiB-p(OEGMA)$_{50}$-*co*-(PEGDMA)$_{0.2}$ and DBiB-p(OEGMA)$_{50}$-*co*-(PEGDMA)$_{0.5}$. Analysis performed by GPC with mobile phase of DMF (+ 0.01M) at 1mL/min 60 ˚C. All of the RI traces were normalised. Ret.; retention. Vol.; volume.

2.2.6 *n*-dodecane emulsion studies of linear and branched DBiB-p(OEGMA)$_{10\text{-}50}$

The stabilising properties of synthesised linear and branched DBiB-p(OEGMA)$_{10\text{-}50}$ were tested using a *n*-dodecane in water emulsion study. For this homogenisation was used as a method and was earlier reported by Weaver *et al.*[191] The formation of emulsion using homogenisation is illustrated Fig. 2.17.

In this method, *n*-dodecane was redispersed 1:1 v/v ratio in water with polymer concentrations of 60-300 mg /mL water as shown in Fig. 2.17I). The sample was homogenised for 10 min at ambient temperature with a homogenisation speed of 25,000 rpm, Fig. 2.17a). This process results in an emulsion that is stabilised by a linear or branched DBiB-p(OEGMA)$_{10\text{-}50}$ based polymer, Fig. 2.17II).

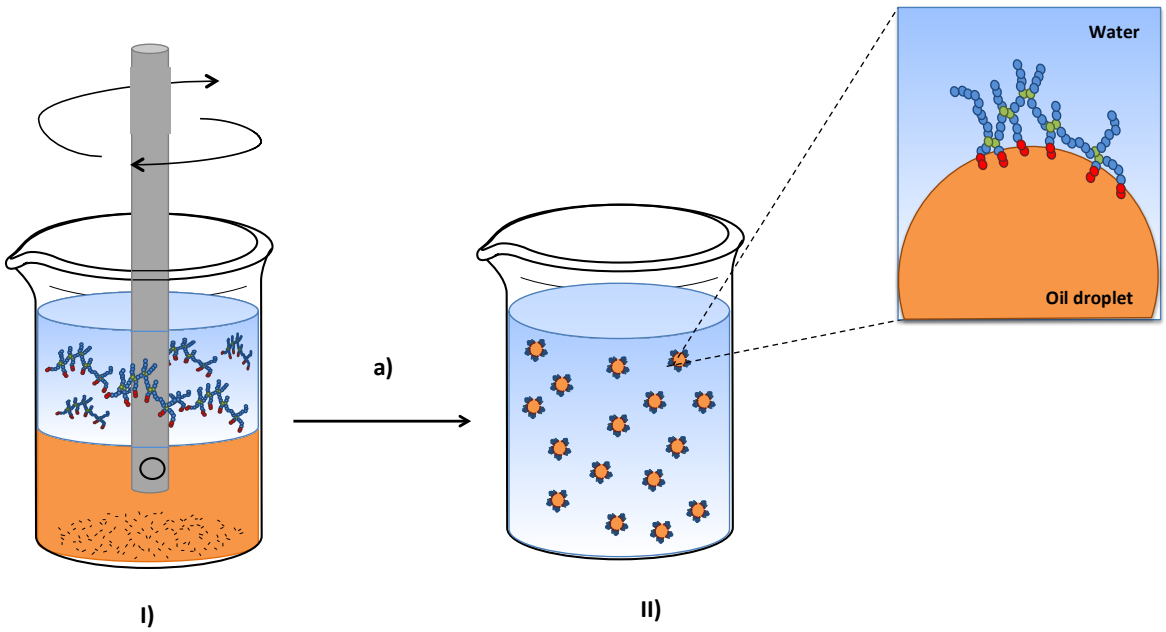

Fig. 2.17. Formation of emulsion using homogenisation technique. The selected DBiB-p(OEGMA) homo- or copolymers were dissolved in the water phase. **I)** The water phase combined with the oil phase were **a)** homogenised 10 minutes at 25,000 rpm at ambient temperature to yield **II)** DBiB-p(OEGMA) homo – or copolymer stabilised *n*-dodecane oil in water emulsion.

Droplet sizes in resulting emulsions were measured using a laser diffraction technique. The diffraction pattern is measured using wide angle and backscattering detectors.[247,248] The signal obtained is used to calculate the particle size by Mie Theory.[247,248] As a result of those measurements many parameters can be obtained such as D(10 %), D(50%) and D(90 %), D[3,2] and D[4,3] and the span of a distribution.[247,248] The volume weighted mean average (D[4,3]) and the span were analysed with the aim to provide information about the resulting droplet in the *n*-dodecane emulsion. D[3,2] is the surface volume mean D[3,2] and measures the diameter of droplet surface as if they were flat objects. The calculation of D[3,2] does not take the third dimension into account but the calculation for D[4,3] does. D[4,3] is also known as De Brouckere mean diameter and it is calculated using the sum of diameters of all particles spheres of the same volume divided by the sum the number of particles in the same volume.[247,248] The span is the width of the distribution and is calculated fitting three parameters. It can be calculated for any of the distribution types such as volume weighted mean (v), surface weighed mean (s), length of the distribution (l) and number of the resulting

distribution (n). All those distributions has a set of parameters which are D(10 %), D(50 %) and D(90 %). The equation used to calculate the span is given as follows:[249,248]

$$Span = \frac{D(90\ \%) - D(10\ \%)}{D(50\ \%)} \quad \textbf{(2.2)}$$

Where D(10 %) is the size distribution size of particles below 10 %, D(50 %) is the distribution size of particles below 50 % and D(90 %) is the distribution size particles below 90 %.[248]

2.2.6.1. n-dodecane in water emulsion study of linear DBiB-p(OEGMA)$_{10}$, DBiB-p(OEGMA)$_{20}$ and DBiB-p(OEGMA)$_{50}$

n-dodecane emulsion studies were initially generated with the synthesised linear homopolymers of DBiB-p(OEGMA)$_{10}$, DBiB-p(OEGMA)$_{20}$ and DBiB-p(OEGMA)$_{50}$. The purpose of this study was to investigate stabilising properties based on the chain length of the primary chains. In order to do so, the number of chain ends in a composition was kept constant while the size of the primary chain was the only variable to change. With this the polymer concentrations in the aqueous phase were chosen to be 60 mg/mL of DBiB-p(OEGMA)$_{10}$, 120 mg/mL of DBiB-p(OEGMA)$_{20}$ and 300 mg/mL of DBiB-p(OEGMA)$_{50}$ in deionised water. These different concentrations were selected so that all so that the molar number of polymer chains within each emulsion was the same as 60 mg/mL of DBiB-p(OEGMA)$_{10}$ in water. The samples with a relative phase ratio of 1:1 v/v ratio of water to oil were homogenised at ambient temperature for 10 min and the sizes of the oil droplets in the emulsions were analysed using laser scattering. The traces obtained for the measurements showed a monomodal distribution after 11 days for DBiB-p(OEGMA)$_{10}$ and DBiB-p(OEGMA)$_{20}$ as illustrated on the diagram, Fig. 2.18 and corresponding data obtained by laser diffraction measurements are given in Appendix A16-A21.

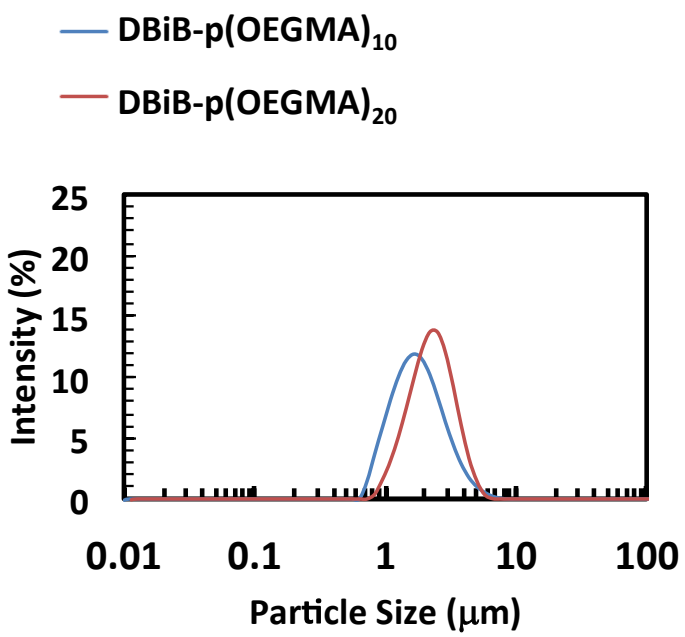

Fig. 2.18. Size distribution of oil droplets in *n*-dodecane emulsion droplets stabilised with DBiB-p(OEGMA)$_{10}$ (60 mg/mL) and DBiB-p(OEGMA)$_{20}$ (120 mg/mL) on day 11.

Data was collected of the droplet sizes measured over 0, 1, 3, 5, 7, and 11 days are plotted to show a of the oil droplets stabilised by linear homopolymers of DBiB-p(OEGMA)$_{10}$, DBiB-p(OEGMA)$_{20}$ and DBiB-p(OEGMA)$_{50}$, Fig. 2.19, poor emulsion stability would be revealed by a tendency for the droplets to increase in size or phase separate.

The droplet diameter of oil droplets stabilised with DBiB-p(OEGMA)$_{10}$ and DBiB-p(OEGMA)$_{20}$ were shown to increase over 11 days, Fig. 2.19. The mechanism, which causes the droplet size was likely due to a phenomenon known as coalescence or Oswald ripening. It is posited that coalescence occurs when oil droplets fuse together. That is, when two oil droplets fuse together to form a single oil droplet.[250] The polymer with the longest chain length, DBiB-p(OEGMA)$_{50}$, was only stable for 2 days and as a separated oil layer were observed on the top of the emulsion day 3 (Fig. 2.19 inset). The corresponding spans of the distributions, Fig. 2.19b, demonstrated that the size distributions, Fig. 2.19a, are narrow over time even though the size increases. The span of the distribution traces indicates that the distribution remains narrow even though the D[4,3] increases over time.

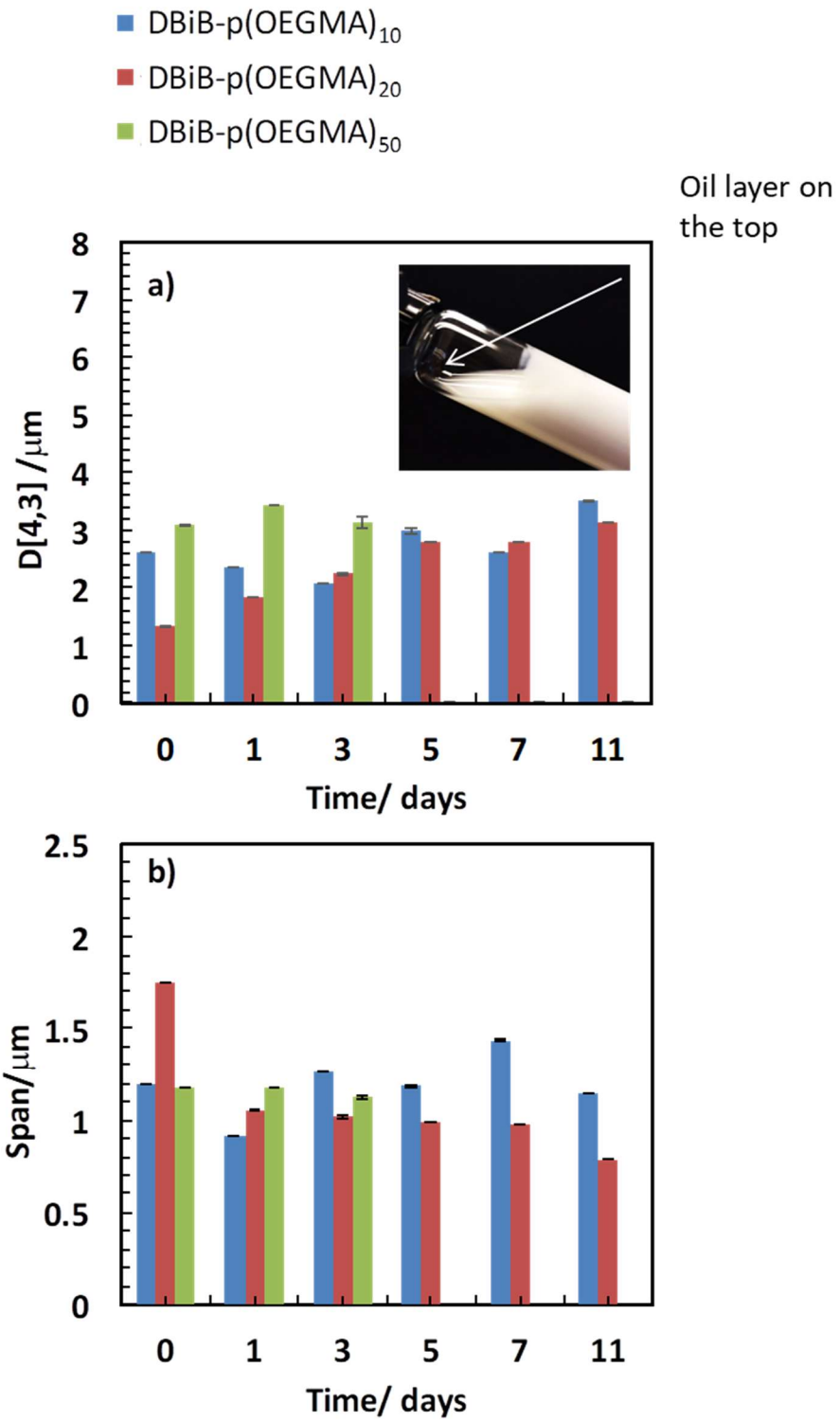

Fig. 2.19. Diagram of volume weighed mean average D [4,3] of oil droplet in 1:1 v/v ratio *n*-dodecane in water emulsions measured over 11 days and stabilised with three different compositions of polymers in water **a)** DBiB-p(OEGMA)$_{10}$ (60 mg/mL), DBiB-p(OEGMA)$_{20}$ (120 mg/mL) and DBiB-p(OEGMA)$_{50}$ (300 mg/mL). Each sample was measured in triplicate and standard deviations are given in the error bars. Inset- Picture of *n*-dodecane emulsion stabilised with DBiB-p(OEGMA)$_{50}$ with an oil layer on the top. **b)** Span of distribution of traces measured over 11 days for DBiB-p(OEGMA)$_{10}$, DBiB-p(OEGMA)$_{20}$ and DBiB-p(OEGMA)$_{50}$. Green bars only present day 0-3 due to DBiB-p(OEGMA)$_{50}$ instability.

When linear polymers were compared against each other it was observed that DBiB-p(OEGMA)$_{10}$ and DBiB-p(OEGMA)$_{20}$ exhibited better activity than DBiB-p(OEGMA)$_{50}$ over a short period of time. However, overall linear polymer it was demonstrated that instability occurred for both DP_{10} and DP_{20} after 11 possibly due to the sample coalescing. This would also lead to the later observation of oil droplets on the of the top of the emulsions. In conclusion, the DBiB-p(OEGMA)$_{10\text{-}50}$ polymers were not good stabilisers for *n*-dodecane emulsion systems. This is thought to be due to the linear polymers only having one chain end to stabilise the surface of an oil droplet and the dynamic nature of such polymer stabilisation. Highly branched polymers have multiple hydrophobic chain ends and present a significant opportunity to create stable emulsions, therefore the materials synthesised in section 2.2.4 and 2.2.5 were evaluated in detail.

2.2.6.2. Study of emulsion stabilised with EGDMA branched DBiB-p(OEGMA)$_{10\text{-}50}$ with WA # of 3-4

As shown in the previous section, the linear polymers with a single chain end did not stabilise the *n*-dodecane emulsion droplets over more than 11 days. Therefore, another study was performed to investigate the stabilising properties of branched copolymer compositions in *n*-dodecane emulsions. In this initial study, DBiB-p(OEGMA)$_{10}$-*co*-EGDMA$_{0.5}$, DBiB-p(OEGMA)$_{20}$-*co*-EGDMA$_{0.2}$ and DBiB-p(OEGMA)$_{50}$-*co*-EGDMA$_{0.5}$ were compared as the low branching in each material gave rise to a similar weight average number of conjoined chains (WA # = 3).

The aqueous continues phase of the emulsion was prepared to contain 60 mg/ mL of branched DBiB-p(OEGMA)$_{10}$, 120 mg/mL of DBiB-p(OEGMA)$_{20}$ and 300 mg/mL of DBiB-p(OEGMA)$_{50}$ to ensure that the amount of chain ends in each formulation were approximately similar. The aim of this study was to investigate the impact of light branching on the stability of branched copolymer stabilised emulsions in direct comparison with the linear copolymers of similar hydrophilic chain length. The size distributions of the selected

samples in the emulsion *n*-dodecane emulsion study are shown in Fig. 2.20 and corresponding data obtained from laser diffraction are given in Appendix Fig. A22-A27 and were compared on day 0 and day 21, respectively

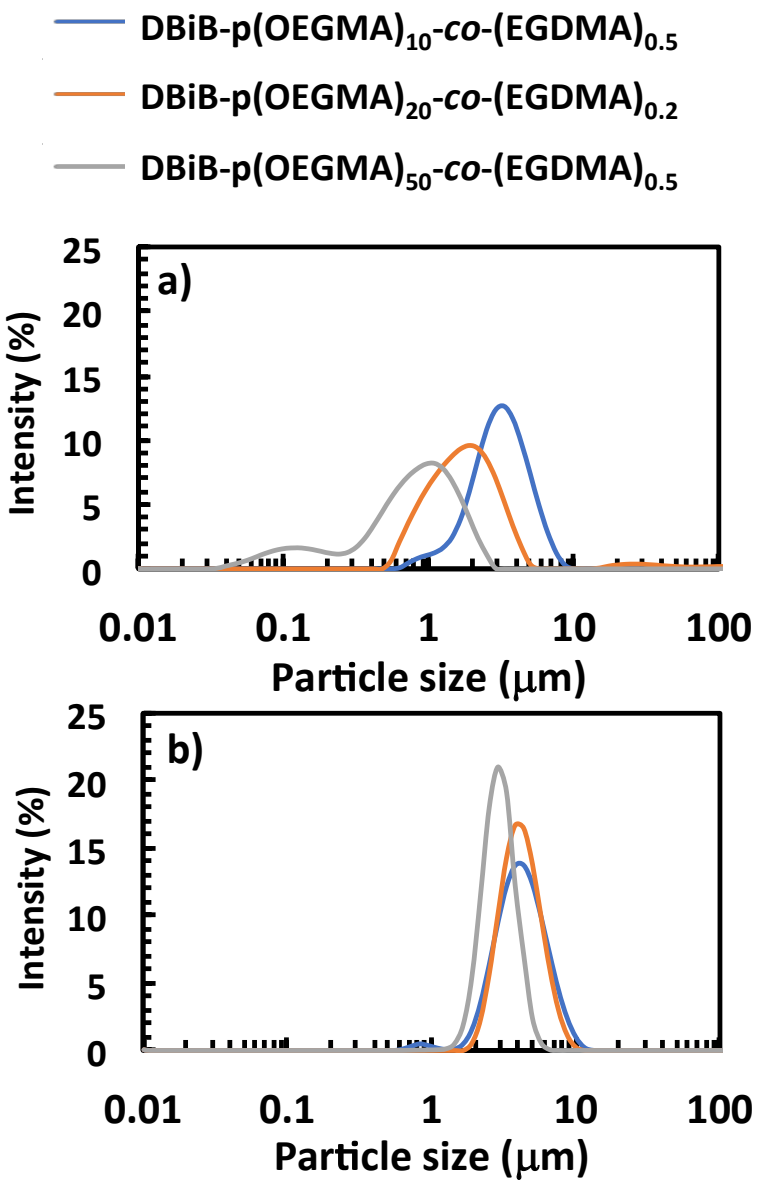

Fig. 2.20. Laser diffraction measurement traces of 1:1 v/v ratio *n*-dodecane in water emulsion recorded on **a)** day 0 and **b)** day 21 with following compositions DBiB-p(OEGMA)$_{10}$-*co*-(EGDMA)$_{0.5}$ (60 mg/mL), DBiB-p(OEGMA)$_{20}$-*co*-(EGDMA)$_{0.2}$ (120 mg/mL) and DBiB-p(OEGMA)$_{50}$-*co*-(EGDMA)$_{0.5}$ (300 mg/mL).

The size distribution of the samples appeared to be broad on day 0 but had become monomodal by day 21. The D[4,3] of the oil droplets stabilised by the different polymers appeared to be different. The initial analysis appeared to show that the shorter primary chain length, DBiB-p(OEGMA)$_{10}$-*co*-(EGDMA)$_{0.5}$, acted as the more efficient stabilisers, generating

the most uniform distribution, however, smaller emulsion droplets were formed in a multimodal distribution when using DBiB-p(OEGMA)$_{50}$-*co*-(EGDMA)$_{0.5}$. When left to stand for several days, the observed behaviour of D[4,3] of the three branched copolymers were very similar as shown on Fig. 2.21a. In both cases D[4,3] increased. For DBiB-p(OEGMA)$_{10}$-*co*-(EGDMA)$_{0.5}$ stabilised oil droplets from 3.57 to 4.73 μm while DBiB-p(OEGMA)$_{20}$-*co*-(EGDMA)$_{0.5}$ stabilised oil droplets increased from 1.69 to 4.21 μm and for oil droplets stabilised with DBiB-p(OEGMA)$_{50}$-*co*-(EGDMA)$_{0.7}$ this increase was from 0.94 to 3.23 μm. It was concluded that DBiB-p(OEGMA)$_{10}$-*co*-(EGDMA)$_{0.5}$ stabilised oil droplets increased 1.32 fold in comparison to DBiB-p(OEGMA)$_{20}$-*co*-(EGDMA)$_{0.5}$ stabilised oil droplets which increased 2.49 fold and oil droplets stabilised with DBiB-p(OEGMA)$_{50}$-*co*-(EGDMA)$_{0.7}$ which increased 3.44 fold. It is speculated that this difference is due to some changes of the chain end functionality when changing the degree of the polymerisation of the primary p(OEGMA) chain. It could be hypothesised that a shorter chain size of p(OEGMA)$_{10}$ will lead to an increase in stability than a longer primary chain size of p(OEGMA)$_{50}$.

The droplet size of selected oil droplets stabilised with DBiB-p(OEGMA)$_{10}$-*co*-(EGDMA)$_{0.5}$, DBiB-p(OEGMA)$_{20}$-*co*-(EGDMA)$_{0.2}$ and DBiB-p(OEGMA)$_{50}$-*co*-(EGDMA)$_{0.5}$ were analysed by laser diffraction and the D[4,3] and corresponding span were assessed over a period of 21 days, Fig. 2.21. The stabilising properties of DBiB-p(OEGMA)$_{10}$-*co*-(EGDMA)$_{0.5}$, DBiB-p(OEGMA)$_{20}$-*co*-(EGDMA)$_{0.2,}$ DBiB-p(OEGMA)$_{50}$-*co*-(EGDMA)$_{0.5}$ were analysed by laser diffraction and the results showed that stabilised *n*-dodecane oil droplets increased significantly in size over 21 days. The behaviour of the size distribution over the 21 days showed DBiB-p(OEGMA)$_{50}$-co-(EGDMA)$_{0.5}$ has increased nearly 3-fold, the DBiB-p(OEGMA)$_{20}$-*co*-(EGDMA)$_{0.2}$ increased with 50% (based on the day 1 result and day 21), and the DBiB-p(OEGMA)$_{10}$-*co*-(EGDMA)$_{0.5}$ has increased by about 35%. Fig. 2.21a. Additionally, the corresponding span of the traces of oil droplets stabilised with DBiB-p(OEGMA)$_{10}$-*co*-(EGDMA)$_{0.5}$ was constant over time, Fig. 2.21b. After 21 days, oil layers were observed on the top of all the emulsions and measurements of those samples were discontinued.

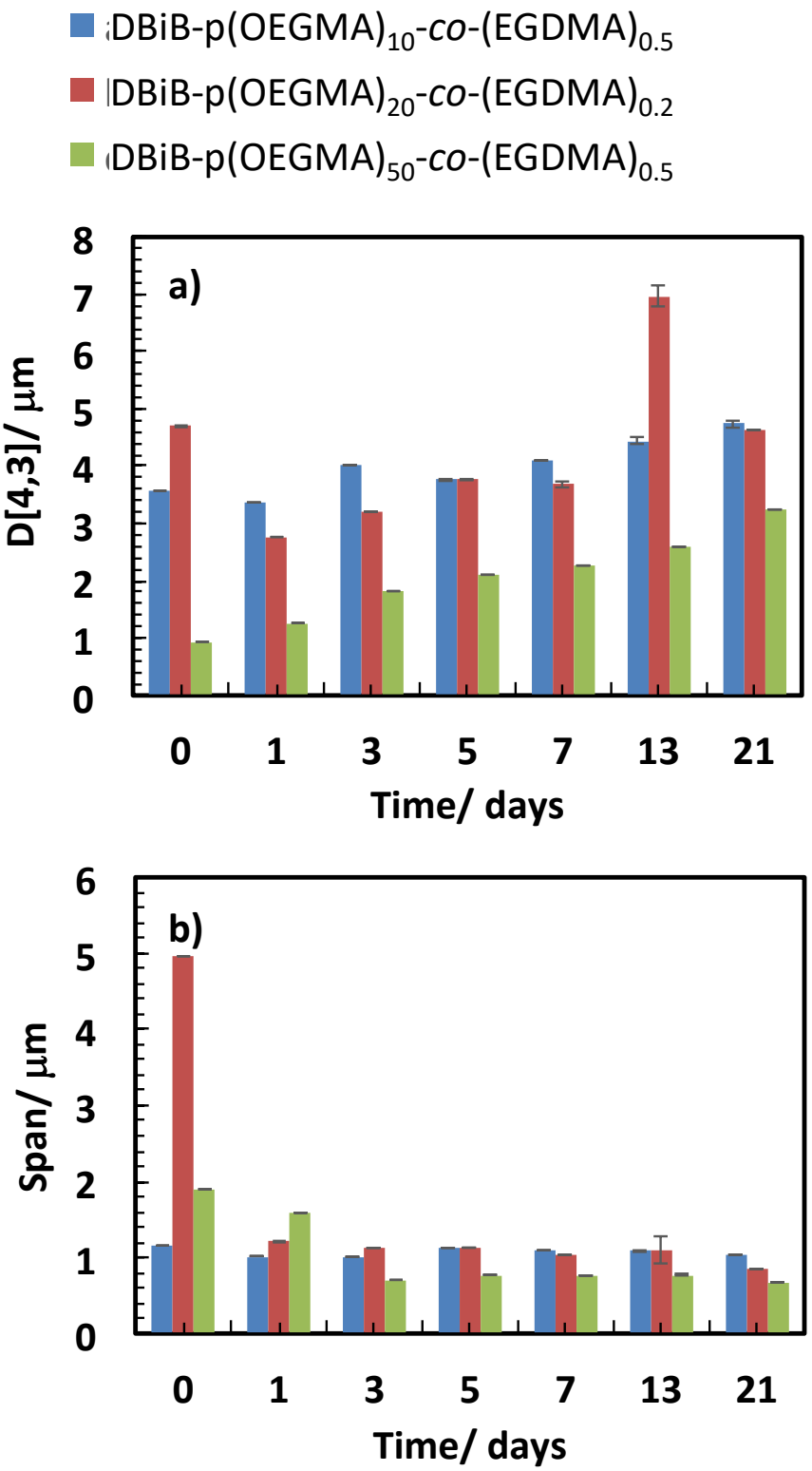

Fig. 2.21. a) Diagram of droplet size distribution in *n*-dodecane in water emulsions given in µm measured over 21 days. The *n*-dodecane in water emulsion was stabilised by three different compositions of polymers DBiB-p(OEGMA)$_{10}$-*co*-(EGDMA)$_{0.5}$ (30 mg/mL), DBiB-p(OEGMA)$_{20}$ -*co*-(EGDMA)$_{0.2}$ (60 mg/mL) and DBiB-p(OEGMA)$_{50}$ -*co*-(EGDMA)$_{0.5}$ (150 mg/mL). Each sample was measured in triplicate and standard deviations are given in the error bars.

2.2.6.3 Study of emulsion stabilised with PEGDMA branched DBiB-p(OEGMA)$_{10\text{-}50}$ with WA # of 3-4

The effect of WA # branched with PEGDMA on the potential for emulsion stabilisation was then investigated. PEGDMA branched copolymers with a WA # between 3-4 were studied with the same compositions were dissolved in water at concentrations between 60-300 mg/mL as described for the former study on EGDMA. This was done with the aim to keep the number of chains the same while varying parameters such as the chain lengths of the primary chain and varying the length of the brancher unit and the chain length of the brancher were changed. The following compositions of selected polymers from the libraries, Table 2.1-2.3, were given as 60 mg/ mL of DBiB-p(OEGMA)$_{10}$-*co*-(PEGDMA)$_{0.2}$, 120 mg/ mL of DBiB-p(OEGMA)$_{20}$-*co*-(PEGDMA)$_{0.3}$ and 300 mg/mL of DBiB-p(OEGMA)$_{50}$-*co*-(PEGDMA)$_{0.5}$ in deionised water were used. The distribution of the emulsion droplets stabilised with the DBiB-p(OEGMA)$_{20}$-*co*-(PEGDMA)$_{0.3}$ and DBiB-p(OEGMA)$_{50}$-*co*-(PEGDMA)$_{0.5}$ were compared on day 0 and 11, Fig. 2.22 and corresponding laser diffraction measurements are given in Appendix A34-A39.

The traces of the selected polymers showed a monomodal distribution after 11 days. The narrowness of the distribution is hypothesised to be caused by Oswald ripening as D[4,3] increases slightly from day 0 to day 11. However, the size distribution of emulsions droplets stabilised with DBiB-p(OEGMA)$_{10}$-*co*-(PEGDMA)$_{0.2}$ was not taken into consideration as some visible phase separation of this sample had occurred with an oil layer observed on the top of the emulsion after 3 days.

The two parameters, D[4,3] and span of the emulsion droplet distribution stabilised by polymers did not remain stable over 11 days in the case of DBiB-p(OEGMA)$_{20}$-*co*-(PEGDMA)$_{0.3}$ and DBiB-p(OEGMA)$_{50}$-*co*-(PEGDMA)$_{0.5}$, Fig. 2.23a.

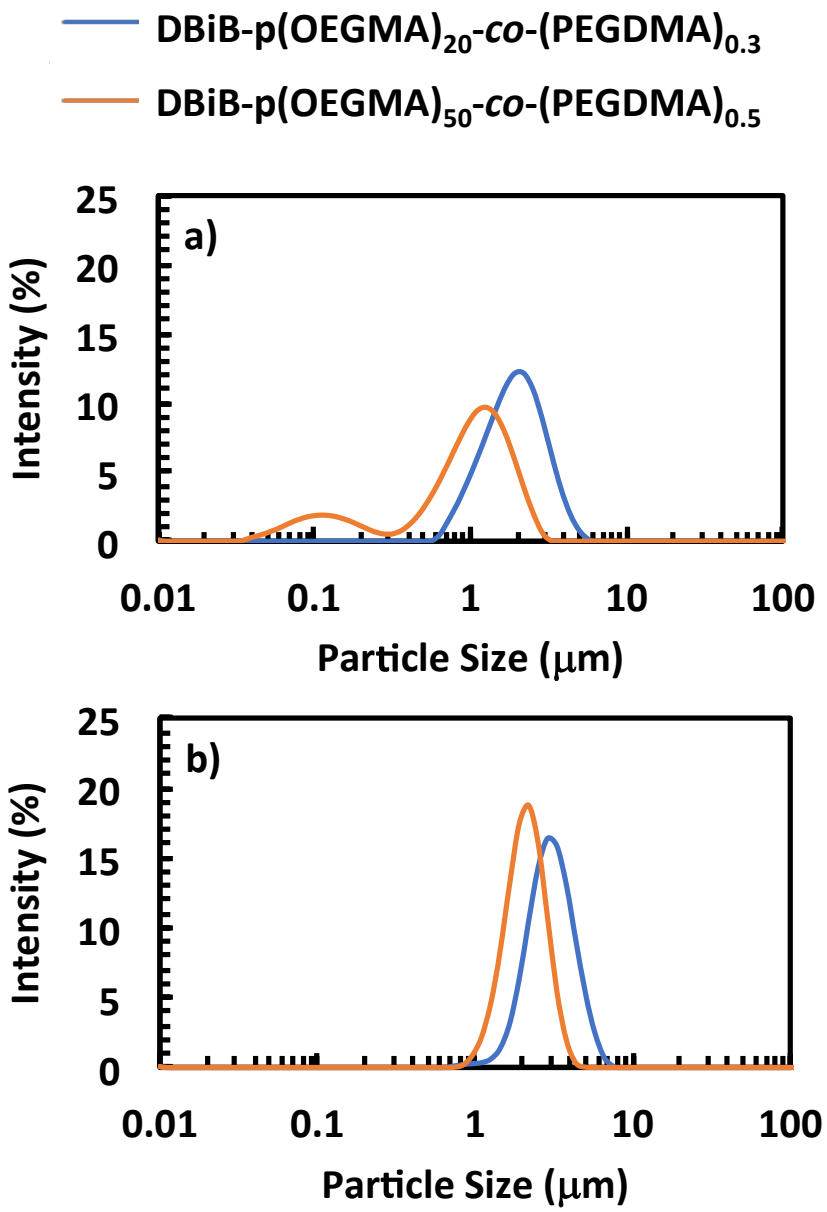

Fig. 2.22. Size distributions of 1:1 v/v ratio dodecane in water emulsion recorded on **a)** day 0 and **b)** day 11 with following composition of DBiB-p(OEGMA)$_{20}$-*co*-PEGDMA$_{0.3}$ and DBiB-p(OEGMA)$_{50}$-co-(PEGDMA)$_{0.5}$.

However, the size distribution of emulsions droplets stabilised with DBiB-p(OEGMA)$_{10}$-*co*-(PEGDMA)$_{0.2}$ was not taken into consideration as some visible phase separation of this sample had occurred with an oil layer observed on the top of the emulsion after 3 days.

The two parameters, D[4,3] and span of the emulsion droplet distribution stabilised by polymers did not remain stable over 11 days in the case of DBiB-p(OEGMA)$_{20}$-*co*-(PEGDMA)$_{0.3}$ and DBiB-p(OEGMA)$_{50}$-*co*-(PEGDMA)$_{0.5}$, Fig. 2.23a.

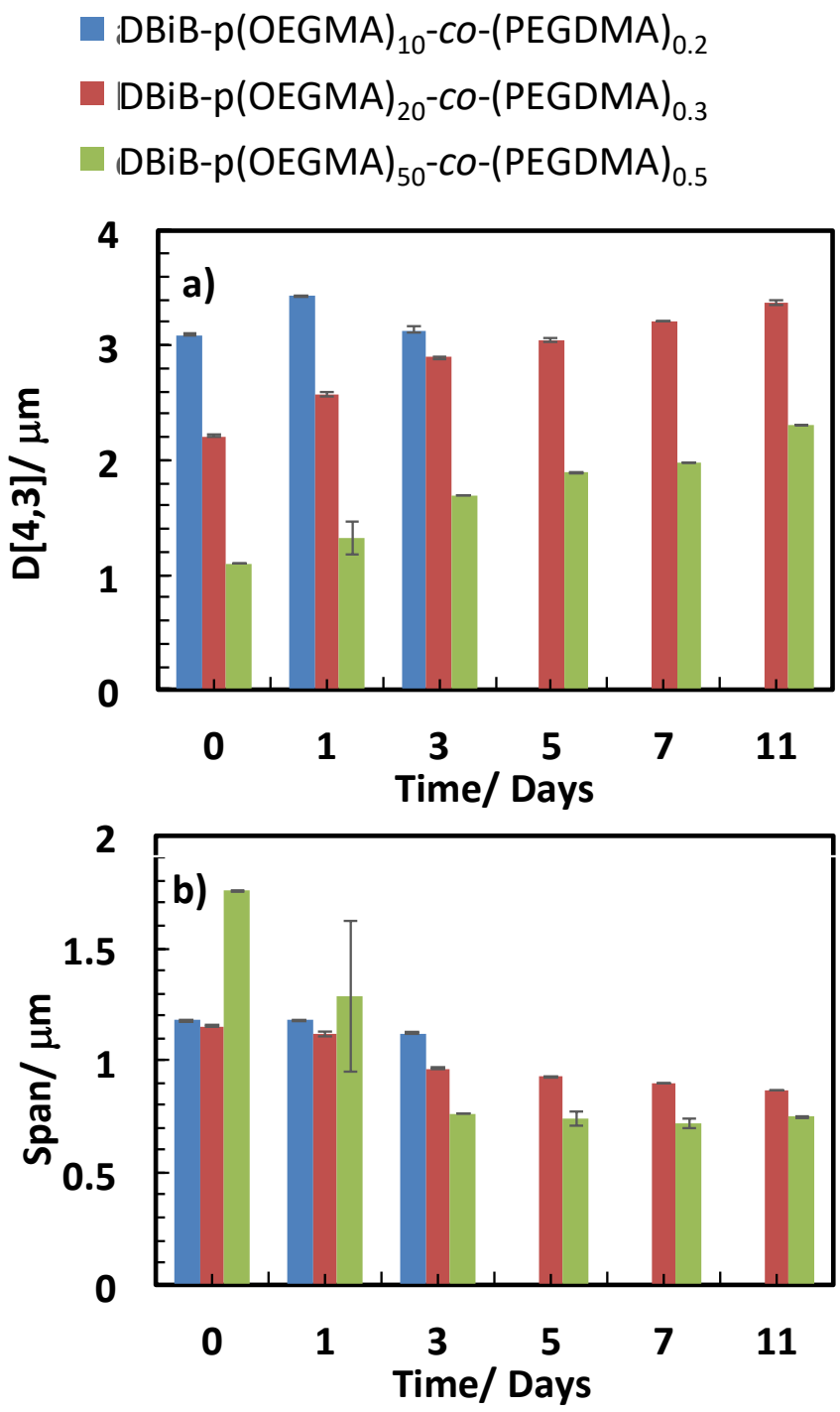

Fig. 2.23. a) Diagram of droplet size distribution and **b)** span in µm droplets in *n*-dodecane in water emulsions measured over 11 days. The *n*-dodecane in water emulsion was stabilised by three different compositions of polymers DBiB-p(OEGMA)$_{10}$-*co*-(PEGDMA)$_{0.2}$ (60 mg/mL), DBiB-p(OEGMA)$_{20}$-*co*-(PEGDMA)$_{0.3}$ (120 mg/mL) and DBiB-p(OEGMA)$_{50}$ -*co*-(PEGDMA)$_{0.5}$ (300 mg/mL). Each sample was measured in triplicate and standard deviations are given in the error bars.

This was due to the DBiB-p(OEGMA)$_{50}$-*co*-(PEGDMA)$_{0.5}$ stabilised emulsion droplet grew by over 200 % and the emulsion droplets stabilised by DBiB-p(OEGMA)$_{20}$-*co*-(PEGDMA)$_{0.3}$ grew with nearly 50 %. However, the D[4,3] and span distribution of DBiB-p(OEGMA)$_{10}$-*co*-(PEGDMA)$_{0.2}$ was only studied for 3 days as thereafter an oil layer was observed on the top of the emulsion. The span of emulsion droplets stabilised by DBiB-p(OEGMA)$_{50}$-*co*-(PEGDMA)$_{0.5}$ decreased considerably. The spans of DBiB-p(OEGMA)$_{20}$-*co*-(PEGDMA)$_{0.3}$ stabilised emulsion droplets were much more strable. This study demonstrated that the composition of p(OEGMA) copolymers branched with PEGDMA used to stabilise *n*-dodecane emulsion droplets only exhibit stability under 11 days which was a much shorter timespan than EGDMA branched copolymer with the same WA # chain which were stable for at least 21 days.

2.2.6.4. Study of emulsion stabilised with EGDMA branched DBiB-p(OEGMA)$_{10-50}$ with WA # of 6-9

In the previous sections it was demonstrated that EGDMA and PEGDMA branched copolymers with WA # chain of 3-4 increase the lifetime of oil droplets but an oil layer forms on the top of the emulsion eventually. However, it takes 21 days before an oil layer on the top of selected emulsions of samples stabilised with EGDMA branched copolymers were observed, Fig. 2.21, in comparison to PEGDMA branched copolymers which was after 11 days, Fig. 2.23. This suggests that the EGDMA branched polymers were better stabilisers. This is possibly due to the more compact nature of branching leading to a more dense arrangement of the polymer chains at the oil-water interphase. This led us to further investigate EGDMA branched DBiB-p(OEGMA)$_{10-50}$ copolymers in *n*-dodecane emulsions. Therefore, a series of polymers with a WA # chains = 6-9 were selected to generate a direct comparison with the stabilising properties of the more lightly branched materials when used in the aqueous continuous phase of the emulsion; namely DBiB-p(OEGMA)$_{10}$-*co*-EGDMA$_{0.6}$

(60 mg/mL), DBiB-p(OEGMA)$_{20}$-*co*-EGDMA$_{0.5}$ (120 mg/mL) and DBiB-p(OEGMA)$_{50}$-*co*-EGDMA$_{0.95}$ (300 mg/mL).

The droplet size distribution was measured by laser diffraction of the samples on day 0 and 21 were shown for all three copolymers in *n*-dodecane emulsions, Fig. 2.24. and corresponding laser diffraction measurements are given in Appendix A28-A33 The traces showed a broad polydisperse distribution on day 0 for all three copolymers that becomes more monomodal after 21 days. The monomodal distributions suggest that the samples are stable over 21 days.

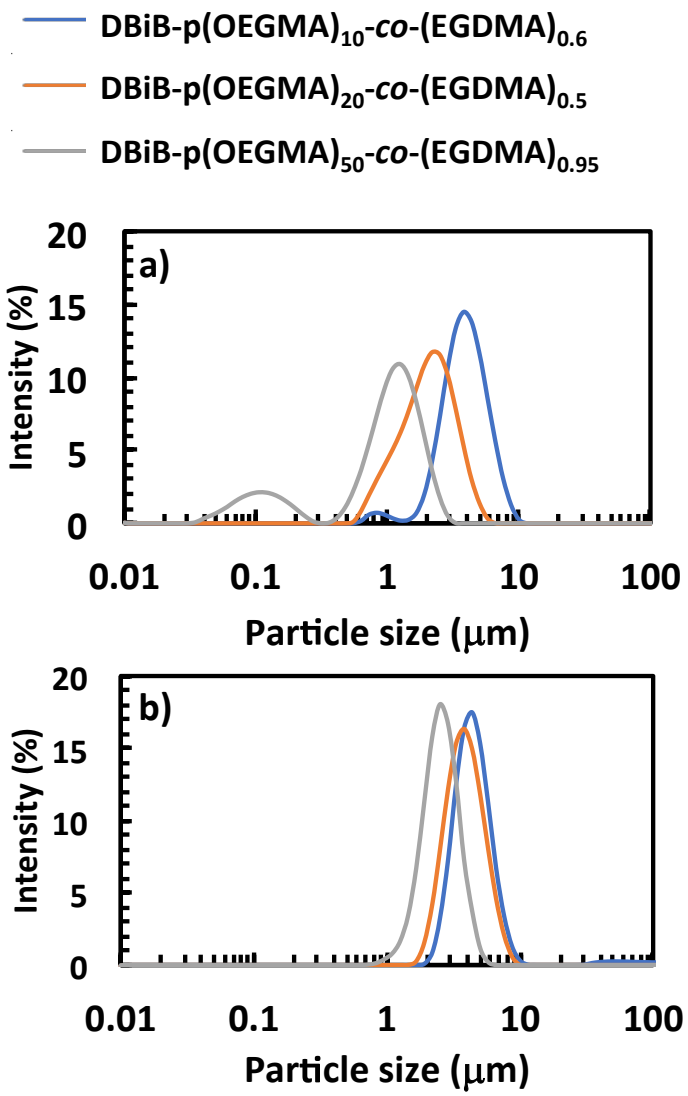

Fig. 2.24. Traces obtained from laser diffraction measurements of 1:1 v/v ratio *n*-dodecane in water emulsion recorded on **a)** day 0 and **b)** day 21 with following composition DBiB-p(OEGMA)$_{10}$-*co*-(EGDMA)$_{0.6}$, DBiB-p(OEGMA)$_{20}$-*co*-(EGDMA)$_{0.5}$ and DBiB-p(OEGMA)$_{50}$-*co*-(EGDMA)$_{0.95}$.

The D[4,3] and span of emulsions stabilised with DBiB-p(OEGMA)$_{10}$-*co*-(EGDMA)$_{0.6}$, DBiB-p(OEGMA)$_{20}$-*co*-(EGDMA)$_{0.5}$ and DBiB-p(OEGMA)$_{50}$-*co*-(EGDMA)$_{0.95}$ were then compared after 0, 1, 3, 5, 7, 13, and 21 days, Fig. 2.25. The results showed that D[4,3] of *n*-dodecane emulsions stabilised with DBiB-p(OEGMA)$_{10}$-*co*-(EGDMA)$_{0.6}$ nearly constant over time while the trend for DBiB-p(OEGMA)$_{20}$-*co*-(EGDMA)$_{0.5}$ and DBiB-p(OEGMA)$_{50}$-*co*-(EGDMA)$_{0.95}$ were similar and the size increased significantly over time.

Moreover, the size of *n*-dodecane in water emulsions stabilised with DBiB-p(OEGMA)$_{10}$-*co*-(EGDMA)$_{0.6}$ remained stable with a D[4,3] ~ 5 μm after 21 days and no oil layer was observed on the top of the emulsion. By comparison, the D[4,3] of *n*-dodecane in water emulsion stabilised with DBiB-p(OEGMA)$_{20}$-*co*-(EGDMA)$_{0.5}$ stabilised *n*-dodecane droplets increased from 2 to 4 μm over 21 days and an oil layer was observed on the top of the emulsion after 21 days, and the D[4,3] of *n*-dodecane in water emulsions stabilised with emulsions stabilised with DBiB-p(OEGMA)$_{50}$-*co*-(EGDMA)$_{0.95}$ droplets increased from 1 to 3 μm over 21 days and the oil layer was observed on day 21. Overall this study demonstrated that the increased number of chains impacts the stability and the shorter the chains, branched with the shorter brancher are more efficient.

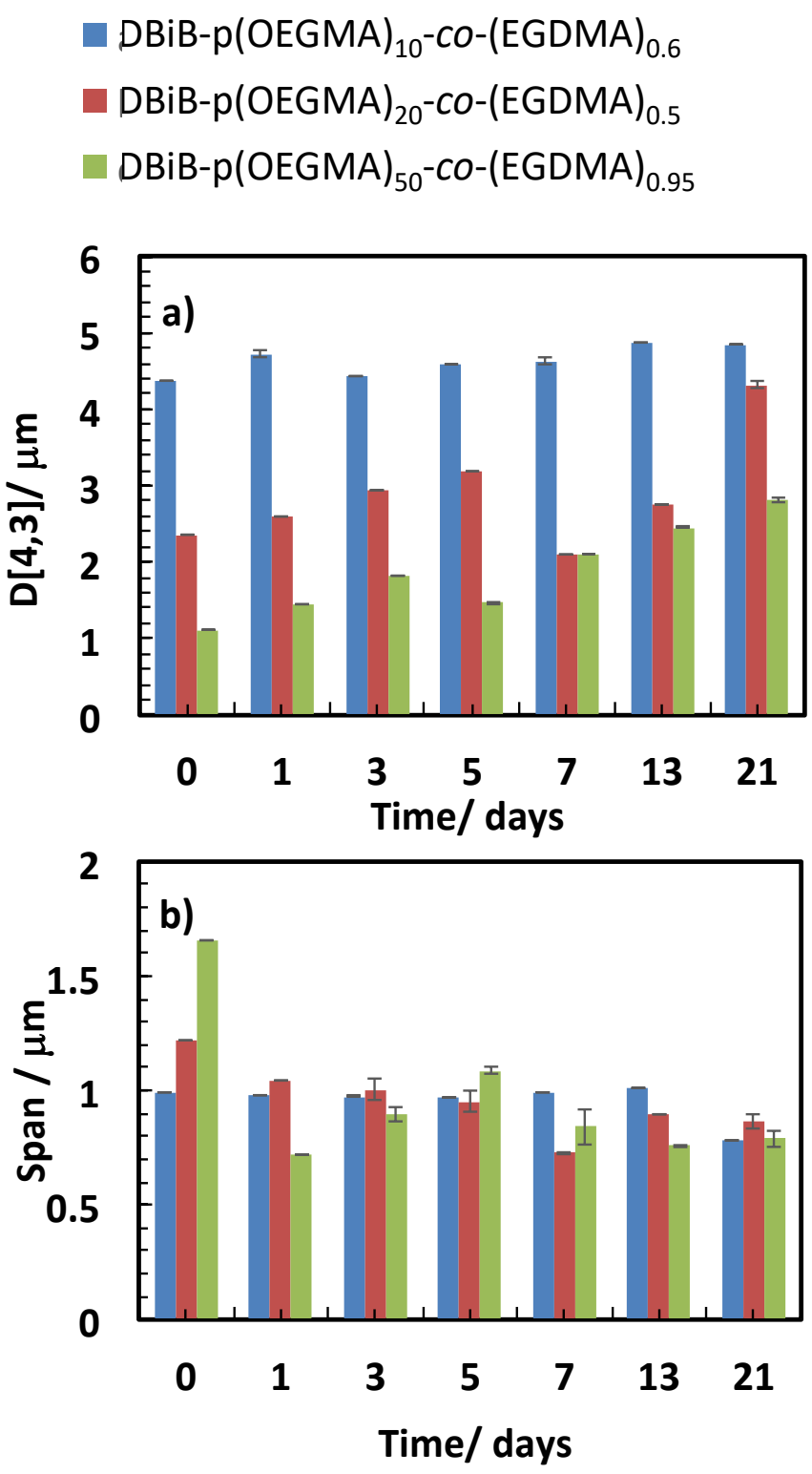

Fig. 2.25. a) Diagram of droplet size distribution and **b)** span of μm droplets in *n*-dodecane in water emulsions measured over 11 days. The *n*-dodecane in water emulsion was stabilised by three different compositions of polymers DBiB-p(OEGMA)$_{10}$-*co*-(EGDMA)$_{0.6}$ (60 mg/mL), DBiB-p(OEGMA)$_{20}$-*co*-(EGDMA)$_{0.5}$ (120 mg/mL) and DBiB-p(OEGMA)$_{50}$-*co*-(EGDMA)$_{0.95}$ (300 mg/mL). Each sample was measured in triplicate and standard deviations are given in the error bars.

2.2.6.5 Pursued studies on n-dodecane emulsions stabilised with EGDMA branched DBiB-p(OEGMA)$_{10}$ polymers

Further studies of the effect of changing the EGDMA brancher to initiator ratio in compositions of DBiB-p(OEGMA)$_{10}$-*co*-(EGDMA)$_{0.6\text{-}0.8}$ in *n*-dodecane emulsion were pursued. A composition of DBiB-p(OEGMA)$_{10}$-*co*-(EGDMA)$_{0.6}$ (30 mg/mL), DBiB-p(OEGMA)$_{10}$-co-(EGDMA)$_{0.7}$ (30 mg/mL) and DBiB-p(OEGMA)$_{10}$-co-(EGDMA)$_{0.8}$ (30 mg/mL) and the *n*-dodecane emulsions were prepared using the homogenisation procedure described in Chapter 7, section 7.1. The stability of the emulsion droplet in presence of DBiB-p(OEGMA)$_{10}$-*co*-(EGDMA)$_{0.6}$ (30 mg/mL), DBiB-p(OEGMA)$_{10}$-co-(EGDMA)$_{0.7}$ (30 mg/mL) and DBiB-p(OEGMA)$_{10}$-co-(EGDMA)$_{0.8}$ (30 mg/mL) were analysed by laser diffraction using laser diffraction and optical microscopy (Fig. 2.26 and 2.27).

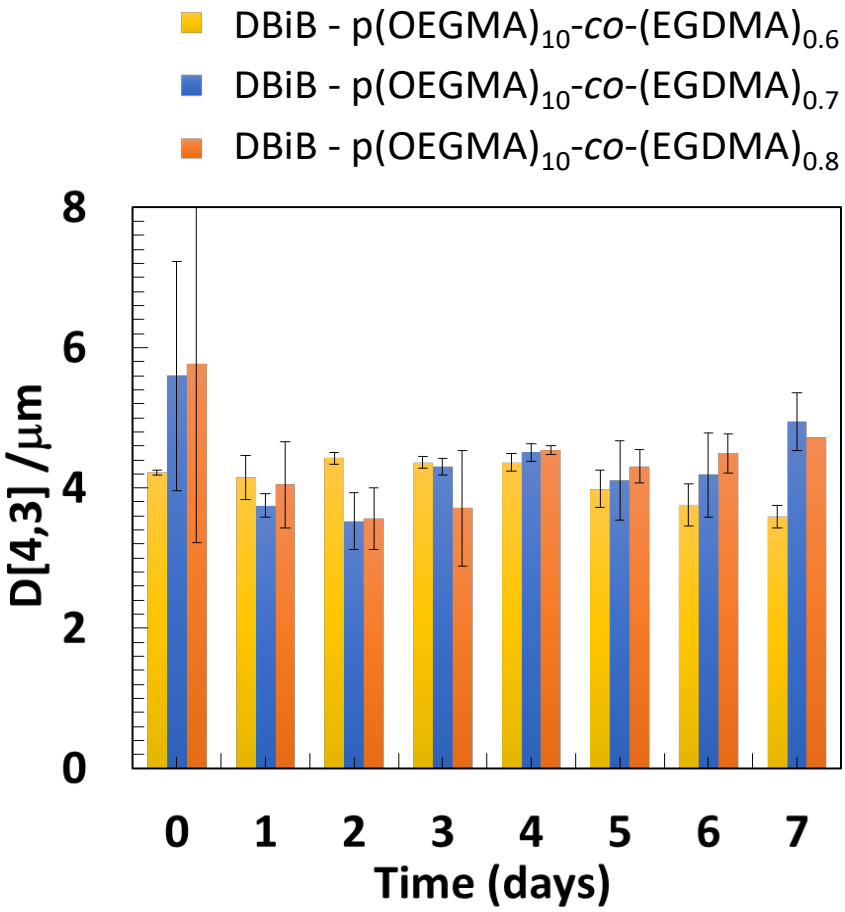

Fig. 2.26. Diagram of droplet size distribution of µm droplets in *n*-dodecane emulsions measured over 7 days. The *n*-dodecane emulsion was stabilised by three different compositions of polymers DBiB-p(OEGMA)$_{10}$-*co*-(EGDMA)$_{0.6\text{-}0.8}$ (60 mg/mL). Each sample was measured in triplicate and standard deviations are given in the error bars.

The size distribution of *n*-dodecane oil droplets stabilised with the copolymer compositions DBiB-p(OEGMA)$_{10}$-*co*-(EGDMA)$_{0.7\text{-}0.8}$ remained constant over 7 days and showed similar trend as its corresponding reference copolymer DBiB-p(OEGMA)$_{10}$-*co*-(EGDMA)$_{0.6}$, Fig. 2.26. No oil layer was observed on the top of the DBiB-p(OEGMA)$_{10}$-*co*-(EGDMA)$_{0.6\text{-}0.8}$ stabilised emulsions over 7 days. Moreover, the laser diffraction results obtained with laser diffraction measurement was compared to microscopy images collected for a *n*-dodecane emulsion stabilised by DBiB-p(OEGMA)$_{10}$-*co*-(EGDMA)$_{0.6}$ composition after 21 days, Fig. 2.27. The average sizes of the oil droplets measured to be $D_{average}$ = 2.1 μm, Fig. 2.27 b which is in agreement with data obtained by the laser diffraction Appendix Fig. A28.

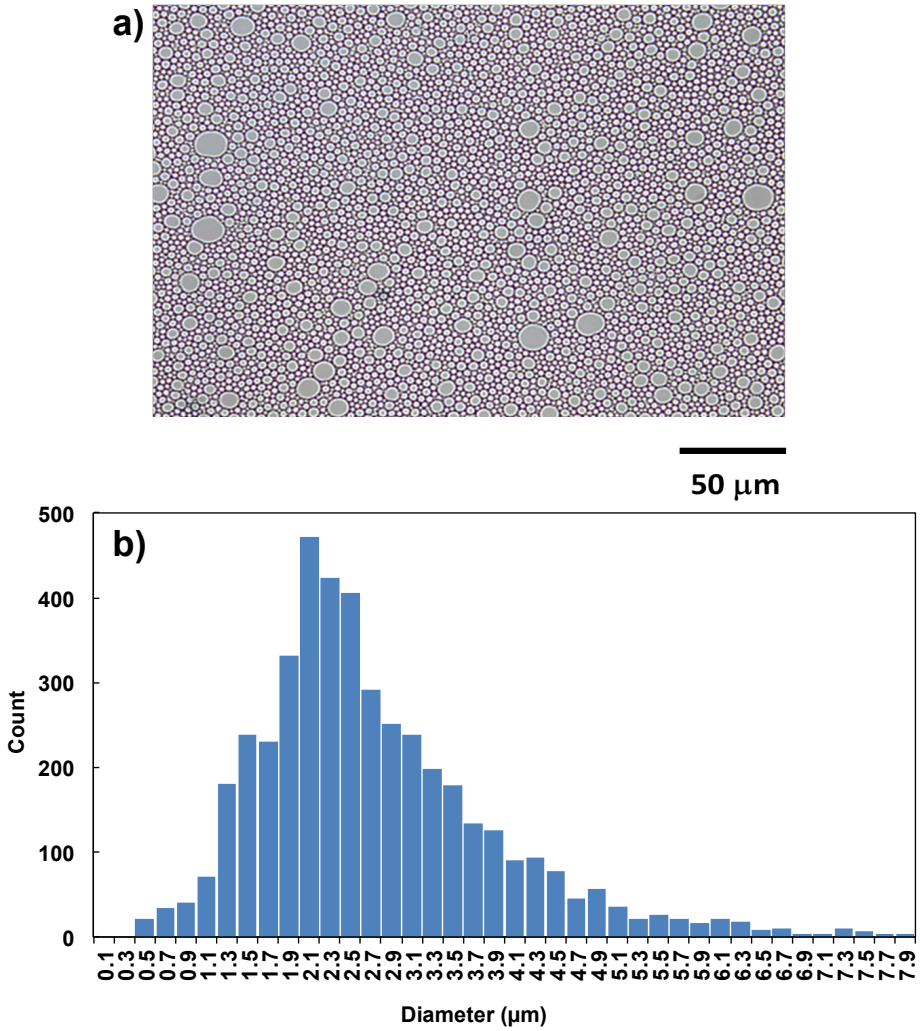

Fig. 2.27. a) *n*-dodecane oil droplets stabilised with DBiB- p(OEGMA)$_{10}$-*co*-(EGDMA)$_{0.6}$ in emulsion after day 21. **b)** Histogram of the *n*-dodecane oil droplets in water emulsion stabilised with DBiB-p(OEGMA)$_{10}$-*co*-(EGDMA)$_{0.6}$.

2.2.7 Surface tension measurements

To understand how the different polymer architectures might have different abilities to stabilise an oil in water emulsion the surface tensions of selected polymers were investigated: DBiB-p(OEGMA)$_{10}$, DBiB-p(OEGMA)$_{10}$-*co*-(EGDMA)$_{0.6}$, p(OEGMA)$_{50}$ and DBiB-p(OEGMA)$_{50}$-*co*-(EGDMA)$_{0.6}$. DBiB-p(OEGMA)$_{50}$ and DBiB-p(OEGMA)$_{50}$-*co*-(EGDMA)$_{0.6}$ were chosen to investigate how the size of a primary chain can have an impact on the surface tension. These experiments were performed in triplicate on samples prepared with concentrations between 0.004 – 10 mM. The surface tension is given in mN m^{-1} and is plotted against the concentration of the polymer in mM. The surface tension was measured using the preparation procedure described in Chapter 7 section 7.1.

The surface tensions and CMC concentrations of linear DBiB-p(OEGMA)$_{10}$ were compared against branched DBiB-p(OEGMA)$_{10}$-*co*-(EGDMA)$_{0.6,}$ Fig. 2.28 and Table 2.15, as well as against two commercial surfactant SDS and poloxamer 188.

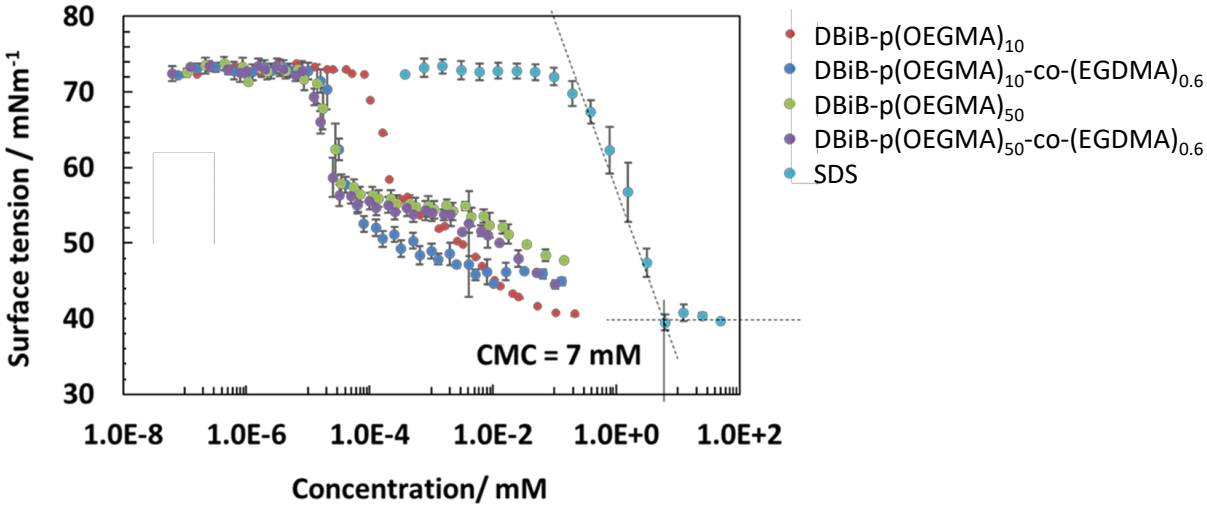

Fig. 2.28. Overlap of all of the surface tension measurements DBiB-p(OEGMA)$_{10,}$ DBiB-p(OEGMA)$_{10}$-*co*-(EGDMA)$_{0.6}$, DBiB-p(OEGMA)$_{50}$, DBiB-p(OEGMA)$_{50}$-*co*-(EGDMA)$_{0.6}$**,** SDS.

The CMC of SDS was measured to be 7 mM which was in good agreement with literature.[251] The CMC of linear DBiB-p(OEGMA)$_{10}$ was measured to be 7x10^{-3} mM which is low in comparison to SDS and poloxamer. However, the increase in targeted degree of branching, DBiB-p(OEGMA)$_{10}$-*co*-(EGDMA)$_{0.6}$, results in a much lower CMC concentration of low of

$3x10^{-4}$ mM. This showed that an increase in WA # chains from 1 to 6 for DBiB-p$(OEGMA)_{10}$ based polymers has a considerable impact on the surface activity.

In another study, the CMC concentration of linear DBiB-p$(OEGMA)_{50}$ was measured with the aim to investigate how the size of chain can have an impact on the formation of micelles by the polymer. The CMC concentration of DBiB-p$(OEGMA)_{50}$ was measured to be $7x10^{-4}$ mM. The CMC concentration of DBiB-p$(OEGMA)_{50}$ appeared to be lower than that measured for DBiB-p$(OEGMA)_{10}$. This shows that an increase in number of chain ends has an impact on the CMC concentration. The concentration of the prepared compositions were diluted from the maximum concentration of 10 mM. Due to that the measured curves did not fully reach the plateau.

Finally, the CMC concentration of synthesised linear DBiB-p$(OEGMA)_{50}$ was compared against branched DBiB-p$(OEGMA)_{50}$-*co*-$(EGDMA)_{0.6}$ and was slightly lower than that of linear DBiB-p$(OEGMA)_{50}$ of $6.5x10^{-4}$ mM.

Table 2.15. Table overviewing CMC concentration values of selected polymers.

Compound	CMC/mM
DBiB-p$(OEGMA)_{10}$	$7.0 \cdot 10^{-3}$
DBiB-p$(OEGMA)_{10}$-co-$(EGDMA)_{0.6}$	$3.0 \cdot 10^{-4}$
DBiB-p$(OEGMA)_{50}$	$7.0 \cdot 10^{-4}$
DBiB-p$(OEGMA)_{50}$-co-$(EGDMA)_{0.6}$	$6.5 \cdot 10^{-4}$
SDS	7.0
Poloxamer 188	3.2

2.2.8 Thermo responsive behaviour of DBiB-p$(OEGMA)_{10}$-*co*-$(EGDMA)_{0.6}$

OEGMA based polymers have been reported in the literature to exhibit thermoresponsive behaviour.[252,253] The thermoresponsive behaviour is entropy driven and leads to the polymer releasing bound water and essentially becoming hydrophobic; this also leads to insolubility in

water, shown schematically in Fig. 2.29. Since the applications of these materials are for the stabilisation of SLNs and some processing methods require heating, the thermoresponsive behaviour of the branched polymers was investigated.

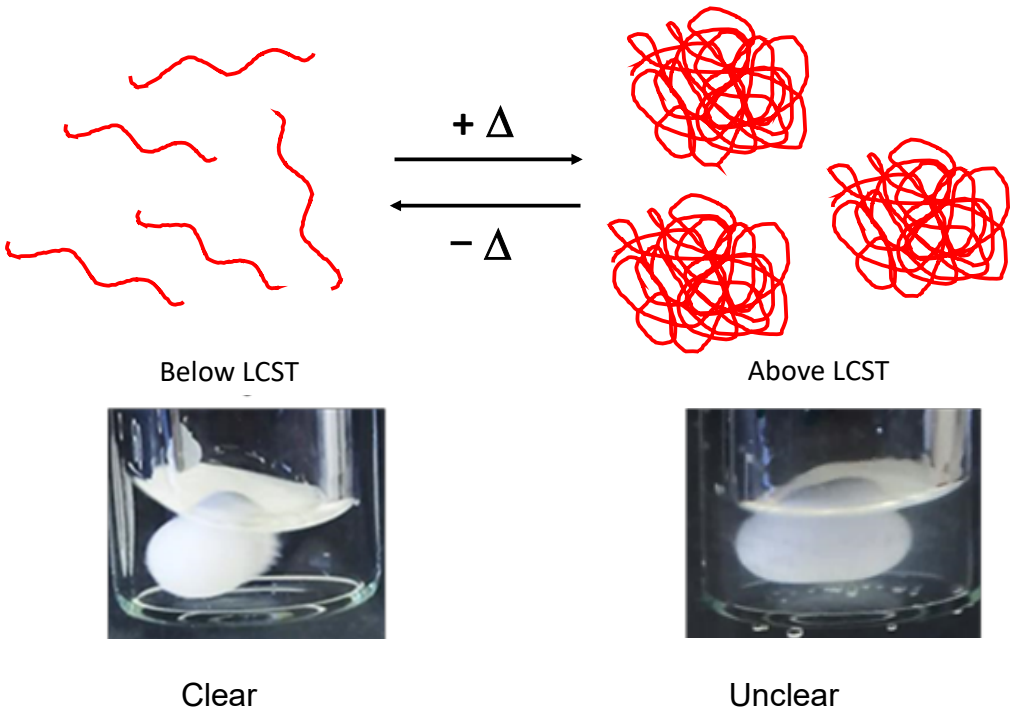

Fig. 2.29. The behavior of LCST in water. Adapted and modified from Phillips *et al*.[254]Picture on the left demonstrate a clear solution of 10 mg/mL DBiB-p(OEGMA)$_{10}$-*co*-(EGDMA)$_{0.6}$ in water and picture to the right is 10 mg/mL DBiB-p(OEGMA)$_{10}$-*co*-(EGDMA)$_{0.6}$ in water at temperature above LCST (> 52 ^{o} C) .

The cloud point of DBiB-p(OEGMA)$_{10}$-*co*-(EGDMA)$_{0.6}$ was measured at different compositions in water from 5 to 35 mg/ mL. The samples were measured using OptiMelt which is an instrument that continuously records real-time images of heated samples, and uses digital image processing to determine results.[255] The experiments were performed in triplicate of three different samples with same compositions and the cloud points (LCSTs) were determined from an extrapolation of the SRS OptiMelt automated melting-point apparatus at a heating rate of 1-2 °C/min as described in Chapter 7 section 7.1. Cloud points were determined from an extrapolation of the measured opacity above and below the cloud point back to the baseline which are indicated as a) and b) in Fig. 2.30 The cloud points were then plotted as composition of DBiB-p(OEGMA)$_{10}$-*co*-(EGDMA)$_{0.6}$ as a function of temperature, respectively. The plot showed that the cloud point was higher at lower

concentrations of the polymer where it is observed at 5 mg/mL at temperatures between 60 and 70 °C. The temperature, at which the cloud point was observed, decreases to between 52 and 53 °C when the concentration was increased to 10 mg/ mL.

The temperature at which the cloud point was possible between 55 and 65 °C while the concentration was increased to above 10 mg/ mL. The LCST of the branched polymer DBiB-p(OEGMA)$_{10}$-*co*-(EGDMA)$_{0.6}$ was concluded to vary between 52-65 °C depending on the concentration. This behaviour was reported by Luzon *et al.*[253]

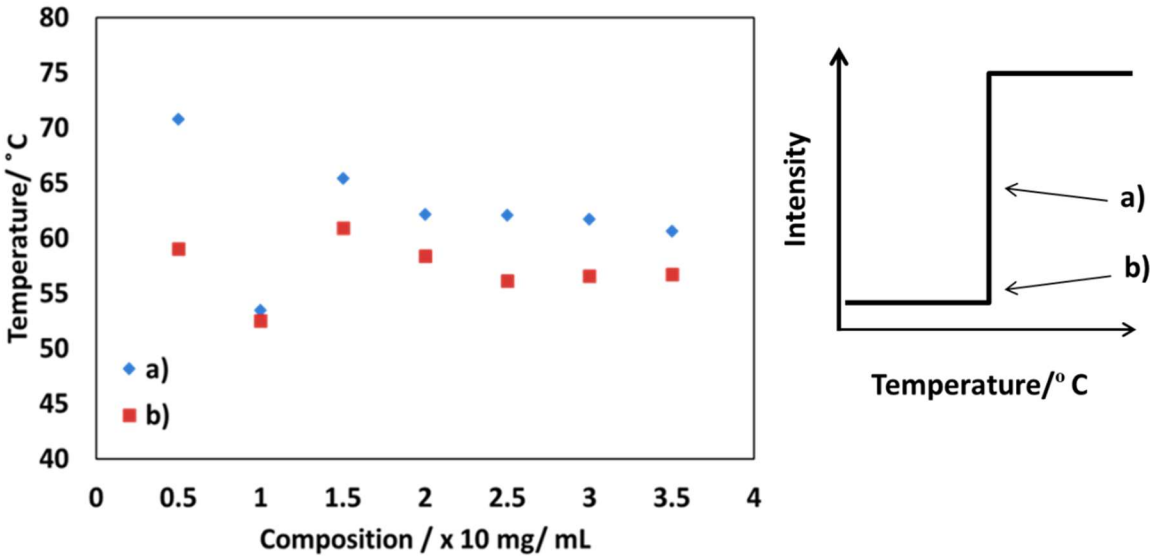

Fig. 2.30. Cloud point DBiB-p(OEGMA)$_{10}$-*co*-(EGDMA)$_{0.6}$ in water using SRS OptiMelt automated melting-point apparatus with a heating rate of 1-2 ºC. Samples were recorded with compositions of 5-35 mg/mL of DBiB-p(OEGMA)$_{10}$-*co*-(EGDMA)$_{0.6}$ in deionised water. a) and b) indicates measured opacity a) above and b) below the cloudpoint back to the baseline.

It is possible the LCST of a polymer may be modified by adding a so-called 'good' solvent to a system. Examples of research carried out with the purpose to investigate the impact of an external 'good' solvent on LCST was reported in many articles[256,257,258] and showed that addition of a 'good' solvent to a polymer composition can shift the temperature. Therefore, the cloud point of DBiB-p(OEGMA)$_{10}$-*co*-(EGDMA)$_{0.6}$ in water was investigated and effect of additional 'good' solvent on the cloud point was investigated. To modify the cloud point three solvents; ethanol, propan-1-ol and propan-2-ol were added to 1 mL a

solution of 1 mg/mL of p(OEGMA)$_{10}$-co-(EGDMA)$_{0.6}$ which was then was heated until the cloud point was observed. The solvents were added in 25 μL aliquots, which corresponded to 2.5 v/v % to separate samples with the same composition of DBiB-p(OEGMA)$_{10}$-*co*-(EGDMA)$_{0.6}$ in deionised water until the cloud points of the samples were modified to a temperature between 70 and 90 °C. The full experimental process is described in detail in chapter 7 section 7.1. The effect of the addition of the different solvents is shown in Fig. 2.31. The observed cloud points all showed a linear relationship as increasing the volume of solvent added resulted in higher cloud points. However, a factor to take into account was that the addition of more co-solvent to the same composition does lead to the dilution of the polymer. However, dilution of the polymer in deionised water can also have a minor impact on the cloud point as investigated earlier, Fig. 2.31.

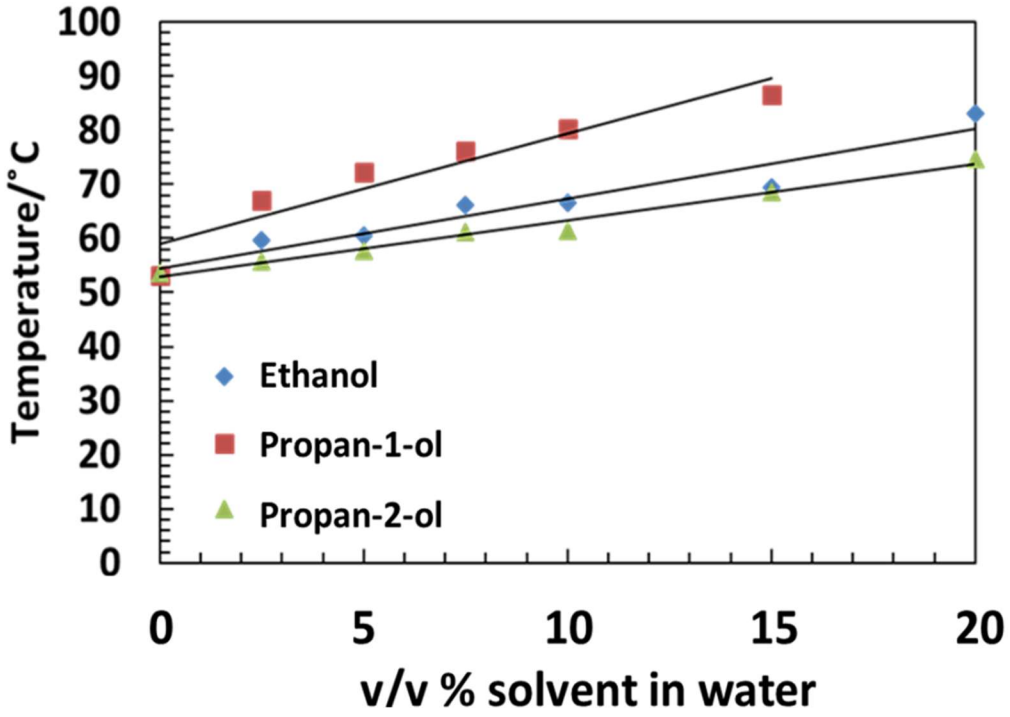

Fig. 2.31. Experiments performed to measure how addition of a co-solvent (ethanol, propan-1-ol or propan-2-ol) to the 10 mg/ml DBiB-p(OEGMA)$_{10}$-*co*-(EGDMA)$_{0.6}$ can shift the LCST.

In conclusion, the solubility of the polymer changed as more solvent was added to the copolymer mixture. It was demonstrated that adding 15.0 v/v % of propan-1-ol to 1 mL of 10

mg/mL of DBiB-p(OEGMA)$_{10}$-*co*-(EGDMA)$_{0.6}$ alters the cloud point from 53 to 87 °C. However, this maximum change in cloud point was only observed for propan-1-ol. The maximum addition of ethanol to 1 mL of 1 mg/mL DBiB-p(OEGMA)$_{10}$-*co*-(EGDMA)$_{0.6}$ was 20.0 v/v % led to an increase in cloud point from 53 to 83 °C. While, the maximum addition of propan-2-ol to 1 mL of 10 mg/mL DBiB-p(OEGMA)$_{10}$-*co*-(EGDMA)$_{0.6}$ 20.0 v/v % and this lead to a shift in cloud point from 53 to 74 °C.

2.3 Conclusion

A library of OEGMA based polymers synthesised with DBiB-p(OEGMA)$_{10\text{-}50}$ The performance of the polymers as stabilisers for an emulsion was tested using *n*-dodecane as a model oil. This study allowed the effect of the different composition variables of the polymers in the library to be investigated These variables included the length of the primary chain, the targeted degree of branching, the effect of concentration and the effect of the number average chain ends WA #. The *n*-dodecane emulsion studies demonstrated that DBiB-p(OEGMA)$_{10}$-*co*-(EGDMA)$_{0.6\text{-}0.8}$ were the best stabilisers to continue with in subsequent studies of SLNs with a concentration of 60 mg/ mL.

The subsequent studies of DBiB-p(OEGMA)$_{10}$-*co*-(EGDMA)$_{0.6}$ were to measure the CMC concentration and compare it against DBiB-p(OEGMA)$_{10}$. The results demonstrated that DBiB-p(OEGMA)$_{10}$-*co*-(EGDMA)$_{0.6}$ has lower CMC concentration of $3x10^{-4}$ mM than that of DBiB-p(OEGMA)$_{10}$. This demonstrates that the CMC concentration of the polymer does not have any impact on how the polymer stabilise the 1:1 v/v ratio *n*-dodecane in water emulsion.

The final experiment that was performed with the aim to measure the cloud point of DBiB-p(OEGMA)$_{10}$-*co*-(EGDMA)$_{0.6}$ which was 52 - 53 ° C for 10 mg/ mL composition. The understanding of the cloud point of DBiB-p(OEGMA)$_{10}$-*co*-(EGDMA)$_{0.6}$ was useful, as SLN processing required lots of heat, often 5-10 degrees above the melting point of a solid lipid.

However, in case that heat interfered with the functionality of DBiB-p(OEGMA)$_{10}$-*co*-(EGDMA)$_{0.6}$ in the SLN production other compositions were investigated. Nevertheless, it was demonstrated that the cloud point of DBiB-p(OEGMA)$_{10}$-*co*-(EGDMA)$_{0.6}$ could be modified about 10-20 °C by adding an additional water miscible solvent such as ethanol, propan-1-ol and propan-2-ol to a resulting composition of 1 mg/ mL of DBiB-p(OEGMA)$_{10}$-*co*-(EGDMA)$_{0.6}$ in deionised water.

Chapter 3 Synthesis, optimisation and stability studies of OEGMA based polymer stabilised SLNs

3.1 Introduction

In Chapter 2 the performance of oligo (ethylene glycol) methacrylate (OEGMA) based stabilisers in *n*-dodecane emulsion studies was studied. The copolymer architecture with the best performance was the branched copolymer, DBiB-p(OEGMA)$_{10}$-*co*-(EGDMA)$_{0.6}$. This polymer will be tested on SLN platforms for anti-HIV treatments which have been developed with the aim of encapsulating drugs with poor water solubility and bioavailability.[104,202,214,215] In addition, a series of comparison materials, namely DBiB-p(OEGMA)$_{10}$ and poloxamer 188, were selected and studied to establish stability of various SLN candidates. Those were chosen with the aim to compare the stability of the surfactant in solid lipid system with liquid lipid emulsion, which was synthesised in Chapter 2.

The excipient chosen to use as the core of the SLNs was Compritol ATO 888, which is also known as glycerol dibehenate.[94] It has a molecular weight of 737.23 Da and its structure is given in Fig. 3.1.

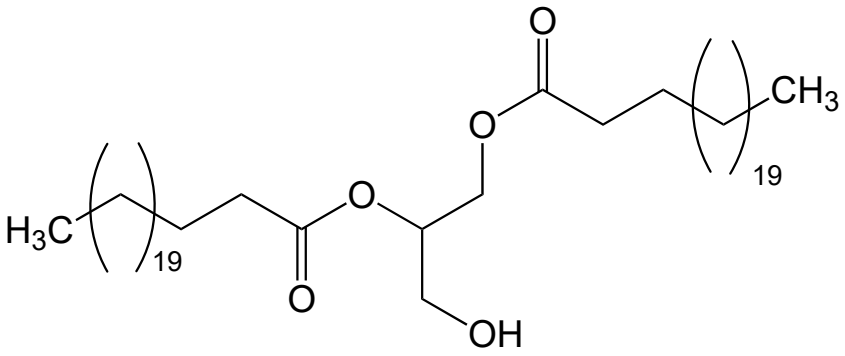

Fig. 3.1. Chemical structure of glyceryl dibehenate (Compritol ATO 888).[94]

Compritol ATO 888 a commonly used excipient in SLN preparation.[94,105,138,202,259] It is considered to be safe according to generally recognised as safe (GRAS) status.[260] Compritol ATO 888 is considered a high melting point lipid with a melting point of 70˚C.[94] This high melting point rules out various preparation procedures described in Chapter 1 which could otherwise be used to process drug loaded SLNs. Specifically, only heat processing or the use of an organic solvent such as chloroform or dichloromethane is applicable to Compritol ATO 888.[122,137] The hot homogenisation process requires Compritol ATO 888 to be heated 5-15 °C above its melting temperature[104,150,261] in order to be dispersed into water in

presence of a polymer/stabiliser.[104] However, it was shown in Chapter 2 section 2.2.5 that the lower critical solvent temperature (LCST) of the polymer we have selected DBiB-p(OEGMA)$_{10}$-*co*-(EGDMA)$_{0.6}$ of 52 - 53 °C for a composition of 1 mg/ mL water, is below the melting point of Compritol ATO 888 which is 70 °C. In this chapter will discuss the results obtained for different processing procedures assessed to produce SLNs of Compritol ATO 888 stabilised by DBiB-p(OEGMA)$_{10}$-*co*-(EGDMA)$_{0.6}$. Specifically, the processing procedures which were attempted were hot high shear homogenisation, hot probe sonication and solvent injection method with the purpose to optimise and reproduce the formation of SLNs in a system stabilised with DBiB-p(OEGMA)$_{10}$-*co*-(EGDMA)$_{0.6}$.

Hot high shear homogenisation is the most commonly used method to prepare SLNs and its process was described in Chapter 1, Fig. 1.6. [12,15] The process involves heating the lipid, in presence or absence of a solvent, 5-15 °C above the melting temperature of the lipid, in the presence or absence of drug. Hot homogenisation is performed differently in some literature reports. In one case, the lipid and drug is heated separately and added to a solution of water containing a polymer followed by homogenisation. In another case the lipid, polymer and drug are heated in the water followed by homogenisation.[104] One use of hot homogenisation has been to prepare lopinavir loaded SLNs. This experiment was performed by melting 100 mg lopinavir and 5.334 g Compritol 888 ATO at 80 °C. Poloxamer 188 was dissolved in double distilled water to obtain a 25 mg/mL solution and the resulting sample was heated up to 80 °C in a beaker. Once a clear homogenous lipid phase was obtained, the hot aqueous surfactant solution was added to hot lipid phase and homogenisation was carried out at 10,000 rpm, for 2 min. The temperature was maintained at 80 °C during the homogenisation step. The conclusion of this study was that they obtained lopinavir loaded SLNs with mean particle diameter of 230 nm (PDI < 0.27). [104]

Alternatively, hot probe sonication was considered for the synthesis of SLNs, as it has a stronger mechanical power than hot homogenisation.[263,228,264] One use of probe sonication has been to make ramipril loaded SLNs.[228] This procedure was carried out by adding a hot

solution of polymeric surfactants (tween 80, poloxamer or span 20) to an oil phase that was heated 5 °C above the lipid's melting temperature, then this was homogenised for 30 min at 25,000 rpm at 70 °C followed by probe sonication for 25 min before finally being cooled down and stored at 4 °C.[228]

Finally, solvent injection can be used to produce SLNs. This method was first introduced by Müller-Goymann and Schubert *et al* in 2003.[124,125] In this experiment they used various lipids (Softisan® 100, Softisan® 142, Softisan® 154, Witepsol® H35, Cetyl palmitate, Softisan®, Softisan® 100, Softisan 142, Witepsol® H35, Cetyl palmitate) dissolved in a range of water-miscible solvents (acetone, ethanol, ethylacetate, methanol, isopropanol, 85% glycerol, bidistilled water) in a water-miscible solvent mixture (1-100 mg/ml) heated up to 80 °C. Subsequently, the hot mixture was rapidly injected through an injection needle into a stirred (330 rpm aqueous phase with or without surfactant. They concluded that the resulting SLNs had a size distributions ranging from 80 and 300 nm depending on the preparation conditions.[124] Other similar studies have been performed with other lipid excipients such as glycerine monostearate (GMS), tefose-63,[125,265] and Compritol ATO 888.[266] The solvent injection method features many similarities to polymer nanoprecipitation.[267] Polymer nanoprecipitation uses a water miscible 'good solvent' for a hydrophobic polymer used for the core of the particles such as acetone, ethanol, propanol and isopropanol and active pharmaceutical ingredients (API) which is then precipitated it into a 'poor solvent' of stabiliser polymer dissolved into water[267,192] and these approaches has been widely studied over the past years using other water miscible solvents such as tetrahydrofuran, dimethylformamide and acetone with the aim to synthesise branched copolymer nanoparticles.[192,189,188,185] The preparation of SLNs by solvent injection includes a water miscible 'good solvent' that is heated above the melting temperature of the lipid along with the API. This solvent solution of lipid and API is then injected into the 'bad solvent' which contains the polymer stabiliser in water. This method was considered useful for this current study as it allows the temperature

of the water to be kept at a temperature below the LCST of the OEGMA-based polymer (52 - 53 °C) discussed in Chapter 2 section 2.2.5.

3.2 Results and discussion

3.2.1. Synthesis of p(OEGMA) based polymer stabilised drug-free SLNs using homogenisation approach

The hot high-shear homogenisation method, previously proposed for the preparation of solid lipid microparticles (SLM)[268] was evaluated using the experimental procedure described in Chapter 7 section 7.2. The use of hot high-shear homogenisation appeared to be a suitable and rapid technique for the production of SLNs and was a typical method used in literature.[104,153,262] High-shear homogenisation was an attractive method to use for SLN production due to its one-step process that resembles the simple preparation of an O/W emulsion, Fig. 3.2.

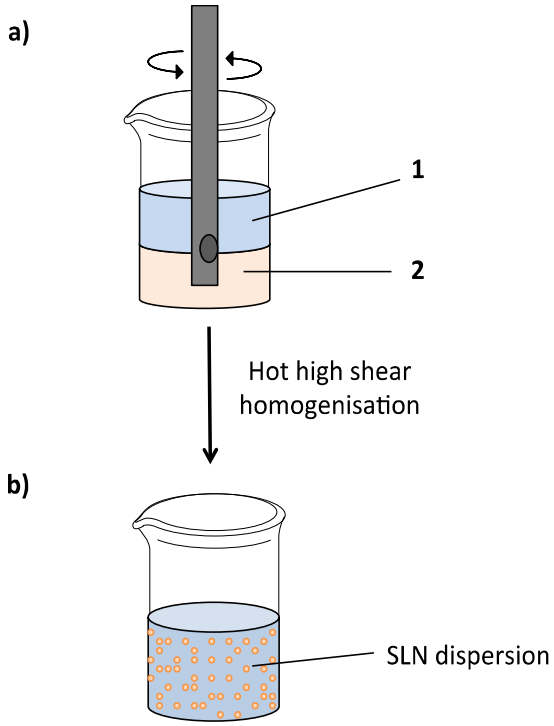

Fig. 3.2. Hot high shear homogenisation for synthesis of SLNs. a) stirring with homogeniser and b) formation of SLN dispersion. 1 is the water phase with a polymer dissolved and 2 is the oil phase in presence or absence of a water miscible solvent.

As reported in experimental section Chapter 7 section 7.2, various polymer to lipid (DBiB-p(OEGMA)$_{10}$-*co*-(EGDMA)$_{0.6}$ to Compriol ATO 888) w/w ratios were studied, namely 1:1-1:4, 1:7 and 1:10, with the total solid content (polymer + lipid) kept to 1.1 g in 10 mL of deionised water. The process was conducted in the absence of additional solvent or utilised a range of water-miscible solvents such as IPA, n-propanol, acetone or ethanol to establish the optimum conditions. All prepared formulations were studied by DLS. The DLS measurements showed no traces or abnormal measurements on the runs. Those observations indicated none of the materials generated using this approach were successful. The selected samples of 1:1-1:3 w/w % ratio of DBiB-p(OEGMA)$_{10}$-*co*-(EGDMA)$_{0.6}$ to Compritol ATO 888 given, Fig. 3.3, were observed to sediment or form turbid and white suspension straight after cooling from the hot high-shear homogenisation.

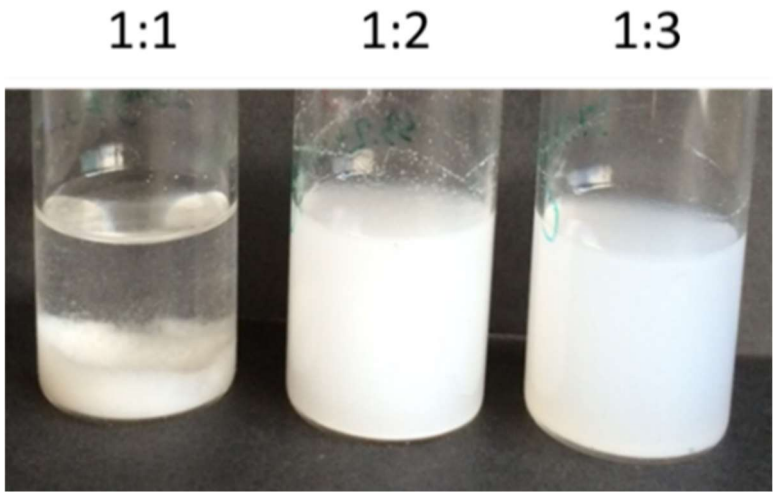

Fig. 3.3 Selected unsuccessful samples with 1:1 - 1:3 w/w ratio of DBiB-p(OEGMA)$_{10}$-*co*-(EGDMA)$_{0.6}$: Compritol ATO 888 with a total solid content of of 1.1 g in deionized water prepared by hot high shear homogenisation 5 min at 25,000 rpm. Photo of the samples were taking straight after cooling. Photos show tubid solutions with sedimentation.

As the hot high-shear homogenisation experiment did not work for the former mentioned compositions other preparation methods were investigated to understand the conditions in which SLNs can form. There are no literature studies investigating the effect of probe sonication *versus* homogenisation of drug-loaded SLNs, therefore a study of the effectiveness of probe sonication was undertaken.

3.2.2 Synthesis of p(OEGMA) based polymer stabilised drug-free SLNs using sonication

As the hot high shear homogenisation technique used in former section 3.2.1 resulted in sedimentation a hot probe sonication procedure was attempted. The hot probe sonication was performed using a modified literature approach.[134] The compositions were chosen as for the hot high shear homogenisation experiments which were described in the previous section and comprise samples with different ratios of polymer to lipid (DBiB-p(OEGMA)$_{10}$-*co*-(EGDMA)$_{0.6}$: Compritol ATO 888) w/w ratio of 1:1-1:10. The total solids content of (Compritol ATO 888 and DBiB-p(OEGMA)$_{10}$-*co*-(EGDMA)$_{0.6}$) was maintained at 1.1 g in 10 mL. The resulting lipid dispersions also failed to make SLNs. A photograph of selected samples is shown in Fig. 3.4. All three selected samples were analysed by observing their appearance straight after cooling with the naked eye and an attempt to measure the diameter of the SLNs present in the sample was made using DLS. All of the samples showed visual sedimentation and the DLS analysis was unable to provide reliable data. Based on those observations the experiment was considered to be unsuccessful.

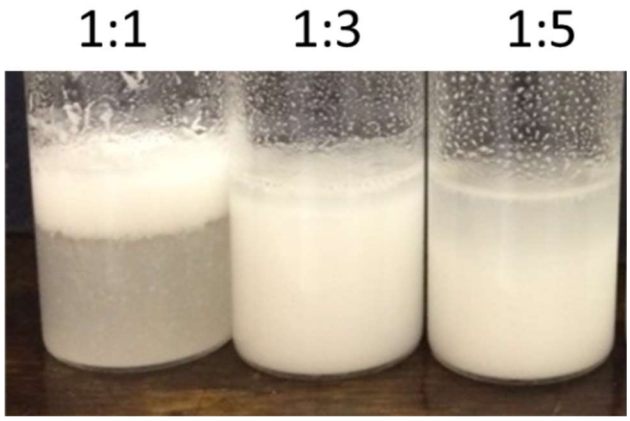

Fig. 3.4. Selected unsuccessful samples prepared with 1:1, 1:3 and 1:5 DBiB-p(OEGMA)$_{10}$-*co*-(EGDMA)$_{0.6}$ to Compritol ATO 888 w/w ratio with a total solid content of 1.1 g in deionised water prepared by hot sonication: 5 min, 100 %, 1 cycle and immediate cooling in ice bath at 0 °C. Samples show turbid solutions with sedimentation.

Using high mechanical power methods such as hot high shear homogenisation and hot sonication to form SLNs were unsuccessful. The reason why these approaches did not work

is unknown. However, we hypothesised that the heating of DBiB-p(OEGMA)$_{10}$-*co*-(EGDMA)$_{0.6}$ might have an impact on the formation of SLNs due to the observed low LCST values of this branched copolymer. This could also be due to the power of the mechanical stirring. The lack of success of homogenisation and sonication techniques suggested that other SLN processing methods would be needed for the current system and solvent injection methods were therefore adopted.

3.2.3 Synthesis of p(OEGMA) based polymer stabilised SLNs using solvent injection

3.2.3.1 Initial optimisation of solvent injection method – optimisation of Lipid: polymer ratio and total mass

Solvent injection was initially described by Schubert and Müller Goymann in 2003[124], and subsequent studies demonstrated the use of solvent injection for synthesis of SLNs.[125,110,269] A schematic illustration of the solvent injection method is given in Fig 3.5. This figure illustrates the parameters, which can be controlled such as stirring, temperature and angles in while the injection is performed. All the controlled parameters determine the outcome of the SLN product. Schubert and Müller Goymann in 2003[124] tested this method with many polymers or surfactants and lipids in water miscible organic solvents such as acetone, ethanol and isopropanol (IPA).[124] However, the system needs to be optimised so that we can integrate the use of DBiB-p(OEGMA)$_{10}$-*co*-(EGDMA)$_{0.6}$ into the solvent injection approach. IPA was chosen as the water miscible solvent in the solvent injection as it has a high boiling point of 82.6 °C which is needed to dissolve Compritol ATO 888 that has a melting temperature of 70 °C. Many considerations were made in choosing these conditions. This approach only heats the lipid in this case Compritol ATO 888 in a water miscible solvent, Fig. 3.5I). Importantly, this approach avoids heating the polymer as shown in Fig. 3.5 II). The polymer, DBiB-p(OEGMA)$_{10}$-*co*-(EGDMA)$_{0.6}$, can be dissolved in water at 25 °C which is below the low critical solution temperature (LCST) above which the polymer can no longer

be dissolved. The LCST was found for DBiB-p(OEGMA)$_{10}$-*co*-(EGDMA)$_{0.6}$ to be = 52 °C in Chapter 2. The hot mixture of lipid in water-miscible solvent can be rapidly injected into a stirred mixture of DBiB-p(OEGMA)$_{10}$-*co*-(EGDMA)$_{0.6}$ in water followed by rapid cooling to, Fig. 3.5a. This results in a SLN dispersion stabilised by DBiB-p(OEGMA)$_{10}$-*co*-(EGDMA)$_{0.6}$ 25 °C, Fig. 3.5 III). It is not known for certain whether the LCST influences the outcome for the SLN creation. However, solvent injection is unique in that it allows control over this parameter.

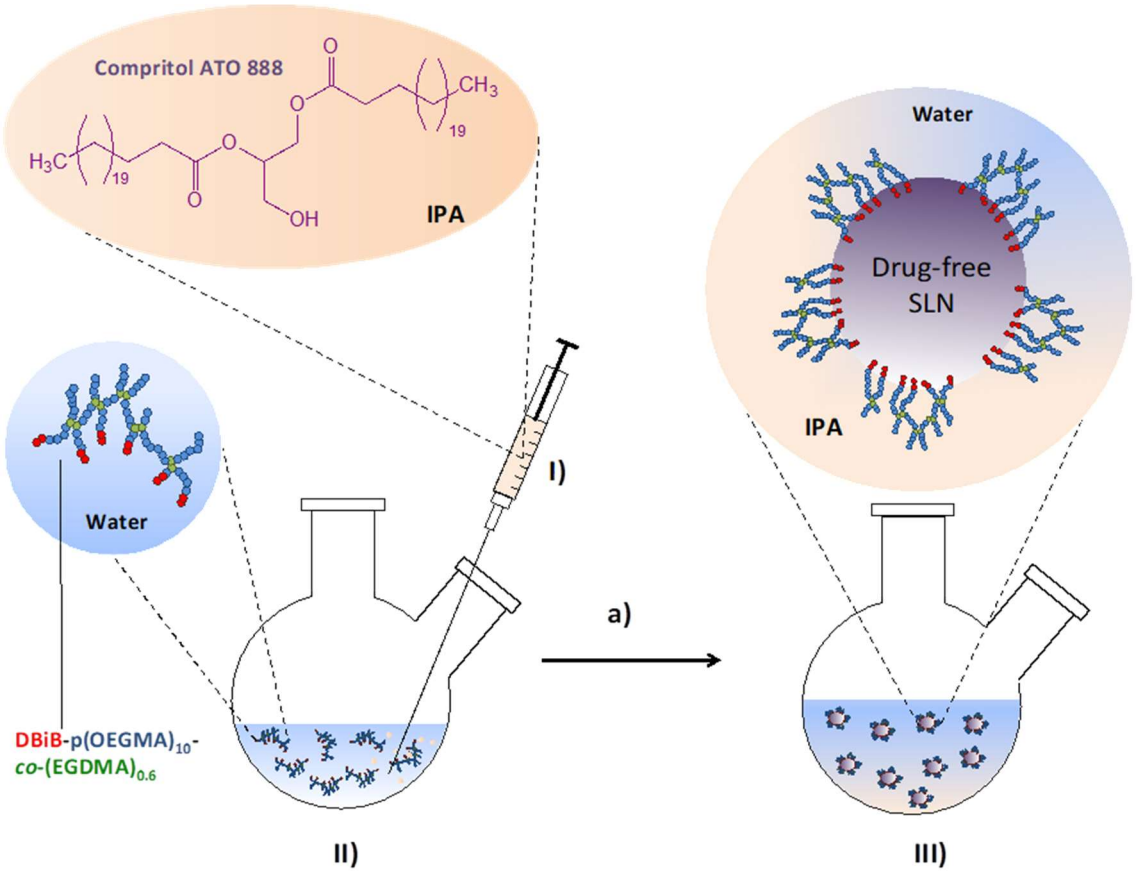

Fig. 3.5. Illustration of solvent injection method conditions and principles. **I)** IPA containing Compritol ATO 888 at 80 °C **II)** Deionised water and DBiB-p(OEGMA)$_{10}$-*co*-(EGDMA)$_{0.6}$ at 25 °C, **a)** 5 min, 300 rpm stirring at ambient temperature, **III)** drug-free SLN dispersion.

In the studies of this method the w/w ratios of DBiB-p(OEGMA)$_{10}$-*co*-(EGDMA)$_{0.6}$ to Compritol ATO 888 was varied and the tested ratios were given on Table 3.1.

Table 3.1. Compositions of Lipid (Compritol ATO 888) to polymer (DBiB-p(OEGMA)$_{10}$-*co*-(EGDMA)$_{0.6}$) ratios tested in the solvent injection method. The code given in the table is the sample number.

Code	Lipid/mg	pol./mg	Ratio lipid:pol.	Water/ mL
a	6	36	1:6	10
b	6	18	1:3	10
c	6	12	1:2	10
d	6	6	1:1	10
e	12	6	2:1	10
f	18	6	3:1	10

The experiments follow procedures described on Chapter 7 section 7.2. After the injection step the samples were immediately cooled down to 4 °C and stored in the fridge for later purification the cooling was performed as it prevents the resulting formulation in forming a turbid solution followed by aggregation of the particles in the sample. It was hypothesised that cooling is necessary for the resulting suspension as the IPA present after the injection could have an impact on dissolving the SLNs or causing SLN to agglomerate. Furthermore, the storage of SLNs in the fridge has been demonstrated in similar types of systems.[270,95] However, it has not been reasoned why it is necessary to store the SLNs in the fridge after formulation processing. The samples that were stored in the fridge at 4 °C were analysed and characterised by DLS with the aim to assess the size and stability of the different compositions derived from experiments with varying parameters as shown in Table 3.1 with a range of total solid contents of DBiB-p(OEGMA)$_{10}$-*co*-(EGDMA)$_{0.6}$ + Compritol ATO 888 from of 4.2 - 0.6 mg/mL in deionised water containing IPA. The samples were stored in the fridge and D_z was analysed by DLS after day 1, 3 and 5 in presence of IPA, see Fig. 3.6 and corresponding measurements are given in Appendix Fig. A40-41. The w/w ratio of 1:6 DBiB-p(OEGMA)$_{10}$-*co*-(EGDMA)$_{0.6}$ to Compritol ATO 888 were not stable after just 3 days according to the DLS measurements due to aggregation of the sample. Visual observation, Fig. 3.6, of the resulting sample of 1:6 DBiB-p(OEGMA)$_{10}$-*co*-(EGDMA)$_{0.6}$ showed a turbid dispersion that could be formed due to aggregation of materials in the dispersion, Fig. 3.6.

The analysed w/w ratio of 3:1 DBiB-p(OEGMA)$_{10}$-*co*-(EGDMA)$_{0.6}$ to Compritol ATO 888 SLN sample did not show reliable DLS data due to sedimentation. However, DLS measurements analysed for ratios of 1:3, 1:2, 1:1 and 2:1 of DBiB-p(OEGMA)$_{10}$-*co*-(EGDMA)$_{0.6}$ to Compritol ATO 888 showed that the resulting formulations were stable after 5 days with a an SLN diameter of 150-200 nm and a PDI distribution between 0.2-0.3. The observation of the samples on the photograph in Fig. 3.6 showed clear SLN dispersions.

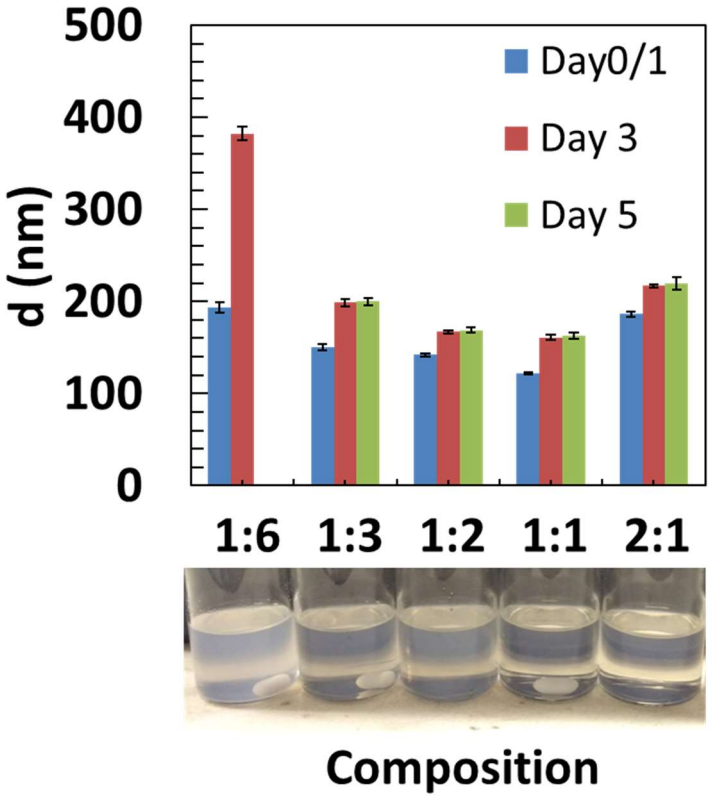

Fig. 3.6. Initial experiments with different ratios of DBiB-p(OEGMA)$_{10}$-*co*-(EGDMA)$_{0.6}$ and Compritol ATO 888 in deionised water. The solvent injection method was performed with DBiB-p(OEGMA)$_{10}$-*co*-(EGDMA)$_{0.6}$ to Compritol ATO 888 w/w ratios of 1:6, 1:3, 1:2, 1:1 and 2:1 in deionised water.

In general, w/w ratios of DBiB-p(OEGMA)$_{10}$-*co*-(EGDMA)$_{0.6}$ to Compritol ATO 888 ranging from 1:3 to 2:1 appeared to generate stable SLNs with D_z values <250 nm. However, interest in this study was directed towards minimising the amount of polymer to stabilise the highest amount of Compritol ATO 888 in a system. Therefore, the ratio of 1:3 (DBiB-p(OEGMA)$_{10}$-*co*-(EGDMA)$_{0.6}$ to Compritol ATO 888), containing the least amount of polymer, was progressed to more detailed studies.

3.2.4 Optimisation of solvent injection method

In summary, it has been demonstrated that a system with a 1:3 (DBiB-p(OEGMA)$_{10}$-*co*-(EGDMA)$_{0.6}$ to Compritol ATO 888) ratio is the most favourable studied ratio to continue with as it allows maximum hydrophobic material to be encapsulated with the use of minimum stabilisers. In addition to that, we focussed on optimising the system in terms of the total mass of polymer and lipid varied within the ratio of 1:3 in 10 mL of deionised water. The aim here was to investigate if it was possible to tune parameters such as particle size and stability in the resulting empty SLN formulations. From the results obtained in the previous section three different total compositions were considered and those were between 1.2-4.2 mg (DBiB-p(OEGMA)$_{10}$-*co*-(EGDMA)$_{0.6}$ + Compritol ATO 888) pr. 1 mL deionised water containing 0.2 mL IPA. The total concentration of the 1:3 (DBiB-p(OEGMA)$_{10}$-*co*-(EGDMA)$_{0.6}$: Compritol ATO 888) wt./wt. ratio was 2.4 mg/mL water containing 0.2 mL of IPA and interest was focussed on investigating experimental reproducibility and stability of this successfully chosen system. For this study of total solid content of (DBiB-p(OEGMA)$_{10}$-*co*-(EGDMA)$_{0.6}$ + Compritol ATO 888) of 2.4 mg, 1.8 mg and 1.2 mg pr. mL of deionised water containing 0.2 mL of IPA were conducted and the compositions for the three experiments are given in Table 3.2.

Table 3.2. Compositions of DBiB-p(OEGMA)$_{10}$-*co*-(EGDMA)$_{0.6}$ and Compritol ATO 888 used in solvent injection optimisation studies. MC; mass content, TM; total mass, lipid = Compritol ATO 888, Polymer = DBiB-p(OEGMA)$_{10}$-*co*-(EGDMA)$_{0.6}$ in water.

MC/ mmol	TM/mg/mL	Lipid/ mg	Lipid/ mmol	Polymer/ mg	Polymer/mmol	Water/ mL	IPA/mL
0.01208	1.2	9	0.012	3	0.00008	1	0.2
0.01812	1.8	13.5	0.018	4.5	0.00012	1	0.2
0.02416	2.4	18	0.024	6	0.00016	1	0.2

The solvent injection experiments were performed with the solvent injection procedure optimised in earlier section and as described in chapter 7 section 7.2. The size distribution of SLN in the samples containing solid content composition of 2.4 mg/mL, 1.8 mg/mL and 1.2 mg/mL water containing 0.2 mL IPA were measured the DLS traces and corresponding D_z

and PDI of the samples evaluated. The size distribution of 1.8 mg/mL and 1.2 mg/mL are shown in Fig. 3.7a. The size distribution of 2.4 mg/ mL water containing 0.2 mL IPA were not reliable due to aggregation. However, the particle size distribution of 1.8 mg/mL and 1.2 mg/mL were very similar and the D_z values were measured to be 189 and 171 nm, respectively. The increase in the D_z suggests that the slight increase of the solid content of 0.4 mg/mL resulted in only a very small change to the overall sample. The PDI distribution was measured to be in the range of 0.2-0.3, which indicates that the sample has a relatively broad distribution in Fig. 3.7a.

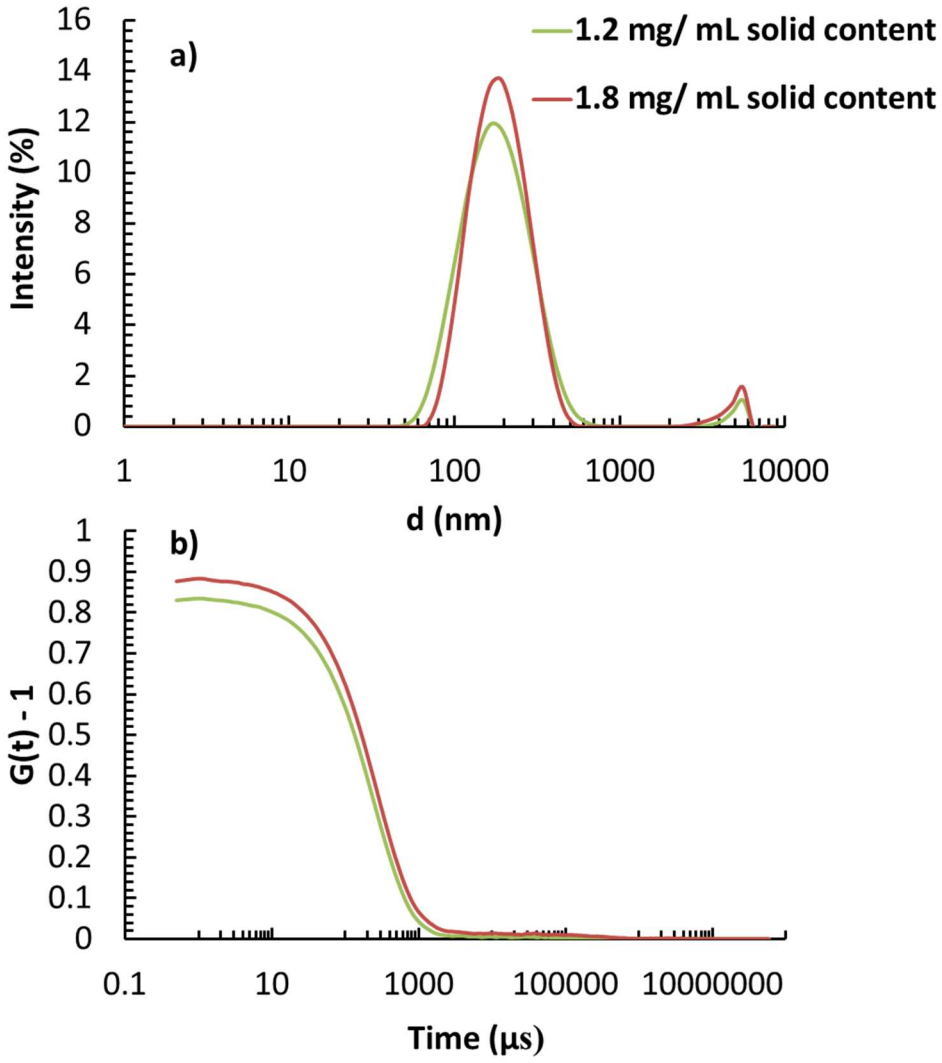

Fig. 3.7 Preliminary SLN experimental conditions: Compritol ATO 888 to DBiB-p(OEGMA)$_{10}$-*co*-(EGDMA)$_{0.6}$ ratio in 10 mL of water (pH= 6), 2 mL isopropanol. **a)** Overlaid size distributions of prepared samples with a total solid content of 1.2 or 1.8 mg/mL (1:3 DBiB-p(OEGMA)$_{10}$-*co*-(EGDMA)$_{0.6}$: Compritol ATO 888). **b)** correlogram of DLS measurements

The observation of the sample with total solid content of 2.4 mg/mL with a ratio of 1:3 w /w (DBiB-p(OEGMA)$_{10}$-*co*-(EGDMA)$_{0.6}$ to Compritol ATO 888) were given in Fig. 3.7b. This Figure showed a turbid drug-free SLN dispersion. When decreasing the total amount of solid content (DBiB-p(OEGMA)$_{10}$-*co*-(EGDMA)$_{0.6}$ to Compritol ATO 888) from 2.4 mg/ mL to 1.8 and 1.2 mg/mL of deionised water containing 0.2 mL IPA the sample becomes more transparent, Fig. 3.8a-b. However, the DLS measurements for the drug-free SLN dispersion with a total solid content of 1.8 mg/mL (DBiB-p(OEGMA)$_{10}$-*co*-(EGDMA)$_{0.6}$ + Compritol ATO 888) in water/ IPA were reliable. As 1.2 mg/mL of solid content in deionised water containing IPA gave the best and most reproducible results this led to creating a system in which it is possible to compare and test other polymers. As a result, the formulation containing a total mass of 1.2 mg/ mL of deionised water containing IPA, Fig. 3.8c, was tested with the three different polymers: linear DBiB-p(OEGMA)$_{10}$, branched DBiB-p(OEGMA)$_{10}$-*co*-(EGDMA)$_{0.6}$ and DBiB-p(OEGMA)$_{50}$-*co*-(EGDMA)$_{0.5}$ and poloxamer 188 which are discussed in the next section.

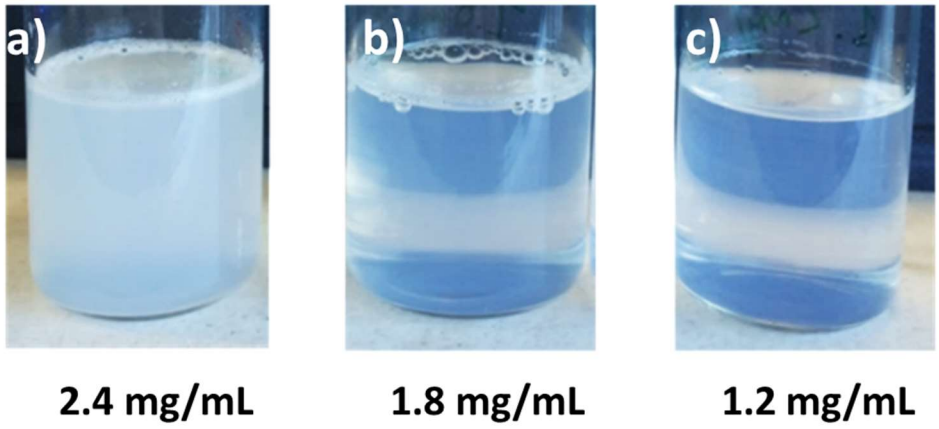

Fig. 3.8. Photography of drug-free SLN dispersions syntesised with following compositions: **a)** 18 mg of Compritol ATO 888 and 6 mg of polymer in 10 mL of water containing 20 v/v % isopropanol resulting in an unclear dispersion **b)** 13.5 mg of Compritol ATO 888 and 4.5 mg of polymer in 10 mL of water containing 20 v/v % isopropanol resulting in a clear dispersion **c)** 9 mg of Compritol ATO 888 and 3 mg of polymer in 10 mL of water containing 20 v/v % isopropanol resulting in a clear dispersion. Samples were photographed 1 hour after solvent injection.

3.2.5 Polymer to lipid ratio optimisation experiment

There were two aims when performing the experiments in this section. The first aim of these experiments was to test how the ratios with a total solid content of 1.2 mg (polymer + Compritol ATO 888) in 10 mL of water can change the behaviour of size and stability of the empty SLNs in a resulting dispersion. The second aim was to compare the behaviour of the different polymers in SLN systems by characterising the morphological behaviours and physio chemical characterisations.

In summary, the optimised solvent injection experiments demonstrated that the 1:3 w/w ratio (DBiB-p(OEGMA)$_{10}$-*co*-(EGDMA)$_{0.6}$ to Compritol ATO 888) with a solid content of 1.2 mg in water/IPA produced the most reproducible results. This lead to an established experimental condition that allow us to test other parameters. One parameter to test in this study was the effect of changing the ratio of polymer to lipid in 1.2 mg/mL of deionised water containing IPA as this composition system has not yet been investigated for DBiB-p(OEGMA)$_{10}$-co-(EGDMA)$_{0.6}$. Another experiment performed was to test the established system with other polymers including DBiB-p(OEGMA)$_{10}$ and poloxamer 188. DBiB-p(OEGMA)$_{10}$ could be interesting to compare with DBiB-p(OEGMA)$_{10}$-*co*-(EGDMA)$_{0.6}$ drug-free SLN systems. This allows us to understand more about the stabilising property of a primary chain *versus* branched copolymer chain in SLN systems. Moreover, the comparison of poloxamer 188 as a stabiliser in the drug-free SLN systems are interesting to compare against DBiB-p(OEGMA)$_{10}$-*co*-(EGDMA)$_{0.6}$ as it has been used widely as a stabiliser in other encapsulation systems.[124,135,230,271] In this study, the focus was directed towards the w/w ratios of polymer to Compritol ATO 888, which were varied with w/w ratio between 1:3, 1:1 and 3:1.

Linear DBiB-p(OEGMA)$_{10}$ was used to synthesis drug free SLNs with ratios of polymer to lipid of 1:3, 1:1 and 3:1 w/w ratio (DBiB-p(OEGMA)$_{10}$ to Compritol ATO 888) with a solid content of 1.2 mg in water/ IPA. The resulting drug free SLN formulations were analysed by

DLS at time points day 0 and 1 and those were given in Fig. 3.9 and corresponding correlation function is given in Appendix Fig. A42.

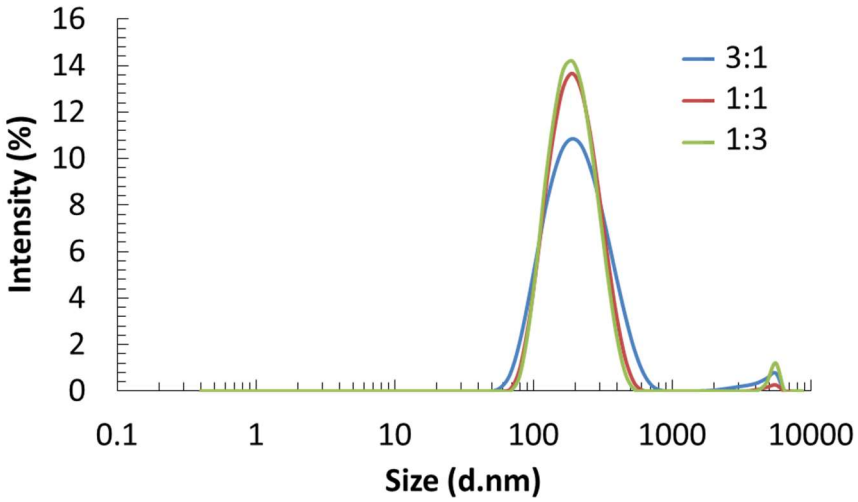

Fig. 3.9. DBiB-p(OEGMA)$_{10}$ in SLN studies. Compritol ATO 888 to DBiB-p(OEGMA)$_{10}$ w/w ratio 1:3, 1:1 and 3:1 and a solid content of 1.2 mg (DBiB-p(OEGMA)$_{10}$ + Compritol ATO 888).

The D_z-value measured for resulting drug free SLN formulations with 1:3, 1:1 and 3:1 w/w ratio of polymer to lipid ratios were monomodal. Moreover, the traces showed that a change in the polymer to lipid ratio of a composition containing a total 1.2 mg/mL (DBiB-p(OEGMA)$_{10}$ + Compritol ATO 888) solid content in water and IPA did not impact the SLNs size distribution of the DLS measurements as the D_z of the measurements were 200 nm (PDI > 0.10). In addition to that, the resulting formulation of linear DBiB-p(OEGMA)$_{10}$ measured by DLS at time points day 0 and day 1, Fig, 3.10. Those results showed that the particle sizes did not change when comparing day 0 with day 1. A photograph was taken of the resulting dispersions and is given in Fig. 3.10. These observations demonstrated that the resulting formulation get slightly turbid as the amount of lipid increased as a fraction of the total solid content of 1.2 mg/mL of deionised water. However, the appearance of the turbidity did not have any impact on the particle size.

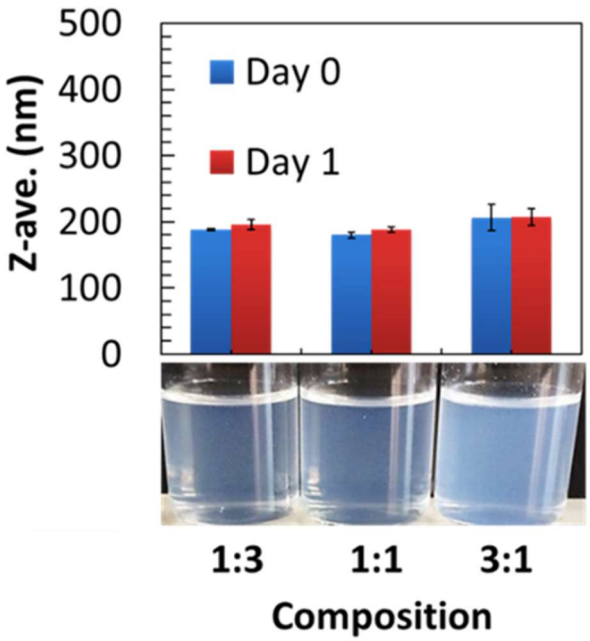

Fig. 3.10. DBiB-p(OEGMA)$_{10}$ in SLN studies. Compritol ATO 888 to DBiB-p(OEGMA)$_{10}$ w/w ratio of 1:3, 1:1 and 3:1 with a total solid content of 1.2 mg (Compritol ATO + DBiB-p(OEGMA)$_{10}$) in deionised water. Bar chart of the Z-average distribution on day 0 and day 1 and photography of observation of different compositions used to prepare SLN dispersions. Synthesis of each SLN formulation was done once. However, each formulation was measured three times using DLS. The results were averaged for each formulation to produce the figures above.

The second polymer in this study was the branched DBiB-p(OEGMA)$_{10}$-*co*-(EGDMA)$_{0.6}$ which was studied in earlier sections. This polymer was varied relative to Compritol ATO 888 in aforementioned w/w 1:3 (polymer to Compritol ATO 888) ratios with the aim to investigate the trend in size and stability of increased or decreased fraction of polymer and lipid in a total solid content of 1.2 mg/mL of deionised water. The resulting formulations DBiB-p(OEGMA)$_{10}$-*co*-(EGDMA)$_{0.6}$ stabilised drug-free SLNs were analysed by DLS in Fig. 3.11. The resulting traces of the DLS measurements showed a monomodal distribution, which indicate that the polymer to lipid ratio has no significant impact on the size or distribution of the particle. These traces showed the there is no trend in the behaviour as for the corresponding linear DBiB-p(OEGMA)$_{10}$, Fig. 3.11. However, D_z of the particles stabilised by branched DBiB-p(OEGMA)$_{10}$-*co*-(EGDMA)$_{0.6}$, see Fig. 3.12 appeared to be smaller than the corresponding SLNs made with linear polymer, Fig. 3.10. DBiB-p(OEGMA)$_{10}$-*co*-(EGDMA)$_{0.6}$

stabilised empty SLNs were also analysed at two different time points day 0 and day 1, Fig. 3.11 and Appendix Fig. A43 and compared with its empty SLN dispersion stabilised with its linear counterpart, linear DBiB-p(OEGMA)$_{10}$.

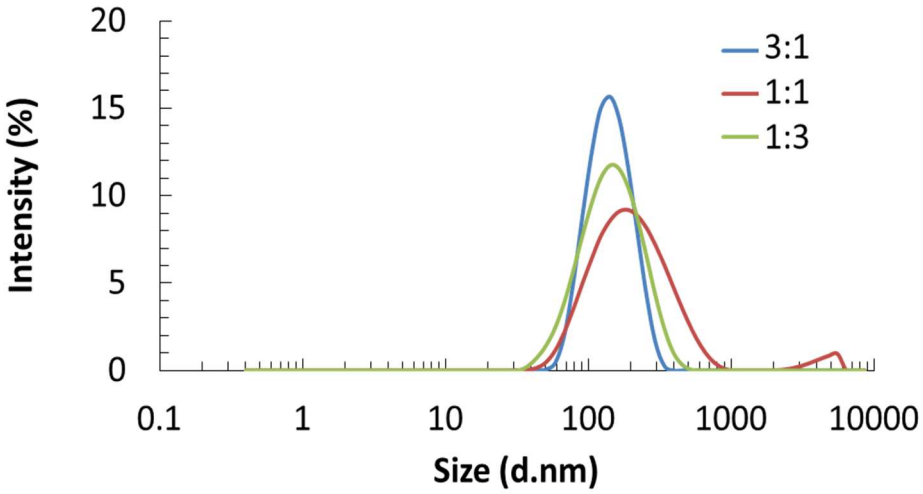

Fig. 3.11. DBiB-p(OEGMA)$_{10}$-*co*-(EGDMA)$_{0.6}$ in SLN studies. Compritol ATO 888 to DBiB-p(OEGMA)$_{10}$-*co*-(EGDMA)$_{0.6}$ ratio 1:3, 1:1 and 3:1 in the solid content 1.2 mg (DBiB-p(OEGMA)$_{10}$-*co*-(EGDMA)$_{0.6}$ + Compritol ATO 888) in deionised water.

The D_z values obtained for the drug free SLNs stabilised with DBiB-p(OEGMA)$_{10}$-*co*-(EGDMA)$_{0.6}$, Fig. 3.12, were lower than those obtained for DBiB-p(OEGMA)$_{10}$ stabilised dispersions, Fig. 3.10. This indicated that the branching of DBiB-p(OEGMA)$_{10}$ can have an impact on the size of the SLN particles in the dispersion. The resulting formulations of DBiB-p(OEGMA)$_{10}$-*co*-(EGDMA)$_{0.6}$ stabilised empty SLNs in the resulting formulations were also observed by the naked eye, photography in Fig. 3.12. It could be seen that the dispersions were clear.

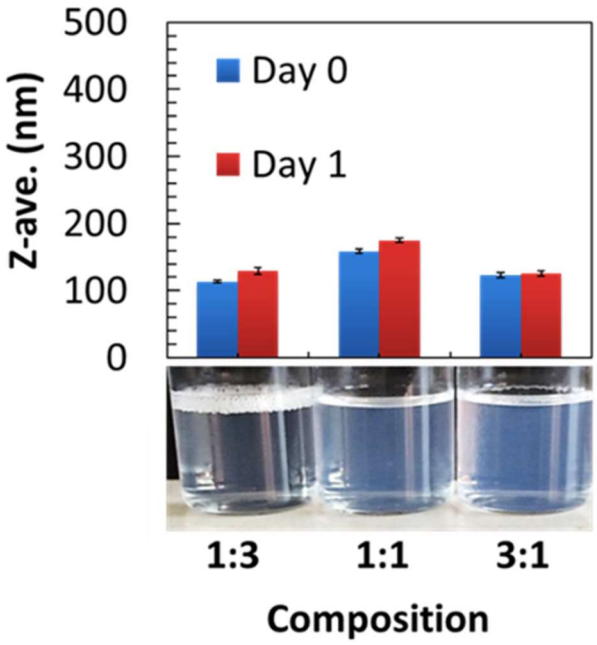

Fig. 3.12. DBiB-p(OEGMA)$_{10}$-*co*-(EGDMA)$_{0.6}$ in SLN studies. Compritol ATO 888 to DBiB-p(OEGMA)$_{10}$-*co*-(EGDMA)$_{0.6}$ w/w ratio of 1:3, 1:1 and 3:1 with a total solid content of 1.2 mg (Compritol ATO + DBiB-p(OEGMA)$_{10}$-*co*-(EGDMA)$_{0.6}$) in deionised water. Bar chart of the Z-average distribution on day 0 and day 1 and photography of observation of different compositions used to prepare SLN dispersions. Synthesis of each SLN formulation was done once. However, each formulation was measured three times using DLS. The results were averaged for each formulation to produce the figures above.

Poloxamer 188 which was the common used polymer for SLN production in literature was also tested as a polymer with same ratios and compositions as for DBiB-p(OEGMA)$_{10}$ and DBiB-p(OEGMA)$_{10}$-*co*-(EGDMA)$_{0.6}$. The resulting poloxamer 188 formulations were measured by DLS and given in Fig. 3.13, Fig. 3.14 and Appendix Fig. A44. The resulting traces of DLS measurements showed a monomodal distribution, Fig. 3.13, which indicate that that the polymer to lipid ratio has no significant impact on the size or distribution of the particle. These traces showed that there is no trend in the behaviour as for DBiB-p(OEGMA)$_{10}$, see Fig. 3.11, and DBiB-p(OEGMA)$_{10}$-*co*-(EGDMA)$_{0.6}$, see Fig. 3.12.

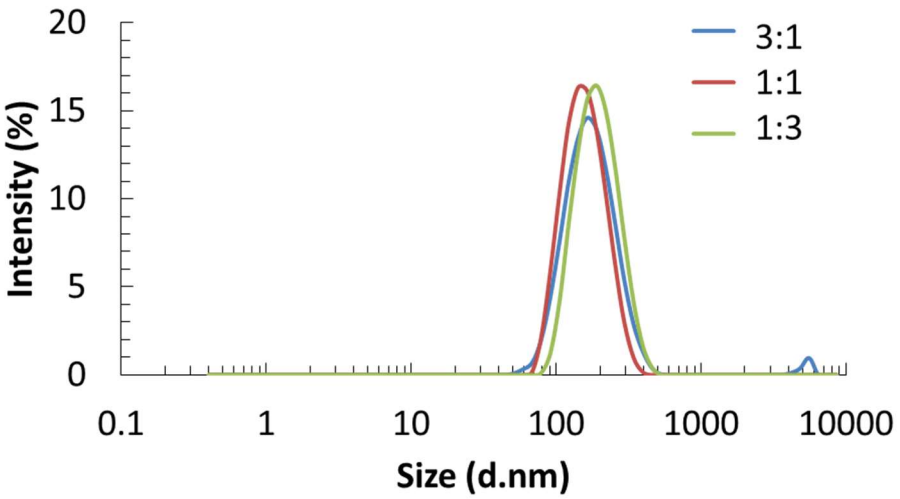

Fig. 3.13. Poloxamer 188 in SLN studies. Compritol ATO 888 to poloxamer ratio w/w 1:3, 1:1 and 3:1 and a total solid content of 1.2 mg of (Compritol ATO 888 + poloxamer 188) in deionised water.

The D_z values obtained for the drug free SLNs stabilised with poloxamer 188, Fig. 3.14, were slightly higher than those obtained for DBiB-p(OEGMA)$_{10}$ stabilised drug free SLN dispersions, Fig. 3.10 and similar to those with DBiB-p(OEGMA)$_{10}$-*co*-(EGDMA)$_{0.6}$ stabilised drug-free SLN dispersions, see Fig. 3.12. Based on those observations it could be hypothesised that poloxamer 188 might have similar stabilising properties as DBiB-p(OEGMA)$_{10}$-*co*-(EGDMA)$_{0.6}$ in the short term (day 0-1). The resulting formulations of poloxamer 188 stabilised drug free SLN were also observed by the naked eye, photography in Fig. 3.14. It could be seen that the dispersions were clear.

Overall, the stability of drug-free SLN particles stabilised with DBiB-p(OEGMA)$_{10}$, DBiB-p(OEGMA)$_{10}$-*co*-(EGDMA)$_{0.6}$ and poloxamer 188 was demonstrated with three different compositions of w/w ratios of 1:3, 1:1 and 3:1 Compritol ATO 888 to polymer in water containing IPA. It was shown that drug-free SLNs stabilised with DBiB-p(OEGMA)$_{10}$ and poloxamer 188 have larger D_z values than drug-free SLN stabilised with DBiB-p(OEGMA)$_{10}$-*co*-(EGDMA)$_{0.6}$ in dispersion containing IPA. This may indicate that the branching of a polymer can have an impact on the particle size. The number of conjoined chains per branched copolymer were calculated for DBiB-p(OEGMA)$_{10}$-*co*-(EGDMA)$_{0.6}$ in Chapter 2 and was WA # = 6 and for DBiB-p(OEGMA)$_{10}$ it was WA # = 1. These values may also have an impact on the D_z values measured for the drug free SLNs in the dispersion.

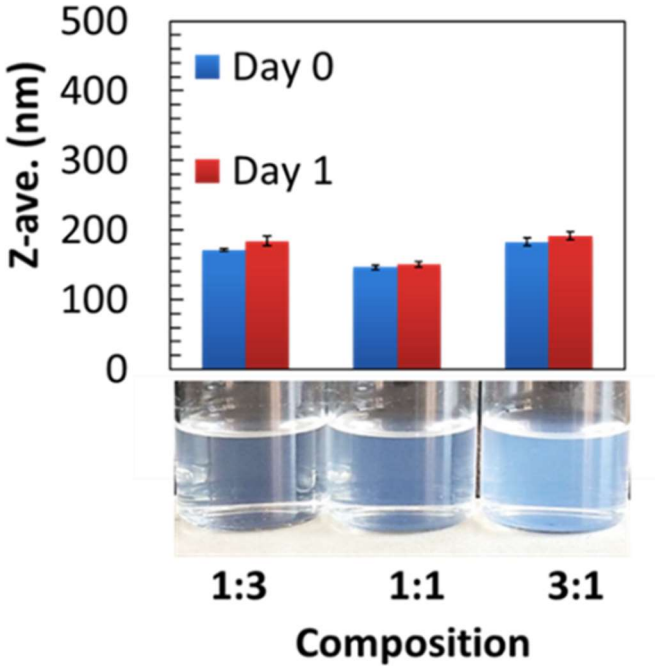

Fig. 3.14. Poloxamer 188 in SLN studies. Compritol ATO 888 to poloxamer 188 w/w ratio of 1:3, 1:1 and 3:1 with a total solid content of 1.2 mg (Compritol ATO + poloxamer 188) in deionised water. Bar chart of the Z-average distribution on day 0 and day 1 and photography of observation of different compositions used to prepare SLN dispersions. Synthesis of each SLN formulation was done once. However, each formulation was measured three times using DLS. The results were averaged for each formulation to produce the figures above.

3.2.6 Stability studies of dialysed versus non-dialysed empty SLN dispersions

The importance of storing the resulting SLN formulations in the fridge straight after the solvent injection procedure was performed was discussed earlier. This was due to observation that the empty SLN dispersions forms aggregate at room temperature straight after the solvent injection procedure was performed. It was hypothesised that this could be due to the use of IPA as a water miscible solvent in the solvent injection process that potentially could dissolve the resulting formed SLN straight after solvent injection. However, very little literature describes why this type of aggregation can occur. In the literature, various methods were used to remove solvents after preparation of SLNs and those procedures include dialysis, freeze drying or evaporation. The removal of solvent from these SLNs was

also evaluated to enable later use of the materials in an in vivo setting and to establish the optimal conditions that would not lead to disruption of the SLN stability. Initially dialysis was selected as the solvent removal procedure as this is well understood and relatively simple to carry out. As mentioned earlier, temperature may play a major role in the SLN stability after processing. The dialysis procedures were initially evaluated in two different temperature conditions. One of the temperature conditions was to dialyse the sample at ambient temperature and the other condition was to dialyse the sample in the fridge. The drug-free SLN dispersions synthesised earlier were dialysed over 3 days with regular change of water after time points 30 min, 1 hr, 6 hrs, day 1, and day 3. After 3 days, the content in the dialysis bag was analysed by ^{1}H NMR. The spectra showed no IPA signals were observed in the analysed dialysis material. Fig. 3.15a on the left showed that the dispersion that was dialysed in the fridge did not form any aggregates after 3 days. However, Fig. 3.15b on the right showed that the dispersion dialysed at ambient temperature did aggregate. It can be concluded from this observation that the temperature does have an impact on the stability of the SLN dispersion upon dialysis. The concern over the presence of IPA in the sample was tested by leaving a dialysed drug-free SLN dispersion it in a closed vial at ambient temperature for 2 days. The sample was frequently observed over 2 days. After 2 days, it was observed that no aggregation was formed as a result. This indicated that IPA might play a role in dissolving the empty SLN particles after solvent injection processing.

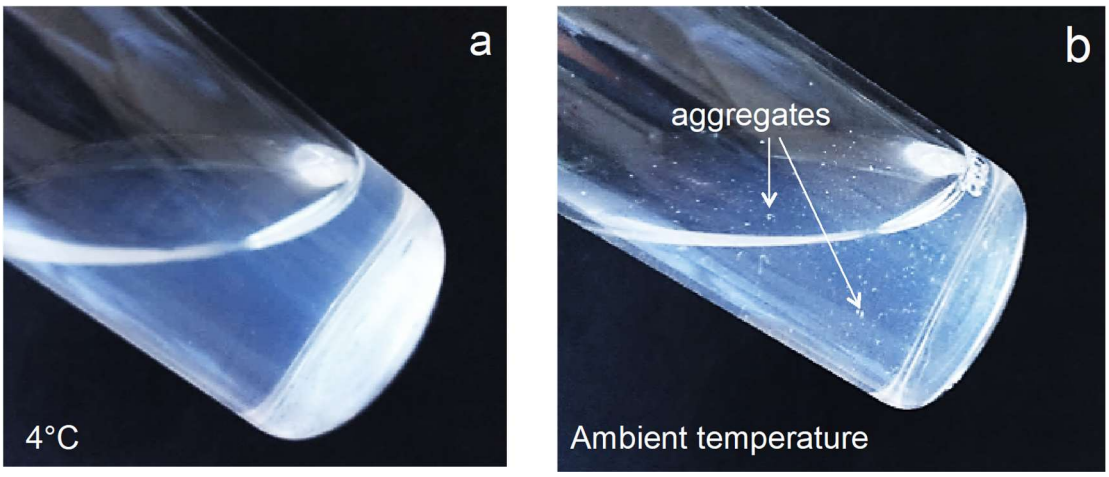

Fig. 3.15. Samples stabilised with poloxamer 188. **a)** Dialysed and **b)** non-dialysed are not stable after 25 days

The effect of solvent removal from SLN samples generated from DBiB-p(OEGMA)$_{10}$, DBiB-p(OEGMA)$_{10}$-*co*-(EGDMA)$_{0.6,}$ and poloxamer 18 was studied by performing dialysis 4°C individually for each sample.

The results were collected by DLS analysis to establish D_z and PDI of the resulting SLN dispersions was undertaken and the results are shown on Table 3.2.

Table 3.2. DBiB-p(OEGMA)$_{10}$, DBiB-p(OEGMA)$_{10}$-*co*-(EGDMA)$_{0.6}$ or Poloxamer 188 stabilised SLNs were analysed with and without dialysis. Samples were analysed at time points 0,1,3 and 24 days.. All measurements were measured in triplicates with an average of 3 different runs. All measurements had an attenuator 6-7. D_z is the average diameter in nm, PDI is the polydispersity index, ZP is the zetapotential in mV.

Polymer	Method	D_z (nm)				PDI	ZP (mV)
DBiB-p(OEGMA)$_{10}$		**Day 0**	**Day 1**	**Day 3**	**Day 24**	**Day 24**	-17.5
	No dialysis	195.0	207.2	204.9	-	-	
	Dialysis	190.7	-	-	114.7	0.144	
DBiB-p(OEGMA)$_{10}$-*co*-(EGDMA)$_{0.6}$		**Day 0**	**Day 1**	**Day 3**	**Day 24**	**Day 24**	-16.0
	No Dialysis	122.9	125.9	126.6	121.3	0.197	
	Dialysis	163.9	-	-	98.2	0.175	
Poloxamer 188		**Day 0**	**Day 1**	**Day 3**	**Day24**	**Day 24**	-16.8
	No Dialysis	182.8	192.0	133.3	182.2	0.097	
	Dialysis	189.0	-	-	118.4	0.237	

The SLN D_z of the drug-free SLNs stabilised with DBiB-p(OEGMA)$_{10}$, DBiB-p(OEGMA)$_{10}$-*co*-(EGDMA)$_{0.6}$ and poloxamer 188 stabilised empty SLNs that were either dialysed or non-dialysed were compared against each other using the most successful procedure which was to dialyse the resulting SLN suspension in the fridge for 3 days. This was done with the aim to show the effect of dialysis *versus* non-dialysis processing on the diameter of the empty SLN particle, Table 3.2. The results demonstrated that the use of dialysis to remove IPA in the fridge after solvent injection does have an impact on the Z-average of the empty DBiB-p(OEGMA)$_{10}$, DBiB-p(OEGMA)$_{10}$-*co*-(EGDMA)$_{0.6}$ and poloxamer 188 stabilised SLNs. As seen on Table 3.2 the DBiB-p(OEGMA)$_{10}$ stabilised drug-free SLN is 190.7 nm on day 0 before dialysis. However, after dialysis the size of the DBiB-p(OEGMA)$_{10}$ stabilised drug free SLNs decrease to 114.7 nm. The same was observed for DBiB-p(OEGMA)$_{10}$-*co*-(EGDMA)$_{0.6}$

stabilised drug free SLNs where the particle size decreased from 163.9 nm to 98.2 nm and for poloxamer 188 stabilised drug free SLNs where the particle size decreased from 189.0 nm to 118.4 nm. We have been unable to produce a hypothesis to explain this observation.

The empty DBiB-p(OEGMA)$_{10}$-*co*-(EGDMA)$_{0.6}$ stabilised SLNs were analysed using scanning electron microscopy (SEM) as shown in Fig. 3.16. The D_z, PDI and zetapotential (ZP) were measured by DLS. The sample were also morphologically characterised by SEM to give number average of dry drug-free SLN size. The SEM images showed that the SLNs flat shapes aggregated together. With this observation the evidence of SLN formation has been seen however the appearance of the morphology of the empty DBiB-p(OEGMA)$_{10}$-*co*-(EGDMA)$_{0.6}$ stabilised SLNs lead us hypothesise that some of the empty SLN particles have aggregated during the drying process. Another possibility is that the branched polymer forms a film on the surface of the sample which makes it hard to see or distinguish the aggregated SLN particles. A similar observation has been made by another researcher in this group, Ford et *al*,[185] who discussed the complications with SEM analysis became increasingly difficult with increasing amounts of A−B block copolymer, that lead to some film formation and observation of objects resembling flattened vesicles at higher ratios.[185]

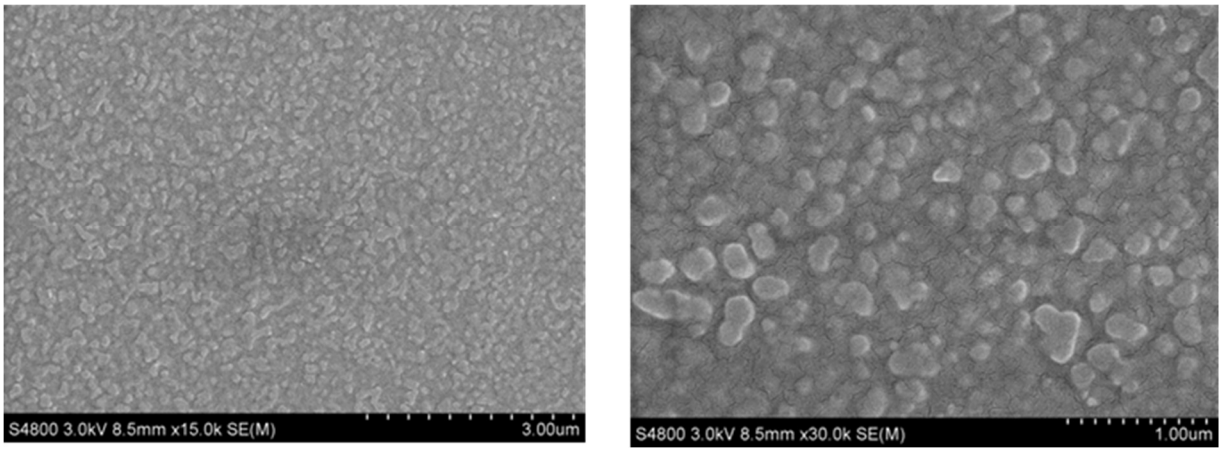

Fig. 3.16. SEM images of a drop of DBiB-p(OEGMA)$_{10}$-*co*-(EGDMA)$_{0.6}$ stabilised SLN dispersion (non-dialysed) dried overnight. The pictures are taken at different scales left 3 μm and right 1 μm.

Zeta potential measurements of the empty SLNs stabilised with either DBiB-p(OEGMA)$_{10}$, DBiB-p(OEGMA)$_{10}$-*co*-(EGDMA)$_{0.6}$ or poloxamer 188 showed values of -16 to -17.5 mV after

day 24. The relatively low amount of surface charge indicates that the long-term stability of the SLNs was due to steric stabilisation provided by the polymer. It has been reported in former studies[185,272] that the ZP of similar nanoprecipitated compounds such as p(HPMA)$_{50}$-*co*-(EGDMA)$_{0.9}$ was -40.5 mV and nanoparticles formed solely of A-B block copolymers showed values of -10.5 mV.[272] This was consistent with PEG-stabilised particles or micelles.[185,272,273]Moreover, Ford *et al*,[185] showed that addition of a block copolymer such as p(PEG$_{45}$-b-HPMA$_{12}$ to p(HPMA)$_{50}$-*co*-(EGDMA)$_{0.9}$ in a ratio of 10:90 weight % results in a decrease in ZP from - 40.5 mV to - 16.7 mV. [185] There is no explanation to why PEG stabilised nanoparticles has a negative charge. It can be hypothesised that the cause of the negative charge can be due to PEG absorbing negative charged ions the dispersion media.

The optimised DBiB-p(OEGMA)$_{10}$ and poloxamer 188 stabilised drug-free SLNs stored in the fridge appeared to aggregate after 39 and 25 days, respectively, based on the assessment by DLS. However, the dialysed drug free SLN sample stabilised with DBiB-p(OEGMA)$_{10}$-*co*-(EGDMA)$_{0.6}$ were stable over 39 days when stored at 4 °C kept in the fridge. This sample did not form large aggregates after 39 days.

The stability of DBiB-p(OEGMA)$_{10}$-*co*-(EGDMA)$_{0.6}$ stabilised drug free SLNs was assessed through several batches and it could be concluded that temperature plays a major rule in terms of the physical observation as the sample kept at ambient temperature results in aggregation or crystallisation. The underlying mechanism behind this observation was unclear, but potentially keeping the samples at a lower temperature reduced the solubility of the lipid in the continuous phase. However, the removal of the solvent IPA by dialysis helped the drug-free SLN dispersion stabilised by DBiB-p(OEGMA)$_{10}$-*co*-(EGDMA)$_{0.6}$ stable over a longer period of time at ambient temperature.

3.2.7 Temperature stability studies of dialysed versus non-dialysed empty SLN dispersions

A study was done to compare the behaviour of a non-dialysed sample with a dialysed sample, Fig. 3.17, at temperatures between 5 to 60 °C. The purpose was to investigate how the empty SLNs behave at different temperature conditions in presence and absence of IPA.

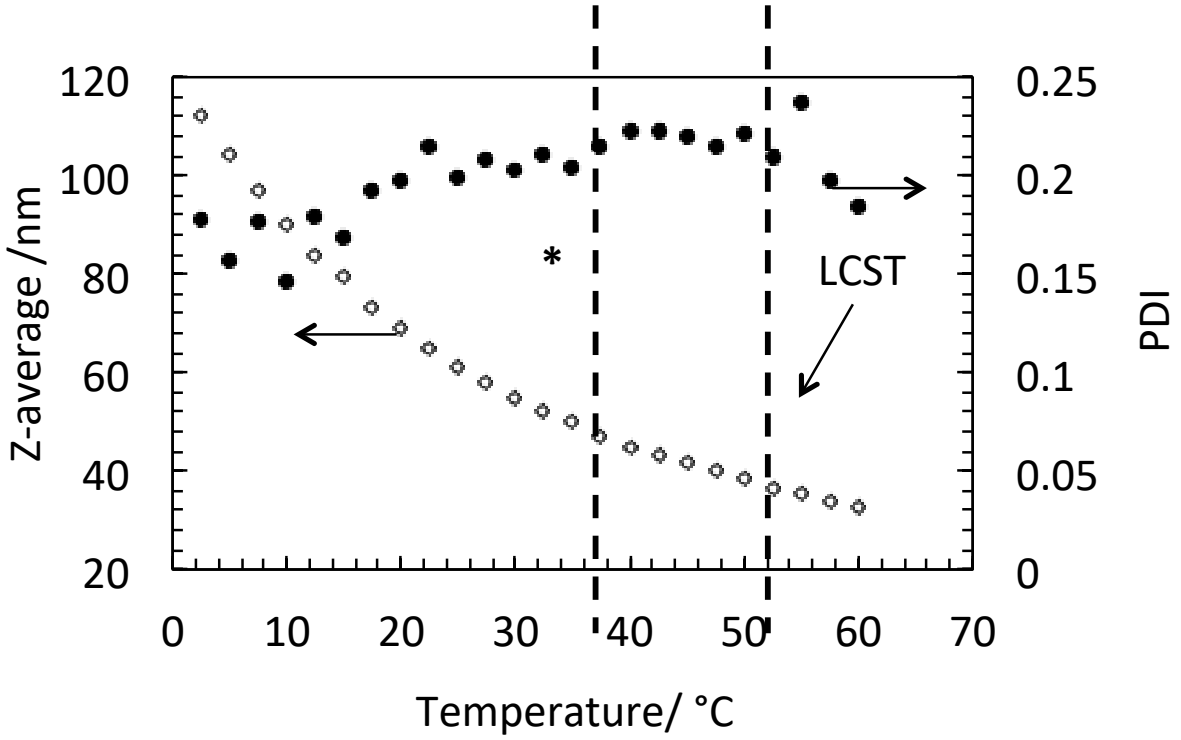

Fig. 3.17. 1:3 w/w ratio; DBiB-p(OEGMA)$_{10}$-*co*-(EGDMA)$_{0.6}$ to Compritol ATO 888 empty SLN dispersion. 1 mL non-dialysed sample containing empty SLNs dispersed into deionised water, IPA (20 v/v %). *body temperature 37 °C.

The diameters and PDI obtained from the DLS measurements between temperatures of 5 to 60 °C of 1 mL of non- dialysed sample is given in Fig. 3.17. These results showed that diameter decreased slightly as the temperature of the sample was increased. Since the sample has IPA present it could was be hypothesised that the empty SLN particle got smaller as IPA dissolved parts of the particle when the sample is heated up.

The Z-average diameters and PDI obtained from the DLS measurements between temperatures of 5 to 60 °C of 1 mL of dialysed sample was given in Fig. 3.18 These results

showed that the diameter of the dialysed sample remained constant as the temperature increased. The derived count rate for the dialysed sample did also remain stable throughout the DLS at different temperatures. This suggests that the sample did not dissolve and remained stable throughout the heat process. Another observation showed that the dialysed sample did not form aggregate after cooling as shown on the photograph in Fig. 3.15.

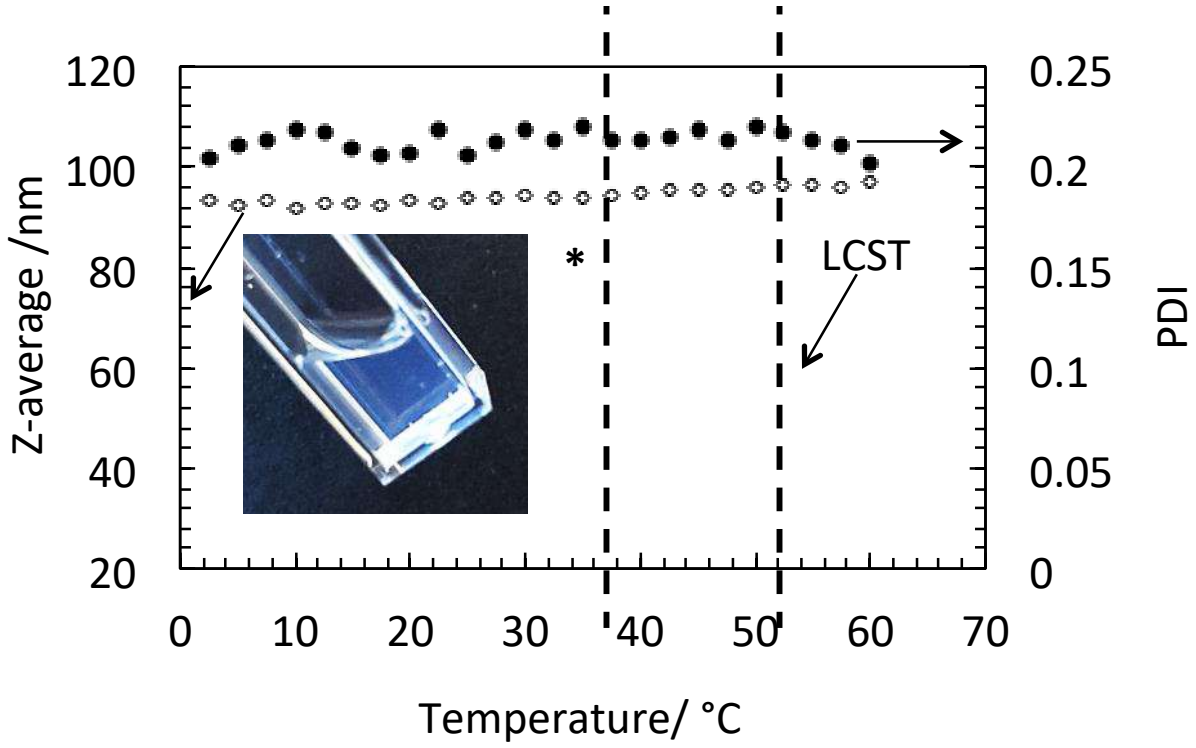

Fig. 3.18. 1:3; DBiB-p(OEGMA)$_{10}$-*co*-(EGDMA)$_{0.6}$: Compritol ATO 888 empty SLN dispersion 1 mL dialysed sample in deionised water. Body temperature 37 °C.

To understand this mechanism another parameter measured by DLS was analysed. The derived count rate (DCR) can be used to monitor any potential dissolution of the particle by the scattering intensity that is directly proportional to the size and number of a particle present in a sample.[274] The DCR of the sample measurement throughout the temperatures 5-60 °C, Fig. 3.19, remained unchanged throughout the measurements at different temperatures. Another hypothesis was that IPA was present in the empty SLN particle straight after injection and diffused out of the empty SLN particle upon heat thereby shrinking the particle

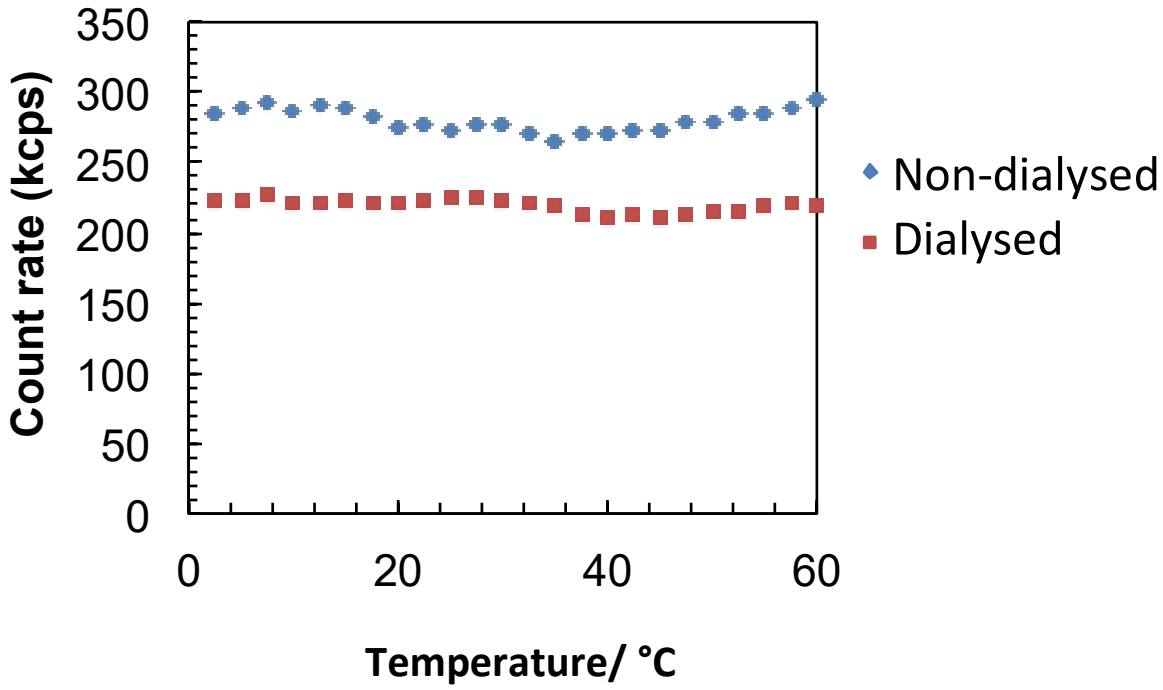

Fig. 3.19. Derived count rate of DBiB-p(OEGMA)$_{10}$-*co*-(EGDMA)$_{0.6}$ stabilised SLNs. Recorded with a composition of 3:1 Compritol ATO 888: DBiB-p(OEGMA)$_{10}$-*co*-(OEGMA)$_{0.6}$ and a total solid content of 1.2 mg/mL of deionised water. Samples were recorded at temperatures between 0-60 ^{o}C.Count rate does not change upon heating in temperature studies.

3.3 Conclusion

This chapter successfully demonstrated that DBiB-p(OEGMA)$_{10}$-*co*-(EGDMA)$_{0.6}$ may be used to form stable SLN systems when an optimised solvent injection method is employed and in the absence of drug compound. However, there was several challenges involved with solvent injection processing. One of the challenges was that visible particles were observed in the formulations after solvent injection processing when kept at room temperature. However, when storing the DBiB-p(OEGMA)$_{10}$-*co*-(EGDMA)$_{0.6}$ stabilised drug-free SLN formulation in the fridge the formulation was stable for 38 days. Dialysis was used to successfully remove the IPA. The resulting formulation was compared against the non-dialysed drug free SLN formulations stabilised with three different types of polymers: DBiB-p(OEGMA)$_{10}$, DBiB-p(OEGMA)$_{10}$-*co*-(EGDMA)$_{0.6}$ and poloxamer 188 with a w/w ratio of 1:3 polymer to Compritol ATO 888 and a solid content of 1.2 mg/ mL water in presence and

absence of IPA. The best performing polymers was concluded to be DBiB-p(OEGMA)$_{10}$-*co*-(EGDMA)$_{0.6}$ as DBiB-p(OEGMA)$_{10}$ and poloxamer 188 stabilised empty SLN formulations start forming aggregates after 25 and 39 days, respectively.

Chapter 4. Synthesis, optimisation and stability studies of OEGMA based polymer stabilised maraviroc loaded SLNs

4.1 Introduction

Maraviroc (MVC) is the only approved entry inhibitor in oral formulation and the only drug in the antiretroviral armamentarium, which targets the human receptor.[275] Hence, it is able to be long-term effective only if the infecting virus uses, exclusively, the CCR5 receptor[275] and in a combination treatment with other antiretroviral drugs discussed in Chapter 1. Nonetheless, MVC is a potent medication for eligible patients and helps to improve the outcome of antiretroviral treatment (ART) of HIV infection.[275] However, it is a poorly bioavailable drug, which has limited its use as it requires a high daily dosage of 300 mg twice daily[276,277] which results in side effects discussed in chapter 1.[18,35] Nanocarrier platforms have been shown to improve the bioavailability other drugs with poor pharmaco-kinetics[2,5,104,278] and therefore may offer benefits if used to deliver MVC. However, currently the literature about MVC encapsulation into nanoparticles is scarce. One example in literature showed MVC loaded in poly(lactic-co-glycolic acid (PLGA) particles.[212] A nominal initial drug loading of 10 wt.% relative to PLGA was used, which resulted in formulated MVC-nanoparticles (NPs).[212] The drug loading of MVC into PLGA particles was measured to be 1.2±0.1 wt.% and the respective drug loading translated to encapsulation efficiency (EE) was 12%.[212] Drug loading of MVC into other nanocarrier systems such as SLNs has to the best of our knowledge not been studied. Encapsulation of MVC into SLNs may offer several advantages such as the biocompatibility of the materials that is used to make them, simple processing methods, suitability to large scale production and cost-effectiveness.[130]

SLNs have been demonstrated to encapsulate poorly bioavailable anti-HIV drugs including examples such as lopinavir,[104] darunavir,[215,216] tenofovir[217] and efavirenz.[214] For example, Alex *et al*, [104] synthesised SLNs using 1.9 wt. % of lopinavir (LPV relative to the lipid (Compritol ATO 888) in the processing of Lo-SLNs with a EE of above 99 %.[104] Alex *et al*,[104] optimised their LPV-SLN system and selected the formulation with the highest encapsulation parameter.[104] This was done based on the conclusion that a mean particle size below 100 nm could be obtained by reducing lipid percentage and increasing surfactant

concentration.[104] In addition to that they also found that the reduction in particle size was followed by decrease of drug payload per ml of water and EE %.[104] Two other examples in literature, Bhalekar *et al*,[216] used 25 wt. % darunavir relative to lipid (GMS) in the processing of DRV-SLNs with EE of 74 % and Gaur *et al*,[214] used 25 wt. % efavirenz relative to lipid (GMS) in their SLNs with an EE of 46-86 %. These articles managed to encapsulate drug relative to lipid in ranges between 2-25 wt. % using homogenisation as a processing method. However, the use of polymers and cryoprotectants are not always specified in the mentioned reports.[214–217] Hence, this makes it unclear how significantly lower the drug encapsulation will be relative to total content of materials (polymer + drug + lipid + cryoprotant) used to produce SLNs.[124] Solvent injection has been used to load 2.5 - 7.5 wt.% of other drugs relative to lipid into similar SLN particles with EE of 38-68 %.[125,266] However, the limit of maximum drug loadings into SLN systems synthesised by solvent injection has not been studied in detail in literature. However, the drug loading in SLNs produced by solvent injection has not been shown to be significantly higher than what has been obtained using homogenisation. As explained in Chapter 1, there are several problems with using SLNs as drug delivery systems, including those made using solvent injection, such as poor drug loading capacity and drug expulsion. It has been proposed that these limitations are caused by the instability and interconversion between ordered and disordered lipid structural arrangements in SLNs.[94] Some methods have been developed to overcome those problems.[94,102,101,93] For example another lipid such as a liquid lipid could be added to the SLN formulation to make the structure less ordered in order to encapsulate a larger proportion of drugs. Such systems are referred to as NLC particles.[279]

Due to the relative obscurity of solvent injection studies in literature we believe there is an opportunity to improve the drug loading of MVC in SLNs using the solvent injection procedure. Therefore, this chapter will investigate drug loading of the SLNs by varying the ratios of drug and lipid and how they influence the stability in order for them to be useful in drug delivery systems.

Many methods have been reported in literature to assess drug loading and stability of SLNs loaded with drugs. These methods include DSC to assess the crystallinity of lipids in the SLNs,[104,133,202,271,280,153] DLS to measure the particle size, dispersity and stability of SLNs, SEM and TEM to assess morphology of a dry SLN,[110,147,281,282–285] ^{1}H NMR,[286] HPLC[104,287] and UV-vis[121,288,289] to quantify drug loading in SLNs. The drug loadings of the MVC in SLNs can be characterised, assessed and quantified using various methods including UV-vis,[290] ^{1}H and ^{19}F NMR (MVC contains two fluorine atoms). UV-vis has already been used to characterise MVC in water, ethanol, phosphate buffer (pH =7.4) and 0.1M NaOH with an absorption spectrum measured in the range 200-400 nm. However, the in this article the signal of the UV-vis spectrum appeared to be weak at a low absorbance with concentrations of 15 µg/mL phosphate buffer.[290] However, UV measurement of MVC in other solvents such as Chloroform has not yet been reported and will be attempted as part of this chapter. Alternatively, ^{1}H and ^{19}F NMR have been considered as tools to measure the drug loading in MVC loaded SLNs. ^{1}H NMR can be used to make a standard calibration curve that can be used to interpret amount of MVC encapsulated in SLNs. This type of experiment has been tried in other NP systems in literature.[291] This study described a rapid, specific, and direct method for the real-time quantification of *in vitro* tenofovir (TNF) release in simulated varginal fluid (VFS).[291] For this they developed a standard curve of TNF in VFS with a linear relationship between the integration of a peak area obtained from a given ^{1}H NMR spectra of TNF as a function of TNF in mM.[291] This curve can be used to interpret the amount of TNF released from microparticles in VFS. [291] A unique feature of MVC is that it contains two ^{19}F atoms. ^{19}F shares the advantage as of being very sensitive and have is a 100 % NMR active isotope, due to the fact that there is only a single isotope. With the choice of a sufficient internal reference it is possible to make a standard calibration curve that can be used to quantify MVC loading in SLN.

4.2. Optimisation of methodology and synthesis of drug loaded MVC in SLNs

In Chapter 3 the solvent injection method was optimised with a composition of DBiB-p(OEGMA)$_{10}$-*co*-(EGDMA)$_{0.6}$ and Compritol ATO 888 but without any drug. It was shown that the most stable drug-free SLN formulation was that of 1:3 w/w ratio of DBiB-p(OEGMA)$_{10}$-*co*-(EGDMA)$_{0.6}$ to Compritol ATO 888 were dialysed to yield an IPA free SLN dispersion with a total solid content of 1.2 mg in 1 mL of water.

In this study, the incorporation of MVC was calculated as wt. % of MVC relative Compritol ATO 888 within 1:3 w/w % ratio of DBiB-p(OEGMA)$_{10}$-co-(EGDMA)$_{0.6}$ to Compritol ATO 888 system established in Chapter 3. A range of compositions of MVC relative to Compritol ATO 888 were prepared as shown Table 4.1 and the compositions were calculated as follows:

$$\text{wt.\% drug rel. to lipid} = \frac{m_{MVC}}{m_{Compritol}+m_{MVC}} \cdot 100\ \% \qquad \textbf{(4.1)}$$

Where m_{MVC} is the mass of the drug in mg, $m_{Compritol}$ is the mass of the lipid in mg and wt. % drug is the weight % of the MVC relative to Compritol ATO 888.

Table 4.1. Composition of MVC relative to Compritol ATO in wt.% in targeted drug encapsulation studies. The w/w ratio of DBiB-p(OEGMA)$_{10}$-co-(EGDMA)$_{0.6}$ to Compritol ATO 888 was 1:3. The total solid content of DBiB-p(OEGMA)$_{10}$-co-(EGDMA)$_{0.6}$ + Compritol ATO 888 + MVC is 1.0 mg/ mL water/IPA.

wt. % drug rel. to lipid	MVC/mg	Compritol/ mg	Polymer/ mg	Water/mL	IPA/mL
10	1.8	16.2	6	20	4
20	3.6	14.4	6	20	4
40	7.2	10.8	6	20	4
50	9	9	6	20	4
70	12.6	5.4	6	20	4
90	16.2	1.8	6	20	4
100	18	0	6	20	4

The same process for solvent injection that was optimised in chapter 3 for drug free SLNs was reused but with MVC included in the compositions are shown in Fig. 4.1, and Table 4.1. The solvent injection method for the MVC-SLN studies are illustrated in Fig. 4.1.

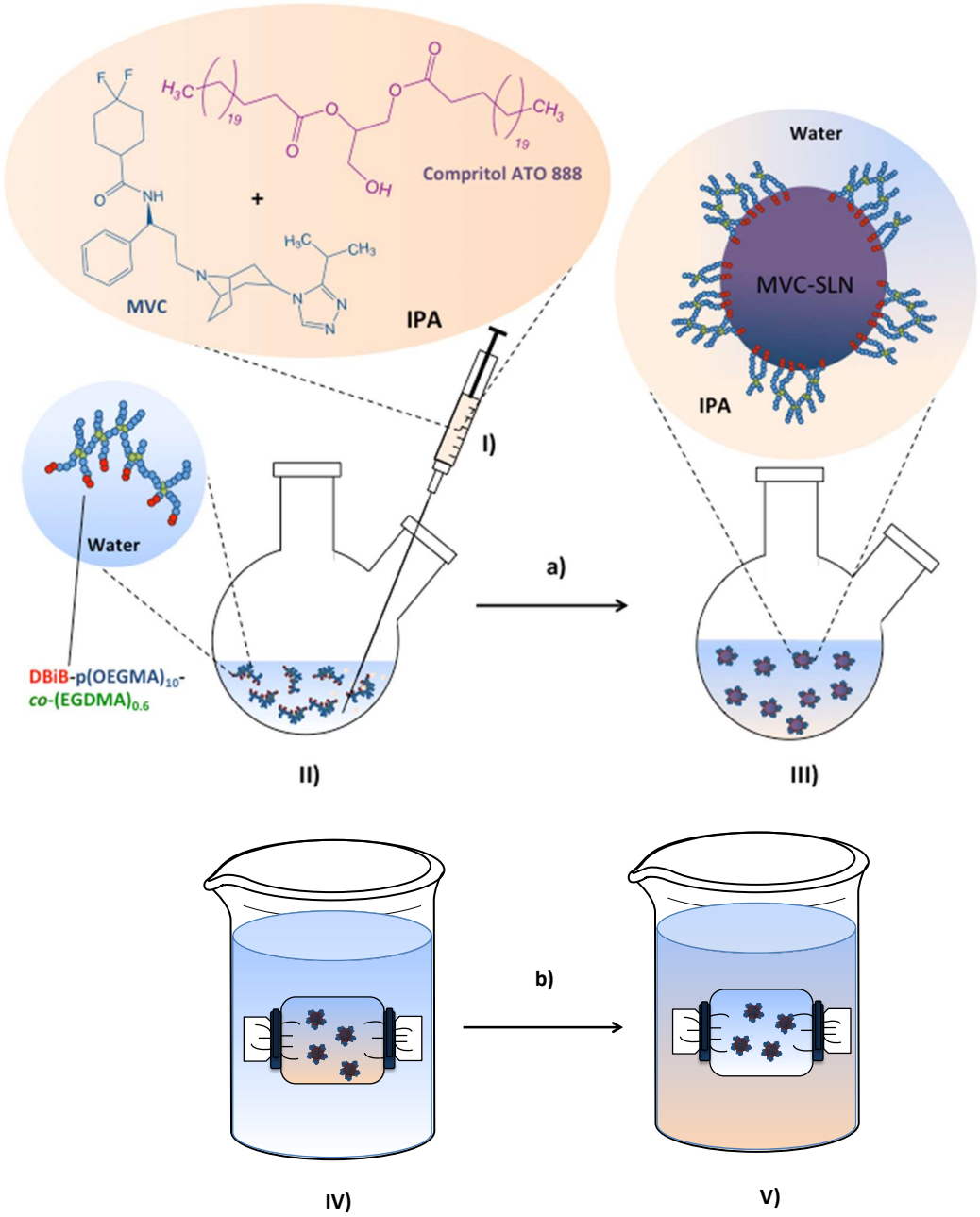

Fig. 4.1. Illustration of solvent injection method conditions and principles. **a)** Deionised water and DBiB-p(OEGMA)$_{10}$-*co*-(EGDMA)$_{0.6}$ at 25 °C 5 min, 300 rpm stirring at ambient temperature IPA containing MVC and Compritol ATO 888 at 80 °C, **b)** removal of IPA from MVC-SLN dispersion using dialysis technique at 4 °C. Conditions: **I)** IPA, Compritol ATO 888 and MVC at 80 °C,**II)** DBiB-p(OEGMA)$_{10}$-*co*-(EGDMA)$_{0.6}$ in water, **III)** MVC-SLN dispersion containing IPA, **IV)** dialysis of MVC-SLN dispersion in a dialysis bag containing IPA and **V)** IPA free SLN dispersion in dialysis bag.

MVC was included in a solution of IPA and Compritol ATO 888 as shown in Fig. 4.1I. The solubility of MVC in IPA was tested at ambient temperature and 80 °C in presence or absence of Compritol ATO 888 to ensure that the solvent injection procedure established in Chapter 3 can be used in presence of MVC. The solubility of MVC in IPA as well as IPA mixed with Compritol ATO 888 has not reported in literature. However, it has been reported that MVC is highly soluble in similar organic solvents such as ethanol and DMF.[290] In the experiment, Fig. 4.2a, MVC (2 mg) was added to IPA 1 mL and was shaken a few times at ambient temperature. It was observed that the solution went clear and this indicated that MVC was soluble with a concentration of 2 mg/mL in IPA at ambient temperature, Fig. 4.2a. In another study, the solubility of MVC (4.5 mg) in IPA (4 mL) in presence of Compritol ATO 888 (4.5 mg) was heated to 80 °C, Fig. 4.2b. The photograph of the heated solution of MVC, Fig. 4.2b, in presence of IPA and Compritol ATO 888 showed a clear solution, which indicated that MVC has dissolved. The other parameters in the optimisation which is DBiB-p(OEGMA)$_{10}$-*co*-(EGDMA)$_{0.6}$ dissolved in deionised water remain unchanged, Fig. 4.1II.

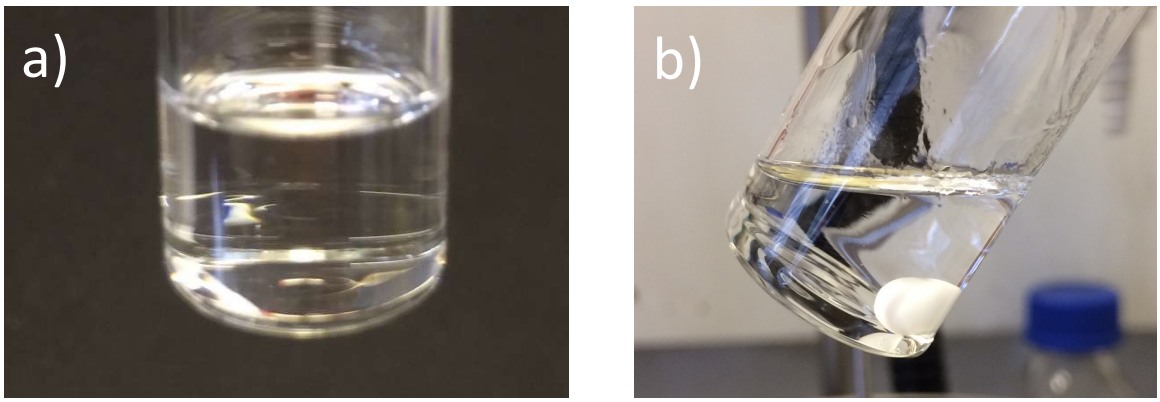

Fig. 4.2. Test of solubility of **a)** 2 mg MVC in 1 mL of IPA at ambient temperature shows a clear solution indicating that MVC is soluble in IPA and **b)** MVC (4.5 mg) in 80 °C IPA containing Compritol ATO 888 (4.5 mg) forms a clear solution indicating that MVC is soluble in IPA containing Compritol ATO 888.

The solvent injection method, Fig. 4.1a was performed in the same way as established in chapter 3. IPA with dissolved MVC and Compritol ATO 888 at 80 °C was rapidly injected into the solution of DBiB-p(OEGMA)$_{10}$-*co*-(EGDMA)$_{0.6}$ in water at 25 °C, Fig. 4.1a. The sample

was stirred for 5 min with a stirring speed of 300 rpm at 25 °C. The last step of MVC-SLN production is to remove the solvent from the dispersion, Fig. 4.1d. Methods reported to remove solvent after solvent injection is freeze drying[265] and solvent evaporation.[124,292] Dialysis against water in Chapter 3 has been used to remove water miscible solvents IPA from a SLN dispersion where it was used to remove drug-free SLNs,[293] this approach was used in the work presented in Chapter 3 using empty SLNs. Therefore, dialysis was also used remove the IPA from the MVC loaded SLNs presented in this Chapter.

4.2.1. DLS measurements of MVC encapsulation SLNs after dialysis

MVC loaded SLNs were synthesised using the compositions shown on Table 4.1. The ratio of 1:3 w/w% of DBiB-p(OEGMA)$_{10}$-*co*-(EGDMA)$_{0.6}$ and Compritol ATO 888 established in Chapter 3 was kept constant throughout this chapter. The experimental procedure was described on chapter 7, section 7.3. IPA was removed from the MVC-SLN dispersion by dialysis against water over 3 days. The MVC-SLNs with targeted drug loadings of 0-90 wt.% and MVC nanodispersion of 100 wt. % relative to lipid were analysed by DLS with a concentration of 1.2 mg/ mL deionised water at 25 °C. In order to analyse the stability of the SLNs over time the MVC-SLNs were analysed after 3 days where IPA was removed. The four selected DLS traces of 30, 50, 70 and 90 wt. % were measured in triplicate on day 3 after dialysis and overlaid for each sample, Fig. 4.3 and corresponding correlograms are given in Appendix Fig A45-A48. The traces of the targeted 30, 50 and 70 wt. % MVC relative to Compritol ATO 888 showed monomodal size distributions and provided consistent measurements with good agreement between the repeat measurements. However, the size distribution of the MVC SLNs synthesised with a targeted drug loading of 90 wt. % relative to Compritol ATO 888 showed a polydisperse distribution. The variability between the overlaid triplicate measurements indicated that 90 wt. % targeted drug loading relative to lipid did not result in a consistent size distribution and some of the measurements appeared to be unreliable. In conclusion, 30-70 wt. % gave monomodal distribution while the sample

became polydisperse as we increased the drug loading from 70 wt. % to 90 wt. % relative to Compritol ATO 888. There is no literature about why highly drug loaded SLNs become unstable when a maximum point of encapsulation has been done. However, it has been hypothesised that Compritol ATO 888 loses its effect as an excipient when the MVC-SLNs have been encapsulated with 90 wt. % MVC relative to Compritol ATO 888.

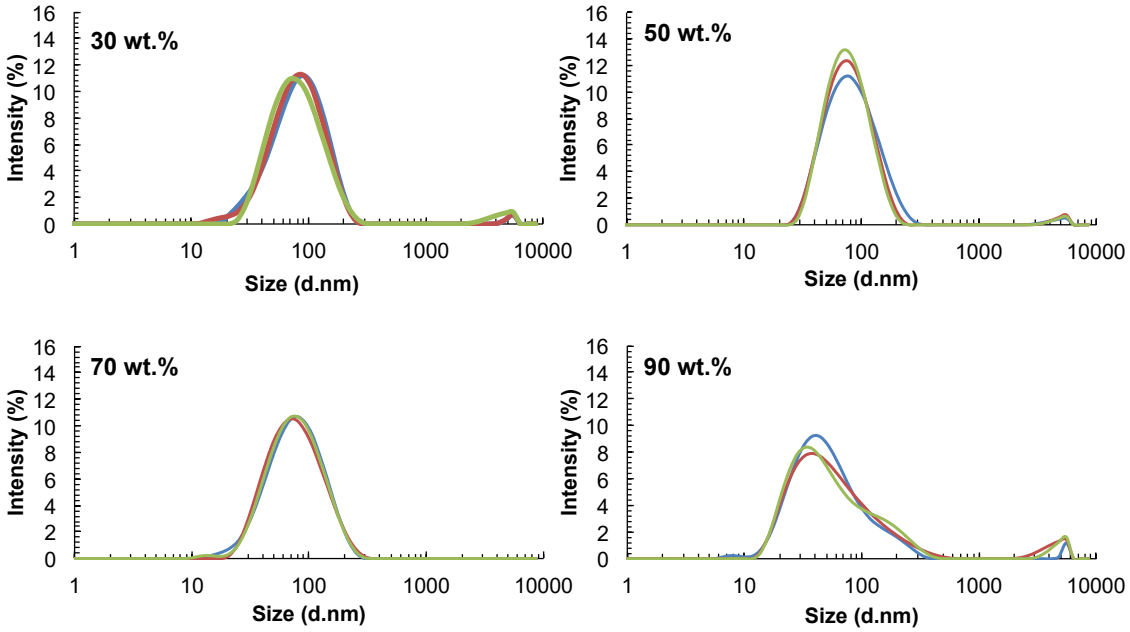

Fig. 4.3. Selected DLS traces of three repeat measurement of MVC –SLN dispersions with targeted loadings of 30, 50, 70 and 90 wt. % of MVC relative to Compritol ATO 888 after day 3.

The D_z and PDI from the measured DLS data obtained from the dialysed MVC-SLNs with targeted drug loadings of 10-90 wt. % MVC relative to Compritol ATO 888 and MVC dispersion of 100 wt. % are given on Table 4.2. From the table is can be seen that 10-30 wt. % of drug loading results in slightly higher D_z values 74-83 nm than those with MVC loading of 40-70 wt. %, which have D_z values of 68-70 nm. The PDI distribution of all the samples were above 0.190, which indicates that the samples were polydisperse. In conclusion, the change in the drug loading does not result in a significant change in particle diameter of the MVC-SLNs. However, it has been hypothesised that since MVC is hydrophobic it could blend in with Compritol ATO 888 in the resulting matrix of MVC-SLN. This hypothesis is consistent with that explaining how oil droplets could blend in with solid lipids NLC

particles.[279] In NLC particles the SLN matrix composition is altered by adding a lipid, which is often an oil. The oil can be incorporated to the NLC particle to prevent the lipid in crystallising upon storage due to its polymorphic transitions described in chapter 1 and literature.[94]

Table 4.2. D_z and PDI values of dialysed MVC loaded SLNs with 10-100 wt. % of MVC relative to lipid in water dispersion comparison of D_z and PDI values. All samples were dialysed for 3 days and measured with a concentration of 1.2 mg/ mL of water at 25 °C. Samples were measured in triplicates and standard deviations are given in ().

wt. % drug rel. to lipid	D_z/nm	PDI
10	79 (0.41)	0.24(0.01)
20	83(3.54)	0.28(0.01)
30	74 (1.41)	0.25(0.00)
40	68(1.15)	0.22(0.01)
50	70(0.72)	0.19(0.01)
70	68 (2.69)	0.21(0.02)

4.2.2 Stability studies of MVC encapsulation SLNs after dialysis

The stable formulations obtained from the solvent injection method with resulting initial MVC drug loadings of 10-70 wt. % relative to Compritol ATO 888 were analysed over 40 days to investigate the stability of the MVC-SLN formulations. The formulations were stored at 4 °C between each measurement as described in Chapter 3. Furthermore, the samples were measured with the same concentrations of 1.2 mg/mL water at 25 °C. The long-term stability of the samples with initial MVC loadings of 10-70 wt.% were then analysed over an extended time range and samples were analysed after 0, 3, 5, 7, 10, and 40 days shown in Fig. 4.4. In addition, three samples with targeted 30, 50, and 70 wt. % MVC loading were kept at 4 °C and measured 150 days after synthesis as shown in Fig. 4.4. The D_z values obtained from DLS measurement at different time points showed no change over time. This indicated excellent colloidal stability of MVC-SLNs with targeted 10-70 wt. % MVC relative to

Compritol ATO 888 over 40 days, Fig. 4.4. However, after dialysis the size of the 10-70 wt. % MVC relative to Compritol ATO 888 increased significantly.

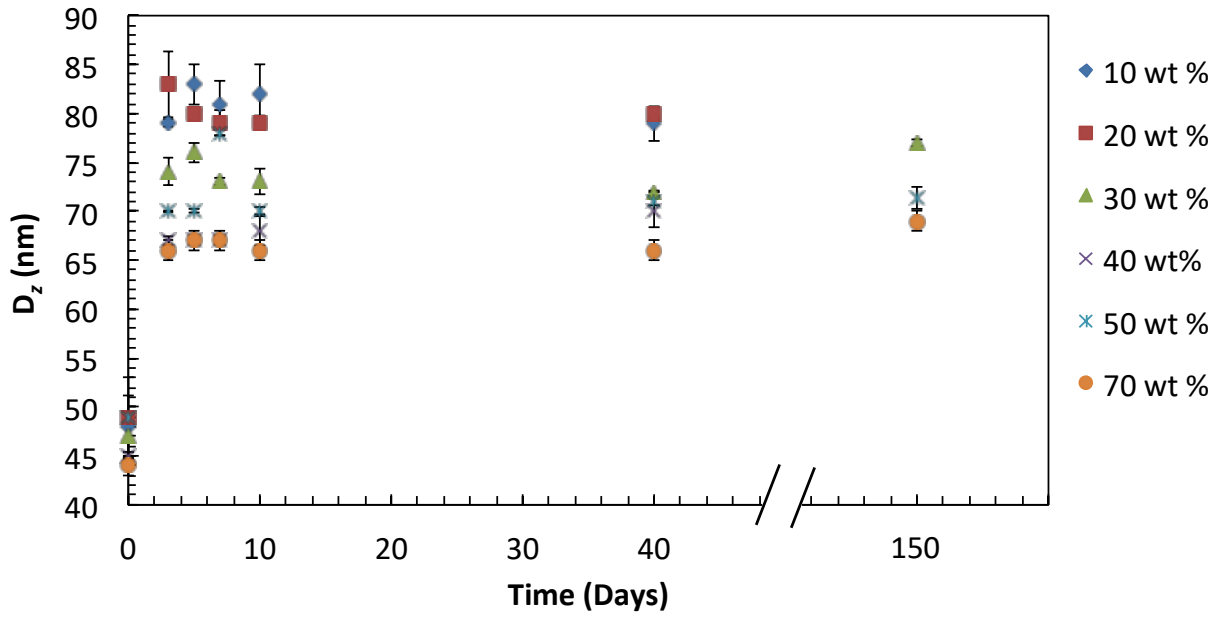

Fig. 4.4. Stability study of MVC encapsulation into SLNs with targeted drug loading of 10-70 wt. % relative to Compritol ATO 888- 1:3 w/w % (DBiB-p(OEGMA)$_{10}$-*co*-(EGDMA)$_{0.6}$ to Compritol ATO 888) analysed over 150 days. Samples were kept in the fridge for 150 days.

It has not been reported why particle sizes of drug loaded SLNs increase after dialysis. However, two possible explanations were given by Müller-Goymann and Schubert for empty SLNs.[124] The first possible explanation was that the emulsifier induced a decrease of the surface tension between organic and aqueous phases that allow the formation of initially smaller solvent droplets causing the observed particle size to decrease.[124] The other explanation is that the SLN particle sizes can be influenced by the viscosity of the outer phase.[124] For example it is mentioned that an increase in viscosity of the aqueous phase on addition of glycerol lead to concentration dependent increase of particle size.[124] Based on this we hypothesise that the addition of IPA to water during the solvent injection lead to a higher viscosity than water and this may cause the particle size to increase.

The corresponding PDI distributions for the same DLS measurements were carried out for SLNs with targeted 10-70 wt. % MVC relative to Compritol ATO 888 and shown in Fig. 4.5. The data showed that the PDIs of measured MVC-SLNs with targeted 10-70 wt. % MVC

relative to Compritol ATO 888 were above 0.19. This indicated that the samples were polydisperse. The samples with high targeted drug loading of 50-80 wt. MVC % relative to Compritol ATO 888 showed lower PDI distributions than those with MVC of 10-30 wt. % relative to Compritol ATO 888. This may suggest that high targeted drug loadings can influence the PDI distribution. Overall, The PDI measured for all MVC-SLNs did not appear to change significantly in either direction. This suggested that MVC-SLNs retained their polydispersity across the time period of measurement.

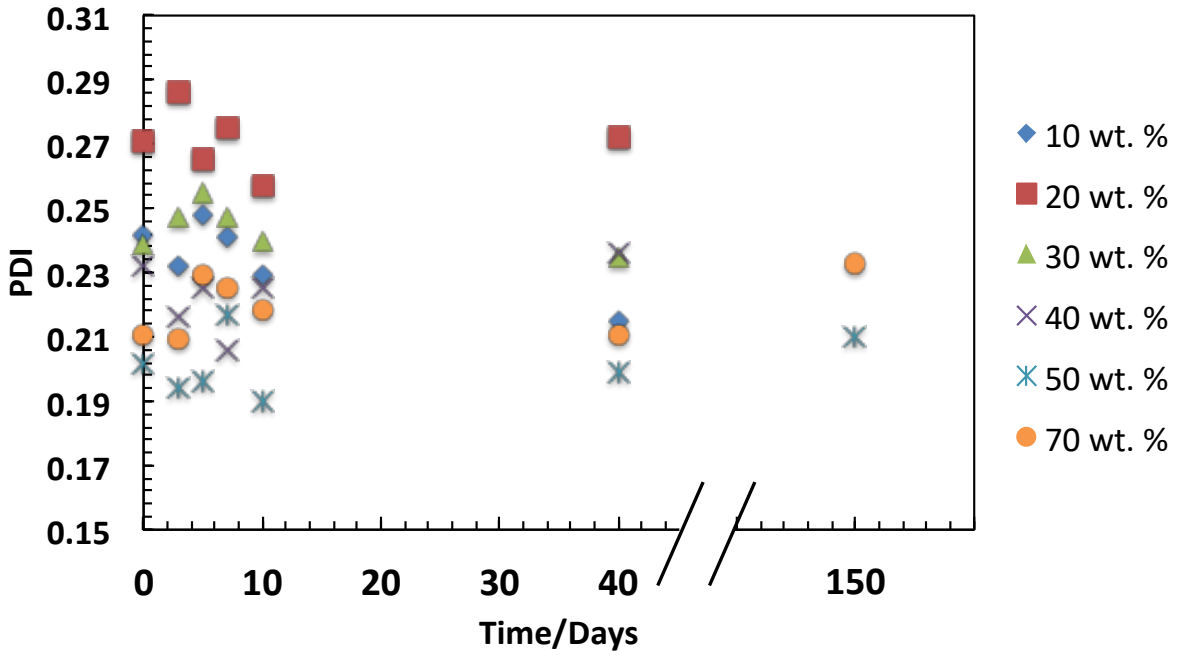

Fig. 4.5. PDI distributions of MVC encapsulation into SLNs with targeted drug loading of 10-70 wt. % relative to Compritol ATO 888- 1:3 (DBiB-p(OEGMA)$_{10}$-*co*-(EGDMA)$_{0.6}$: Compritol ATO 888) analysed over 150 days. Samples were kept in the fridge for 150 days.

The derived count rate (DCR) which is given in kilo counts per second (kcps) was also measured in our studies.[274] DCR represents the scattering intensity that is directly proportional to the size and number of a particle present in a sample.[274] DCR can be used to monitor any potential dissolution of the particle.[274] DCR from DLS measurement of the samples 10-70 wt. % of targeted MVC loading relative to Compritol ATO 888 is shown in Fig. 4.6. The DCR of all of the samples appeared decrease significantly between day 0 and day 3 for targeted MVC loadings of 10-50 wt. % relative to Compritol ATO 888. However, the

DCR for targeted MVC loading of 70 wt. % relative to Compritol ATO 888 only showed a slight decrease from day 0 to day 3 after dialysis. Such a decrease in the DCR when accompanied by an increase D_z suggested that the MVC-SLNs were experiencing swelling. It further suggests that the swelling is reduced when the drug loading is increased as the 70 wt. % MVC loaded SLNs exhibits only a very small decrease in the DCR. A similar effect has been observed for gold polymer hybrid nanoparticles.[294]

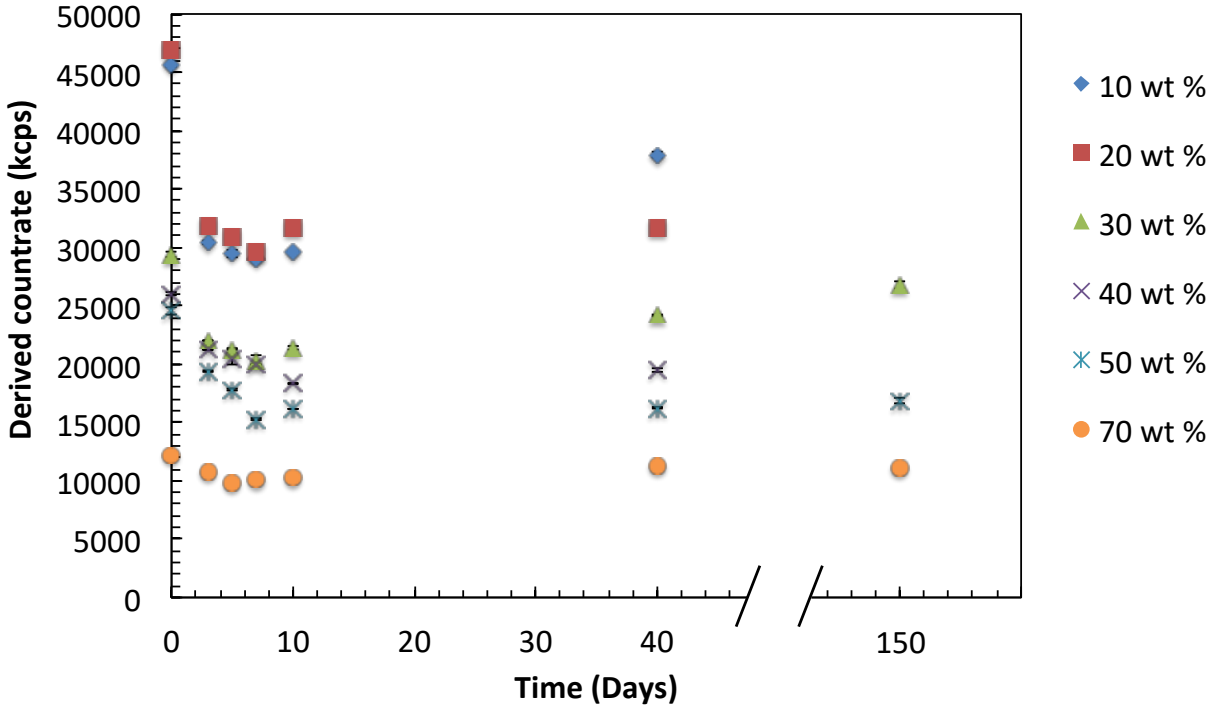

Fig. 4.6. Derived count rate measurements of MVC encapsulation into SLNs with targeted drug loading of 10-70 wt. % relative to Compritol ATO 888- 1:3 (DBiB-p(OEGMA)$_{10}$-*co*-(EGDMA)$_{0.6}$: Compritol ATO 888) analysed over 150 days stored at 4°C.

Three selected samples 30, 50 and 70 wt. % MVC relative to Compritol ATO 888 were kept at 4 °C and analysed after 150 days. The DLS distributions for these at 3, 40 and 150 days are shown in Fig. 4.7 and corresponding correlograms are given in Appendix Fig. A49-A51. The size distributions of 30-70 wt. % were all monomodal and showed no change in the distribution over the 150 days' time period. Moreover, the MVC loaded SLNs loaded with 30-70 wt. % have similar D_z values of 68-74 nm and PDI below 0.25. This indicated that drug loading does not change the stability of the drug over time. In conclusion the stability studies

of MVC-SLNs stored 4 °C with targeted loading of 30-70 wt. % MVC and a 1:3 w/w % DBiB-p(OEGMA)$_{10}$-*co*-(EGDMA)$_{0.6}$:Compritol ATO 888 showed stability over 150 days as aqueous dispersions.

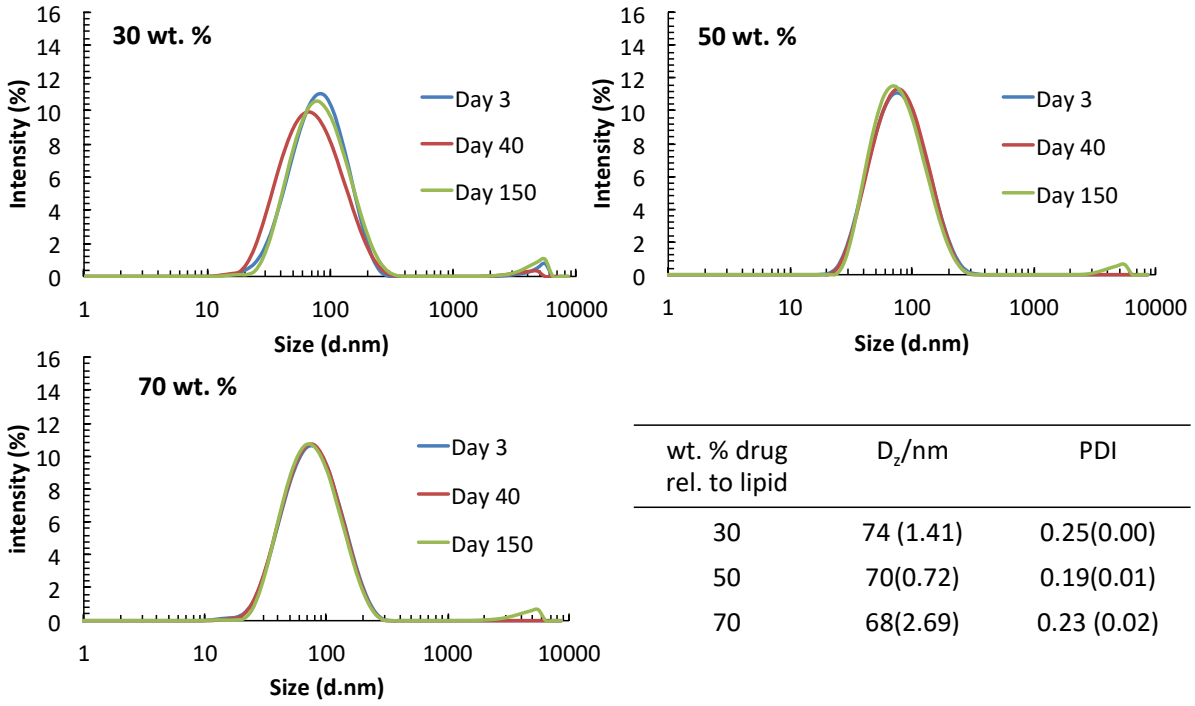

wt. % drug rel. to lipid	D_z/nm	PDI
30	74 (1.41)	0.25(0.00)
50	70(0.72)	0.19(0.01)
70	68(2.69)	0.23 (0.02)

Fig. 4.7. Removing IPA after 3 days of dialysis - Stability test of dialysed samples 30, 50 and 70 wt.% relative to Compritol ATO 888 Z-average over 150 days. Table shows measured Z-average of dialysed MVC-SLN dispersions with targeted MVC loadings of 30,50 and 70 wt. % of MVC relative to MVC on day 3. Standard deviations are given in ().

4.2.3 Stability studies of MVC loaded SLNs after dialysis in PBS

The stability of the dialysed MVC-SLN samples with targeted loadings of 70 wt. % and 50 wt. % relative to Compritol ATO 888 and were analysed at body temperature and physiological ionic strength. This was done to obtain a better understanding of the colloidal stability of the particles under simple conditions mimicking a body fluid. A solution phosphate buffer saline (PBS) was prepared (Chapter 7, section 7.3.1) and 1 mL of concentrated PBS stock solution was added to 1 mL of MVC SLN containing 1.2 mg/mL of either 70 wt. % or 50 wt. % targeted drug loading relative to Compritol ATO 888. The sample was analysed by DLS both

before and after addition of PBS. The samples were then left to incubate at 37 °C. On day 1 and 2 after incubation was initiated the samples were investigated again by DLS and the traces are shown in Fig. 4.8 and corresponding correlograms given in Appendix Fig. A52-A53.

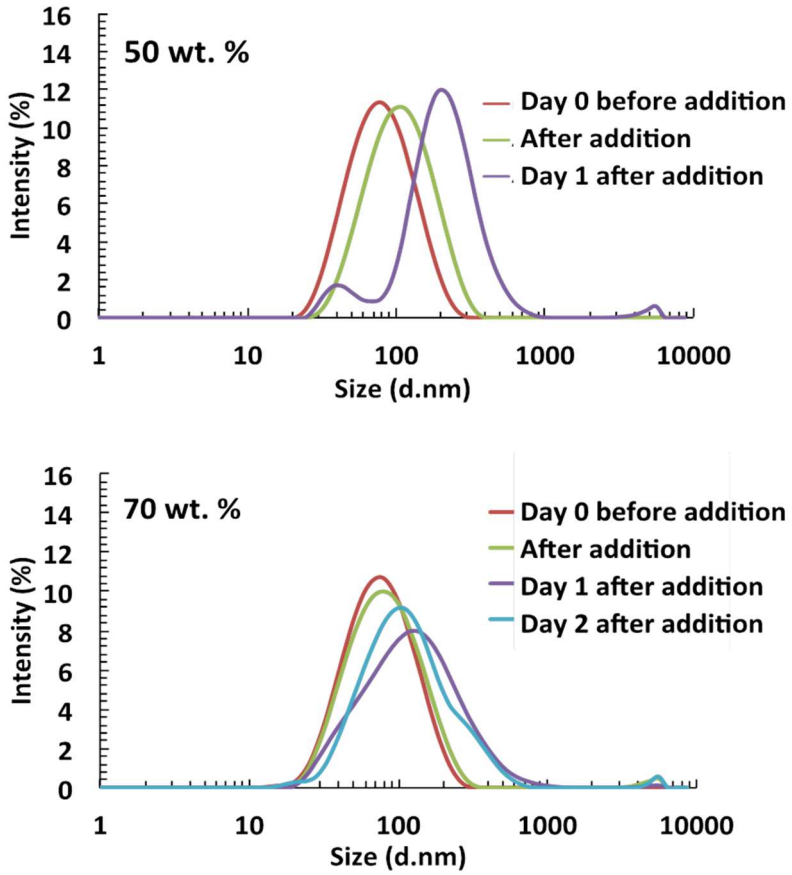

Fig. 4.8. MVC loaded SLNs with 50 and 70 wt. % targeted MVC loading before and after addition of PBS (phosphate buffer saline) solution. The PBS was added to a dialysed 40 days old MVC loaded SLNs (day 0) and after addition of PBS on day 0. The samples were incubated for 1-3 days at 37 °C and analysed by DLS. Measurement on day 2 was not possible for 50 wt. % targeted MVC due to sample instability.

The size distribution of MVC-SLNs with a targeted loading of 70 wt. % MVC loading relative to Compritol ATO 888 showed monomodal distribution over 2 days. This indicated that the sample was stable over 2 days after addition of PBS and incubation of the sample at 37 °C. Thereafter, the DLS measurements of 70 wt. % MVC loading relative to Compritol ATO 888 were no longer reliable due to formation of aggregations in the sample. This indicated that the particles were not stable after day 2. The traces obtained for 50 wt. % of MVC loading

relative to Compritol ATO 888 showed the formation of a bimodal distribution after day 1 incubation at 37 °C. However, the sample was still stable on day 1 due to reproducibility of 3 repeat measurements. However, the stability of MVC-SLNs with targeted MVC loading of 50 wt. % relative to Compritol ATO 888 incubated at 37 °C did not give reliable measurement after 1 day. The D_z, PDI and DCR measured for MVC-SLNs with targeted encapsulation of 70 wt. % MVC relative to Compritol ATO 888 was given on Table 4.3.

Table 4.3. D_z, PDI and derived count rate (DCR) of MVC loaded SLNs with 70 wt. % targeted MVC loading before and after addition of PBS (phosphate buffer saline) solution. The PBS was added to a dialysed 40 days old MVC loaded SLNs (which is indicated as day 0) and incubated for 1-2 days at 37 °C and analysed by DLS. Numbers in () is the standard deviation.

	D_z/nm	PDI	DCR/kcps
Day 0 Before addition	66 (0.7)	0.21(0.04)	11180 (42.7)
Day 0 After addition	72(0.7)	0.23 (0.00)	5882 (63.3)
Day 1	99 (1.0)	0.37(0.01)	7902(48.6)
Day 2	111 (12.1)	0.33 (0.08)	8024 (141.4)

As shown on Table 4.3, D_z increased from 66 - 72 nm after addition of PBS and increased further through to day 2 where it reached 111 nm. This increase indicated that the particle aggregated in the PBS solution. However, DCR obtained from the DLS measurements of MVC-SLNs with targeted encapsulation of 70 wt. % MVC relative to Compritol ATO 888 showed a decrease from 11180 on day 0 to 8024 on day 2. The combined D_z and DCR figures are consistent with the MVC-SLNs with targeted encapsulation of 70 wt. % MVC relative to Compritol ATO 888 swelling after addition of PBS. This further suggests the cause of SLN loss is excessive swelling leading to a rupture. This might also be why an SLN with a lower amount of drug loading is more vulnerable as it already has a slightly larger diameter when PBS is added the dispersion as seen in Fig. 4.8.

In conclusion, the studies suggested that 50 wt. % MVC relative to Compritol ATO 888 was less stable than 70 wt. % of MVC relative to Compritol ATO 888. This indicated that the colloidal stability of MVC-SLNs with targeted MVC loadings above 70 wt. % MVC relative to Compritol ATO 888 show better stability under conditions that mimics physiological conditions in the body, therefore the 70 wt. % MVC sample was selected for further analysis.

4.2.4 ^{1}H NMR studies of MVC encapsulation SLNs after dialysis

^{1}H NMR allows us to integrate resonances which have been assigned to Compritol ATO 888 and MVC separately and the ratio can then be used to quantify the drug loading using previously established calibration curve. To the best of our knowledge calculating the drug loadings in SLN systems by either ^{1}H or ^{19}F NMR using a standard calibration curve has not yet been demonstrated. ^{1}H NMR of MVC, Compritol ATO 888, and DBiB-p(OEGMA)$_{10}$-*co*-(EGDMA)$_{0.6}$ were acquired in $CDCl_3$ at 50 °C and was assigned separately, see Fig. 4.9, 4.10 and 4.11 respectively. The ^{1}H NMR spectra of MVC at 50 °C was shown in Fig. 4.9. The ^{1}H NMR (400 MHz; $CDCl_3$) resonances were assigned as follows δ = 7.32-7.36 (2H, m), 7.26 (3H, m), 6.36–6.38 (1H, m), 5.15-5.18 (1H, dd, *J* 6.7 Hz, 6.7 Hz), 4.25-4.35 (1H, m), 3.34-3.38 (2H, m), 2.95-3.02 (1H, m), 2.49 (3H, s), 2.43 (2H, t, J=7Hz), 1.59-2.28 (20H, m), 1.37-1.39 (6H, d, *J* 7.0 Hz). The assignments of the MVC signals in $CDCl_3$ were in agreement with literature.[295]

The ^{1}H NMR spectra of Compritol ATO 888 at 50 °C in $CDCl_3$ was given in Fig. 4.10. The ^{1}H NMR (400 MHz; $CDCl_3$) resonances were assigned as follows δ = 3.57-4.33 ppm (4H,m), 2.28-2.35 ppm (4H, m), 1.62 (4H,m), 1.26 ppm (72 H, m), 0.88 ppm (6H, t, J=7 Hz).

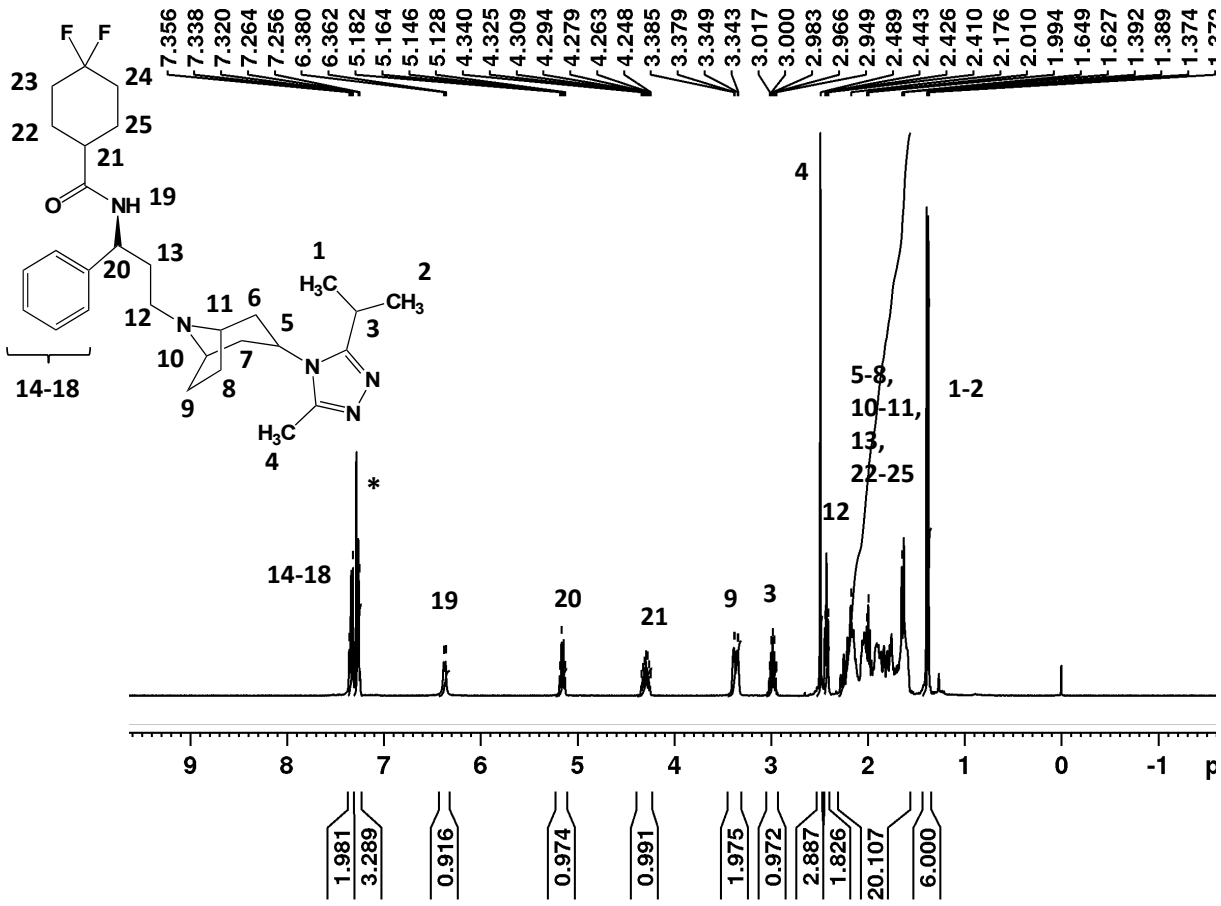

Fig. 4.9. ^{1}H NMR (400 MHz) of 4.5 mg of MVC in $CDCl_3$ at 50 °C. The spectra of MVC was characterised based on literature.[295] The $CDCl_3$ solvent residual peak was assigned to δ = 7.26 ppm in agreement with literature.[296] The signals were referenced to TMS at δ = 0 ppm.

The ^{1}H NMR spectra of DBiB-p(OEGMA)$_{10}$-*co*-(EGDMA)$_{0.6}$ at 50 °C in $CDCl_3$ was given in Fig. 4.10. ^{1}H NMR (400 MHz; $CDCl_3$) resonances of DBiB-p(OEGMA)$_{10}$-co-(EGDMA)$_{0.6}$ were assigned as follows δ = 0.9 ppm (42 H), 1.3 (18 H), 1.5-1.9 ppm (30 H), 3.4 ppm (32 H), 3.5 ppm (22 H), 3.6 ppm (146 H) and 4.1 (25 H).

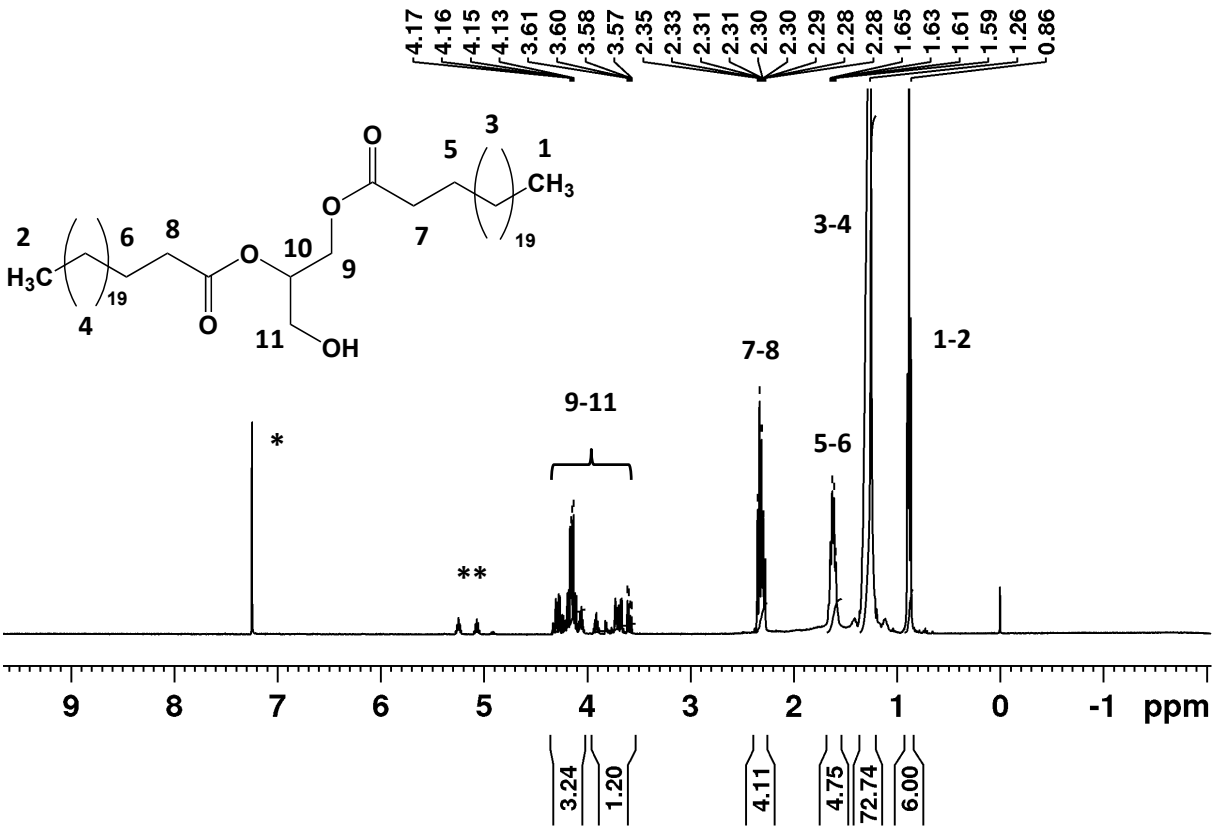

Fig. 4.10. ^{1}H NMR (400 MHz) of 4.5 mg of Compritol ATO 888 in $CDCl_3$. The solvent residual peak was assigned to 7.26 ppm in agreement with literature.[296] The signals were referenced to TMS at δ = 0 ppm. ** Is an unknown impurity.

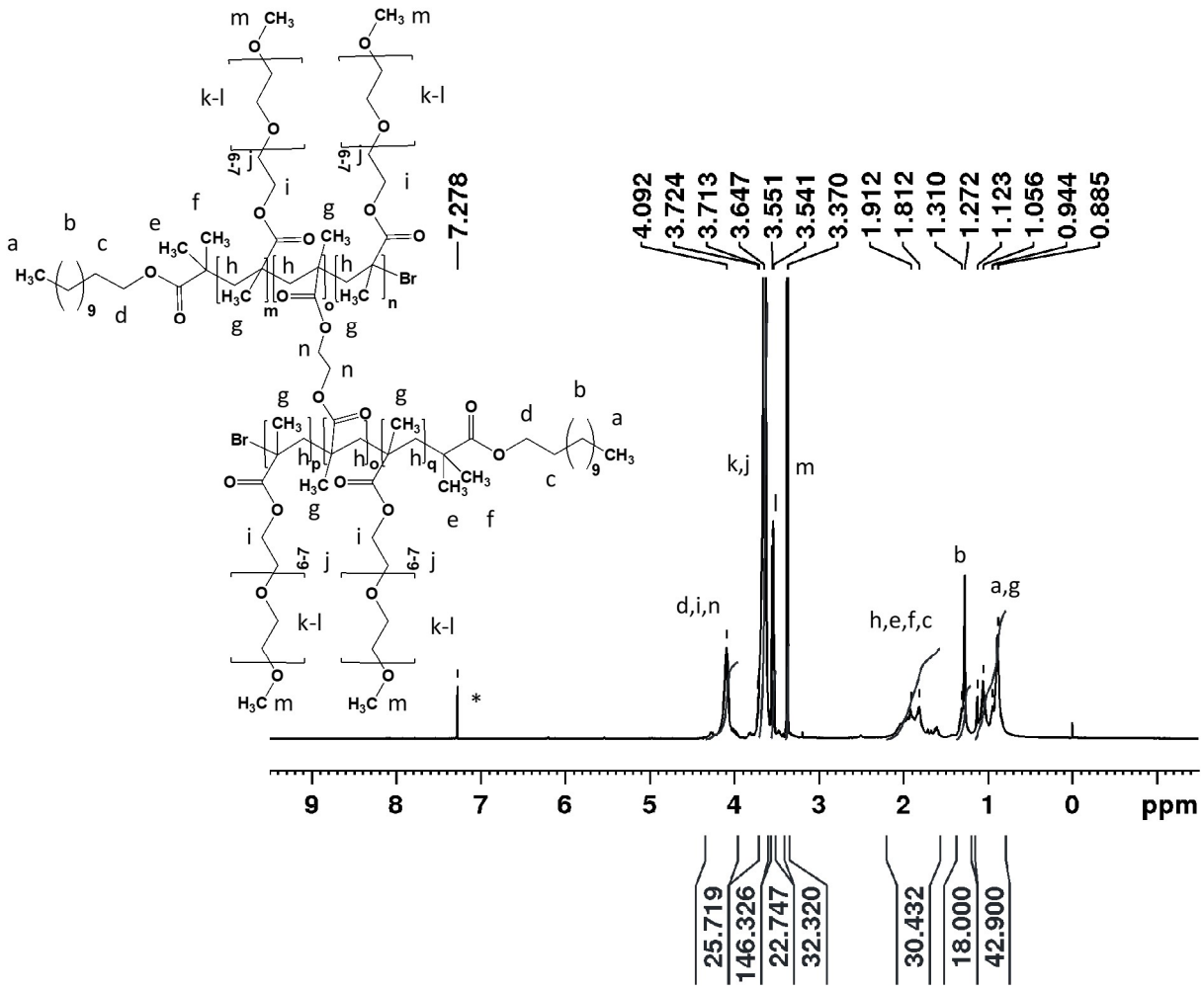

Fig. 4.11. ^{1}H NMR (400 MHz) of 3 mg of DBiB-p(OEGMA)$_{10}$-*co*-(EGDMA)$_{0.6}$ in $CDCl_3$ at 50 °C. The solvent residual peak was assigned to 7.26 ppm in agreement with literature.[296] The signals were referenced to TMS at δ = 0 ppm. *Is solvent $CDCl_3$ residual peaks.

The ^{1}H NMR spectra of DBiB-p(OEGMA)$_{10}$-*co*-(EGDMA)$_{0.6}$, MVC and Compritol ATO 888 at 50 °C in $CDCl_3$ are shown overlaid each other in Fig. 4.12. Individual resonances of DBiB-p(OEGMA)$_{10}$-*co*-(EGDMA)$_{0.6}$, MVC and Compritol ATO 888 were identified for each of the compounds present each has at least one of the following problems: Insufficient signal to noise, overlapping with nearby resonance which prevents accurate integration, or the resonance is composed of multiple protons in a very similar environment appearing at the same chemical shift and as one resonance. Since there are no unique peaks observed for both the MVC and Compritol ATO 888 in the mixtures of ^{1}H NMRs of DBiB-p(OEGMA)$_{10}$-*co*-

(EGDMA)$_{0.6}$, MVC and Compritol ATO 888 it was not possible to integrate a signal from MVC and quantify this against Compritol ATO 888.

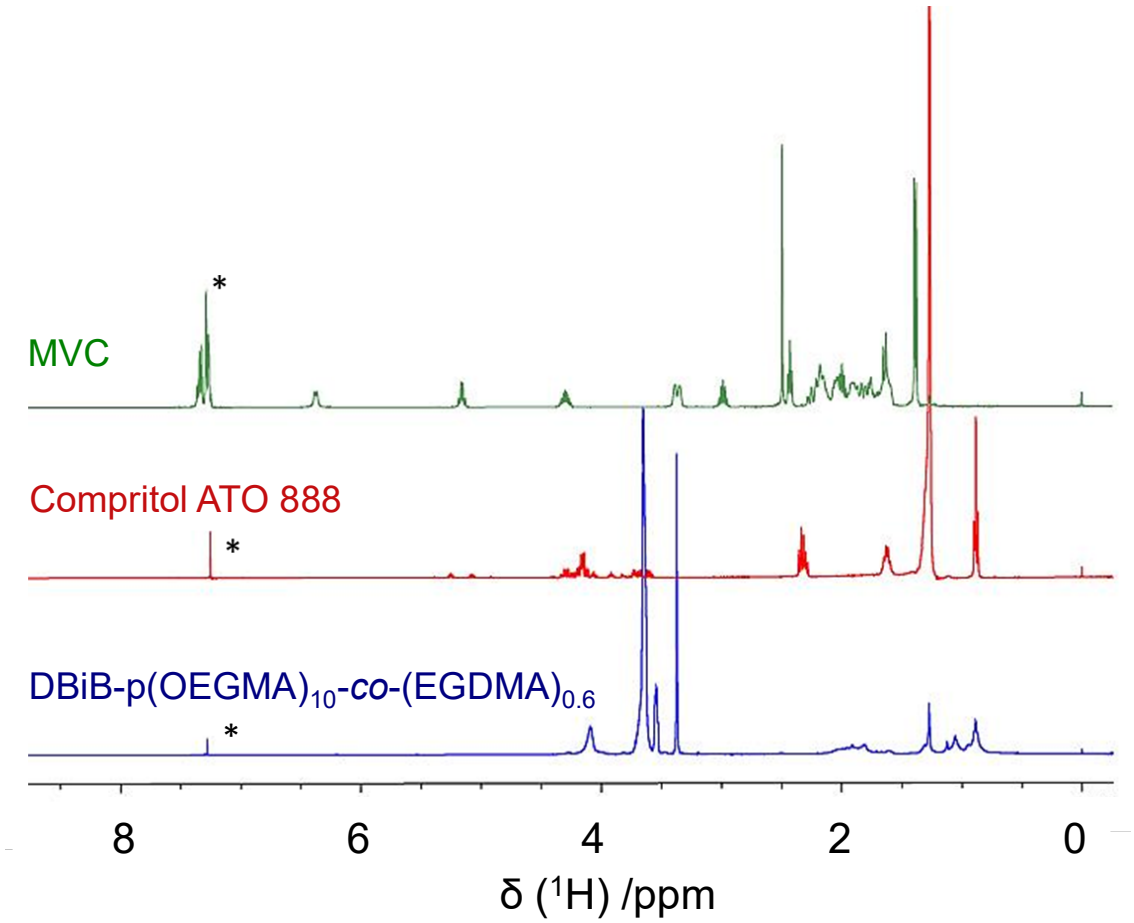

Fig. 4.12. Overlaid ^{1}H NMR (400 MHz) spectra of MVC, Compritol ATO 888 and DBiB-p(OEGMA)$_{10}$-*co*-(EGDMA)$_{0.6}$ in $CDCl_3$ at 50 °C. The signals were referenced to TMS at δ = 0 ppm.

4.2.5 ^{19}F NMR studies of MVC encapsulation SLNs after dialysis and freeze drying

4.2.5.1 Optimisation of temperature and solvent conditions in ^{19}F NMR of MVC and TBHF

MVC contains two fluorine atoms, which can be observed using ^{19}F NMR spectroscopy. Therefore, a method was devised using ^{19}F NMR to quantify the amount of MVC loaded into SLNs. The solvent, $CDCl_3$, used for the quantification experiments was selected because SLNs are soluble in this solvent at any temperature, which would enable the MVC to be easily extracted from the SLNs.

Tetrabutylammonium hexafluorophosphate (TBHF), Fig. 4.13, was used as an internal reference as it is a non-reactive chemical used as a phase transfer catalyst in electrochemical reactions[297] and also has good solubility in $CDCl_3$.

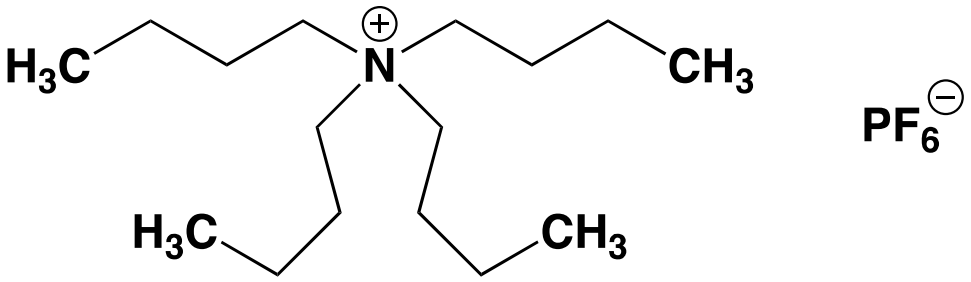

Fig. 4.13. Chemical structure of tetrabutyl hexaflourophosphate (TBHF).

Stock solutions of MVC were created as described in Chapter 7 and were diluted to give different concentrations of MVC in $CDCl_3$ equivalent to loading SLNs with 25, 50, 75 and 100 wt. % relative to lipids. This was done with the purpose of mimicking the total amount of MVC in SLN systems. Initial experiments were done with MVC (18 mg, 1 eq.) in non-dried $CDCl_3$ and a spectrum was acquired at two different temperature 25 °C and at 50 °C in the presence of the internal reference TBHF (1 eq.) as described in Chapter 7 section 7.3. The resulting ^{19}F NMR spectra are given in Fig. 4.14. The internal reference TBHF signals were assigned to $\delta =$ - 71.25 ppm and - 73.11 ppm. The two resonances observed are due to ^{31}P splitting the ^{19}F signal into a doublet due to J-coupling of 714 Hz.

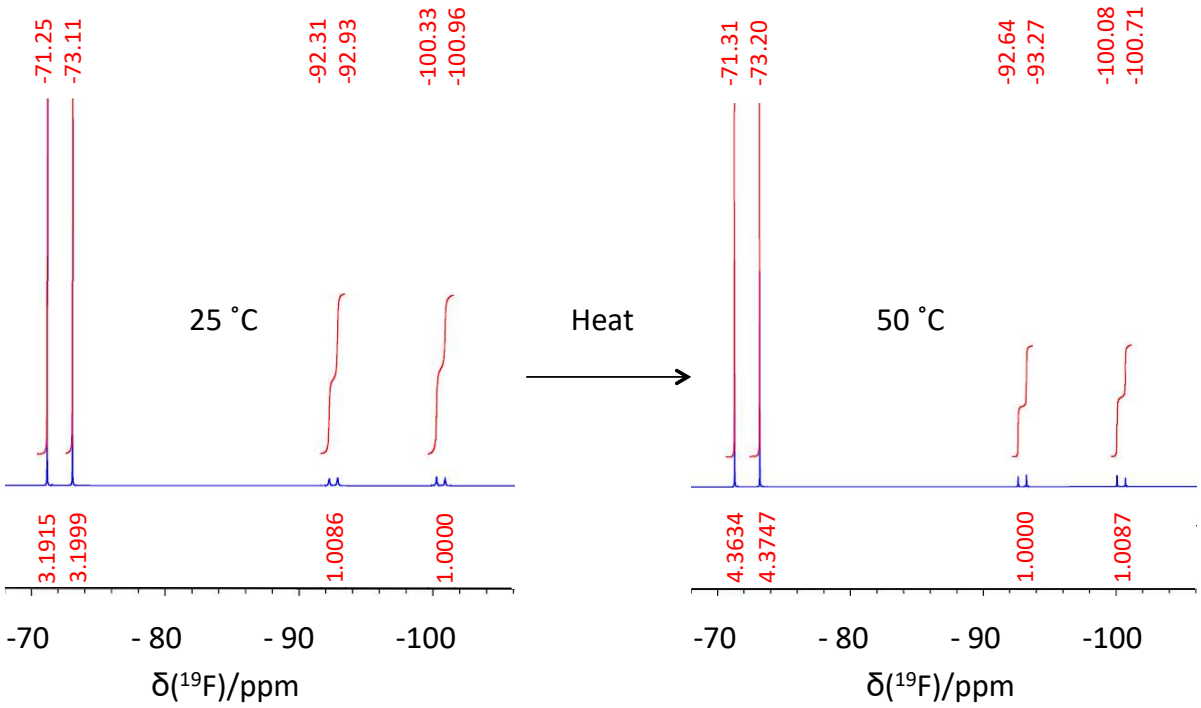

Fig 4.14. ^{19}F NMR spectra of MVC in non-dried $CDCl_3$ recorded at room 25˚C and at 50˚C. Internal reference is TBHF.

The signals from the two ^{19}F atoms on MVC appear as two doublets. This is because the fluorine atoms are inequivalent and their J-coupling splits each other's resonance. The first doublet was assigned to ^{19}F δ = -92.31 and -92.93 ppm while the other doublet was assigned to ^{19}F δ = -100.33 and -100.96 ppm. The J-coupling is therefore measured as 237 Hz and 235 Hz, respectively.

It was discovered the signal intensity of MVC was affected by whether the NMR solvent $CDCl_3$ was contaminated with water. It was initially observed that when a sample of MVC and TBHF was acquired at 25 °C and 50 °C the intensity of TBHF relative to MVC increased from 3.19 to 4.36 as shown in Fig. 4.14. This meant that the intensity measurements were sensitive to temperature in presence of water. Such a sensitivity is undesirable as in order to measure the concentration of MVC in SLNs the temperature would need to be increased to 50 °C. In our efforts to reduce the sensitivity of the resonances to temperature, we found that drying $CDCl_3$ in the presence of molecular sieves completely eliminates the problem. The resulting spectra at 25 °C and 50 °C after drying $CDCl_3$ are shown in Fig. 4.15 where the

relative intensities between TBHF and MVC are 2.8 and 2.8, respectively. On this basis, it was concluded that water interferes with MVC and therefore ^{19}F resonances. However, the mechanism for this is unknown, but it is likely to be caused by a relaxation phenomenon possibly due to fluorine hydrogen bonding. Therefore, sieve dried $CDCl_3$ was used in all subsequent experiments.

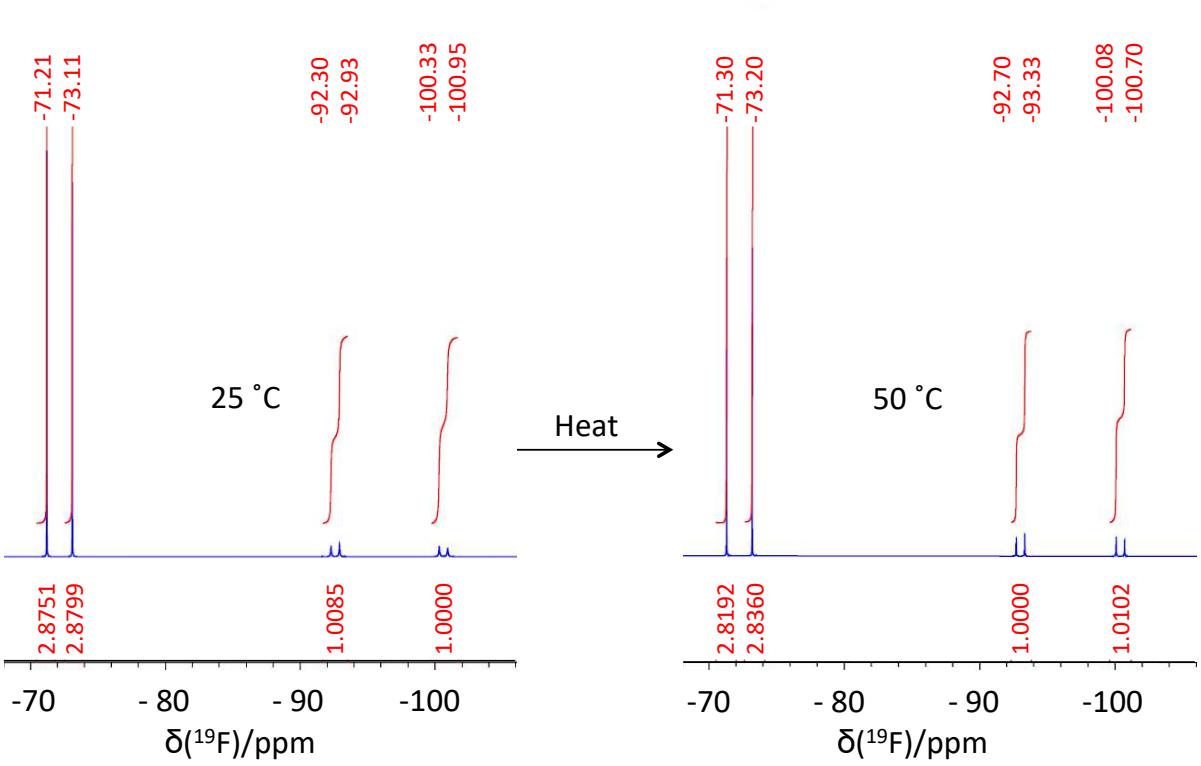

Fig 4.15. ^{19}F NMR spectra of MVC at 25 °C and 50 °C in $CDCl_3$. MVC signals does not change relative to TBHF at 50 °C the heat in $CDCl_3$ dried over molecular sieves. Internal reference is TBHF

MVC and TBHF were studied in the presence of the polymer and lipid in order to determine whether there were any interactions which would interfere with the ^{19}F resonances and therefore the quantification of MVC. In Fig. 4.16 ^{19}F NMR spectra acquired at 25 and 50 °C of samples with MVC and TBHF in the presence of DBiB-p(OEGMA)$_{10}$-*co*-(EGDMA)$_{0.6}$ are shown. From these spectra, it can be seen that the intensity ratio between TBHF and MVC increase from 1.9 at 25 °C to 2.7 at 50 °C. The expected intensity ratio is 3 as there are two fluorine on MVC and six on TBHF. It was therefore concluded that MVC interacts with the polymer at 25 °C but this interaction disappears when the sample is heated to 50 °C.

Therefore, in order to accurately quantify the amount of MVC using ^{19}F NMR the samples were heated to 50 °C.

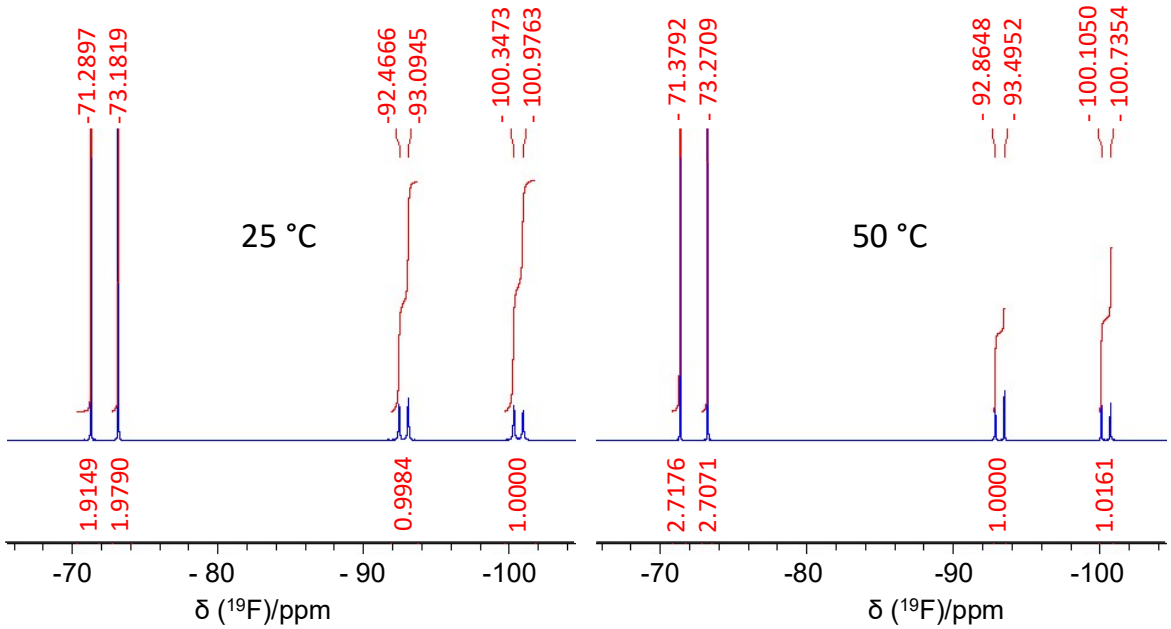

Fig. 4.16. ^{19}F NMR spectra of MVC (9 mg) and DBiB-p(OEGMA)$_{10}$-co-(EGDMA)$_{0.6}$ at 25 °C and 50 °C in $CDCl_3$. MVC signals do not change relative to TBHF at 50 °C the heat in $CDCl_3$ dried over molecular sieves. Internal reference is TBHF

In Fig. 4.17 the ^{19}F NMR spectra of MVC and TBHF acquired at 25 and 50 °C in the presence of Compritol ATO 888 are shown. From these spectra, it can be seen that the intensity ratio between MVC and TBHF are 3.2 at both temperatures as would be expected. It was therefore concluded that MVC does not interact with Compritol ATO 888 in such manner that the ^{19}F NMR resonances are affected as was observed with the polymer. However, the temperature of future concentration measurements using ^{19}F NMR were conducted at 50 °C due to the interaction observed between MVC and the polymer.

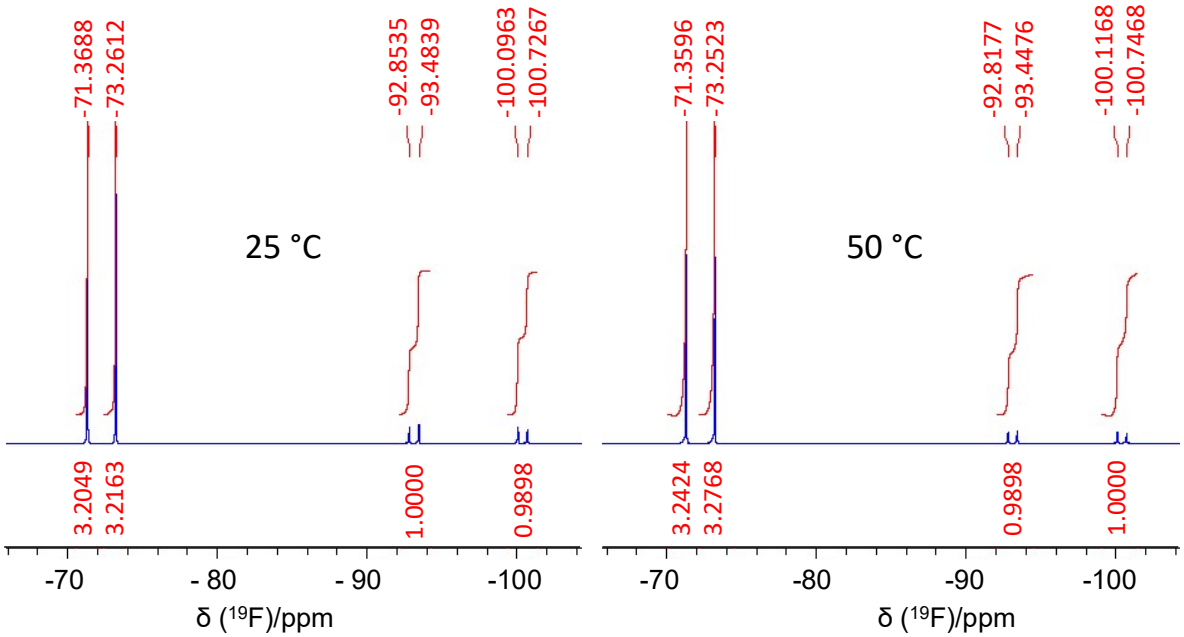

Fig. 4.17. ^{19}F NMR spectra of MVC (9 mg) and Compritol ATO 888 at 25 °C and 50 °C in $CDCl_3$. MVC signals does not change relative to TBHF at 50 °C the heat in $CDCl_3$ dried over molecular sieves. Internal reference is TBHF

4.2.5.2 ^{19}F NMR of MVC and TBHF calibration curve

The optimised conditions from the previous section were used to record a series of MVC concentrations in dry $CDCl_3$ to obtain a calibration curve. This curve can be used to calculate the concentration of MVC loaded into SLNs while dissolved dry $CDCl_3$ at 50 °C and using TBHF as the internal reference. The concentrations of MVC and TBHF in dry $CDCl_3$ used to record ^{19}F NMR spectra to obtain a calibration curve are given in Table 4.4.

Table 4.4. Concentrations of MVC and TBHF in dry $CDCl_3$ used for ^{19}F NMR experiment calibration curves.

wt % MVC	m_{TBHF} (mg)	n_{TBHF} (mmol)	TBHF eq.	m_{MVC} (mg)	n_{MVC} (mmol)	MVC eq.
25	13.6	26.2	1	4.5	8.7	0.25
50	13.6	17.5	1	9.0	17.5	0.5
75	13.6	8.7	1	13.5	26.2	0.75
100	13.6	35.0	1	18.0	35	1

The concentration of TBHF was kept constant in all solutions to act as an internal reference. The concentration of MVC was varied between each preparation. Initially, MVC was prepared in a concentration, which would correspond to an SLN with a targeted drug loading of 100 wt. % MVC relative to lipid. Such solutions were also prepared with MVC in concentrations corresponding to 25, 50, 75 wt. % of the maximum amount of MVC used in MVC-SLN synthesis. The exact amounts used in mmol and mg equivalents are shown in Table 4.4.

The theoretical intensities of MVC were normalised to 1 and the theoretical and experimental intensities of TBHF was expected to change as MVC was diluted. The theoretical intensity of TBHF, $I_{TBHF,\ Theo}$, was calculated as follows:

$$I_{TBHF,Theo} = \frac{100\ \text{wt.\% MVC}}{X\ \text{wt.\% MVC}} \cdot 3 \qquad \textbf{(4.2)}$$

Where $I_{TBHF,\ Theo}$ is the theoretical intensity of TBHF at a given X wt. % drug loading into SLNs. 100 wt. % MVC is the maximum amount of drug added to the system and X wt. % is any arbitrary amount of drugs added to the system. 3 it the number of ^{19}F pr. Signal of the TBHF. The Theoretical $I_{TBHF,\ Theo}$ are calculated on Table 4.

Table 4.5. Calculated theoretical and experimental intensities of MVC and TBHF in dry $CDCl_3$ used for ^{19}F NMR experiment calibration curves.

wt % MVC	TBHF intensities (theo.)	TBHF Intensities (exp.)	MVC intensities (theo.)	MVC Intensities (exp.)	MVC eq.
25	12	12.3	1	1	0.25
50	6	5.9	1	1	0.5
75	4	3.7	1	1	0.75
100	3	2.9	1	1	1

An overlay of ^{19}F NMR spectra recorded in dry $CDCl_3$ at 50 °C of MVC in presence of TBHF is at different concentrations 25% - 100% are given in Fig. 4.18. The resonances were assigned as in previous sections. The four spectra overlaid in Fig. 4.18 show samples where an increasing proportion of MVC was added relative to TBHF going from the bottom to the top. As expected the signal intensity of MVC increases linearly with the increased

concentration of MVC as can be seen in Fig. 4.19. The relationship derived from this linear regression curve shown in Fig. 4.19 was used to calculate the concentration of MVC in MVC loaded SLNs.

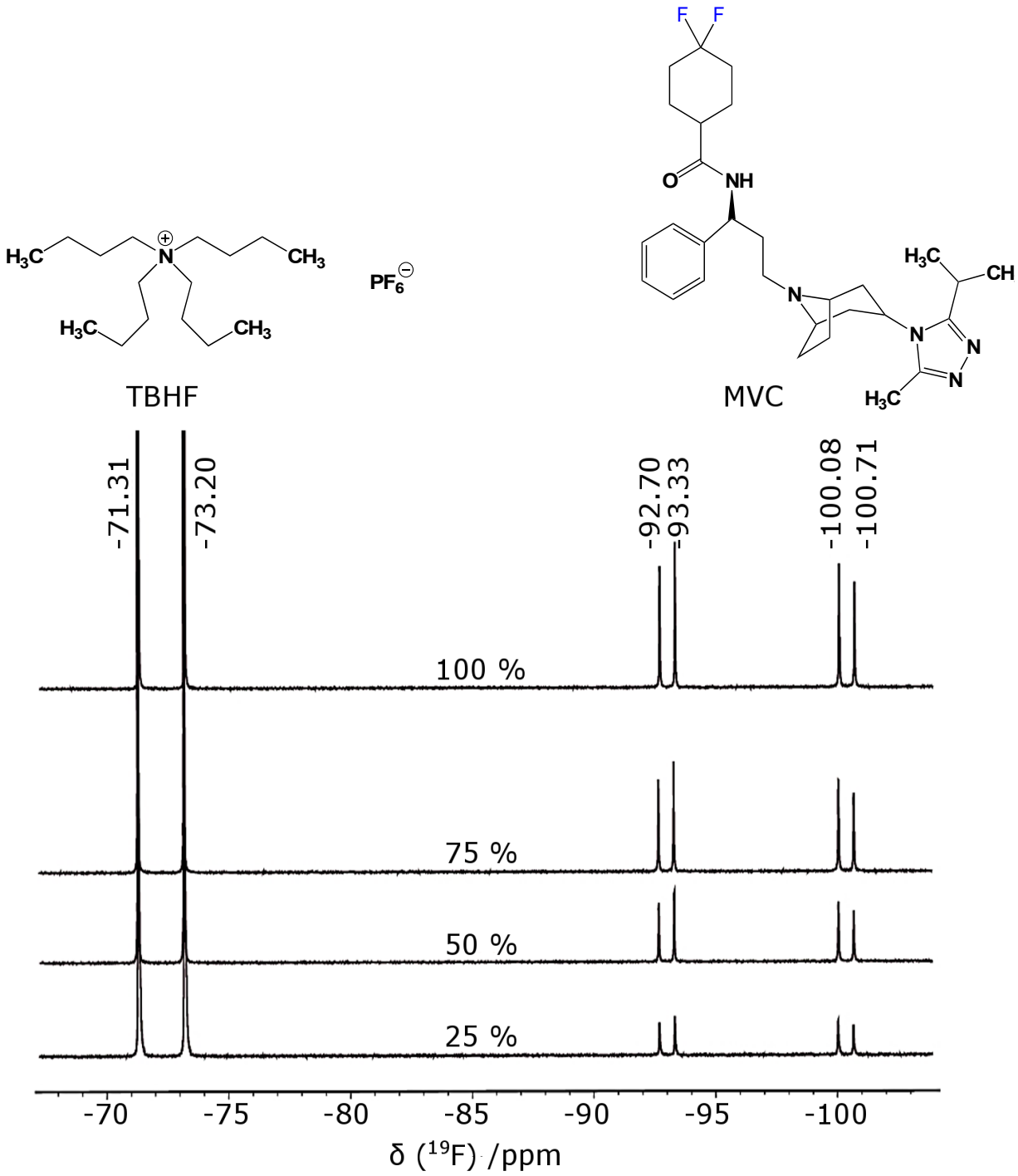

Fig. 4.18. Overlay of ^{19}F NMR spectra (376.42 MHz) in dry $CDCl_3$ of MVC in presence of TBHF at different concentrations 25% - 100%. Were 100 % is 18 mg MVC.

Concentrations of MVC can be used to calculate a signal intensity ratio when compared to the signal intensity of TBHF to produce a calibration curve with the following linear relationship:

$$\frac{3 \cdot \mathrm{I_{MVC}}}{\mathrm{I_{TBHF}}} = a \cdot C \qquad \textbf{(4.3)}$$

where I_{MVC} is the intensity of MVC resonances, I_{TBHF} is the intensity of TBHF resonances, *C* is the concentration which would be used to create an SLN with a wt. % of MVC relative to lipid, and *a* is the gradient.

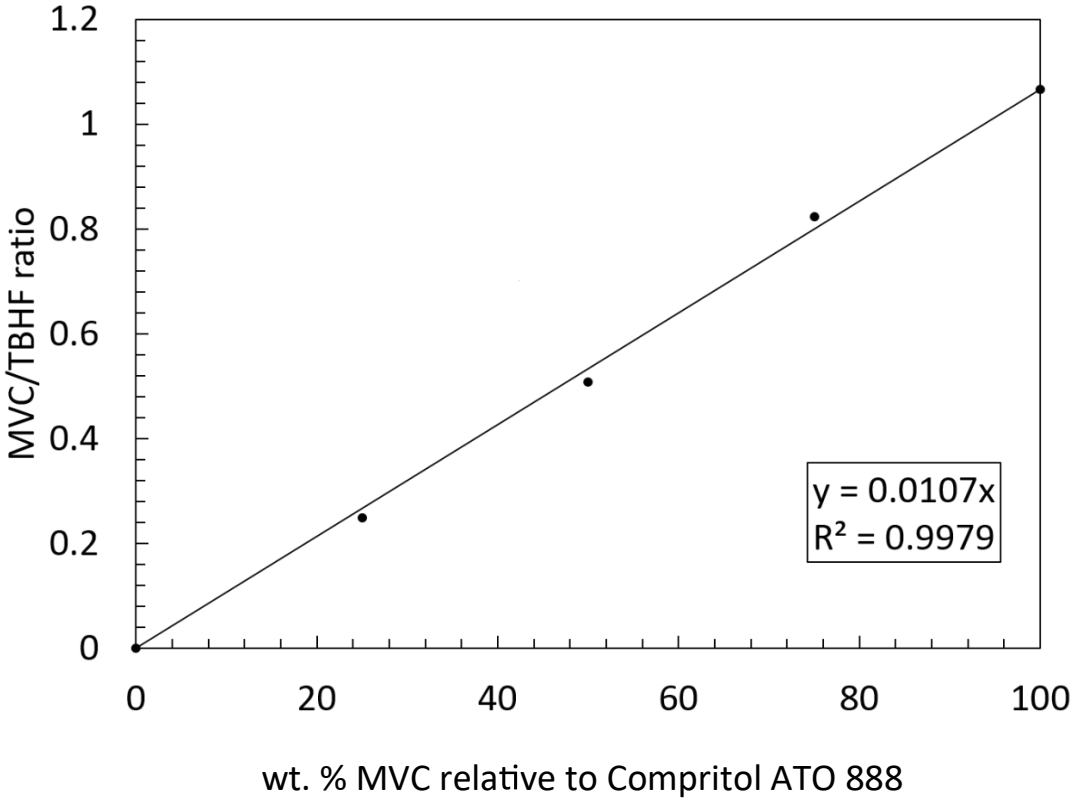

Fig. 4.19. Linear relationship of MVC/TBHF ratio against concentration of MVC in wt. % relative to Compritol ATO 888.

The study was also replicated with same compositions of MVC and TBHF as well as the presence of Compritol ATO 888 and DBiB-p(OEGMA)$_{10}$-*co*-(EGDMA)$_{0.6}$. Another ^{19}F NMR measurement was also conducted with the additional presence of freeze dried SLNs. Both calibration curves are shown in Fig. 4.20. The purpose of this study was to investigate

whether Compritol ATO 888 or DBiB-p(OEGMA)$_{10}$-*co*-(EGDMA)$_{0.6}$ interfered with MVC and therefore with the resonance intensities in the ^{19}F spectra. The results showed that the derived calibration curves achieved by the ratio of TBHF and MVC gave a straight line for MVC, Compritol ATO 888 and DBiB-p(OEGMA)$_{10}$-*co*-(EGDMA)$_{0.6}$ and the same for freeze dried SLNs. Furthermore, the results showed that a slight difference in gradient was apparent when the calibration curve of MVC with DBiB-p(OEGMA)$_{10}$-*co*-(EGDMA)$_{0.6}$ and Compritol ATO 888 was compared against the calibration curve for MVC alone.

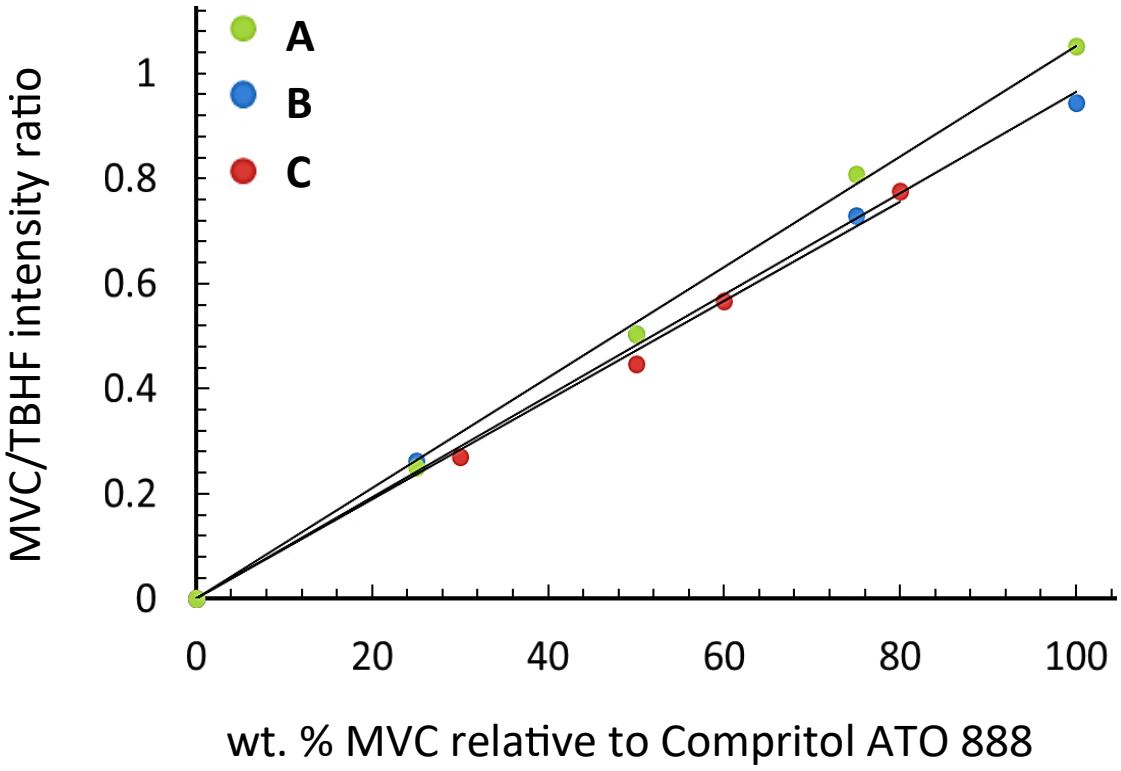

Fig. 4.20. Comparison of calibration curves obtained by ^{19}F NMR of **A)** MVC (green), **B)** Compritol ATO 888 + DBiB-p(OEGMA)$_{10}$-*co*-(EGDMA)$_{0.6}$ + MVC (blue) and **C)** Freeze dried SLNs (red) at 50 ˚C

The amount of MVC lost during the dialysis has been calculated and ranges between 25% and 60%. The complete data is shown in Table 4.6.

Table 4.6. Values obtained for the ^{19}F-NMR studies of SLNs with 30-80 wt. % MVC relative to lipid (Compritol ATO 888). MVC/TBHF is the ratio of intensities obtained from ^{19}F NMR spectra of SLNs.

wt % MVC rel. lipid	MVC/TBHF intensity ratios	% Drug encapsulated	% lost drug	Exp. encapsulated drug	Theo. encapsulated drug
30	0.050	4.8	25.2	0.9	5.4
50	0.151	14.4	35.6	2.5	9.0
60	0.095	9.0	50.9	1.6	10.8
80	0.202	19.3	60.7	3.4	14.4

Additionally, a calibration curve was created using SLNs with MVC which have been both freeze-dried and dialysed. This calibration curve is compared to the one from SLNs with MVC, which have only been freeze-dried in Fig 4.21. This figure appears to show that a significant amount of MVC has been lost during the dialysis as the calibration curve for the dialysed particles has a significantly shallower slope.

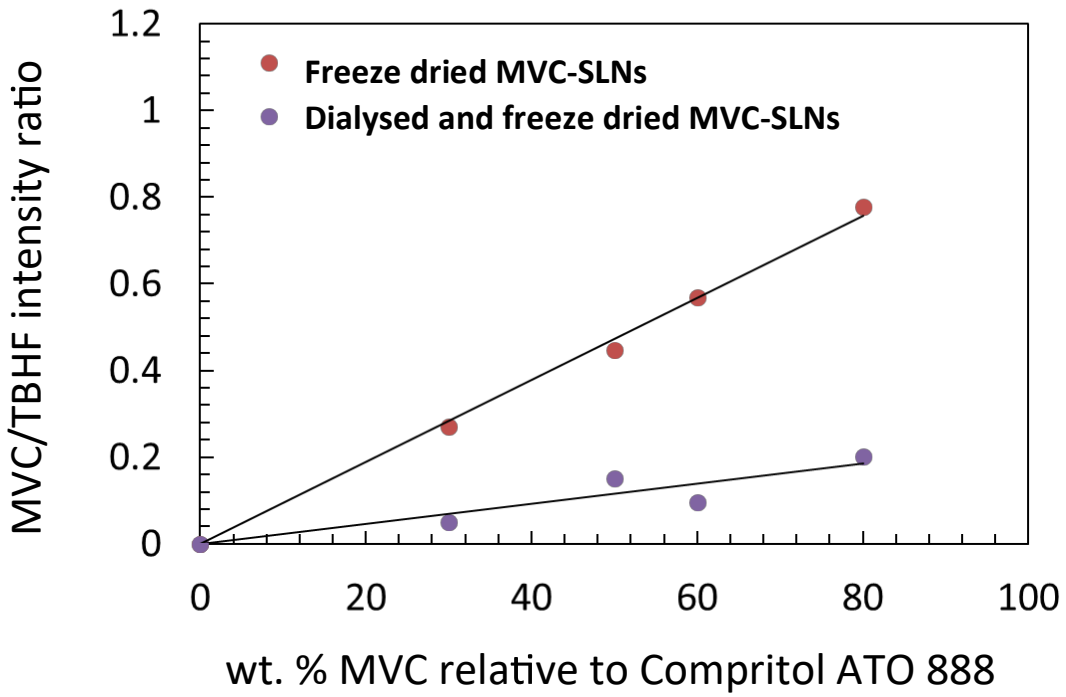

Fig. 4.21. ^{19}F NMR of freeze dried SLNs compared against dialysed SLNs at 50 ˚C. The loss of MVC during dialysis led us to examine the leftovers from the dialysis water.

This was studied using ^{1}H NMR at 25 °C and compared to the spectra of pure MVC as shown in Fig. 4.22. From this comparison, it is clear that no resonances observed in the spectra of the dialysis wastewater and MVC are the same. This suggests that no MVC is present is in the wastewater. We have been unable to detect were this loss of MVC occurred. It is possible that MVC is trapped on the dialysis membrane. As we were unable to remove this loss of MVC the use of dialysis was discontinued as a means of removing the IPA solvent. Freeze-drying was therefore optimised to remove IPA for SLN use in vivo. This will be described in Chapter 5.

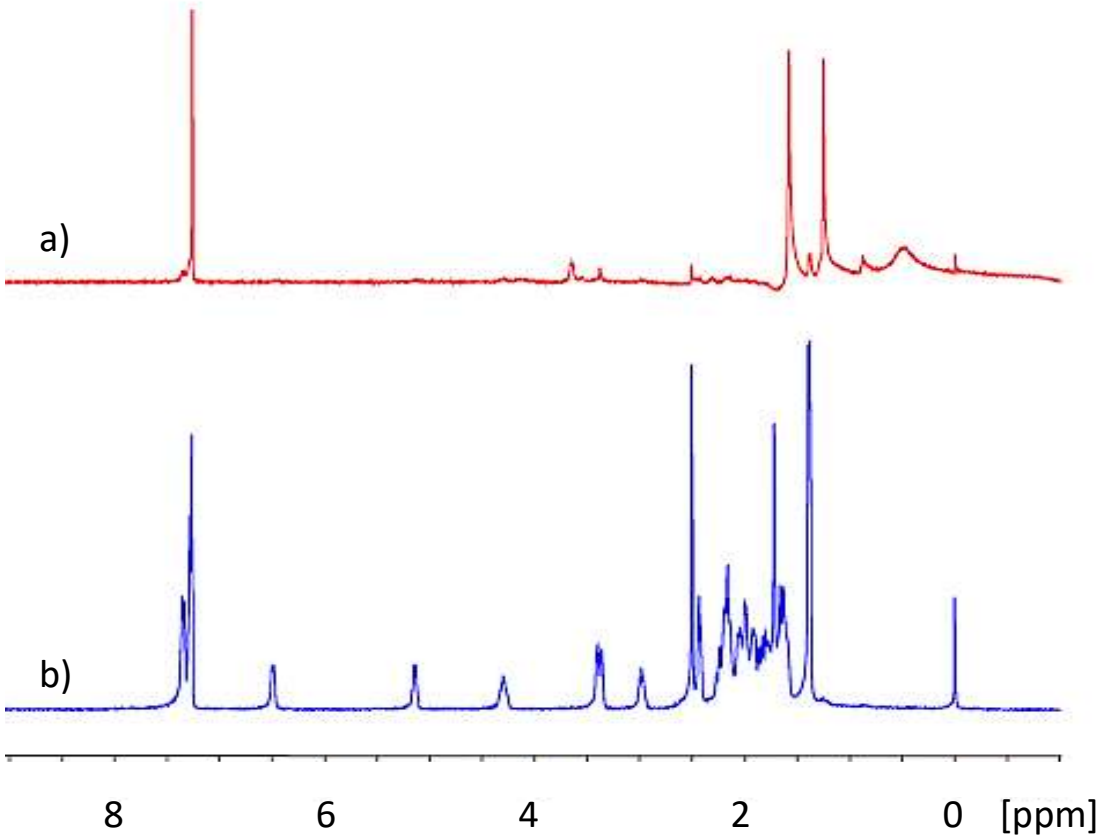

Fig. 4.22. ^{1}H NMR recordings of **a)** dialysis beaker and **b)** MVC (4.5 mg) at 25 °C.

4.2.6. Differential scanning calorimetry (DSC) of MVC-SLNs

Differential scanning calorimetry (DSC) was used with the aim of assessing the crystallinity of the SLNs loaded with MVC. The SLNs loaded with 60 wt. % MVC relative to Compritol ATO 888 were examined using DSC as shown in Fig. 4.23. The DSC confirmed that the

melting temperature of MVC, shown in green, was ~200 °C and that the melting temperature of Compritol ATO 888, shown in red, was ~ 70 °C. Both these are consistent with literature values.[94] The DSC of SLNs loaded with MVC, shown in blue, had two melting temperatures one at ~180 °C and one at 75 °C. The melting temperature at 180 °C corresponds to a 20 °C decrease in the melting temperature of MVC. The second melting point at 75 °C of DSC of SLNs loaded with MVC corresponds to a 5 °C increase in the melting temperature of Compritol ATO 888. Additionally, it is noted that this melting point occurs over broader range of temperatures than in pure Compritol ATO 888. There is also a second bump in this peak at 85 °C that is highlighted in red in Fig. 4.23. As we observe definite melting temperature from the DSC it can be concluded that both Compritol ATO 888 and MVC within the SLNs loaded with MVC remain in a crystalline form. However, the changes in the melting temperatures may represent some co-crystallisation as their melting temperatures have converged partially.

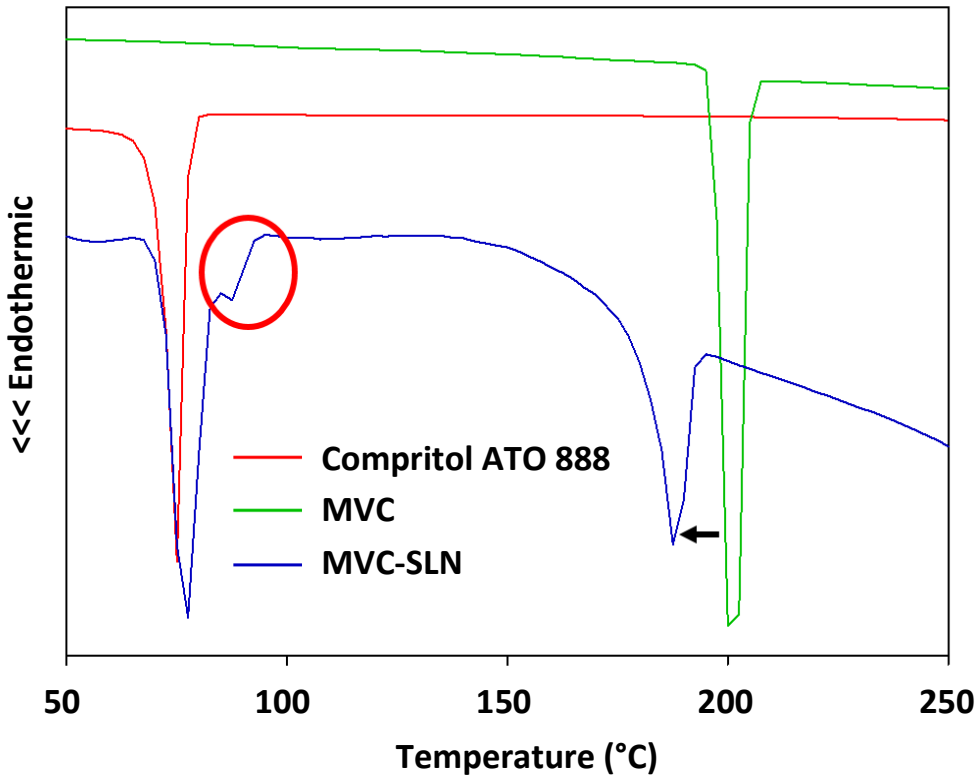

Fig. 4.23. DSC diffraction scanning calorimetry. Of Compritol ATO 888, MVC and MVC-SLN loaded with 60 wt. % MVC-SLN.

4.3 Conclusion

The empty SLN studies were optimised and the optimised procedure was used to synthesise MVC loaded SLNs. It was shown that it was possible to increase the targeted drug loading of MVC up to 70 wt. % relative to MVC while retaining the stability of SLNs as determined by DLS. However, the SLN stability was ambiguous for MVC-SLNs loaded with 90 wt. % loaded. The SLNs were not formed when using 100 wt. % SLN relative to Compritol ATO 888.

The drug loading of MVC SLNs were quantified with ^{19}F NMR using standard calibration curves relating the ^{19}F signals of MVC to that of an internal reference TBHF at different concentrations. Before dialysis the MVC-SLNs were shown to contain the expected amount of MVC. However, after dialysis there was a significant decrease in the loading of MVC in the MVC-SLNs. It was hypothesised that this could be due to the drug being captured by the dialysis bag. However, after analysing the material in the dialysis beaker by ^{1}H NMR it was demonstrated that MVC did not go outside the dialysis bag. Where the drug goes after dialysis is unknown.

Chapter 5. Optimisation of freeze dried MVC loaded SLNs for *in vitro* and *in vivo* studies

5.1 Introduction

The synthesis of MVC-SLNs stabilised with DBiB-p(OEGMA)$_{10}$-co-(EGDMA)$_{0.6}$ was shown in Chapter 4 using a modified solvent injection method. However, to use the solvent injection process one must use an organic solvent to dissolve the polymer; these organic solvent needs to be removed prior to any biological evaluation. Both dialysis and freeze-drying were used to remove isopropanol (IPA) solvent from MVC-SLNs with targeted drug loading of 10-70 wt. %. Dialysis was attempted first to remove IPA. However, as discussed in Chapter 4, the use of dialysis appeared to result in a large reduction in the concentration of MVC in the SLNs. Therefore, freeze-drying was considered to remove IPA from the MVC-SLN dispersion. However, freeze-drying can result in the aggregation of SLNs due to mechanical stress caused by ice.[298] To prevent the mechanical stress from causing aggregation a cryoprotectant can be used as it vitrifies at a specific temperature, and the glassy matrix of cryoprotectant can protect nanoparticles from the mechanical stress caused by ice.[298]

Freeze-drying SLNs has been well studied.[299,300–302,303] Schwarz and Mehnert studied the effect of different cryoprotectants on the SLNs for Freeze drying.[299] They optimised the freeze drying conditions that resulted in a lyophilisate with good reconstitution properties.[299] To achieve this they used Compritol ATO 888 as a lipid matrix for the SLN and stabilisers such as poloxamer 188.[299] A range of cryoprotectants were used in a thaw pre-test to screen the effect of the cryoprotectants on the freezing and those included trehalose, glucose, maltose, mannose, lactose, sorbitol, glycine, PVP and gelatine.[299] It was concluded that the sugar trehalose proved to be most effective in preventing ice crystal growth during freezing and thawing and also in the freeze-drying process.[299]

Polyethylene glycol (PEG) has also been used as a cryoprotectant in other systems.[298,304] In a study of RIF-loaded PCL-PEG-PCL it was demonstrated that PEG acted as a cryoprotectant due to the successful lyophilization of RIF-loaded PCL–PEG–PCL micelles with an acceptable particle size after reconstitution.[304] Moreover, It was concluded that the use of cryoprotective additives were essential in order to avoid micellar aggregation.[304]

For *in vitro* and *in vivo* biological evaluation of SLNs the organic solvent needs to be removed. *In vitro* evaluations can be used to assess the release profile of a drug encapsulated in SLNs. The *in vitro* drug release of oral formulation of SLNs over time can be determined using the dialysis bag diffusion technique. These experiments typically use UV-spectrometry to measure drug release from aliquots withdrawn from the dialysis bag at different time points.[305,306,307] In case of drugs that have weak UV-Vis chromophores as is the cause of MVC, methods such as tritium labelling can be considered. This method using the radioactive isotope of hydrogen, tritium to label drugs and allows the concentration of the drug to be rapidly and accurately determined by liquid scintillation counting. *In vivo* studies are used to assess the oral bioavailability and pharmacokinetic release profile by orally administering the drug loaded SLNs in to rats.

5.2 Results and discussion

5.2.1 Freeze drying of MVC loaded SLNs using sugars as cryoprotection

Cryoprotectants such as trehalose, galactose, sucrose and mannose were tested as cryoprotectants in this study. They were used with concentrations between 0 to 25 mg/mg to the MVC-SLNs. The MVC-SLNs used in this study were 50 wt. % MVC which were quantified using the ^{19}F NMR calibration described in Chapter 4. The samples were analysed by DLS before and after addition of cryoprotectants at given concentrations between 0 to 25 mg/mg MVC-SLNs. It was attempted to re-disperse the freeze-dried nanoparticles in water. However, it was not possible to redisperse any freeze-dried SLN sample using vortexing and aspiration.

5.2.2. Freeze drying of MVC loaded SLNs with PEGs as cryoprotant *versus* no cryoprotectant

5.2.2.1 Initial optimisation using PEG-2k-20k cryoprotectant in freeze drying of MVC-SLNs

As the use of sugars as cryoprotectant in the freeze-drying process of 50 wt. % were unsuccessful we continued by testing PEG 2k, 4k, 10k, and 20k as a cryoprotectant during freeze-drying. The concentration of PEG 2k-20k used was between 15 and 30 mg/mg relative to MVC-SLNs. The amount of cryoprotectant was varied in order to investigate the effect its concentration has on the reconstitution size after freeze-drying. Redispersion was achieved using vortexing and then aspirating the sample in deionised water.

First, PEG 20k was tested in concentrations of 15 and 30 mg PEG 20k for every mg of 50 wt. % MVC SLNs freeze dried. The size distribution of the resulting SLNs were analysed using DLS and the traces before and after freeze drying and redispersion are shown in Fig. 5.1A-B and corresponding correlograms are given in Appendix Fig. A54 and A55. The traces before and after freeze-drying were monomodal and showed similar particle mode diameter. This indicates that the MVC-SLN particles freeze dried with 15 and 30 mg PEG 20k per mg MVC-SLN were still stable after freeze-drying and potentially very little aggregation of the particles had occurred during the freeze drying step. It also indicates that the reconstitution of the MVC-SLN particles is possible after freeze drying and re-dispersion when using 15 and 30 mg PEG 20k per mg MVC-SLNs. Overall, PEG 20k were similar in terms of both size and morphology when compared to a freshly prepared sample. These experiments do not directly show that the stability under freeze drying is a result of the cryoprotection by PEG and no further experiments were carried out to make this connection as the sample stability was primary goal of these experiments.

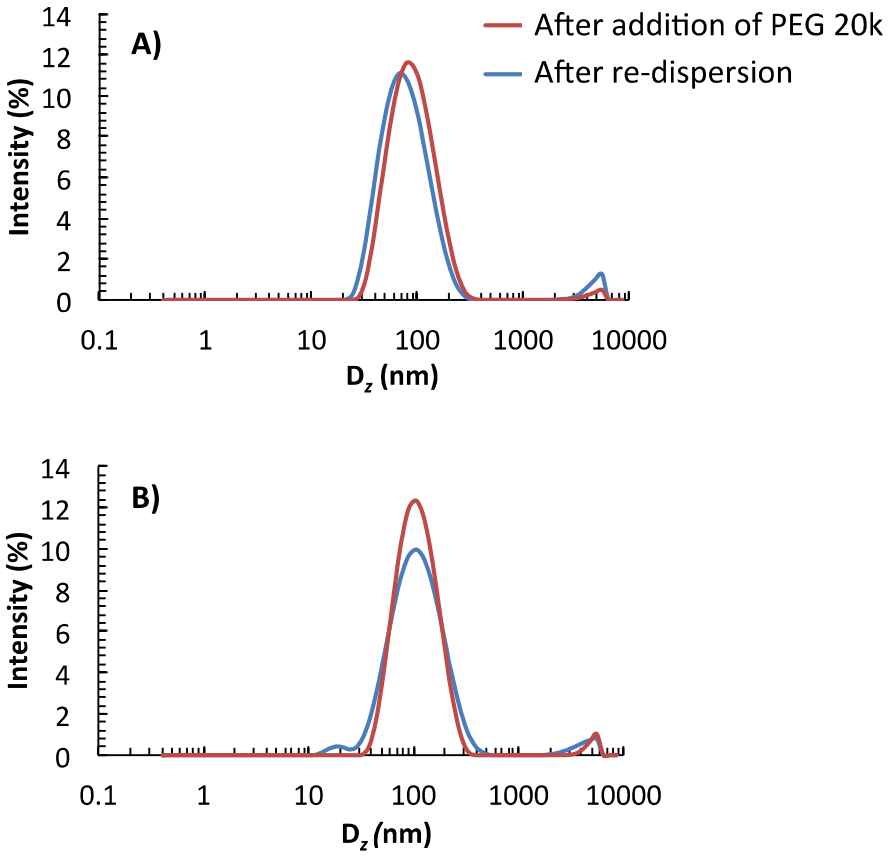

Fig. 5.1. A) 30 mg/mg PEG 20 k relative to 1 mg 50 wt. % MVC SLN **B)** 15 mg/mg PEG 20 k relative to 1 mg 50 wt. % MVC SLN.

The D_z-values of MVC-SLNs freeze dried 50 wt. % MVC-SLNs using PEG 2k-20k as a cryoprotection in concentrations of 15-30 mg/mg MVC-SLNs are in Fig. 5.2. For samples where PEG 2k, 5k and 10k were added to the 50 wt. % MVC SLNs it was observed that the size after redispersion was significantly larger than before redispersion. In addition, it is observed that adding 15 mg PEG per mg MVC SLNs results in a larger size distribution than when 30 mg per MVC SLNs is added. The only exception from this trend was when PEG 20k was added. In this case, the size of the redispersed SLNs were similar in size both before and after redispersion. Furthermore, this was observed when both 15 and 30 mg of PEG 20k was added per mg MVC SLNs.

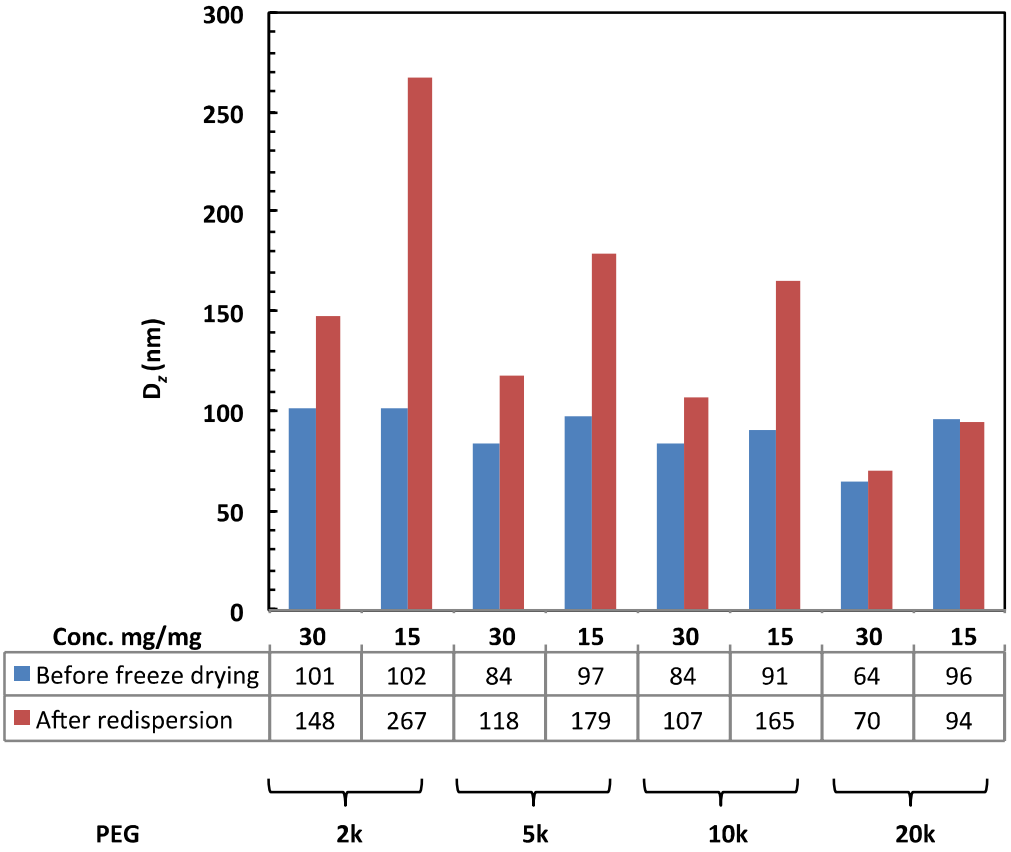

Fig. 5.2. D_z measurements of 1 mg 50 wt. % MVC SLN freeze dried with PEG-2k-30k in concentrations of 15 and 30 mg per mg of 50 wt.% MVC SLNs. Samples were analysed after adding PEG 2k-20k. Samples were measured as three repeat measurements and given as an average value.

5.2.2.2 Later optimisation using PEG- 2k-4k cryoprotectant in freeze drying of MVC-SLNs

Given the high concentrations of cryoprotectants required to prevent SLN aggregation during the freeze drying step, a higher energy dispersion approach was tested to investigate the use of lower cryoprotectant concentrations. Therefore ultrasonication was used to redisperse the freeze-dried MVC-SLNs material instead of vortexing and aspiration. For this work, 80 % wt. MVC SLNs were used and PEG 2k and 4k were added as cryoprotectants in concentrations varying between 0 and 4 mg per mg of MVC SLNs to investigate how the minimum amount of cryoprotectant can result in stable MVC-SLNs. We decided not to move on with 50 wt. % as our aim was to encapsulate maximum amount of drug in SLNs. Results obtained for 50 wt. % can be found in Appendix Fig. A56-A57.

The size distributions of MVC SLNs with 0.5, 1, 2, 4 mg added PEG 2k and 4k after freeze-drying and redispersion are shown in Fig. 5.3. Additionally, the SLN size distribution of MVC SLNs before freeze-drying is shown in Fig. 5.3 where it is labelled 0. It was observed that using ultrasonication to redisperse the MVC SLN freeze dried with PEG 2k and 4k resulted in D_z size distributions which were significantly similar after reconstitution. Furthermore, it was observed that adding more cryoprotectant also decreased the SLNs size distribution after freeze-drying, Fig. 5.3.

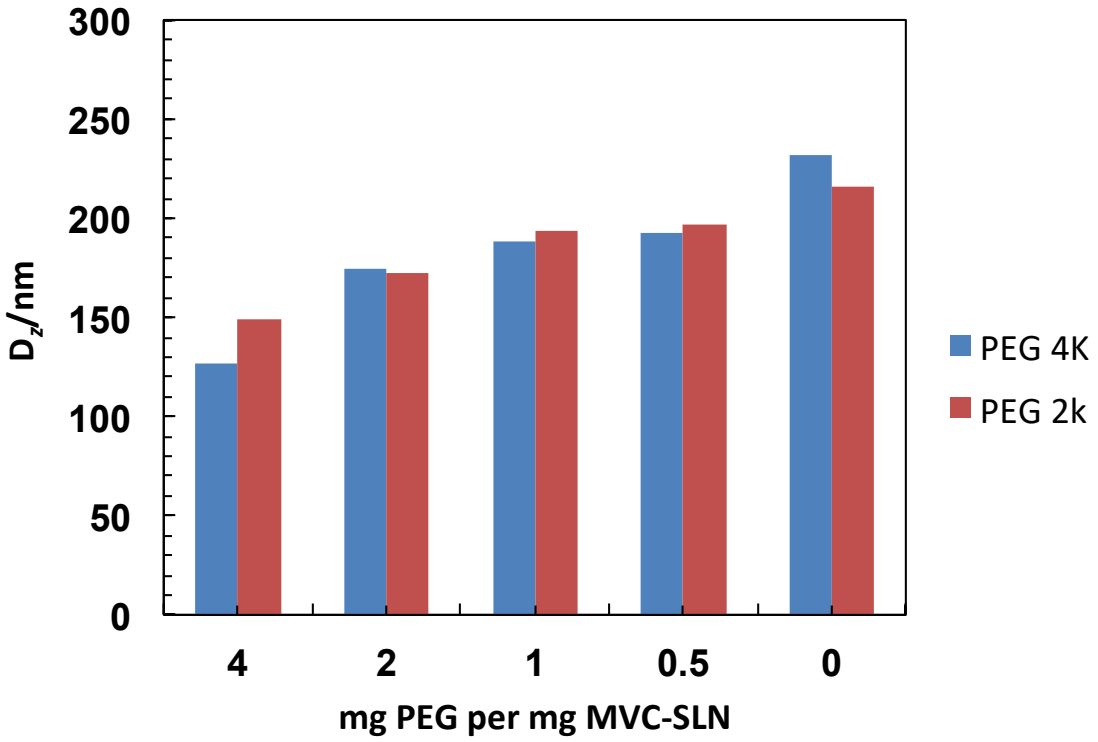

Fig. 5.3. DLS measurement of SLNs freeze dried using cryoprotectants PEG 2k and PEG 4k with concentrations 4 mg/ mg of MVC-SLNs with 80 wt. % drug loading. Sonicated 4x15 sec. 0 mg of PEG per mg MVC-SLNs is the blank.

Freeze-dried SLNs with 80 wt. % MVC loading cryoprotected using 0, 0.5 and 4 mg of PEG 4k were kept as a powder for 2 weeks at 25 °C. They were then redispersed and compared with newly freeze-dried but otherwise identical SLNs, which were also redispersed. The samples kept for 2 weeks were analysed by DLS and the results are given on Table 5.3. They showed that after 2 weeks of storage larger particle sizes (D_z) were obtained when compared the particle sizes of the MVC-SLNs redispersed immediately after freeze drying,

Table 5.1. The trend of the D_z values measured for samples kept for 2 weeks and immediately redispersed after freeze drying are shown in Fig. 5.4. The effect of the duration of the ultrasonication was tested. Samples were sonicated for 15 sec and for 4x15 sec to redisperse them and then measured using DLS. The results are shown in table 5.2 for 15 sec and table 5.3 for 4x15 sec. This showed that a longer period of ultrasonication resulted in smaller SLNs. This method for freeze-drying was considered best as it used the least amount of cryoprotectant and was used in all further studies.

Table. 5.1. D_z and PDI values of redispersed MVC loaded SLNs immediately after freeze-drying was sonicated 4 x 15 sec sonication. S= Solid Content = Compritol ATO 888 + DBiB-p(OEGMA)$_{10}$-*co*-(EGDMA)$_{0.6}$+ MVC, PEG-4k.

wt. MVC % rel. lipid	m_{PEG4k}/mg	m_s/ mg	wt. MVC % Rel. S	D_z/ nm	PDI
80	4	5	12	127	0.18
80	0.5	1.5	40	193	0.22
80	0	1	60	232	0.24

Fig. 5.2. Redispersion of MVC loaded SLNs stored for 2 weeks freeze-drying was sonicated 1 x 15 sec sonication. S= Solid Content = Compritol ATO 888 + DBiB-p(OEGMA)$_{10}$-*co*-(EGDMA)$_{0.6}$+ MVC, PEG-4k.

wt. MVC % rel. lipid	m_{PEG4k}/mg	m_s/ mg	wt. MVC % Rel. S	D_z/ nm	PDI
80	4	5	12	209	0.29
80	0.5	1.5	40	270	0.27
80	0	1	60	320	0.26

Fig. 5.3. Redispersion of MVC loaded SLNs stored for 2 weeks freeze-drying was sonicated 4 x 15 sec sonication. S= Solid Content = Compritol ATO 888 + DBiB-p(OEGMA)$_{10}$-*co*-(EGDMA)$_{0.6}$+ MVC, PEG-4k.

wt. MVC % rel. lipid	m_{PEG4k}/mg	m_s/ mg	wt. MVC % Rel. S	D_z/ nm	PDI
80	4	5	12	187	0.23
80	0.5	1.5	40	269	0.26
80	0	1	60	262	0.21

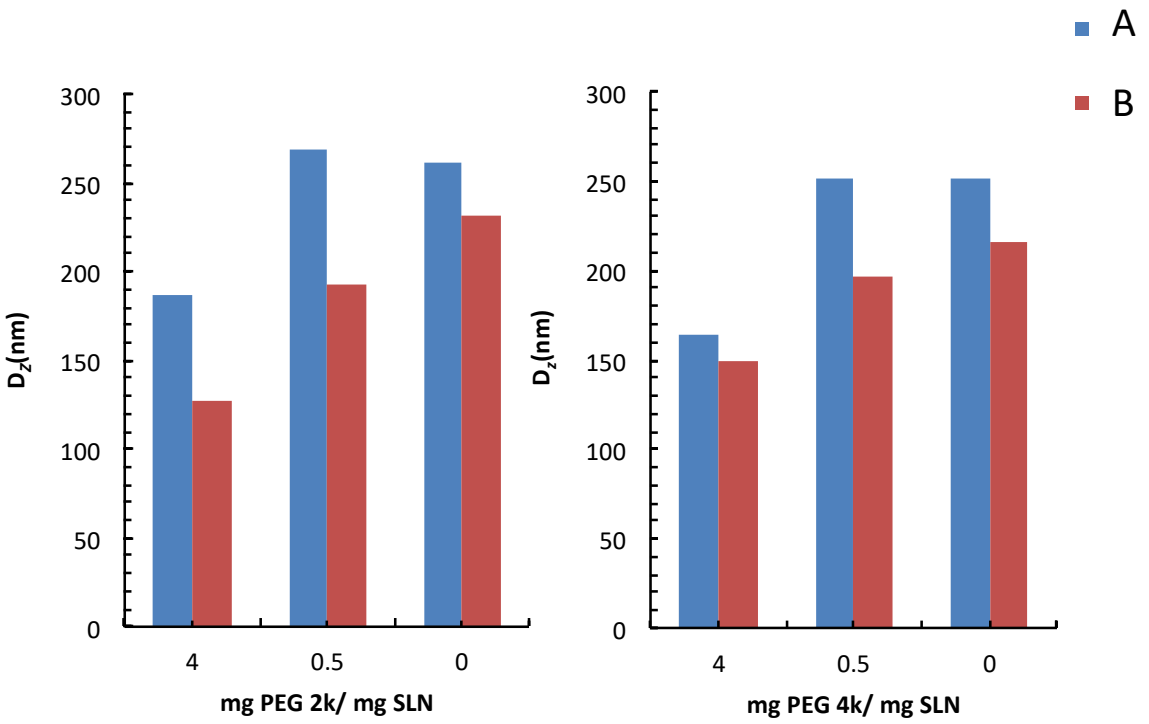

Fig. 5.4. A) redispersion of freeze dried MVC SLNs after 2 weeks storage at 25 °C, **B)** redispersion just after freeze drying of 80 wt. % MVC SLNs relative to Compritol ATO 888 using PEG 4k as a cryoprotectant. Samples were redispersed using 4x15 sec sonication.

5.2.3 Role of MVC, Compritol ATO 888 and DBiB-p(OEGMA)$_{10}$-co-(EGDMA)$_{0.6}$ in MVC-SLNs

MVC-SLNs stabilised with DBiB-p(OEGMA)$_{10}$-co-(EGDMA)$_{0.6}$ were synthesised in Chapter 4 using solvent injection. However, the roles which MVC, Compritol ATO 888 and DBiB-p(OEGMA)$_{10}$-*co*-(EGDMA)$_{0.6}$ play during solvent injection and freeze drying has not yet been understood throughout this thesis. Therefore, focus has been directed towards investigating the role of MVC, Compritol ATO 888 and DBiB-p(OEGMA)$_{10}$-*co*-(EGDMA)$_{0.6}$ in SLN particle formation using the 80 wt. % MVC loaded SLNs previously described.

In the first experiment MVC was investigated. A sample of MVC was heated to 80 °C in IPA and rapidly injected into stirred water at 25 °C (Fig. 5.5). Thereafter, 1 mL of sample was analysed by DLS. The sample was subsequently freeze dried and redispersed in water followed by 4x15 sec sonication. The DLS results of D_z, PDI and ZP measured for samples

before and after freeze drying were not reliable due to the sample dissolving. This indicated that this approach did not form any MVC nanoparticles as expected.

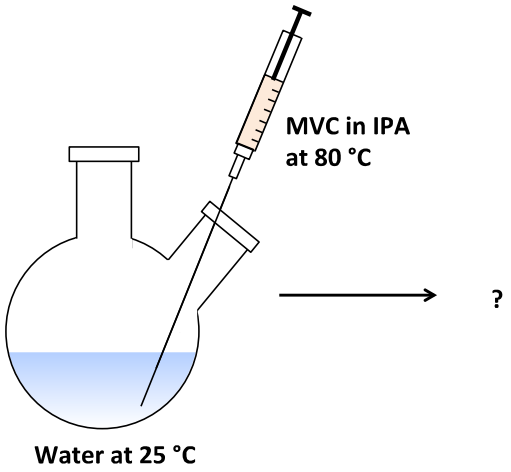

Fig. 5.5. MVC in IPA at 80 °C was injected into deionised water 25 °C.

In another experiment Compritol ATO 888 was heated to 80 °C in IPA and rapidly injected into stirred water (Fig 5.6). The sample was analysed by DLS straight after the solvent injection and after redispersing the freeze-dried material using sonication. The DLS results of the SLN dispersion before and after freeze-drying are shown in Fig. 5.6. D_z, PDI and ZP of the SLN dispersion before freeze drying showed formation of SLNs with a small particle diameter of D_z of 43.5 nm (PDI 0.18) and a ZP of -23.3 mV. This indicated that this approach result in the formation of stable SLN particles.

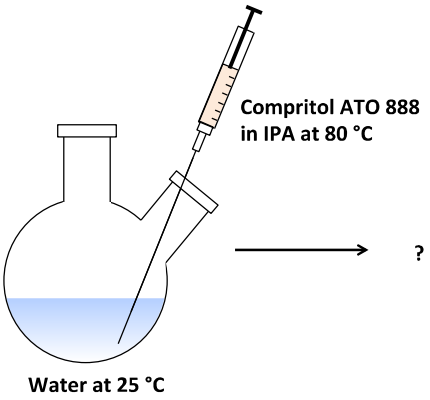

	D_z/nm	PDI	ZP (mV)
After solvent injection	43.5	0.176	-23.3
After freeze drying	-	-	-

Fig. 5.6. Compritol ATO 888 in IPA at 80 °C was injected into deionised water 25 °C. (-) = no results.

However, the DLS results for the freeze-dried and redispersed material did not give any reliable results due to sedimentation of the particles in the sample. This suggests that Compritol ATO 888 may crystallise during freeze-drying.

In a third experiment, DBiB-p(OEGMA)$_{10}$-(EGDMA)$_{0.6}$ dissolved in stirred water was injected with MVC dissolved in hot IPA. The sample was analysed by DLS after the solvent injection as well as after redispersing the freeze-dried material using sonication. The results are shown in Fig. 5.7. The DLS results for the SLN dispersion before and after freeze-drying and redispersion did not give any reliable results. Overall, this suggests that MVC does not form any particles in presence of DBiB-p(OEGMA)$_{10}$-co-(EGDMA)$_{0.6}$.

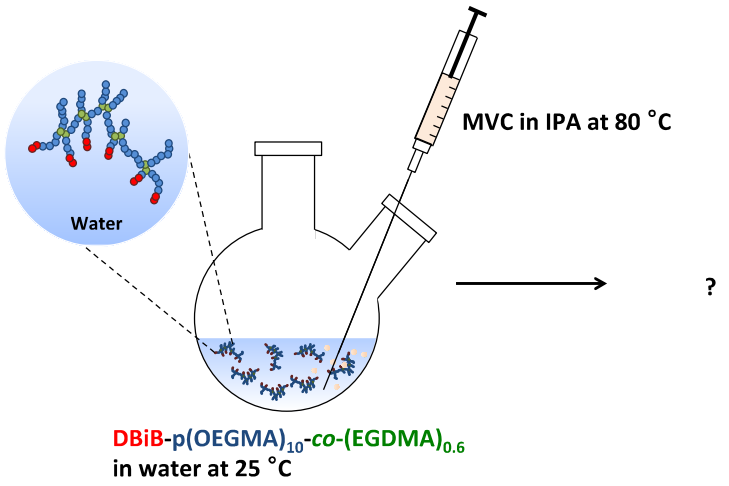

Fig. 5.7. MVC in IPA at 80 °C was injected into deionised water containing dissolved DBiB-p(OEGMA)$_{10}$-*co*-(EGDMA)$_{0.6}$ 25 °C.

In another study Compritol was dissolved in IPA at 80 °C was injected into a stirred mixture of water and DBiB-p(OEGMA)$_{10}$-*co*-(EGDMA)$_{0.6}$. The size distributions obtained for the samples before and after DLS measurements are given in Fig. 5.8. The results showed that stable particles were formed with a D_z value of 43.4 nm (PDI of 0.21). After freeze drying stable SLN particles were formed with size distributions of 353 nm (PDI 0.37). Overall this indicated that the size of SLNs made of Compritol ATO 888 stabilised with DBiB-p(OEGMA)$_{10}$-*co*-(EGDMA)$_{0.6}$ increase in particle diameter after freeze drying. It could be suggested that Compritol ATO 888 crystallise during freeze-drying process.

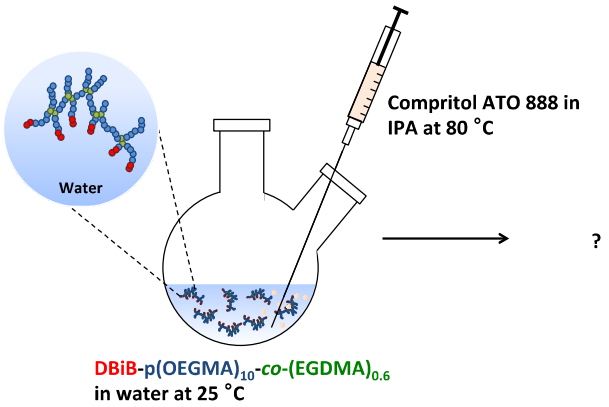

	D_z/nm	PDI	ZP (mV)
After solvent injection	43.4	0.208	-
After freeze drying	353.5	0.369	-

Fig. 5.8 Compritol ATO 888 in IPA at 80 °C was injected into deionised water containing dissolved DBiB-p(OEGMA)$_{10}$-*co*-(EGDMA)$_{0.6}$ 25 °C. (-) = no results

Finally, in the last study we investigated the impact of MVC and Compritol ATO 888 in the formation of MVC SLNs in solvent injection experiment. In this experiment MVC and Compritol ATO 888 heated to 80 °C was rapidly injected into a stirred solution of water at 25 °C. The size distribution of the SLNs in the dispersion was analysed before and after freeze-drying and re-dispersion and shown in Fig. 5.9.

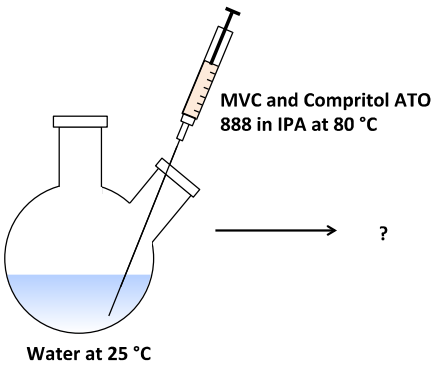

	D_z/nm	PDI	ZP (mV)
After solvent injection	38.0	0.221	-
After freeze drying	328.8	0.323	5.29

Fig. 5.9 MVC and Compritol ATO 888 in IPA at 80 °C was injected into deionised water containing dissolved DBiB-p(OEGMA)$_{10}$-*co*-(EGDMA)$_{0.6}$ at 25 °C. (-) = no results.

The size distributions of SLNs made of MVC and Compritol ATO 888 before freeze drying showed a D_z of 38 nm (PDI of 0.22). This indicated that MVC and Compritol ATO 888 can form a stable particle in a dispersion of water in presence of IPA. The D_z of the MVC-Compritol ATO 888 particles after freeze-drying and redispersion was 328.8 nm (PDI of 0.32). This suggests that the SLN particles made of Compritol ATO 888 and MVC remain stable after freeze drying. Another parameter measured for the MVC-Compritol ATO 888 particle was the ZP value which was determined to be 5.29 mV. This value indicate that MVC and Compritol ATO 888 may form a short-term stable particles as the ZP is low.[308]

Overall it can be concluded that the size of the resulting SLN particles formed by Compritol ATO 888 and DBiB-p(OEGMA)$_{10}$-*co*-(EGDMA)$_{0.6}$, Compritol and MVC or Compritol, MVC and DBiB-p(OEGMA)$_{10}$-*co*-(EGDMA)$_{0.6}$ get larger after freeze drying and redispersion. The understanding of how a drug and a lipid stabilise each other is not discussed in literature. However, from the above results it is hypothesised that they may co-crystallise after solvent injection is performed. The role of each components in the formed nanoparticles showed that Compritol ATO 888 injected into water does not form any nanoparticle. However, the presence of DBiB-p(OEGMA)$_{10}$-co-(EGDMA)$_{0.6}$ or MVC does result in particle formation. These results suggest that Compritol ATO 888 presence in the solvent injection is crucial in

order to form particles. Analysis of MVC injected into water or water and DBiB-p(OEGMA)$_{10}$-co-(EGDMA)$_{0.6}$ does not form nanoparticles. This suggest that MVC does not play any role in nanoparticle formation.

5.2.4 Stability studies of freeze dried MVC-SLNs with 80 wt. % MVC loading

So far the 80 wt. % MVC-SLN has been formulated with a total solid content of 1.2 mg/mL water. However, in order to deliver a sufficient to dose of MVC in formulated MVC-SLNs via oral administration to rats this concentration needs to be increased.

Pharmacokinetics and distribution in rats after oral delivery of MVC has been studied in literature.[309,310] Based on this work the formulation aimed to obtain an orally administrate 10 mg/ kg MVC dose per rat. This dose was considered to be feasible to ensure that the ^{3}H MVC in plasma and tissue can be detected.[309,310] To achieve this concentration 80 wt. % MVC relative to Compritol ATO 888 was encapsulated in SLN using solvent injection and 1 mL samples were distributed in 4 mL vials, frozen and then freeze dried over 1 day. The individual vials were sonicated and combined until a concentration of 3.4 mg/mL MVC in deionised water was obtained. A photograph of the resulting dispersions with 0.6, 1.2, 2.4 and 3.4 mg/mL are given in Fig. 5.10 A. The photograph shows that the sample looks more turbid as the concentration of MVC-SLNs in water increases. The size distribution of the final sample was measured by DLS over 2 days to ensure that the resulting MVC-SLN dispersion containing 3.4 mg/mL MVC remain stable over 2 days, Fig. 5.10 and corresponding correlogram is given in Appendix Fig. A58.

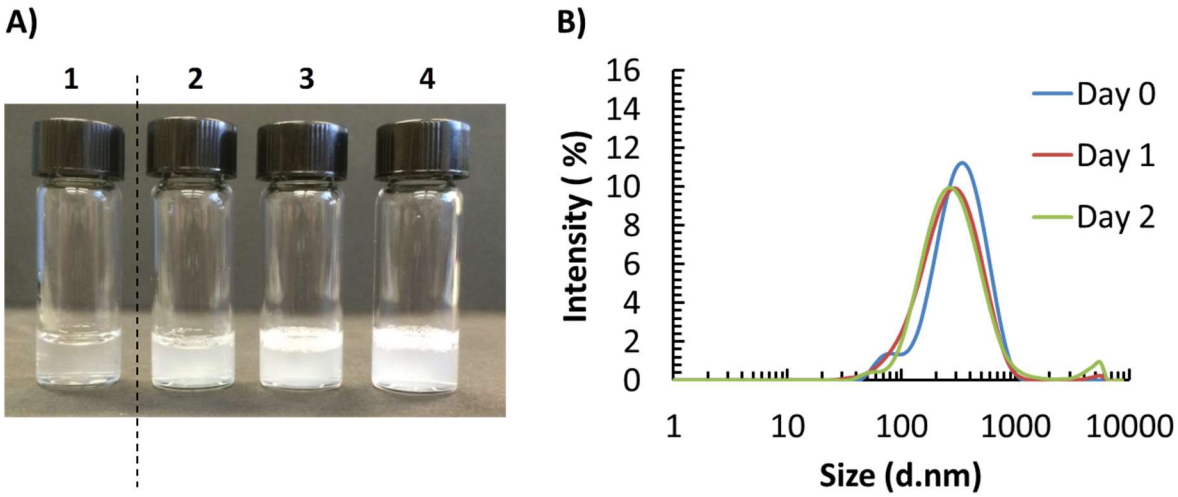

Fig. 5.10. A) Photograph of MVC-SLN with 80 wt. % MVC relative to lipids **1** = 0.6 mg MVC/ per mL water, **2** = 1.2 mg MVC/mL water, **3** = 2.4 mg MVC / mL water and **4** = 3.4 mg MVC/ mL water. 7.2 mg 80 wt. % MVC-SLNs/mL of water. The samples look more turbid as the concentration of MVC-SLN in water increases. **B)** DLS size distribution traces of **4** = 3.4 mg MVC/ mL water on day 0-2.

The size distributions indicate that the resulting concentrated MVC-SLN formulation remains stable over 2 days. Moreover the particle diameter D_z of the MVC-SLNs in the concentrated solution were analysed and the results are given on Table 5.11. The results showed that the MVC-SLN particles sizes have the same diameter in the resulting concentrated solution over a period of 2 days. Therefore, it was concluded that the 80 wt. % MVC-SLN concentration of 3.4 mg/mL was successfully achieved by combining the freeze-dried samples by sonicating and redispersing them.

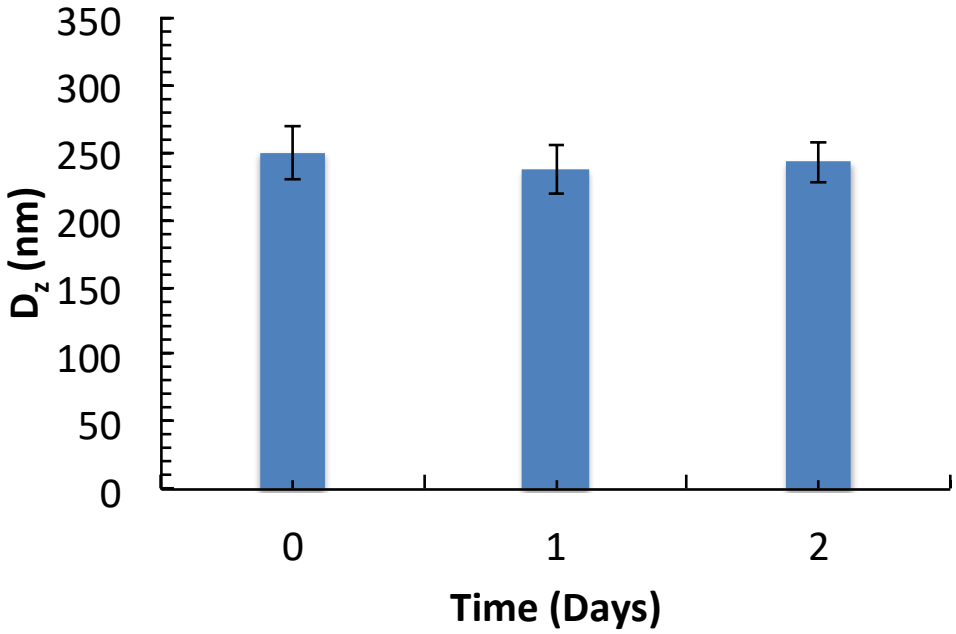

Fig. 5.11. MVC-SLNs containing 80 wt. % MVC relative to Compritol ATO 888. Composition of 3.4 mg MVC/mL deionised water day 0-2. Samples were analysed after redispersion.

A morphological investigation of the freeze dried and concentrated MVC SLNs was performed using SEM. SEM allows visualisation of the particles after freeze drying providing information on the particle size and shape. SEM micrographs of the 80 wt. % MVC sample after being redisperse were acquired at two magnifications as shown in Fig. 5.12a and b. The MVC-SLN formulation had an irregular shape and surface. It was observed that MVC-SLN also tends to aggregate near each other. This could be due to the processing of SEM samples or due to the sonication.

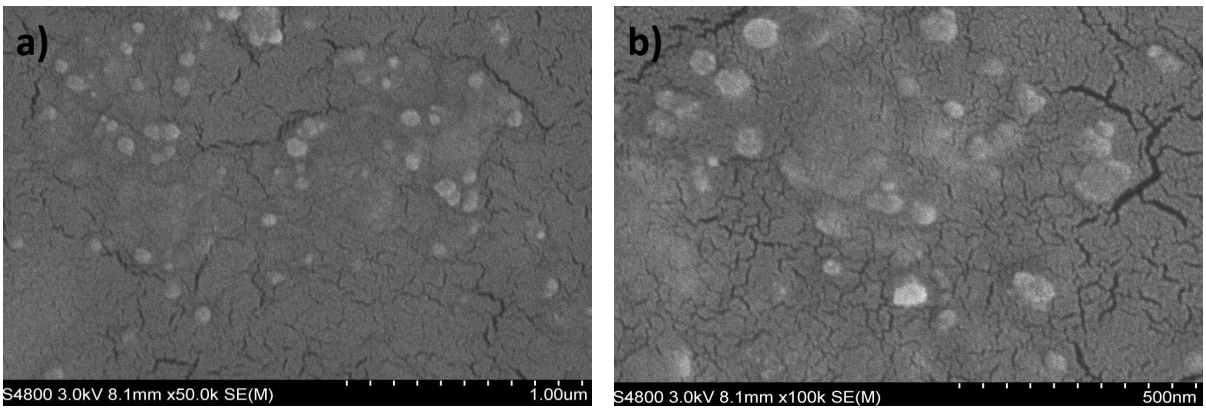

Fig. 5.12. SEM images of tissue dried MVC-SLN dispersion samples containing 80 wt. % MVC relative to Compritol ATO 888 at two magnifications A) x 50k and (B) x 100k.

5.2.5. Synthesis of Radiolabelled MVC loaded SLNs and biological evaluation

5.2.5.1 Synthesis and characterisation of radiolabelled MVC loaded SLNs

It was shown in Chapter 4 that MVC resulted in a weak signal using UV-vis spectroscopy when recorded with concentrations of 1.8-18 mg of MVC dissolved in chloroform. Therefore other methods were used to assess MVC *in vitro* and *in vivo*. Specifically, MVC labelled with tritium (^{3}H) isotopes were used.[311] Tritium is: an isotope of hydrogen, which has two extra neutrons, a beta emitter that produces a maximum energy of 0.0186 MeV and it can be detected via liquid scintillation counting.[311] The sample was measured using a liquid scintillation counter (LSC) that works by converting the beta decay energy (from the radiolabelled ^{3}H-MVC) into photons of light. Scintillation cocktails help with the transfer of this energy. Photomultiplier tubes within the LSC then detect the light and convert this into an electrical signal, Fig. 5.13.

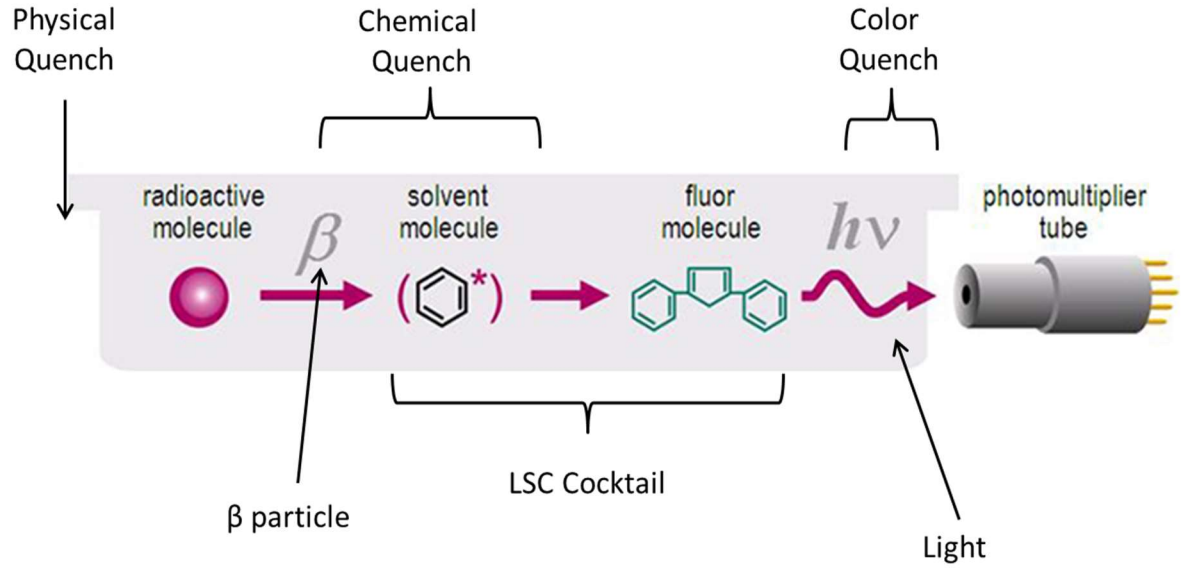

Fig. 5.13. Principle of scintillation counting. Modified from link.[312]

As LSC makes a measurement of radioactive decay there is no need for a calibration curve. However, anything which interrupts/ reduces the efficiency of the energy transfer/ absorbs the photons of light quenches the sample. There are two main types of quenching, chemical and colour. Chemical quenching interrupts the radioactive decay converting to photons of

light whereas colour quenching interrupts the photons of light being converted to electrical signals. We perform a quench curve with 10 standards of known radioactivity and various amounts of quenching allowing determining counting efficiency of the LSC to be determined. Quenching of samples is automatically corrected for by the LSC depending on counting efficiency when measuring radioactivity.

MVC-SLNs with 80 wt. % relative to Compritol ATO 888 were synthesised using, MVC and ^{3}H MVC and DBiB-p(OEGMA)$_{10}$-*co*-(EGDMA)$_{0.6}$. Tritiated MVC was generated by RCTritec using a sample of MVC provided and the certificate analysis has been included in the Appendix Fig. A59. Tritiated MVC (288 µCi, specific activity 20 µCi/mg), MVC (14.4 mg, 28.03 µmol) and compritol (3.6 mg, 8.68 µmol) were added to a 20 mL vial equipped with a stirrer bar and solubilised in IPA (4 mL) at 80 °C. DBiB-p(OEGMA)$_{10}$-*co*-(EGDMA)$_{0.6}$ (6 mg) solubilised in H_2O (20 mL) was added to a 100 mL round-bottomed flask equipped with a magnetic stirrer and stirred at ambient temperature. The rapid addition of the MVC mixture to the polymer solution was conducted *via* a cannula. The mixture was stirred for a further 5 minutes and the solution was freeze-dried over 4 days and re-dispersed in H_2O (4 mL) via vortex mixing and sonication. The formulation and studies of MVC + ^{3}H-MVC encapsulated SLNs were done by Dr Helen Cauldbeck, Dr Pierre Chambon and Dr Alison Savage from the Rannard group at the Department of Chemistry, University of Liverpool. The samples were analysed before and after freeze drying by DLS. The D_z and PDI are given in Table 5.4. Overall the obtained D_z and PDI values of ^{3}H labelled 80 wt. % MVC SLNs are comparable to those obtained for non-labelled MVC-SLNs after freeze-drying. This indicated that the size distribution after freeze-drying remains the same. The non-labelled MVC-SLNs were shown to be approximately 2-fold smaller than that of ^{3}H-labelled MVC SLNs. However, this can be due to a different processing method used to synthesise ^{3}H-labelled MVC i.e. canula injection rather than solvent injection. This method was used for safety reasons to avoid handling a needle with ^{3}H-labelled MVC.

Table 5.4. D_z and PDI distributions measured for 80 wt. % MVC-SLNs and ^3H labelled MVC- SLNs. D_z and PDI before and after freeze-drying. Standard deviations are given in ().

80 wt. % SLNs containing	D_z before freeze drying (nm)	PDI before freeze drying	D_z after freeze drying (nm)	PDI after freeze drying (nm)
MVC	45 (0.6)	0.33(0.01)	258 (8.1)	0.37(0.04)
^3H-labelled MVC	92 (0.7)	0.25(0.01)	263(3.6)	0.29(0.01)

For dialysis 1 mL of this formulation was taken and added to a dialyser with 1000 MWCO membrane and placed in a reservoir of 100 mL deionised water. At the time points of 0.5,1,2,3,4,5,6,7,8 -350 hrs 1mL sample of the 100mL reservoir was taken and LSC cocktail added. The sample was measured by LSC. The LSC gives a reading of disintegrations per minute which is converted to μCi by dividing by a constant of 2.22 x 10^6, to determine radioactivity in the 100 mL reservoir this amount is multiplied by 100 (see Equation 5.1). The amount of MVC in mass (mg) in the reservoir is calculated by dividing the radioactivity by the specific activity (mentioned earlier, this is the amount of tritiated MVC added to the mass of unlabelled in this case 20 μCi/mg) (see Equation 5.1).

$$\text{Radioactivity in Reservoir } (\mu\text{Ci}) = \frac{\text{DPM}}{(2.22*106)} \text{ x } 100 \qquad \textbf{(5.1)}$$

Conversion of dispersions per minute (DPM) is given by LSC to amount of radioactivity (μCi) in 100 mL dialysis reservoir. Calculation of mass of MVC in 100 mL from amount of radioactivity is given by Equation 5.2:

$$m_{MVC}(\text{mg}) = \frac{\text{Radioactivity in 100 mL reservoir}}{\text{Specific activity}} \qquad \textbf{(5.2)}$$

5.2.5.2 In vitro release studies of radiolabelled MVC loaded SLNs

MVC-SLNs with 80 wt. % relative to Compritol ATO 888 (containing 14.4 mg of MVC) were formulated as in section 5.2.5.1 and Chapter 7, section 7.4.3. Unformulated MVC (14.4 mg,

28.03 μmol) was used as a control; DMSO was used as the carrier solvent for the unformulated MVC as MVC is soluble within this solvent and it is a common carrier solvent within pharmacological experiments.[309,313]

The drug release of the synthesised ^{3}H-labelled MVC-SLN with 80 wt. % loading and former mentioned lipid polymer ratio 3:1 Compritol ATO 888 to DBiB-p(OEGMA)$_{10}$-*co*-(EGDMA)$_{0.6}$ were investigated in a dialysis release study. The cumulative release of MVC is given in mass (μg) and as a percentage is plotted against time in hours for MVC-SLN and MVC in DMSO at ambient temperature was calculated using equation 5.1 and 5.2, Fig. 5.14 and Fig. 5.15. The *in vitro* release studies at ambient temperature suggested that MVC encapsulated in the MVC-SLN formulation released 0.50 % drug after 8 hours in comparison to conventional MVC formulation, which released 0.78 % drug after 8 hours.

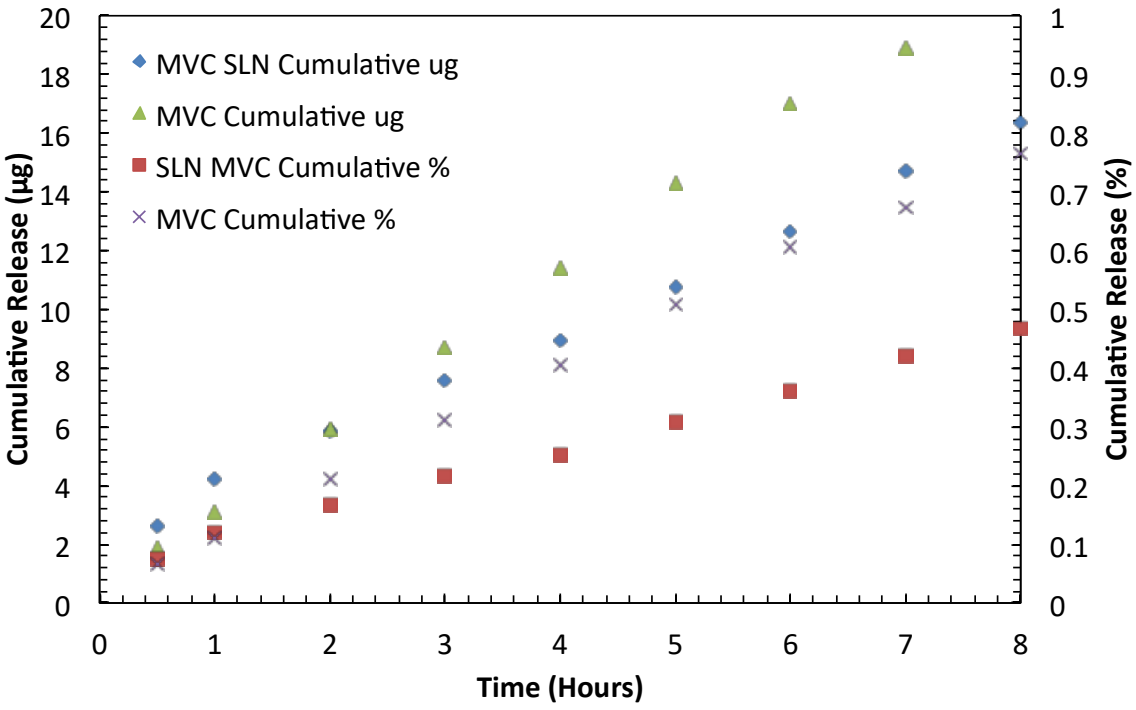

Fig. 5.14. *In vitro* cumulative release profile of MVC-SLN formulation and unformulated MVC at ambient temperature. Samples were taken over 8 hrs. 3.5 mg (3514 μg) of MVC-SLN and MVC formulation were tested. Table was provided by Dr Helen Cauldbeck.

Since the MVC-SLNs showed a first-order kinetic release profile over several days the release studies were continued over 311 hrs were 95 % MVC was released, Fig. 5.15. This

suggests that the use of Compritol ATO 888 and DBiB-p(OEGMA)$_{10}$-*co*-(EGDMA)$_{0.6}$ slow down the release of MVC.

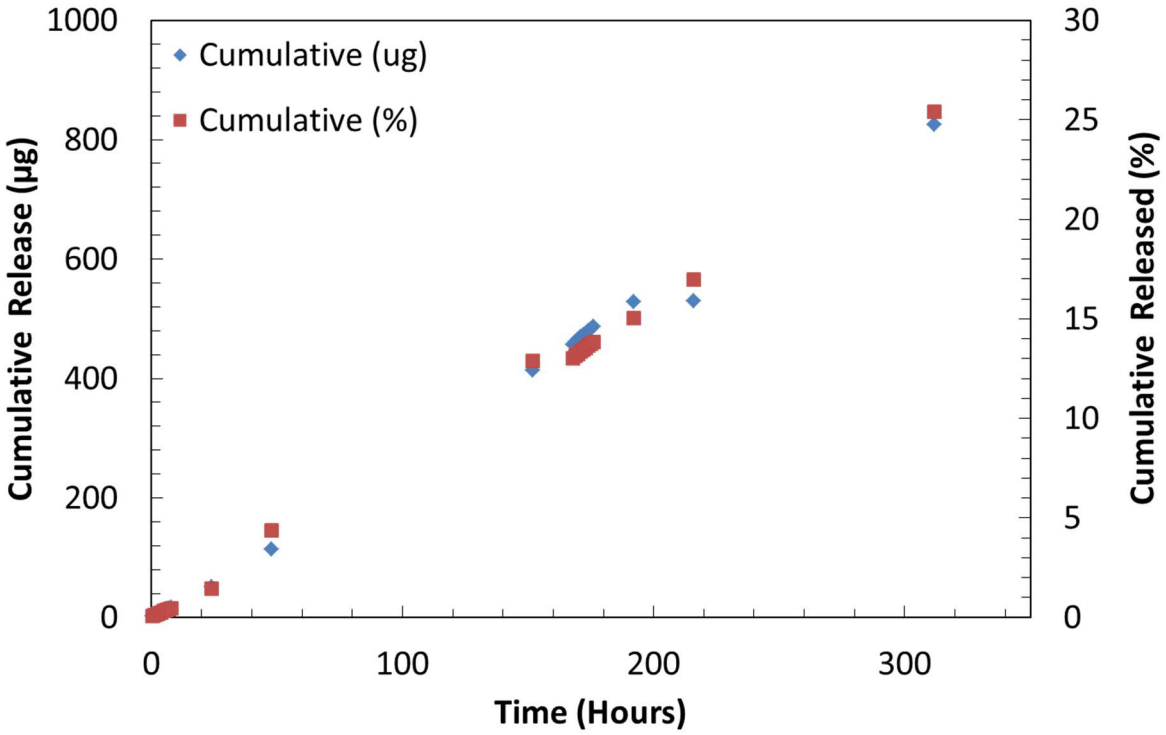

Fig. 5.15 *In vitro* cumulative release profile of MVC-SLN formulation and unformulated MVC at ambient temperature samples were taken over 311 hrs. 3.5 mg (3514 µg) MVC in MVC-SLN formulation were tested. Figure was provided by Dr Helen Cauldbeck.

Another *in vitro* release profile was conducted at 80 °C which is above the melting point of Compritol ATO 888. The aim with this study was to investigate how the release behaviour would change when the Compritol ATO 888 was liquid. Again, the cumulative release in mass (µg) and percentage were plotted against time in hours for MVC-SLN and MVC in DMSO at 80 °C and the graph is given in Fig. 5.16. This study showed that MVC-SLN formulation released 36 % drug after 3 hours while unformulated MVC released 3 % drug. This observation led us to conclude that the drug release profile of MVC in both non-formulated and formulated form is temperature dependent.

Overall the *in vitro* stability studies showed the slow release and stability of 80 wt.% MVC encapsulated in SLNs relative to Compritol ATO 888.

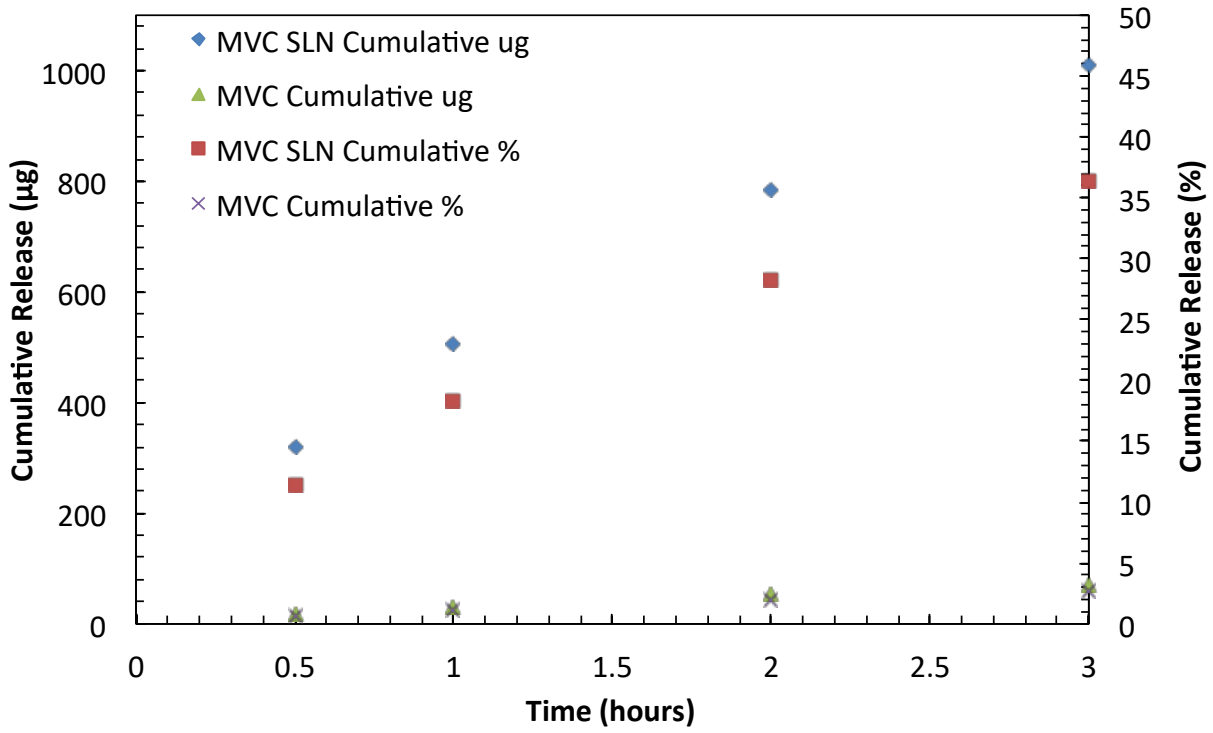

Fig. 5.16. *In vitro* cumulative release profile of MVC-SLN formulation and unformulated MVC at 80 °C samples were taken over 3 hrs. 3.5 mg (3514 µg) of MVC was tested in each formulation. Figure was provided by Dr Helen Cauldbeck.

5.2.6. *In vivo* evaluation of ^{3}H-labelled MVC loaded SLNs

In vivo tests were done in collaboration with the department of Pharmacology by Dr Lee Tatham. The evaluation of the *in vivo* effectiveness of freeze-dried 80 wt. % MVC-SLN was done by performing *in vivo* pharmacokinetic study using male Wistar (280-330 g) adult rats (2.8-3.3 mg of MVC/ rat). During the study the rats were dosed with either a conventional formulation of MVC in DMSO or a MVC SLN preparation using 10 mg/kg MVC that contains 20 µCi/mg ^{3}H activity in deionised water via oral gavage. Formulation of MVC in DMSO was used as it is commonly used in pharmacokinetic studies of MVC in literature.[309,314] Food and water were provided throughout the study. *In vivo* plasma concentrations profile of MVC and 80 wt. % MVC-SLN in rats are given in Fig. 5.17. The *in vivo* plasma concentrations showed an increase of unformulated MVC 70 min after oral administration and the plasma concentration dropped after 240 min. The SLN formulated MVC showed a sustainable release over 240 min.

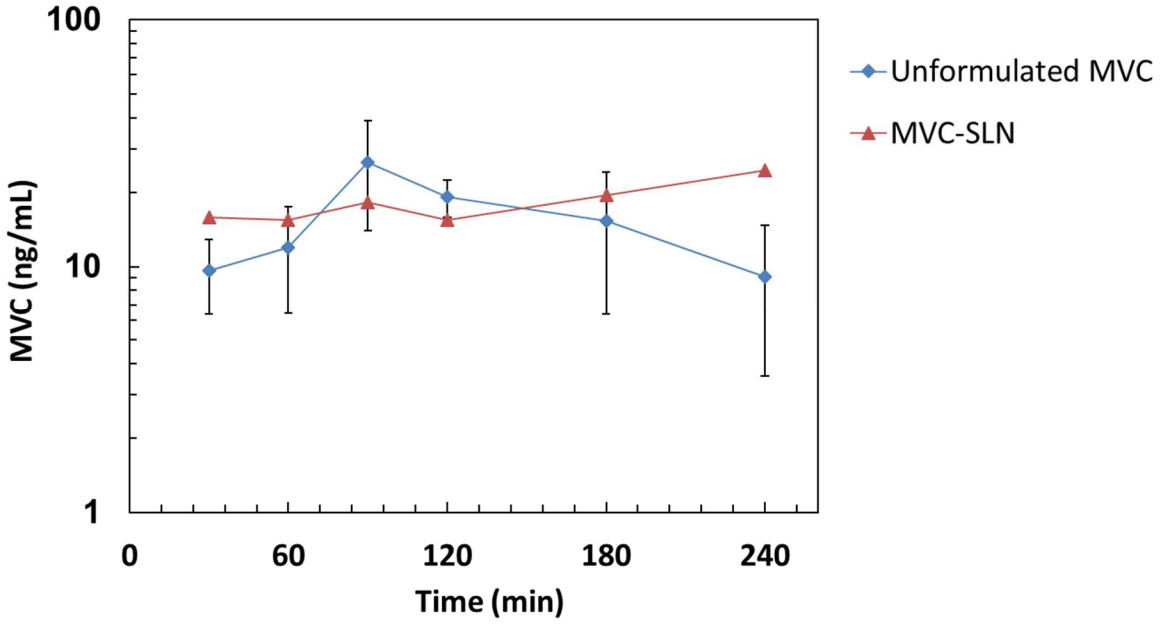

Fig. 5.17. *In-vivo* plasma concentrations profile of MVC and MVC-SLN in Wistar rats (n= 4, ± SD). Data was provided by Dr Lee Tatham.

The corresponding pharmacokinetics (PK) parameter for *in vivo* plasma concentrations of unformulated MVC versus MVC-SLN formulation are given on Table 5.5.

Table 5.5. *In vivo* oral study PK parameters obtained by oral administration of MVC-SLN or unformulated MVC in Wistar rats. Data was provided by Dr Lee Tatham.

PK parameters (n=4, ±SD)	Unformulated MVC	SLN	Fold-difference	Paired t-test (two-tailed)
C_{max} (ng/mL)	26.52	24.47	0.92	P=0.217 (n/s)
C_{min} (ng/mL)	8.16	15.42	1.89	P=0.204 (n/s)
T_{max} (h)	1.5	4.0	-	-
AUC (ng.h/mL)	58.71	67.97	1.16	P=0.547 (n/s)
C_{max}/C_{min} ratio	3.25	1.87	0.57	P=0.089 (n/s)

Compared to the unformulated MVC, a significant increase in the AUC and T_{max} was observed for MVC-SLN formulations on Table 5.5 for the MVC-SLN. It was shown that when MVC was incorporated in SLNs the C_{max} reached 24 ng/mL after T_{max}= 4 hrs. This indicated that MVC-SLNs have resulted in the drug remaining in the plasma for longer time periods

compared to the MVC alone. Moreover, the 1.16 fold increase of AUC with the administration of MVC-SLN indicated that the oral bioavailability has improved in comparison to oral administration of unformulated MVC. The minimum concentration of oral administered, C_{min}, MVC-SLN formulation increased 1.89 fold, which indicated that the MVC plasma concentration did not drop as quickly as it was seen for C_{min} concentration of unformulated MVC. Overall, the measured PK parameters showed that the MVC-SLN formulation resulted in sustainable release and improved bioavailability.

In vivo tissue analysis was performed on the same rats used for the preliminary *in vivo* plasma release studies. The study was used to demonstrate the presence of MVC from oral administered MVC-SLN formulations and unformulated MVC in rats. The results are given in Table 5.6. and Fig. 5.18.

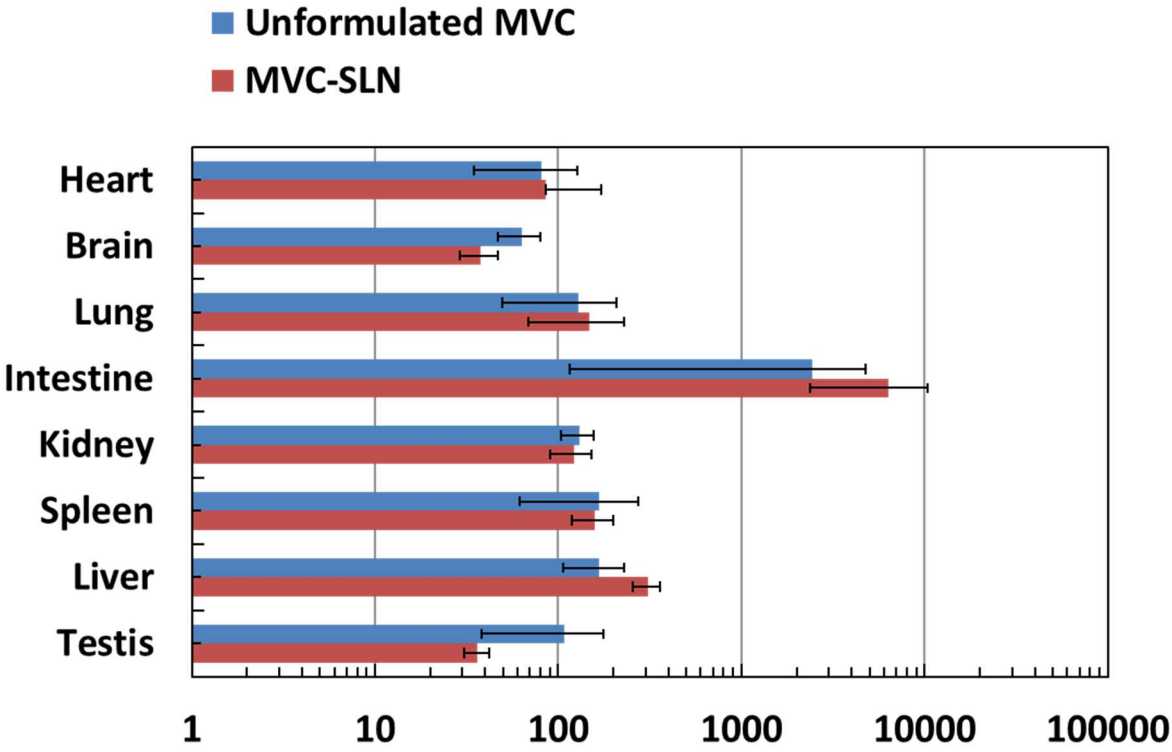

Fig. 5.18. Following solubilisation of ~100 mg of each tissue, radioactivity was determined for each using scintillation counting. MVC concentration as ng per g of dissected tissue. Organs were from MVC-SLN and unformulated treated Wistar rats. Data was provided by Dr Lee Tatham.

As seen in Table 5.6 the concentration of MVC from orally administered MVC-SLN formulations increases significantly with a fold difference of 2.61 in the intestine and 1.83 in

the liver when compared to the amount of MVC in those organs when the rats were administered with unformulated MVC. Moreover, concentration of MVC from orally administered MVC-SLNs increase 1.05 fold in the heart and 1.16 fold in the lung. The concentration of MVC in organs from rats administered with MVC-SLNs decreased in the brain, kidney, spleen and testis.

Table 5.6. In vivo oral study tissue analysis of MVC from orally administered MVC SLNs and unformulated MVC.

Tissue (n=12)	Unformulated MVC (ng/g)	MVC-SLN (ng/g)	Fold-difference	Paired t-test (two-tailed)
Heart	81.33	85.64	1.05	P=0.749 (n/s)
Brain	63.10	37.91	0.60	P=0.033
Lung	128.60	148.65	1.16	P=0.166 (n/s)
Intestine	2433.69	6352.79	2.61	P=0.006
Kidney	130.47	121.63	0.93	P=0.166 (n/s)
Spleen	167.36	159.34	0.95	P=0.249 (n/s)
Liver	167.84	307.37	1.83	P=0.0004
Testis	107.84	36.34	0.34	P=0.026

5.3. Conclusion

In this chapter, 80 wt. % MVC-SLNs were lyophilised in presence of cryoprotectants. It was found that sugars were not effective cryoprotectants in order to freeze-dry 80 wt. % MVC SLNs. However, it was found that PEG 2k-20k could be used as a cryoprotectant and that it resulted in a reconstituted MVC-SLN size after redispersion using vortexing and aspiration. However, the use of high concentrations of PEG 20k resulted in a significant reduce of drug loading in the particles. Therefore, other redispersion by ultrasonication was investigated. It was found that PEG 2k and 4k at concentrations 0.5-4 mg/mg MVC SLNs could act as cryoprotectants if the samples were redispersed using an ultrasonicator. When SLN particle diameters of the samples were analysed using DLS the samples showed as more

cryoprotectant was used a smaller difference in SLN particle diameter obtained when comparing it before and after freeze drying.

For samples used in *in vivo* and *in vitro* studies no cryoprotectant during freeze-drying of 80 wt. % MVC-SLNs was used due to the necessity of a high drug concentration during *in vitro* and *in vivo* studies. This caused the particle size of 80 wt. % MVC-SLNs to increase from 44 to 258 nm after freeze-drying. However, a highly concentrated dispersion containing 3.4 mg 80 wt. % MVC-SLNs that remained stable over 2 days. A corresponding ^{3}H-labelled MVC-SLN formulation was synthesised and the SLN particle diameters obtained were comparable to those that were unlabelled. The resulting formulation was tested *in vitro* and it was concluded that the release of ^{3}H-labelled MVC-SLN formulation released the drug with 50 % over a period of 8 hours when compared to the conventional ^{3}H-labelled MVC formulation which released the drug 78 % over the same amount of time. Therefore, we concluded that the incorporation of MVC into SLNs stabilised with DBiB-p(OEGMA)$_{10}$-*co*-(EGDMA)$_{0.6}$ resulted in sustainable release over time.

In vivo studies were carried out by administering ^{3}H-labelled MVC-SLN formulations orally into healthy rats. The plasma concentrations measured over 240 min showed that MVC obtained a maximum concentration after 4 hours which was significantly lower than the plasma concentrations obtained for commercial ^{3}H-labelled MVC. Moreover, the increase in AUC indicated that the bioavailability improved when MVC was incorporated into SLNs. Finally, the tissue analysis showed significantly higher concentrations of ^{3}H-labelled MVC in the intestine and liver when MVC was orally administered using ^{3}H-labelled MVC-SLNs compared to conventional ^{3}H-labellend MVC.

Chapter 6. Overall conclusions and future work

6.1 Overall conclusions

The research of this thesis investigated the application of branched copolymers in stabilising SLN systems that encapsulate MVC and biological evaluation.

In Chapter 2 a library of p(OEGMA) based homo and copolymers were synthesised and the stabilising properties were tested using a model oil study with *n*-dodecane as model oil. The stabilising properties of the OEGMA polymers which were varied were the chain length, the degree of branching, the number of chain ends and the concentration were tested. It was demonstrated that the number of chain ends was an extremely important factor in predicting whether a polymer was able to stabilise a *n*-dodecane emulsion. The polymer which was the best stabiliser of the *n*-dodecane emulsion was determined to be DBiB-p(OEGMA)$_{10}$-*co*-(EGDMA)$_{0.6}$. The CMC concentration of DBiB-p(OEGMA)$_{10}$-*co*-(EGDMA)$_{0.6}$ was measured and compared to its correspondent linear counterpart DBiB-p(OEGMA)$_{10.}$ This result showed that branching of a primary chain does have an impact on the CMC concentrations. Finally, measurements of the cloud point of the OEGMA polymer showed that it is insoluble in water at the temperature 52 °C but that it could be solubilised by adding organic water miscible solvents such as IPA to the aqueous phase.

In Chapter 3 DBiB-p(OEGMA)$_{10}$-co-(EGDMA)$_{0.6}$ was tested using a range of SLN preparation methods with the aim of synthesising drug-free SLNs, these methods were homogenisation, sonication and solvent injection**.** Homogenisation and sonication resulted in turbid solutions and the experiments were unsuccessful. Solvent injection led us to synthesis stable drug-free SLNs. This method was optimised and the optimal composition was DBiB-p(OEGMA)$_{10}$-co-(EGDMA)$_{0.6}$ to Compritol ATO 888 1:3 w/w %. The water miscible solvent used to synthesis IPA was used to dissolve the surfactant was removed using dialysis.

In Chapter 4 MVC loaded SLNs were produced using the solvent injection. It was possible to add up to 70 wt % MVC in relation to total solid lipid while maintaining SLN stability. The amount of drug loading was confirmed using a novel approach involving ^{19}F NMR. However,

after IPA removal by dialysis it was found there was a significant loss of MVC from the SLNs which we could not ascertain what happened to.

In Chapter 5 it was shown that IPA used in the processing of the MVC-SLNs could be removed using freeze-drying. It was found that the resulting MVC-SLNs could be redispersed with the significantly same properties after freeze drying as they possessed before including size if a cryoprotectant was used. PEG 20k was found to be optimal at both 15 and 30 mg per mg MVC SLN if vortexing and aspiration was used to redisperse the MVC-SLNs. However, if ultrasonication was used to redisperse as little as 0.5 mg PEG 2k or 4k could be used per mg MVC SLN as cryoprotectant. It was also possible to redisperse MVC-SLNs with 80 wt. % MVC relative to Compritol ATO 888 using ultrasonication. The optimised procedure of 80 wt. % MVC relative to Compritol ATO 888 was used to synthesis 80 wt. % MVC-SLNs with tritium labelled MVC to allow rapid and accurate quantification of MVC concentrations for *in vitro* and *in vivo* evaluations. *In vitro* studies showed that 80 wt. % MVC-SLNs have a first order rate of drug release over a period of 8 hours with a slower release rate than that measured for unformulated MVC. In addition, *in vivo* studies of oral administration of MVC-SLNs and unformulated MVC in rats showed that MVC-SLN formulation reached maximum plasma concentration 4 fold slower than unformulated MVC. Moreover, the AUC measured for MVC-SLNs increased in comparison to that measured for unformulated SLNs. This demonstrated that MVC-SLNs resulted in slower release *in vivo* compared to unformulated MVC. The MVC tissue distribution studies demonstrated that the concentration of MVC increased in the liver and intestine when the formulation was administered as MVC-SLN formulation.

Overall this work has shown the successful synthesis of stable MVC loaded SLNs with a drug loading of up to 80 wt. % relative to Compritol ATO 888 using solvent injection procedure. This is to our knowledge a very high drug loading by a significant margin, which has been achieved for SLNs. Furthermore, there are early indications that this procedure might be more generally usable on other hydrophobic drugs such as the anti-HIV drug DRV.

In order to synthesise these SLNs numerous obstacles were overcome in novel and unexpected ways. Among these is the use of the solvent injection procedure to create both empty and MVC loaded SLNs. The use of highly branched polymers to stabilise the drug free and MVC loaded SLNs has been demonstrated. The use of PEG polymers as cryoprotectants during freeze drying which result in easily redispersed SLNs with similar properties before and after freeze drying. Furthermore, we have used novel ^{19}F NMR techniques in order to characterise the SLNs and quantify their MVC content.

6.2 Future work

6.2.1 Synthesis of DRV loaded SLNs using solvent injection

The optimised solvent injection procedure was tried on other drugs such as darunavir (DRV). This was done by using a procedure significantly similar to that used to encapsulate MVC into SLNs another anti-HIV drug DRV appears to have been encapsulated into SLNs. When these SLNs were measured using DLS they have similar properties including size distribution to those of MVC loaded SLNs (table 6.1).

Table 6.1. D_z and PDI distribution of 80 wt. % DRV-SLNs and 80 wt. % MVC-SLNs.

80 wt. % SLNs containing	D_z before freeze drying (nm)	PDI before freeze drying	D_z after freeze drying (nm)	PDI after freeze drying (nm)
MVC	45 (0.6)	0.33 (0.01)	258 (8.1)	0.37 (0.04)
DRV	62 (0.4)	0.44 (0.07)	287 (0.04)	0.38 (0.03)

However, further characterisation has not yet been undertaken and it is not known how much DRV has in fact been encapsulated. It is expected that UV-VIS characterisation would be informative with this respect as DRV absorbs much more strongly in this range when compared to MVC.

6.2.2 Synthesis and characterisation of gemini surfactants for use as stabilisers in MVC-SLNs

It was shown in Chapter 3 that polymers with a high degree of branching are highly effective at stabilising SLNs when compared to less branched or linear polymers. This could be extended by using initiators such as glyceryl dibehenate (GDB-BiB) to synthesise Gemini surfactants instead of DBiB as initiator, Fig. 6.1.

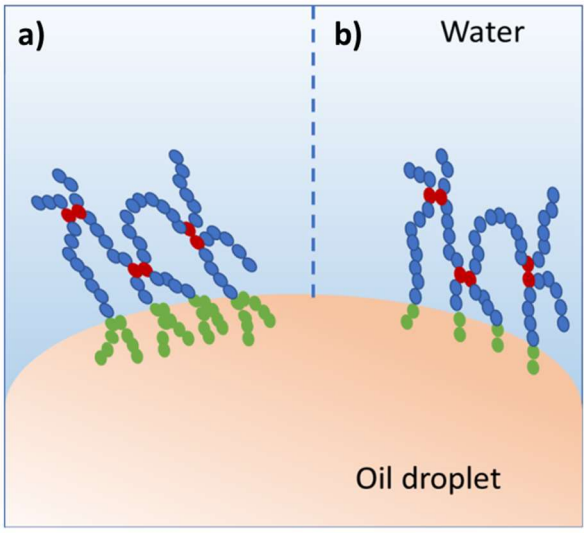

Fig. 6.1. Surface stabilising of an oil droplet using **a)** gemini chain end functional branched polymers *versus* **b)** single chained end functional branched copolymers.

Traditional amphiphilic polymers have only one foot per chain end which can be anchored into a hydrophobic oil droplet or nanoparticle surface, Fig. 6.1b. By contrast Gemini surfactants have two foot per chain end which can be anchored into hydrophobic oil droplet or nanoparticle surface, Fig. 6.1a. When gemini surfactants are used to initiate polymerisation the number of chain ends will double when compared to a linear initiator such as DBiB. This would immediately double the quantity of the branched ends of the polymer which would be able to embed themselves into the SLNs in order to stabilise the particles. The surfactant GDB-BiB-p(OEGMA) has been synthesised and used to encapsulate up to 80 wt. % MVC using Compritol ATO 888. Its size was measure as D_z = 94 nm using DLS (Table 6.2).

Table 6.2. D_z and PDI distribution before and after freeze drying of 80 wt. % MVC-SLNs stabilised with DBiB-p(OEGMA)$_{10}$-*co*-(EGDMA)$_{0.6}$ and 80 wt. % MVC-SLNs stabilised with GDB-BiB.

Polymer used For MVC-SLNs	D_z before freeze drying (nm)	PDI before freeze drying	D_z after freeze drying (nm)	PDI after freeze drying (nm)
DBiB-p(OEGMA)$_{10}$-(EGDMA)$_{0.6}$	45 (0.6)	0.33 (0.01)	258 (8.1)	0.37 (0.04)
GDB-BiB-p(OEGMA)$_{10}$-(EGDMA)$_{0.6}$	31 (1.4)	0.20 (0.01)	94 (0.04)	0.24 (0.00)

Furthermore, these particles retained their properties after freeze-drying and redispersion even without cryoprotectant. To the best of our knowledge this is the first example of gemini surfactants being used to stabilise SLNs before and the production of SLNs which are stable during freeze drying without any cryoprotectant. Furthermore, such initiators could be used to study the effect on stability when using initiators with different chain length. Therefore, these preliminary studies should be continued.

6.2.3 Characterisation of size and structure of SLNs using ^{1}H NMR

It is possible to measure the diffusion rate using an experiment called diffusion ordered spectroscopy (DOSY) NMR for ^{1}H (as well as ^{19}F for MVC). Once the diffusion rate has been measured it can be converted into a particle size using the Stokes-Einstein equation [315]. Such measurements have been used to calculate the size and concentration of low density lipoprotein (LDL) and high density lipoprotein (HDL) in blood serum [316].

It may also be possible to measure the size as well as probe the structure of SLNs using ^{1}H NMR chemical shift of lipids used to encapsulate drugs like MVC. In addition to DOSY another ^{1}H NMR technique is also already used to measure the size of LDL and HDL in blood serum [317]. This technique relies on the particle having a highly ordered layer which separates the surrounding solution from the interior which causes a shift in the ^{1}H frequency of the lipid resonances [318]. The magnitude of this shift in frequency depends on the size of the particle [318].

Applying this technique would require the synthesis of SLNs of different sizes but using the same lipids to encapsulate a drug. Then ^{1}H NMR could be used to determine whether a frequency shift is observed. If successful, this method could become another way of measuring SLN size. However, the frequency shift would need to reference to a separate measure of size for each type of lipid. Both DOSY and DLS measurements could be used in this regard. Most importantly, this experiment would give information about the structure of the SLNs. Specifically, whether an ordered lipid layer is formed between the surrounding solution and the encapsulated drug.

6.2.4 Future work summary

Looking forward, several ways which this work can be developed into the future have been identified. Notably, there are early indications that other hydrophobic drugs might be encapsulated using this technique the preliminary studies using DRV suggests. Additionally, the use of gemini surfactants as candidates may further increase the stability of SLNs which might eventually result a reduction in the amount of surfactant needed and/or in higher drug loadings in the future work. Finally, a novel approach to characterising both the internal order as well as the particle size using ^{1}H NMR has been suggested, this method is inspired by the similarity of SLNs to natural nanoparticles which the body produces using lipoproteins.

If I had several more years I would repeat the experiment details in this thesis using a Gemini surfactant library to investigate if they are better suited stabilisers for the SLNs. Moreover, I would investigate how number of feet and length of foot in the chain ends will be optimal for stabilising SLNs.

Chapter 7 Experimental section

7.1 Materials and methods – Chapter 2

7.1.1 Materials

Poly (ethylene glycol) methyl ether methacrylate (OEGMA, M_w = 300 g mol^{-1}), ethylene glycol dimethacrylate (EGDMA, M_w = 198.2 g mol^{-1}), poly (ethylene glycol) dimethacrylate (PEGDMA, M_n = 875 g mol^{-1}), 2,2'-bipyridine (bpy, 99%), copper (I) chloride (Cu(I) Cl, 99%), α-bromo-isobutyryl bromide (98%), dodecanol, anhydrous dichloromethane (DCM, 99%) and triethylethane (TEA), DOWEX marathon ion-exchange resin (hydrogen form) and aluminium oxide (AlO_3, activated, basic, Brockmann I), mesitylene and NMR solvents $CDCl_3$ (99.8 atom % D) MeOD-d_4 (99.8 atom % D) and *n*-dodecane (≥ 99.9 %) were purchased from Sigma Aldrich and used as received. The solvents Methanol (MeOH, anhydrous 99.99 %), petroleum ether (analytical grade, bp. 40-60°C), N, N- dimethylformamide (DMF, HPLC-grade), propan-2-ol were purchased from Fischer Scientific and used as received. 2-dodecyl-2-bromoisobutyrate initiator was synthesized by a procedure mentioned in the experimental section and characterized by ^1H and ^{13}C NMR as well as ESI-MS before use.

Linear and branched polymers were synthesised and characterised by a procedure described in the experimental section.

7.1.2 Synthesis of DBiB-p(OEGMA) based copolymers

7.1.2.1 Synthesis of 2-dodecyl-2-bromoisobutyrate initiator

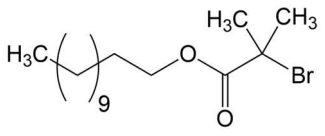

Dodecanol (12.5g, 67.1 mmol) was dissolved in DCM (186.5 mL) and TEA (10 g, 14.2 mL, 100.6 mmol) in a triple neck round bottom flask, which was equipped with a magnetic stirrer and dry N_2 inlet. The mixture was cooled to 0°C in an ice bath and 2-bromo-2-isobutyrate

(18.5 g, 80.5 mmol, 9.94 mL) was added drop wise to the stirring mixture. After complete addition, the reaction was left to heat up to ambient temperature for 24 h. The mixture was washed with $NaHCO_3$ (2 x 200 mL), distilled water (4 x 200 mL) and dried over anhydrous $MgSO_4$. The solvent was evaporated to yield 21.9 g (99 %) dark brown liquid. ^{1}H-NMR (MeOD-d_4, 400 MHz) δ (ppm): 0.92(t, 3H, *J* =7 Hz); 1.40(m, 18H), 1.69 (q, 2H), 1.93(s, 6H), 4.18 (t, 2H, *J* = 6.4 Hz). ^{13}C-NMR (MeOD-d_4, 100.61 MHz) δ (ppm): 13.08 (-**C**H_3), 22.25 (-**C**H_2-), 25.55 (-**C**H_2-), 28.08(-**C**H_2-), 28.87(-**C**H_2-), 29.08(-**C**H_2-), 29.22(-**C**H_2-), 29.26 (-**C**H_2-), 29.37 (-**C**H_2-), 29.75 (-**C**H_2-), 31.69(2x-**C**H_3), 55.75(-**C**-), 65.68 (-**C**-O), 171.60 (-**C**=O). m/z calcd for $C_{16}H_{31}BrO_2$ (M^+): 335.32 Da; found by ESI-MS $[M+Na]^+$ =357.1 Da.

7.1.2.2. Synthesis of grafted linear DBiB-p(OEGMA) based homopolymers

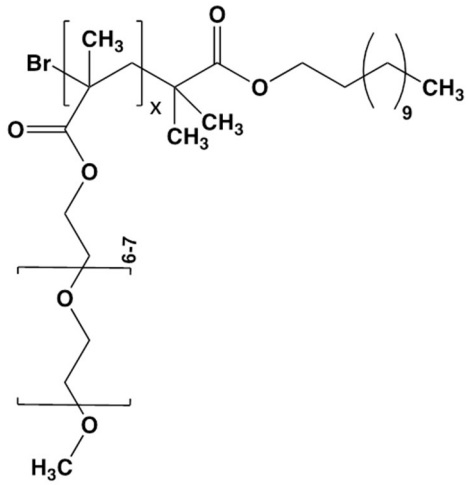

The targeted number average degree of polymerisation DP_n was n =10, 20 or 50 monomer units. Poly (ethylene glycol) methyl ether methacrylate (OEGMA, average M_n = 300 gmol^{-1}) 10-50 eq. was added to a mixture of isopropanol/water (IPA/H_2O; 92.5, 7.5 v/v %) (6 g), 2,2'-bipyridyl (2 eq.), 2-dodecyl-2-bromoisobutyrate bromide (1 eq.) and a few drops of mesitylene (used as an internal reference). The reaction were monitored by ^{1}H NMR and worked up when >90 % conversion was obtained. After > 90 % conversion was obtained 100 mL MeOH or THF was added to the solution and the active copper was inactivated with compressed air, the copper was then removed by stirring the solution with DOWEX and

basic AlO_3 for 15 min. The solution was filtered by gravity and the solvent was removed by reduced pressure. MeOH or THF was added to dissolve the mixture that dropwise was precipitated into petroleum ether at room temperature. The reaction was stirred for 30 min after the precipitation. Petroleum was decanted and excessive solvent was removed be reduced pressure. The resulting polymer product was dried in the vacuum oven at 40 °C overnight at 40 ˚C. The resulting yield was measured 4-5 g was stored in a vial at ambient temperature for later use. ^{1}H-NMR (MeOD-d_4, 400 MHz) assignment for DBiB-p(OEGMA)$_{50}$ δ (ppm): 0.9 ppm (103 H) –C**H$_2$**-, 1.1 ppm (50 H) –C**H$_3$**, 1.3 (18 H) CH_2-C**H$_2$**-O, 1.5-1.9 ppm (102 H) –C**H$_2$**-, C**H$_3$,** Br-CR-C**H$_3$**, 3.4 ppm (151 H) –C**H$_3$**, 3.5-4.1 ppm (803 H) –C**H$_2$**-.

Table 7.1 Reaction time and conditions.

Polymer	Reaction time
DBiB-p(OEGMA)$_{10}$	2
DBiB-p(OEGMA)$_{20}$	4
DBiB-p(OEGMA)$_{50}$	8

7.1.2.3 Synthesis of grafted branched polymers

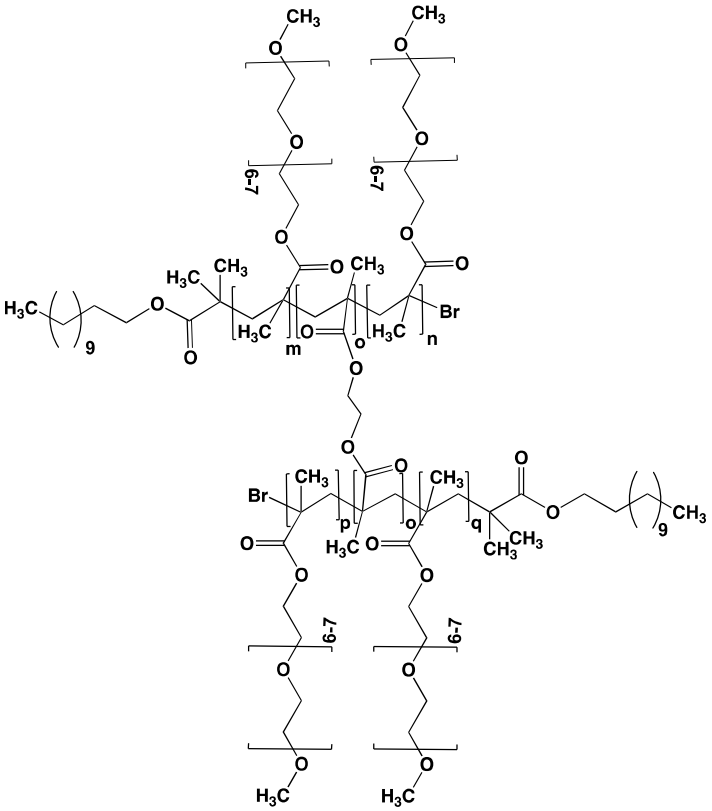

10, 20 and 50 eq. of OEGMA (M_n= 300 gmol^{-1}) was added to a mixture of Ethylene dimethacrylate (EGDMA, M_w=198.22 gmol^{-1}) 0.2-0.95 eq. or (PEGDMA, M_w=875 gmol^{-1}) in IPA/H_2O (92.5, 7.5) (6 g), bpy (2 eq.), 2-dodecyl-2-bromoisobutyrate (1 eq.) and a few drops of mesitylene as an external reference. Oxygen was removed from the mixture through N_2 inlet for 20 min and CuCl (1 eq.,) was added to the solution. Nitrogen was then again blown through the mixture for 5 min. The reaction was stirred at 40 ˚C and analysed at different time point by ^{1}H-NMR and GPC. The reaction was worked up after 93-99 % conversion monitored by ^{1}H NMR. 100 mL MeOH was added to the solution and killed with compressed air, the copper was then removed by stirring the solution with DOWEX and AlO_3 in 15 min. The solution was filtered by gravity and the solvent was removed by reduced pressure. MeOH or THF was then added to dissolve the sample and the mixture was dropwise precipitated into petroleum ether. The after precipitation petroleum ether was decanted and

the excess solvent was removed by reduced pressure. The resulting product was then transferred to a vial and dried in a vacuum oven at 40 ˚C for 2-3 days. The yield of the experiments were 3-5 g. The dried samples were analysed by GPC by dissolving the samples in fresh DMF eluent with a concentration of 20 mg/mL. The purified OEGMA based products were analysed by 1H NMR by preparing 20 mg of sample in 0.6 mL of MeOD-d_4.

Table 7.2 Reaction time and conditions for EGDMA branched DBiB-p$(OEGMA)_{10}$ based polymers

Polymer	Reaction time (hrs)
DBiB-p$(OEGMA)_{10}$ – $(EGDMA)_{0.2}$	3
DBiB-p$(OEGMA)_{10}$ - $(EGDMA)_{0.5}$	3
DBiB-p$(OEGMA)_{10}$-$(EGDMA)_{0.6}$	3.5
DBiB-p$(OEGMA)_{10}$-co-$(EGDMA)_{0.7}$	4
DBiB-p$(OEGMA)_{10}$-co-$(EGDMA)_{0.8}$	4

Table 7.3 Reaction time and conditions for EGDMA branched DBiB-p$(OEGMA)_{20}$ based polymers

Polymer	Reaction time (hrs)
DBiB-p$(OEGMA)_{20}$ –co- $(EGDMA)_{0.2}$	5
DBiB-p$(OEGMA)_{20}$ –co- $(EGDMA)_{0.5}$	6
DBiB-p$(OEGMA)_{20}$-co-$(EGDMA)_{0.6}$	5
DBiB-p$(OEGMA)_{10}$-co-$(EGDMA)_{0.7}$	7
DBiB-p$(OEGMA)_{10}$-co-$(EGDMA)_{0.8}$	7

Table 7.4 Reaction time and conditions for EGDMA branched DBiB-p$(OEGMA)_{50}$ based polymers

Polymer	Reaction time (hrs)
DBiB-p$(OEGMA)_{50}$ –co- $(EGDMA)_{0.2}$	10
DBiB-p$(OEGMA)_{50}$ –co- $(EGDMA)_{0.5}$	9
DBiB-p$(OEGMA)_{50}$-co-$(EGDMA)_{0.6}$	9
DBiB-p$(OEGMA)_{50}$-co-$(EGDMA)_{0.7}$	9
DBiB-p$(OEGMA)_{50}$-co-$(EGDMA)_{0.8}$	8
DBiB-p$(OEGMA)_{50}$-co-$(EGDMA)_{0.95}$	10

Table 7.5 Reaction time and conditions for PEGDMA branched DBiB-p$(OEGMA)_{20}$ based polymers

Polymer	Reaction time (hrs)
DBiB-p$(OEGMA)_{10}$ –co- $(PEGDMA)_{0.2}$	3
DBiB-p$(OEGMA)_{10}$ –co- $(PEGDMA)_{0.5}$	4

Table 7.6 Reaction time and conditions for PEGDMA branched DBiB-p$(OEGMA)_{20}$ based polymers

Polymer	Reaction time (hrs)
DBiB-p$(OEGMA)_{20}$ –co- $(PEGDMA)_{0.2}$	8
DBiB-p$(OEGMA)_{20}$ –co- $(PEGDMA)_{0.5}$	8
DBiB-p$(OEGMA)_{20}$ –co- $(PEGDMA)_{0.7}$	8

Table 7.7 Reaction time and conditions for PEGDMA branched DBiB-p(OEGMA)$_{20}$ based polymers

Polymer	Reaction time (hrs)
DBiB-p(OEGMA)$_{50}$ –co- (PEGDMA)$_{0.2}$	13
DBiB-p(OEGMA)$_{50}$ –co- (PEGDMA)$_{0.5}$	12
DBiB-p(OEGMA)$_{50}$ –co- (PEGDMA)$_{0.7}$	12

7.1.2.4 Dodecane emulsion studies

OEGMA based homo- or copolymers were dissolved into the aqueous phase at the concentrations of 60, 120 and 240 mg/mL into 3 mL of the aqueous phase. The 3 mL aqueous phase was mixed with 3 mL of *n*-dodecane, a ratio of 1:1 v/v ratio. The combined sample was homogenised for 10 min with a speed of 25,000 rpm at ambient temperature.

7.1.3 Characterisation of p(OEGMA) based copolymers

7.1.3.1 NMR

Single pulse ^{1}H and ^{13}C NMR spectra were acquired on a 400 MHz Bruker Avance III HD spectrometer operating at 400.13 MHz for ^{1}H and 100.61 MHz for ^{13}C. The spectrometer was equipped a dual channel 5 mm BBFO Bruker probe. The ^{13}C spectra were 1H decoupled using the TPPM sequence. The ^{1}H pi/2 excitation pulse length was 10 μs and the recycle delay of 1 sec. 16 experiments were co-added. 16 experiments were co-added. The ^{1}H chemical shift was referenced to TMS at 0 ppm and the ^{13}C chemical shift was referenced to TMS at 0 ppm. NMR spectra were obtained from samples prepared with approximately 20 mg of crude/product in 0.6 mL of $CDCl_3$ or MeOD-d_4. Kinetic studies of linear polymers were analysed in MeOD-d_4. Results were processed and analysed by Topspin 3.2, Origin Pro 9 and Excel.

7.1.3.2 Gel Permeation Chromatography (GPC)

Gel permeation chromatography (GPC) was performed using Malvern Viscotek instruments equipped with a GPCmax VE2001 autosampler, two Viscotek D6000 columns (and a guard

column) and a single detector array TDA305 (refractive index, light scattering) with mobile phase of DMF containing 0.01 M lithium bromide and a flow rate of 1 mL/min. Samples were prepared with a concentration of 10 mg/mL in DMF containing 0.01 M Lithium Bromide and the eluent was taken from the machine. Polymethylmethacrylate (PMMA) 65 kDa or 50 kDa was used as a narrow standard and 95 kDa for broad standard for the calibration.

7.1.3.3 CMC - Surface tension measurements

Selected polymers were measured by a Kibron Delta-8 tensionmeter. The machine was calibrated with distilled water at ambient temperature and pressure. Branched or linear polymeric samples with starting concentrations 0.004-10mM were diluted with a dilution factor of 0.5 using Eppendorf robotic sampler and the 50 μL of the diluted samples were transferred to a Kibron plate and analysed.

7.1.3.4 Thermal behaviour of p(OEGMA) based copolymers Optimelt

DBiB-p$(OEGMA)_{10}$-*co*-$(EGDMA)_{0.6}$ was prepared at concentrations of 5-40 mg/mL (0.5-4 v/v %) in deionised water. The samples were injected into OP100MPC capillaries that were 90 mm long. The cloud point of the different compositions of DBiB-p$(OEGMA)_{10}$-*co*-$(EGDMA)_{0.6}$ was measured by SRS MPA100 Optimelt automated melting point instrument with a heating rate at 1-2 °C/min. The cloud points were measured from a resulting plot in MeltView.

7.1.3.5 ESI Mass spectrometry

Electrospray mass spectrometry data (ES-MS) of the samples were collected in the Mass Spectrometry Laboratory at the University of Liverpool. The data was obtained using a Micro Mass LCT mass spectrometer using electron ionisation and direct infusion syringe pump sampling. 10 mg of all the materials were diluted with methanol.

7.1.3.6 Laser diffraction analysis

n-dodecane emulsions were characterized by laser diffraction using a Mastersizer 2000 (Malvern instrument), equipped with a Hydro 2000 SM dispersion unit. 2-3 drops of the resulting linear or branched copolymer stabilised *n*-dodecane emulsion were added to the Hydro 2000 SM dispersion unit with a stirring rate adjusted to 1200 rpm until the laser obscuration was observed to be within 5-20 %. The volume-weighed mean D[4,3] diameter and other parameters of the oil droplets were measured in triplicate. Before and after each of the sample measurements the Hydro 2000 SM dispersion unit was flushed with deionised water to ensure quality between the measurements.

7.1.3.7 Characterisation of DBiB-p(OEGMA)-co-(EGDMA)$_{0.6}$ stabilised n-dodecane oil droplets using optical microscope

The morphology of DBiB-p(OEGMA)$_{10}$-*co*-(EGDMA)$_{0.6}$ (60 mg/mL deionised water) stabilised *n*-dodecane emulsion the emulsion droplets were analysed using an optical microscopy, leica DM4B, transmitted light source. One drop of the emulsion was added to a glass slide and covered with a coverslip.

7.2 Materials and methods – Chapter 3

7.2.1 Materials

The linear and branched polymers were synthesised and characterised as mentioned in former section. Glycerol dibehenate (Compritol ATO 888) was kindly gifted from Gattefossé and analysed by ^{1}H NMR and ESI before use. Poloxamer 188 (Pluronic F64). Spectra/Por 4 dialysis tubing with 12-14 molecular weight cutoff (MWCO), 75 mm flat width, 15 meters/ roll (50 ft) was supplied by spectrum labs. BD Microlance 3 hypodermic needle 21 g (green) 50 mm, 18 g (pink) x 1.5 and Plastipak syringes 1-2 mL was supplied by BD Microlance. 12 and

40 mL vials were used. Magnetic stirring bars, micro, were supplied by VWR ®. Propan-2-ol was supplied from Sigma Aldrich.

7.2.2 Synthesis of empty SLNs by hot high shear homogenisation

DBiB-p(OEGMA)$_{10}$-*co*-(EGDMA)$_{0.6}$ stabilised SLN dispersions were prepared using the hot high shear homogenisation procedure. DBiB-p(OEGMA)$_{10}$-*co*-(EGDMA)$_{0.6}$ were weighed out as given in the Table 7.1 and dissolved in 10 g deionised water (pH = 6±0.2). Compritol ATO 888 was weighed out, as given on Table 7.1, and added to the same sample of polymer in water so that the total solid content of the polymer and lipid in each case was 1.1 g in 10 g of deionised water. The two-phased mixture was heated to 85 °C and subsequently homogenised with 2 cycles of 5 minutes using an Ultra Turaxx T25 digital homogeniser fitted with a S25 N 10G dispersing element, and set to maximum speed of 25,000 rpm. The temperature of the sample was maintained at 85 °C during the homogenisation.

Table 7.1. Compositions of polymers used for hot high shear homogenisation.

Ratio Polymer:lipid	DBiB-p(OEGMA)$_{10}$-co-(EGDMA)$_{0.6}$/ g	Compritol ATO 888/ g
1:1	0.550	0.550
1:3	0.275	0.825
1:5	0.180	0.920
1:7	0.138	0.962
1:10	0.1	1

7.2.3 Synthesis of empty SLNs by hot probe sonication

DBiB-p(OEGMA)$_{10}$-*co*-(EGDMA)$_{0.6}$ was dissolved in 10 g of water in compositions given in Table 7.2. Compritol ATO 888 and 3 g of *n*-propanol solvent was added to the solution containing DBiB-p(OEGMA)$_{10}$-*co*-(EGDMA)$_{0.6}$. The ratios for the polymer to Compritol ATO 888 compositions are given in Table 7.2. The combined samples were heated to 85 °C. The

sample was sonicated 1 cycle of 5 min 100 % power by a probe sonicator. Samples were cooled under ice bath straight after sonication.

Table 7.2. Compositions of polymers used for hot probe sonication.

w/w ratio	DBiB-p(OEGMA)$_{10}$-co-(EGDMA)$_{0.6}$/ g	Compritol ATO 888/ g
1:1	0.550	0.550
1:3	0.275	0.825
1:5	0.180	0.920
1:7	0.138	0.962
1:10	0.1	1

7.2.4 Synthesis of drug-free SLNs by solvent injection methods

DBiB-p(OEGMA)$_{10}$-co-(EGDMA)$_{0.6}$, DBiB-p(OEGMA)$_{10}$ and poloxamer 188 to Compritol ATO 888 were prepared with ratio compositions as given in Table 7.3. The polymer was dissolved in deionised water 10 g (pH=6.0 ±0.2) at heated to 25 °C under stirring. Compritol ATO 888 was heated to 80 °C in 2 mL IPA and rapidly injected into a stirred mixture (330 rpm) of polymer in deionised water at 25 °C. The sample was cooled after 5 min stirring of the sample and stored in the fridge at 4 °C until use.

Table 7.3. Compositions of polymers used for the initial solvent injection method.

Ratio Polymer:lipid	DBiB-p(OEGMA)$_{10}$-*co*-(EGDMA)$_{0.6}$/ mg	Compritol ATO 888/ mg
1:1	6	6
1:2	6	12
1:3	6	18
1:6	6	36
2:1	12	6
3:1	18	6
6:1	36	6
0:1	0	6

DBiB-p(OEGMA)$_{10}$-*co*-(EGDMA)$_{0.6}$, DBiB-p(OEGMA)$_{10}$, DBiB-(OEGMA)$_{50}$ and DBiB-(OEGMA)$_{50}$-*co*-(EGDMA)$_{0.95}$ poloxamer 188 to Compritol ATO 888 were prepared with ratio compositions as given in table 7.4. In each case the total solid content in deionised water was 1.2 mg/ mL. The polymer was dissolved in deionised water 10 g (pH = 6.0 ±0.2) at heated to 25 °C under stirring speed of 150 rpm. Compritol ATO 888 was heated to 80 °C in 4 mL IPA and rapidly injected into the solution of polymer in deionised water. The sample was cooled after 5 min stirring of the sample and stored in the fridge at 4 °C until use.

Table 7.4. Compositions of polymers used for later optimised solvent injection method. * DBiB-p(OEGMA)$_{10}$-*co*-(EGDMA)$_{0.6}$, DBiB-p(OEGMA)$_{10}$ and poloxamer 188.

Ratio Polymer:lipid	*Polymer/ mg	Compritol ATO 888/ mg
1:1	6	6
1:3	3	9
3:1	9	3

7.2.4.1. Characterisation of empty SLNs by DLS

The size and zeta potentials of SLNs in the resulting formulations stabilised by DBiB-p(OEGMA) based polymers or conventional polymer were measured using dynamic light scattering (DLS) . The sizes and were measured in plastic cuvettes or zeta potential cuvettes. The samples were pipetted directly from the formulation that has a concentration of 1.2 mg/mL of SLNs and this resulted in a laser attenuation of 6-7 and this was consistent throughout the whole study. The samples were measured in triplicates both in case of the diameter size and surface charge measurements. The samples were measured with a constant temperature of 25 °C.

7.2.4.2 Characterisation of empty SLNs by SEM

Samples a for SEM imaging 20 µL of SLN formulation containing 1.2 mg/mL SLN formulation pipetted into a was pipetted onto a glass cover slide attached to a carbon adhesive disc on an aluminium SEM specimen stub (12.5 mm diameter). The samples were left to air-dry for 24 hours, followed by sputter coating with gold (EMITECH K550X) with a deposition current of 25 mA for 100 seconds before imaging. SEM images of the samples were then obtained using a Hitachi S-4800 FE-SEM at 3 kV.

7.3 Materials and methods – Chapter 4

7.3.1. Materials

Maraviroc (MVC) donated by ViiV Healthcare. Spectra/Por 4 dialysis tubing with 12-14 molecular weight cutoff (MWCO), 75 mm flat width, 15 meters/ roll (50 ft) was supplied by spectrum labs. BD Microlance 3 hypodermic needle 21 g (green) 50 mm, 18 g (pink) x 1.5 and Plastipak syringes 1-2 mL was supplied by BD Microlance. 12 and 40 mL vials were used. Magnetic stirring bars, micro, were supplied by VWR ®. $CDCl_3$ were purchased from sigma Aldrich and dried with molecular activated molecular sieves overnight. ^{1}H and ^{19}F samples were analysed in Wilmad® NMR tubes 5 mm diam. purchased from Sigma Aldrich. The internal ^{19}F reference Tetrabutylammonium hexafluorophosphate (TBHF) was purchased from Sigma Aldrich and used as received.

7.3.2 Synthesis of MVC loaded SLN dispersion by optimised solvent injection method

DBiB-p$(OEGMA)_{10}$-*co*-$(EGDMA)_{0.6}$ to Compritol ATO 888 ratio of 1:3 were prepared with MVC to Compritol ATO 888 ratio compositions as given in table 7.5. In each case the total solid content in deionised water was 1.2 mg/mL. The polymer was dissolved in deionised water 20 g (pH = 6.0 ±0.2) at heated to 25 °C under stirring at 150 rpm on a stirrer. Compritol ATO 888 and MVC was heated to 80 °C in 4 mL IPA for 2 min and rapidly injected

into the solution of polymer in deionised water. The sample was cooled after 5 min stirring at 300 rpm of the sample and stored in the fridge at 4 °C until use.

Table 7.5. MVC: Compritol ATO 888 ratios used in solvent injection method to synthesis $p(OEGMA)_{10}$-co-$(EGDMA)_{0.6}$ stabilised MVC loaded SLNs.

% MVC rel. to Compritol ATO 888	MVC/mg	Compritol ATO 888/ mg
0	0	18
20	3.6	14.4
30	5.4	12.6
40	7.2	10.8
50	9	9
60	10.8	7.2
70	12.6	5.4
80	14.4	3.6
90	16.2	1.8
100	18	0

7.3.2.1. Characterisation of MVC loaded SLNs by DLS

D_z and zeta potentials of MVC loaded SLNs in the resulting formulations stabilised by DBiB-$p(OEGMA)_{10}$-*co*-$(EGDMA)_{0.6}$ or poloxamer 188 were measured using dynamic light scattering (DLS). The sizes and were measured in plastic cuvettes or zeta potential cuvettes. The samples were pipetted directly from the formulation. 1 mL of sample has a concentration of 1.0 mg/ mL of MVC loaded SLNs in presence of IPA and 1.2 mg/ mL in absence of IPA.

D_z measurements resulted in a laser attenuation of 6-7 and this was consistent throughout the whole study. The zetapotential was measured in a different cuvette resulting in a laser attenuation of 11. The samples were measured in triplicates both in case of the diameter size and surface charge measurements. The samples were measured with a constant temperature of 25 °C.

7.3.2.2 Characterisation of MVC loaded SLNs by SEM

MVC loaded SLNs with 80 wt. % MVC relative to SLN was prepared form SEM. A Sample of 20 µL of SLN formulation containing 1.2 mg/mL of freeze dried and redispersed MVC loaded SLN formulation was prepared as described in former section using the same equipment.

7.3.3 Dialysis of MVC loaded SLN dispersion by optimised solvent injection method

The drug release studies were carried out using a 12-14 kDa MWCO cellulose acetate membrane in a double-sided bio-dialyser containing 1 mL of SLN dispersion with a concentration of 1.2 mg/mL MVC-SLN in deionised water. The dialyser was then placed in a 100 mL reservoir of distilled water, which was replaced on every time-point (i.e. a fresh 100 mL reservoir for every time-point) in order to maintain sink conditions.

7.3.4 Freeze drying of MVC loaded SLN dispersion by optimised solvent injection method

20 g of dialysed MVC loaded SLN dispersions obtained with targeted MVC loadings of 10-90 wt. % MVC relative to Compritol ATO 888 in water/IPA were directly transferred from the dialysis bag to a 40 mL vial. The sample in the vial was frozen using liquid nitrogen and then freeze-dried using VirTis Freeze Dryer BTK4XL -75 °C for 5 days. 24 g of MVC SLN dispersion in water/IPA was transferred to a 40 mL vial from a 50 mL two neck flask. The sample in the vial was frozen down with liquid nitrogen and freeze dried using VirTis Freeze Dryer BTK4XL -75 °C for 5 days. After 5 days freeze drying the samples were dried in the vacuum oven for 1 day.

7.3.5 Quantification of MVC in MVC loaded SLNs

7.3.5.1. Characterisation of MVC loaded SLNs by UV-vis

Thermo Scientific NanoDrop 2000c spectrophotometer monitoring the absorption at λ_{max} = 216 nm was recorded prior to dissolving MVC in solvents such as chloroform or DCM that is known so solubilise Compritol ATO 888. Three sets of samples were prepared and analysed in a quartz cuvette. The compositions of the three sets of experiments are given in the table below. MVC was dissolved in chloroform in different compositions used in the solvent injection experiments.

7.3.5.2. Characterisation of MVC loaded SLNs by ^{1}H NMR

The ^{1}H NMR samples were recorded on a 400 MHz Bruker Avance III HD spectrometer operating at a frequency of 400.13 MHz for ^{1}H. The spectrometer was equipped a dual channel 5 mm BBFO Bruker probe. Samples were recorded using single pulse on ^{1}H with a pi/2 excitation duration of 10 μs. The recycle delay was 1 sec. The chemical shift was referenced to TMS at ^{1}H δ 0 ppm

7.3.5.3. Characterisation of MVC loaded SLNs by ^{19}F NMR

The ^{19}F NMR experiments were done in collaboration with Dr. Konstantin Luzyanin from the NMR facility of the University of Liverpool. The spectra were recorded on a 400 MHz Bruker Avance III HD spectrometer operating at 376.42 MHz for ^{19}F. The spectrometer was equipped a dual channel 5 mm BBFO Bruker probe. Samples were recorded using single pulse on ^{19}F with a pi/2 excitation duration was 12.5 μs. The recycle delay was 20 sec. The spectra were referenced to TBHF ^{19}F δ = -70 ppm.

Samples were prepared for calibration curve of MVC with following compositions 18 mg (100 %), 13.5 mg (75 %), 9 mg (50 %) and 4.5 mg (25 %) relative to Compritol ATO 888 in 0.6 mL of molecular sieve dried $CDCl_3$. The internal reference TBHF was added with the same concentration to all of the samples with a molar ratio of 1:1 relative to MVC. The samples were recorded at 25 ℃ and 50 ℃, respectively. The peaks assigned to MVC were -92 ppm--101ppm (dd 2F, J=236 Hz) and peaks assigned to ^{19}F on TBHF -70 and -73 ppm (6F). The intensity of the ratios of ^{19}F on MVC relative to ^{19}F on TBHF was plotted on a curve shown in chapter 4.

Samples were prepared for calibration curve of MVC, Compritol ATO 888 and DBiB-p(OEGMA)$_{10}$-*co*-(EGDMA)$_{0.6}$. The ratios of Compritol ATO 888 were varied with following compositions MVC 18 mg (100 %) and Compritol ATO 888 (0%) and, MVC 13.5 mg (75 %) and Compritol ATO 888 4.5 mg (25 %), MVC 9 mg (50 %) and Compritol ATO 888 9 mg (50 %), MVC 4.5 mg (25 %) and Compritol ATO 888 13.5 mg (75 %) in 0.6 mL of molecular sieve dried $CDCl_3$. The internal reference TBHF was added in the same concentration with a molar ratio of 1:1 relative to MVC to all of the samples. DBiB-p(OEGMA)$_{10}$-co-(EGDMA)$_{0.6}$ (6 mg) was added with the same concentration to all of the samples. The samples were recorded were recorded under same conditions as started earlier in this section.

Dialysed samples of MVC loaded SLNs were dialysed for 3 days followed by Freeze-drying for 3 days. The samples were dried in the vacuum oven at 40 °C for 1 day. Samples for NMR contained the ratios of Compritol ATO 888 and MVC was varied with earlier mentioned compositions of MVC, Compritol ATO 888 and DBiB-p$(OEGMA)_{10}$-co-$(EGDMA)_{0.6}$ in the dialysed and freeze dried MVC SLNs.

Freeze dried MVC loaded samples were prepared with earlier mentioned compositions of MVC, Compritol ATO 888 and DBiB-p$(OEGMA)_{10}$-co-$(EGDMA)_{0.6}$ and analysed with the optimised method as stated earlier in this section.

7.3.5.4. Analysis of dialysis contents

Analysis of dialysis content study were carried out using a 12-14 kDa MWCO dialysis bag. The dialyser was then placed in a 500 mL beaker containing deionised water. The sample was left in the dialysis bag in the fridge at 4 °C over 4 days and the dialysis bag was removed. The content in the dialysis bag was left to dry over heat at 60 °C a heat plate over a day. The NMR sample was prepared after all of the water was evaporated and the remaining content was dissolved in the beaker in $CDCl_3$ with an unknown concentration. The beaker was weighted out before and after dialysis and no water was change during the dialysis period. However, the mass of the beaker before and after dialysis was the same suggesting that not much material has escaped through the dialysis bag.

7.4 Materials and methods – Chapter 5

ProSafe+ scintillation cocktail (Meridian Biotechnologies Ltd.) was used as received. Maraviroc donated by ViiV Healthcare was tritiated by RCTritec and received in an ethanol solution. The certificate can be found in the Appendix Fig. A59 Ethanol was removed before experiments by evaporating the sample overnight in the fume cupboard. All radiation

measurements were carried out using a liquid scintillation counter (Packard Tri-carb 3100TR; Isotech).

Adult male Wistar rats (280-330 g) were dosed with either SLN formulated MVC or unformulated MVC (10 mg/Kg MVC, 20 µCi/mg ^{3}H activity) via oral gavage. Food and water were provided ad libitum throughout the procedure.

7.4.1 Freeze drying of MVC loaded SLNs using cryoprotection

7.4.1.1. Freeze drying of MVC loaded SLNs with Sugars or PEGs as cryoprotant

1 mL of MVC loaded SLN dispersions prepared by the solvent injection method were transferred into a 4 mL vial straight after synthesis and then 1 mL of cryoprotection solution was added. The sample was then mixed overnight or frozen in liquid nitrogen straight after addition of a 0.5 – 4 mg/mL cryoprotectant solution. This was done as samples in a sample vial containing 1 mL of resulting mixture. The frozen sample was freeze-dried for 2 days dried using a VirTis Freeze Dryer BTK4XL -75 °C. After 2 days the samples were redispersed by adding 1 mL of water to a powder of with concentration of 0.6 mg MVC-SLN (80 wt. % MVC relative to Compritol ATO 888) + 0.5-4 mg of cryoprotectant. The sample was mixed with aspiration and vortex. Particle sizes of the resulting dispersions were measured by DLS.

DBiB-p$(OEGMA)_{10}$-$(EGDMA)_{0.6}$ in 3:1 (Compritol ATO 888: DBiB-p$(OEGMA)_{10}$-$(EGDMA)_{0.6}$; total volume 12 mg in 10 mL of water + 2 mL of IPA) – Dialysis vs. freeze dried MVC and Compritol ATO 888 (total mass of 9 mg) was heated in IPA and rapidly injected into a stirred mixture of DBiB-p$(OEGMA)_{10}$-$(EGDMA)_{0.6}$ (mass of 6 mg) in 10 mL deionised water.

PEG 2k, 5k, 10k and 20k was dissolved in 1 mL of deionised water with following concentrations 7.5 mg/mg, 15 mg/mg and 30 mg/mg. The solution was rolled on the roller o/n and 1 mL was added dropwise to 1 mL of 50 wt. % (MVC relative to Compritol ATO 888)

SLN solution. The solution was vortex and mixed with the pipette and 1mL was transferred to a 4 mL vial and the sample was freeze dried o/n.

7.4.2 Freeze drying of MVC loaded SLNs without cryoprotection

This procedure was done exactly as described in former section with the modifications: 1 mL of water was added to the SLN dispersion when freeze-dried.

7.4.2.1 Optimisation of ultrasonication of MVC loaded SLNs

The resulting MVC loaded SLN powder was redispersed into deionised water with a concentration of 1.2 mg/mL and sonicated 4 cycles of 15 sec with 10 sec break between each cycles using a Covaris S2x with a duty cycle of 20 %, an intensity of 10, cycles per burst in frequency sweeping mode 500 and power 70 W.

7.4.3. Synthesis of ^{3}H-labelled MVC loaded SLNs

Tritiated MVC (288 µCi, specific activity 20 µCi/mg), MVC (14.4 mg, 28.03 µmol) and Compritol ATO 888 (3.6 mg, 8.68 µmol) were added to a 20 mL vial equipped with a stirrer bar and solubilised in IPA (4 mL) at 80 °C. DBiB-p(OEGMA)$_{10}$-*co*-(EGDMA)$_{0.6}$ (6 mg) solubilised in H_2O (20 mL) was added to a 100 mL round-bottomed flask equipped with a magnetic stirrer and stirred at ambient temperature. The rapid addition of the MVC mixture to the polymer solution was conducted *via* a cannula. The mixture was stirred for a further 5 minutes and particle size measured by DLS. The solution was freeze-dried over 4 days and re-dispersed in H_2O (8 mL) via vortex mixing and sonication. Finally, the particle size was analysed by DLS.

7.4.4. Characterisation of radiolabelled MVC loaded SLNs

7.4.4.1 In vitro release studies of radiolabelled MVC loaded SLNs

The drug release studies were carried out using a 1,000 MWCO cellulose acetate membrane in a double-sided bio-dialyser containing 1 mL of SLN solution. The dialyser was then placed in a 100 mL reservoir of distilled water, which was replaced on every time-point (i.e. a fresh 100 mL reservoir for every time-point) to have true sink conditions.

7.4.4.2 In vivo oral study with MVC loaded SLNs

This study is a result of collaboration with the department of pharmacology at the University of Liverpool by Dr Lee Tatham.

Following 7 days habitation, the rats weighed 280-330 g (2.8-3.3 mg of MVC/ rat) received either a single dose of 10mg/ kg of MVC SLNs formulation of 80 wt. % MVC relative to Compritol with a concentration of 1.56-1.83 mL of radioactive MVC I SLN dispersion or unformulated MVC (<5% DMSO) via oral gavage (1 ml total volume in distilled water) as outlined above. Blood samples were collected (300 µl) at 0.5, 1, 1.5, 2 and 3 hrs post-dosing from the tail vein. At the 4h time point, the rats were sacrificed using cardiac puncture under terminal anaesthesia and immediate exsanguination of blood from the heart. Immediately following this, an overdose of Pentoject (Pentobarbitone) was administered to the heart using the same in situ puncture needle. Terminal blood and tissue samples were collected for analysis. All animal work was conducted in accordance with the Animals (Scientific Procedures) Act 1986 (ASPA) implemented by the UK Home Office.

7.4.4.3 Sample collection, storage and processing

Blood samples (300 µl) were collected in heparinised Eppendorf tubes and centrifuged at 3,000 rpm for 5 min, the plasma layer was removed and stored at -20°C prior to analysis. Plasma samples (100 µl) were transferred to scintillation vials before adding Ultima Gold

scintillation fluid (4 ml) (Meridian Biotechnologies, UK) and scintillation counting using a Packard Tri-carb 3100TR.

Brain, heart, lungs, liver, intestine, kidneys, spleen and testis were collected from each rat, rinsed in PBS (pH 7.4) and dried on tissue before storing at -20 °C prior to analysis. Subsequently, each dissected tissue was weighed individually and approximately 100 mg was placed into a 20 ml scintillation vial. The samples were submerged in 1 ml Soluene - 350 (PerkinElmer, USA) and incubated in a water bath at 50 °C for 18 h. Following this, 200 µl of a 30% hydrogen peroxide solution was added to the dissolved sample and incubated for 60 min at room temperature. Subsequently, 90 µl of glacial acetic acid was added to each sample and incubated for a further 15 min at 50 °C. Ultima Gold scintillation fluid (12 ml) was added to each sample and mixed via inversion. Scintillation counting was carried out using a Packard Tri-carb 3100TR.

Bibliography

(1) Edagwa, B.; Zhou, T.; McMillan, J.; Liu, X. M.; Gendelman, H. Development of HIV Reservoir Targeted Long Acting Nanoformulated Antiretroviral Therapies. *Curr. Med. Chem.* **2014**, *21* (36), 4186–4198.

(2) Rohan, L.; Mallipeddi. Progress in Antiretroviral Drug Delivery Using Nanotechnology. *Int. J. Nanomedicine* **2010**, *5*, 533.

(3) WHO. Global Health Observatory HIV/AIDS http://www.who.int/gho/hiv/en/ (accessed Aug 1, 2016).

(4) Wilen, C. B.; Tilton, J. C.; Doms, R. W. HIV: Cell Binding and Entry. *Cold Spring Harb. Perspect. Med.* **2012**, *2* (8), 1–13.

(5) Sharma, P.; Garg, S. Pure Drug and Polymer Based Nanotechnologies for the Improved Solubility, Stability, Bioavailability and Targeting of Anti-HIV Drugs. *Adv. Drug Deliv. Rev.* **2010**, *62* (4–5), 491–502.

(6) Mallipeddi, R.; Rohan, L. C. Nanoparticle-Based Vaginal Drug Delivery Systems for HIV Prevention. *Expert Opin. Drug Deliv.* **2010**, *7* (1), 37–48.

(7) Davis, F. F. The Origin of Pegnology. *Adv. Drug Del. Rev.* **2002**, *54*, 457–458.

(8) Bangham, A. D.; Standish, M. M.; Watkins, J. C. Diffusion of Univalent Ions across the Lamellae of Swollen Phospholipids. *J. Mol. Biol.* **1965**, *13* (1), 238–252.

(9) Regelson, W.; Parker, G. The Routinization of Intraperitoneal (Intracavitary) Chemotherapy and Immunotherapy. *Cancer Invest.* **1986**, *4*, 29–42.

(10) Barré-Sinoussi, F.; Ross, A. L.; Delfraissy, J. F. Past, Present and Future: 30 Years of HIV Research. *Nat. Rev. Microbiol.* **2013**, *11* (12), 877–883.

(11) Khandazhinskaya, A.; Matyugina, E.; Shirokova, E. Anti-HIV Therapy with AZT Prodrugs: AZT Phosphonate Derivatives, Current State and Prospects. *Expert Opin. Drug Metab. Toxicol.* **2010**, *6* (6), 701–714.

(12) Arts, E. J.; Hazuda, D. J. HIV-1 Antiretroviral Drug Therapy. *Cold Spring Harb. Perspect. Med.* **2012**, *2* (4), 1–23.

(13) Autran, B.; Carcelain, G.; Li, T. S.; Blanc, C.; Mathez, D.; Tubiana, R.; Katlama, C.; Debré, P.; Leibowitch, J. Positive Effects of Combined Antiretroviral Therapy on CD4+ T Cell Homeostasis and Function in Advanced HIV Disease. *Science* **1997**, *277* (5322), 112–116.

(14) Sagar, V.; Pilakka-Kanthikeel, S.; Pottathil, R.; Saxena, S. K.; Nair, M. Towards Nanomedicines for neuroAIDS. *Rev. Med. Virol.* **2014**, *24* (2), 103–124.

(15) Mahajan, S. D.; Aalinkeel, R.; Law, W. C.; Reynolds, J. L.; Nair, B. B.; Sykes, D. E.; Yong, K.; Roy, I.; Prasad, P. N.; Schwartz, S. A. Anti-HIV-1 Nanotherapeutics: Promises and Challenges for the Future. *Int. J. Nanomedicine* **2012**, *7*, 5301–5314.

(16) Margolis, A. M.; Heverling, H.; Pham, P. A.; Stolbach, A. A Review of the Toxicity of HIV Medications. *J. Med. Toxicol.* **2014**, *10* (1), 26–39.

(17) Vyas, T. K.; Shah, L.; Amiji, M. M. Nanoparticulate Drug Carriers for Delivery of HIV/AIDS Therapy to Viral Reservoir Sites. *Expert Opin. Drug Deliv.* **2006**, *3* (5), 613–628.

(18) Woollard, S. M.; Kanmogne, G. D. Maraviroc: A Review of Its Use in HIV Infection and Beyond.

Drug Des. Devel. Ther. **2015**, *9*, 5447–5468.

(19) Flexner, C. HIV Drug Development: The next 25 Years. *Nat. Rev. Drug Discov.* **2007**, *6* (12), 959–966.

(20) Barmania, F.; Pepper, M. S. C-C Chemokine Receptor Type Five (CCR5): An Emerging Target for the Control of HIV Infection. *Appl. Transl. Genomics* **2013**, *2*, 3–16.

(21) Feng, Y.; Broder, C. C.; Kennedy, P. E.; Berger, E. A. HIV-1 Entry Cofactor: Functional cDNA Cloning of a Seven-Transmembrane, G Protein-Coupled Receptor. *Science* **1996**, *272* (5263), 872–877.

(22) Fricker, S. P. Targeting Chemokine Receptors for HIV: Past, Present and Future. *Future Med. Chem.* **2015**, *7* (17), 2311–2315.

(23) Kuritzkes, D.; Kar, S.; Kirkpatrick, P. Maraviroc. *Nat. Rev. Drug Discov.* **2008**, *7* (1), 15–16.

(24) Schall, T. J.; Proudfoot, A. E. I. Overcoming Hurdles in Developing Successful Drugs Targeting Chemokine Receptors. *Nat. Rev. Immunol.* **2011**, *11* (5), 355–363.

(25) De Clercq, E. AMD3100/CXCR4 Inhibitor. *Front. Immunol.* **2015**, *6*, 276.

(26) Patel, B.; Pearson, H.; Zacharoulis, S. Mobilisation of Haematopoietic Stem Cells in Paediatric Patients, prior to Autologous Transplantation Following Administration of Plerixafor and G-CSF. *Pediatr. Blood Cancer* **2015**, *62* (8), 1477–1480.

(27) Tan, Q.; Zhu, Y.; Li, J.; Chen, Z.; Han, G. W.; Kufareva, I.; Li, T.; Ma, L.; Fenalti, G.; Li, J. Structure of the CCR5 Chemokine Receptor-HIV Entry Inhibitor Maraviroc Complex. *Science* **2013**, *341* (6152), 1387–1390.

(28) Lieberman-Blum, S. S.; Fung, H. B.; Bandres, J. C. Maraviroc: A CCR5-Receptor Antagonist for the Treatment of HIV-1 Infection. *Clin. Ther.* **2008**, *30* (7), 1228–1250.

(29) Lederman, M. M.; Penn-Nicholson, A.; Cho, M.; Mosier, D. Biology of CCR5 and Its Role in HIV Infection and Treatment. *JAMA* **2006**, *296* (7), 815.

(30) Huang, Y.; Paxton, W. A.; Wolinsky, S. M.; Neumann, A. U.; Zhang, L.; He, T.; Kang, S.; Ceradini, D.; Jin, Z.; Yazdanbakhsh, K. The Role of a Mutant CCR5 Allele in HIV-1 Transmission and Disease Progression. *Nat. Med.* **1996**, *2* (11), 1240–1243.

(31) de Roda Husman, A. M.; Blaak, H.; Brouwer, M.; Schuitemaker, H. CC Chemokine Receptor 5 Cell-Surface Expression in Relation to CC Chemokine Receptor 5 Genotype and the Clinical Course of HIV-1 Infection. *J. Immunol.* **1999**, *163* (8), 4597–4603.

(32) Lehner, T. The Role of CCR5 Chemokine Ligands and Antibodies to CCR5 Coreceptors in Preventing HIV Infection. *Trends Immunol.* **2002**, *23* (7), 347–351.

(33) Fätkenheuer, G.; Pozniak, A. L.; Johnson, M. A.; Plettenberg, A.; Staszewski, S.; Hoepelman, A. I. M.; Saag, M. S.; Goebel, F. D.; Rockstroh, J. K.; Dezube, B. J. Efficacy of Short-Term Monotherapy with Maraviroc, a New CCR5 Antagonist, in Patients Infected with HIV-1. *Nat. Med.* **2005**, *11* (11), 1170–1172.

(34) Carter, N. J.; Keating, G. M. Maraviroc. *Drugs* **2007**, *67* (15), 2277–2288.

(35) Abel, S.; Back, D. J.; Vourvahis, M. Maraviroc: Pharmacokinetics and Drug Interactions. *Antivir. Ther.* **2009**, *14* (5), 607–618.

(36) Abel, S.; Russell, D.; Taylor-Worth, R. J.; Ridgway, C. E.; Muirhead, G. J. Effects of CYP3A4 Inhibitors on the Pharmacokinetics of Maraviroc in Healthy Volunteers. *Br. J. Clin. Pharmacol.* **2008**, *65* (s1), 27–37.

(37) Lu, Y.; Hendrix, C. W.; Bumpus, N. N. Cytochrome P450 3A5 Plays a Prominent Role in the Oxidative Metabolism of the Anti-Human Immunodeficiency Virus Drug Maraviroc. *Drug Metab. Dispos.* **2012**, *40* (12), 2221–2230.

(38) Kamaly, N.; Xiao, Z.; Valencia, P. M.; Radovic-Moreno, A. F.; Farokhzad, O. C. Targeted Polymeric Therapeutic Nanoparticles: Design, Development and Clinical Translation. *Chem. Soc. Rev.* **2012**, *41* (7), 2971–3010.

(39) Duncan, R. Polymer Conjugates as Anticancer Nanomedicines. *Nat. Rev. Cancer* **2006**, *6* (9), 688–701.

(40) Gros, L.; Ringsdorf, H.; Schupp, H. Polymeric Antitumor Agents on a Molecular and on a Cellular Level? *Angew. Chemie Int. Ed. English* **1981**, *20* (4), 305–325.

(41) Malik, N.; Evagorou, E. G.; Duncan, R. Dendrimer-Platinate: A Novel Approach to Cancer Chemotherapy. *Anticancer Drugs* **1999**, *10*, 767–776.

(42) Rizwanullah, M.; Ahmad, J.; Amin, S. Nanostructured Lipid Carriers: A Novel Platform for Chemotherapeutics. *Curr. Drug Deliv.* **2016**, *13* (1), 4–26.

(43) Veiseh, O.; Tang, B. C.; Whitehead, K. A.; Anderson, D. G.; Langer, R. Managing Diabetes with Nanomedicine: Challenges and Opportunities. *Nat. Rev. Drug Discov.* **2014**, *14* (1), 45–57.

(44) Conti, E.; Gregori, M.; Radice, I.; Da Re, F.; Grana, D.; Re, F.; Salvati, E.; Masserini, M.; Ferrarese, C.; Zoia, C. P. Multifunctional Liposomes Interact with Abeta in Human Biological Fluids: Therapeutic Implications for Alzheimer's Disease. *Neurochem. Int.* **2017**, *108*, 60–65.

(45) Kuo, Y. C.; Wang, C. C. Chapter 19 - Colloidal Drug Delivery System for Brain-Targeting Therapy. In *Colloid and Interface Science in Pharmaceutical Research and Development*; Elsevier, 2014; pp 389–410.

(46) Trivedi, R.; Kompella, U. B. Nanomicellar Formulations for Sustained Drug Delivery: Strategies and Underlying Principles. *Nanomedicine* **2010**, *5* (3), 485–505.

(47) Singh, L. P.; Bhattacharyya, S. K.; Kumar, R.; Mishra, G.; Sharma, U.; Singh, G.; Ahalawat, S. Sol-Gel Processing of Silica Nanoparticles and Their Applications. *Adv. Colloid Interface Sci.* **2014**, *214*, 17–37.

(48) Nishiyama, N.; Takemoto, H. Polymeric Micelles. In *Encyclopedia of Polymeric Nanomaterials*; Springer Berlin Heidelberg: Berlin, Heidelberg, Heidelberg, 2014; pp 1–7.

(49) Ahmad, Z.; Shah, A.; Siddiq, M.; Kraatz, H. B. Polymeric Micelles as Drug Delivery Vehicles. *RSC Adv.* **2014**, *4* (33), 17028–17038.

(50) Gao, H.; Tan, Y.; Guan, Q.; Cai, T.; Liang, G.; Wu, Q. Synthesis, Characterization and Micellization of Amphiphilic Polyethylene-B-Polyphosphoester Block Copolymers. *RSC Adv.* **2015**, *5* (61), 49376–49384.

(51) Wu, Q.; Wang, C.; Zhang, D.; Song, X.; Verpoort, F.; Zhang, G. Synthesis and Micellization of Amphiphilic Biodegradable Methoxypolyethylene Glycol/poly(d,l-Lactide)/polyphosphate Block Copolymer. *React. Funct. Polym.* **2011**, *71* (9), 980–984.

(52) Xu, Y.; Shi, L.; Ma, R.; Zhang, W.; An, Y.; Zhu, X. X. Synthesis and Micellization of Thermo- and pH-Responsive Block Copolymer of poly(N-Isopropylacrylamide)-Block-poly(4-Vinylpyridine). *Polymer* **2007**, *48* (6), 1711–1717.

(53) Diaz, I. L.; Perez, L. D. Synthesis and Micellization Properties of Triblock Copolymers PDMAEMA-B-PCL-B-PDMAEMA and Their Applications in the Fabrication of Amphotericin B-Loaded Nanocontainers. *Colloid Polym. Sci.* **2015**, *293* (3), 913–923.

(54) Yu, L.; Yao, L.; You, J.; Guo, Y.; Yang, L. Poly(methyl Methacrylate)/poly(ethylene Glycol)/poly(ethylene Glycol Dimethacrylate) Micelles: Preparation, Characterization, and Application as Doxorubicin Carriers. *J. Appl. Polym. Sci.* **2014**, *131* (1), 1–8.

(55) Blanco, E.; Kessinger, C. W.; Sumer, B. D.; Gao, J. Multifunctional Micellar Nanomedicine for Cancer Therapy. *Exp. Biol. Med.* **2009**, *234* (2), 123–131.

(56) Larson, N.; Ghandehari, H. Polymeric Conjugates for Drug Delivery. *Chem. Mater.* **2012**, *24* (5), 840–853.

(57) Pang, X.; Du, H. L.; Zhang, H. Q.; Zhai, Y. J.; Zhai, G. X. Polymer–drug Conjugates: Present State of Play and Future Perspectives. *Drug Discov. Today* **2013**, *18* (23–24), 1316–1322.

(58) Jatzkewitz, H. An Ein Kolloidales Blutplasma-Ersatzmittel (Polyvinylpyrrolidon) Gebundenes Peptamin (Glycyl-L-Leucyl-Mezcalin) Als Neuartige Depotform Für Biologisch Aktive Primäre Amine (Mezcalin). *Zeitschrift für Naturforsch. B* **1955**, *10* (1), 27–31.

(59) Alconcel, S. N. S.; Baas, A. S.; Maynard, H. D. FDA-Approved Poly(ethylene Glycol)-Protein Conjugate Drugs. *Polym. Chem.* **2011**, *2* (7), 1442–1448.

(60) Kojima, C. Preclinical Studies of Dendrimer Prodrugs. *Expert Opin. Drug Metab. Toxicol.* **2015**, *11* (8), 1303–1315.

(61) Duro-Castano, A.; Movellan, J.; Vicent, M. J. Smart Branched Polymer Drug Conjugates as Nano-Sized Drug Delivery Systems. *Biomater. Sci.* **2015**, *3* (10), 1321–1334.

(62) Li, C.; Wallace, S. Polymer-Drug Conjugates: Recent Development in Clinical Oncology. *Adv. Drug Deliv. Rev.* **2008**, *60* (8), 886–898.

(63) Vasey, P. A.; Kaye, S. B.; Morrison, R.; Twelves, C.; Wilson, P.; Duncan, R.; Thomson, A. H.; Murray, L. S.; Hilditch, T. E.; Murray, T. Phase I Clinical and Pharmacokinetic Study of PK1 [N-(2-Hydroxypropyl)methacrylamide Copolymer Doxorubicin]: First Member of a New Class of Chemotherapeutic Agents—Drug-Polymer Conjugates. *Clin. Cancer Res.* **1999**, *5* (1), 83–94.

(64) Tomalia, D. A.; Christensen, J. B.; Boas, U. *Dendrimers, Dendrons, and Dendritic Polymers*; Dendrimers, Dendrons, and Dendritic Polymers: Discovery, Applications, and the Future; Cambridge University Press: Cambridge, 2012.

(65) Tomalia, D. A.; Baker, H.; Dewald, J.; Hall, M.; Kallos, G.; Martin, S.; Roeck, J.; Ryder, J.; Smith, P. A New Class of Polymers: Starburst-Dendritic Macromolecules. *Polym. J.* **1985**, *17* (1), 117–132.

(66) Buhleier, E.; Wehner, W.; Vögtle, F. "Cascade"- and "Nonskid-Chain-like" Syntheses of Molecular Cavity Topologies. *Synthesis* **1978**, *1978* (2), 155–158.

(67) Medina, S. H.; El-Sayed, M. E. H. Dendrimers as Carriers for Delivery of Chemotherapeutic Agents. *Chem. Rev.* **2009**, *109* (7), 3141–3157.

(68) Abbasi, E.; Aval, S. F.; Akbarzadeh, A.; Milani, M.; Nasrabadi, H. T.; Joo, S. W.; Hanifehpour, Y.; Nejati-Koshki, K.; Pashaei-Asl, R. Dendrimers: Synthesis, Applications, and Properties. *Nanoscale Res. Lett.* **2014**, *9* (1), 247.

(69) Wu, J.; Huang, W.; He, Z. Dendrimers as Carriers for siRNA Delivery and Gene Silencing: A Review. *Sci. World J.* **2013**, *2013*, 630654.

(70) Bertero, A.; Boni, A.; Gemmi, M.; Gagliardi, M.; Bifone, A.; Bardi, G. Surface Functionalisation Regulates Polyamidoamine Dendrimer Toxicity on Blood–brain Barrier Cells and the Modulation of Key Inflammatory Receptors on Microglia. *Nanotoxicology* **2014**, *8* (2), 158–168.

(71) Jain, K.; Kesharwani, P.; Gupta, U.; Jain, N. K. Dendrimer Toxicity: Let's Meet the Challenge. *Int. J. Pharm.* **2010**, *394* (1–2), 122–142.

(72) Svenningsen, S. W.; Janaszewska, A.; Ficker, M.; Petersen, J. F.; Klajnert-Maculewicz, B.; Christensen, J. B. Two for the Price of One: PAMAM-Dendrimers with Mixed Phosphoryl Choline and Oligomeric Poly(Caprolactone) Surfaces. *Bioconjug. Chem.* **2016**, *27* (6), 1547–1557.

(73) Rupp, R.; Rosenthal, S. L.; Stanberry, L. R. VivaGel(™) (SPL7013 Gel): A Candidate Dendrimer – Microbicide for the Prevention of HIV and HSV Infection. *Int. J. Nanomedicine* **2007**, *2* (4), 561–566.

(74) Rao, J. P.; Geckeler, K. E. Polymer Nanoparticles: Preparation Techniques and Size-Control Parameters. *Prog. Polym. Sci.* **2011**, *36* (7), 887–913.

(75) Kumari, A.; Yadav, S. K.; Yadav, S. C. Biodegradable Polymeric Nanoparticles Based Drug Delivery Systems. *Colloids Surfaces B Biointerfaces* **2010**, *75* (1), 1–18.

(76) Kamaly, N.; Yameen, B.; Wu, J.; Farokhzad, O. C. Degradable Controlled-Release Polymers and Polymeric Nanoparticles: Mechanisms of Controlling Drug Release. *Chem. Rev.* **2016**, *116* (4), 2602–2663.

(77) Guterres, S. S.; Alves, M. P.; Pohlmann, A. R. Polymeric Nanoparticles, Nanospheres and Nanocapsules, for Cutaneous Applications. *Drug Target Insights* **2007**, *2*, 147–157.

(78) Li, J.; Wang, X.; Zhang, T.; Wang, C.; Huang, Z.; Luo, X.; Deng, Y. A Review on Phospholipids and Their Main Applications in Drug Delivery Systems. *Asian J. Pharm. Sci.* **2015**, *10* (2), 81–98.

(79) Langer, R.; Folkman, J. Polymers for the Sustained Release of Proteins and Other Macromolecules. *Nature* **1976**, *263* (5580), 797–800.

(80) Kim, H.; Kim, Y.; Lee, J. Liposomal Formulations for Enhanced Lymphatic Delivery. *Asian J. Pharm. Sci.* **2013**, *8* (2), 100–109.

(81) Mei, L.; Zhang, Z.; Zhao, L.; Huang, L.; Yang, X. L.; Tang, J.; Feng, S. S. Pharmaceutical Nanotechnology for Oral Delivery of Anticancer Drugs. *Adv. Drug Deliv. Rev.* **2013**, *65* (6), 880–890.

(82) Zylberberg, C.; Matosevic, S. Pharmaceutical Liposomal Drug Delivery: A Review of New Delivery Systems and a Look at the Regulatory Landscape. *Drug Deliv.* **2016**, 1–11.

(83) Sun-Waterhouse, D.; Waterhouse, G. I. N. Recent Advances in the Application of

Nanomaterials and Nanotechnology in Food Research. In *Novel Approaches of Nanotechnology in Food*; Elsevier, 2016; pp 21–66.

(84) Jesorka, A.; Orwar, O. Liposomes: Technologies and Analytical Applications. *Annu. Rev. Anal. Chem.* **2008**, *1* (1), 801–832.

(85) Akbarzadeh, A.; Rezaei-Sadabady, R.; Davaran, S.; Joo, S. W.; Zarghami, N.; Hanifehpour, Y.; Samiei, M.; Kouhi, M.; Nejati-Koshki, K. Liposome: Classification, Preparation, and Applications. *Nanoscale Res. Lett.* **2013**, *8* (1), 102.

(86) Hyodo, K.; Yamamoto, E.; Suzuki, T.; Kikuchi, H.; Asano, M.; Ishihara, H. Development of Liposomal Anticancer Drugs. *Biol. Pharm. Bull.* **2013**, *36* (5), 703–707.

(87) Ling, L.; Du, Y.; Ismail, M.; He, R.; Hou, Y.; Fu, Z.; Zhang, Y.; Yao, C.; Li, X. Self-Assembled Liposomes of Dual Paclitaxel-Phospholipid Prodrug for Anticancer Therapy. *Int. J. Pharm.* **2017**, *526* (1–2), 11–22.

(88) Alaarg, A.; Jordan, N. Y.; Verhoef, J. J. F.; Metselaar, J. M.; Storm, G.; Kok, R. J. Docosahexaenoic Acid Liposomes for Targeting Chronic Inflammatory Diseases and Cancer: An in Vitro Assessment. *Int. J. Nanomedicine* **2016**, *11*, 5027–5040.

(89) de Sá, F. A. P.; Taveira, S. F.; Gelfuso, G. M.; Lima, E. M.; Gratieri, T. Liposomal Voriconazole (VOR) Formulation for Improved Ocular Delivery. *Colloids Surfaces B Biointerfaces* **2015**, *133*, 331–338.

(90) Xiang, Y.; Wu, Q.; Liang, L.; Wang, X.; Wang, J.; Zhang, X.; Pu, X.; Zhang, Q. Chlorotoxin-Modified Stealth Liposomes Encapsulating Levodopa for the Targeting Delivery against the Parkinson's Disease in the MPTP-Induced Mice Model. *J. Drug Target.* **2012**, *20* (1), 67–75.

(91) Nayak, D.; Boxi, A.; Ashe, S.; Thathapudi, N. C.; Nayak, B. Stavudine Loaded Gelatin Liposomes for HIV Therapy: Preparation, Characterization and in Vitro Cytotoxic Evaluation. *Mater. Sci. Eng. C* **2017**, *73*, 406–416.

(92) Sharma, A.; Sharma, U. S. Liposomes in Drug Delivery: Progress and Limitations. *Int. J. Pharm.* **1997**, *154* (2), 123–140.

(93) Naseri, N.; Valizadeh, H.; Zakeri-Milani, P. Solid Lipid Nanoparticles and Nanostructured Lipid Carriers: Structure, Preparation and Application. *Adv. Pharm. Bull.* **2015**, *5* (3), 305–313.

(94) Aburahma, M. H.; Badr-Eldin, S. M. Compritol 888 ATO: A Multifunctional Lipid Excipient in Drug Delivery Systems and Nanopharmaceuticals. *Expert Opin. Drug Deliv.* **2014**, *11* (12), 1865–1883.

(95) Das, S.; Chaudhury, A. Recent Advances in Lipid Nanoparticle Formulations with Solid Matrix for Oral Drug Delivery. *AAPS PharmSciTech* **2011**, *12* (1), 62–76.

(96) Kalepu, S.; Manthina, M.; Padavala, V. Oral Lipid-Based Drug Delivery Systems – an Overview. *Acta Pharm. Sin. B* **2013**, *3* (6), 361–372.

(97) Svilenov, H.; Tzachev, C. Solid Lipid Nanoparticles—a Promising Drug Delivery System. *Nanomedicine* **2014**, 187–237.

(98) Tamilvanan, S. Oil-in-Water Lipid Emulsions: Implications for Parenteral and Ocular Delivering Systems. *Prog. Lipid Res.* **2004**, *43* (6), 489–533.

(99) Jaiswal, M.; Dudhe, R.; Sharma, P. K. Nanoemulsion: An Advanced Mode of Drug Delivery

System. *3 Biotech* **2015**, *5* (2), 123–127.

(100) Solans, C.; Izquierdo, P.; Nolla, J.; Azemar, N.; Garcia-Celma, M. J. Nano-Emulsions. *Curr. Opin. Colloid Interface Sci.* **2005**, *10* (3–4), 102–110.

(101) Mukherjee, S.; Ray, S.; Thakur, R. S. Solid Lipid Nanoparticles: A Modern Formulation Approach in Drug Delivery System. *Indian J. Pharm. Sci.* **2009**, *71* (4), 349–358.

(102) Üner, M.; Yener, G. Importance of Solid Lipid Nanoparticles (SLN) in Various Administration Routes and Future Perspectives. *Int. J. Nanomedicine* **2007**, *2* (3), 289–300.

(103) Mehnert, W.; Mader, K. Solid Lipid Nanoparticles Production, Characterization and Applications. *Adv. Drug Deliv. Rev.* **2001**, *47* (2–3), 165–196.

(104) Aji Alex, M. R.; Chacko, A. J.; Jose, S.; Souto, E. B. Lopinavir Loaded Solid Lipid Nanoparticles (SLN) for Intestinal Lymphatic Targeting. *Eur. J. Pharm. Sci.* **2011**, *42* (1–2), 11–18.

(105) Alex, A.; Paul, W.; Chacko, A. J.; Sharma, C. P. Enhanced Delivery of Lopinavir to the CNS Using Compritol®-Based Solid Lipid Nanoparticles. *Ther. Deliv.* **2011**, *2* (1), 25–35.

(106) Jenning, V.; Lippacher, A.; Gohla, S. H. Medium Scale Production of Solid Lipid Nanoparticles (SLN) by High Pressure Homogenization. *J. Microencapsul.* **2002**, *19* (1), 1–10.

(107) Dingler, A.; Gohla, S. Production of Solid Lipid Nanoparticles (SLN): Scaling up Feasibilities. *J. Microencapsul.* **2002**, *19* (1), 11–16.

(108) Silva, A. C.; González-Mira, E.; García, M. L.; Egea, M. A.; Fonseca, J.; Silva, R.; Santos, D.; Souto, E. B.; Ferreira, D. Preparation, Characterization and Biocompatibility Studies on Risperidone-Loaded Solid Lipid Nanoparticles (SLN): High Pressure Homogenization versus Ultrasound. *Colloids Surfaces B Biointerfaces* **2011**, *86* (1), 158–165.

(109) Siddiqui, A.; Alayoubi, A.; El-Malah, Y.; Nazzal, S. Modeling the Effect of Sonication Parameters on Size and Dispersion Temperature of Solid Lipid Nanoparticles (SLNs) by Response Surface Methodology (RSM). *Pharm. Dev. Technol.* **2014**, *19* (3), 342–346.

(110) Thatipamula, R. P.; Palem, C. R.; Gannu, R.; Mudragada, S.; Yamsani, M. R. Formulation and in Vitro Characterization of Domperidone Loaded Solid Lipid Nanoparticles and Nanostructured Lipid Carriers. *Daru* **2011**, *19* (1), 23–32.

(111) Khameneh, B.; Halimi, V.; Jaafari, M. R.; Golmohammadzadeh, S. Safranal-Loaded Solid Lipid Nanoparticles: Evaluation of Sunscreen and Moisturizing Potential for Topical Applications. *Iran. J. Basic Med. Sci.* **2015**, *18* (1), 58–63.

(112) Mojahedian, M. M.; Daneshamouz, S.; Samani, S. M.; Zargaran, A. A Novel Method to Produce Solid Lipid Nanoparticles Using N-Butanol as an Additional Co-Surfactant according to the O/w Microemulsion Quenching Technique. *Chem. Phys. Lipids* **2013**, *174*, 32–38.

(113) Kotmakçı, M.; Akbaba, H.; Erel, G.; Ertan, G.; Kantarcı, G. Improved Method for Solid Lipid Nanoparticle Preparation Based on Hot Microemulsions: Preparation, Characterization, Cytotoxicity, and Hemocompatibility Evaluation. *AAPS PharmSciTech* **2017**, *18* (4), 1355–1365.

(114) Charcosset, C.; El-Harati, A.; Fessi, H. Preparation of Solid Lipid Nanoparticles Using a Membrane Contactor. *J. Control. Release* **2005**, *108* (1), 112–120.

(115) Friberg, S. E.; Corkery, R. W.; Blute, I. A. Phase Inversion Temperature (PIT) Emulsification

Process. *J. Chem. Eng. Data* **2011**, *56* (12), 4282–4290.

(116) Gao, S.; McClements, D. J. Formation and Stability of Solid Lipid Nanoparticles Fabricated Using Phase Inversion Temperature Method. *Colloids Surfaces A Physicochem. Eng. Asp.* **2016**, *499*, 79–87.

(117) Battaglia, L.; Gallarate, M.; Cavalli, R.; Trotta, M. Solid Lipid Nanoparticles Produced through a Coacervation Method. *J. Microencapsul.* **2010**, *27* (1), 78–85.

(118) Battaglia, L.; D'Addino, I.; Peira, E.; Trotta, M.; Gallarate, M. Solid Lipid Nanoparticles Prepared by Coacervation Method as Vehicles for Ocular Cyclosporine. *J. Drug Deliv. Sci. Technol.* **2012**, *22* (2), 125–130.

(119) Lee, Y. S.; Johnson, P. J.; Robbins, P. T.; Bridson, R. H. Production of Nanoparticles-in-Microparticles by a Double Emulsion Method: A Comprehensive Study. *Eur. J. Pharm. Biopharm.* **2013**, *83* (2), 168–173.

(120) Shi, L.; Li, Z.; Yu, L.; Jia, H.; Zheng, L. Effects of Surfactants and Lipids on the Preparation of Solid Lipid Nanoparticles Using Double Emulsion Method. *J. Dispers. Sci. Technol.* **2011**, *32* (2), 254–259.

(121) Becker Peres, L. L.; Becker Peres, L. L.; de Araújo, P. H. H.; Sayer, C. Solid Lipid Nanoparticles for Encapsulation of Hydrophilic Drugs by an Organic Solvent Free Double Emulsion Technique. *Colloids Surfaces B Biointerfaces* **2016**, *140*, 317–323.

(122) Pooja, D.; Tunki, L.; Kulhari, H.; Reddy, B. B.; Sistla, R. Optimization of Solid Lipid Nanoparticles Prepared by a Single Emulsification-Solvent Evaporation Method. *Data Br.* **2016**, *6*, 15–19.

(123) Emami, J.; Mohiti, H.; Hamishehkar, H.; Varshosaz, J. Formulation and Optimization of Solid Lipid Nanoparticle Formulation for Pulmonary Delivery of Budesonide Using Taguchi and Box-Behnken Design. *Res. Pharm. Sci.* **2015**, *10* (1), 17–33.

(124) Schubert, M. A.; Müller-Goymann, C. C. Solvent Injection as a New Approach for Manufacturing Lipid Nanoparticles – Evaluation of the Method and Process Parameters. *Eur. J. Pharm. Biopharm.* **2003**, *55* (1), 125–131.

(125) Madan, J. R.; Khude, P. A.; Dua, K. Development and Evaluation of Solid Lipid Nanoparticles of Mometasone Furoate for Topical Delivery. *Int. J. Pharm. Investig.* **2014**, *4* (2), 60–64.

(126) Battaglia, L.; Gallarate, M. Lipid Nanoparticles: State of the Art, New Preparation Methods and Challenges in Drug Delivery. *Expert Opin. Drug Deliv.* **2012**, *9* (5), 497–508.

(127) Jose, S.; Anju, S. S.; Cinu, T. A.; Aleykutty, N. A.; Thomas, S.; Souto, E. B. In Vivo Pharmacokinetics and Biodistribution of Resveratrol-Loaded Solid Lipid Nanoparticles for Brain Delivery. *Int. J. Pharm.* **2014**, *474* (1–2), 6–13.

(128) Olbrich, C.; Gessner, A.; Kayser, O.; Müller, R. H. Lipid-Drug-Conjugate (LDC) Nanoparticles as Novel Carrier System for the Hydrophilic Antitrypanosomal Drug Diminazenediaceturate. *J. Drug Target.* **2002**, *10* (5), 387–396.

(129) Üner, M. Preparation, Characterization and Physico-Chemical Properties of Solid Lipid Nanoparticles (SLN) and Nanostructured Lipid Carriers (NLC): Their Benefits as Colloidal Drug Carrier Systems. *Die Pharm. Int. J. Pharm. Sci.* **2006**, *61* (5), 375–386.

(130) Müller, R. H.; Mäder, K.; Gohla, S. Solid Lipid Nanoparticles (SLN) for Controlled Drug Delivery – a Review of the State of the Art. *Eur. J. Pharm. Biopharm.* **2000**, *50* (1), 161–177.

(131) Olbrich, C.; Schöler, N.; Tabatt, K.; Kayser, O.; Müller, R. H. Cytotoxicity Studies of Dynasan 114 Solid Lipid Nanoparticles (SLN) on RAW 264.7 Macrophages—impact of Phagocytosis on Viability and Cytokine Production. *J. Pharm. Pharmacol.* **2004**, *56* (7), 883–891.

(132) Olbrich, C.; Kayser, O.; Müller, R. H. Lipase Degradation of Dynasan 114 and 116 Solid Lipid Nanoparticles (SLN)—effect of Surfactants, Storage Time and Crystallinity. *Int. J. Pharm.* **2002**, *237* (1), 119–128.

(133) Severino, P.; Pinho, S. C.; Souto, E. B.; Santana, M. H. A. Crystallinity of Dynasan®114 and Dynasan®118 Matrices for the Production of Stable Miglyol®-Loaded Nanoparticles. *J. Therm. Anal. Calorim.* **2012**, *108* (1), 101–108.

(134) Ibrahim, W. M.; Al Omrani, A. H.; B Yassin, A. E. Novel Sulpiride-Loaded Solid Lipid Nanoparticles with Enhanced Intestinal Permeability. *Int. J. Nanomedicine* **2014**, *9*, 129–144.

(135) Vivek, K.; Reddy, H.; Murthy, R. S. R. Investigations of the Effect of the Lipid Matrix on Drug Entrapment, in Vitro Release, and Physical Stability of Olanzapine-Loaded Solid Lipid Nanoparticles. *AAPS PharmSciTech* **2007**, *8* (4), 16–24.

(136) Rawat, M. K.; Jain, A.; Singh, S. In Vivo and Cytotoxicity Evaluation of Repaglinide-Loaded Binary Solid Lipid Nanoparticles After Oral Administration to Rats. *J. Pharm. Sci.* **2017**, *100* (6), 2406–2417.

(137) Kushwaha, A. K.; Vuddanda, P. R.; Karunanidhi, P.; Singh, S. K.; Singh, S. K. Development and Evaluation of Solid Lipid Nanoparticles of Raloxifene Hydrochloride for Enhanced Bioavailability. *Biomed Res. Int.* **2013**, *2013*, 584549.

(138) Sandri, G.; Bonferoni, M. C.; Gökçe, E. H.; Ferrari, F.; Rossi, S.; Patrini, M.; Caramella, C. Chitosan-Associated SLN: In Vitro and Ex Vivo Characterization of Cyclosporine A Loaded Ophthalmic Systems. *J. Microencapsul.* **2010**, *27* (8), 735–746.

(139) Zhang, J.; Smith, E. Percutaneous Permeation of Betamethasone 17-Valerate Incorporated in Lipid Nanoparticles. *J. Pharm. Sci.* **2017**, *100* (3), 896–903.

(140) Montenegro, L.; Campisi, A.; Sarpietro, M. G.; Carbone, C.; Acquaviva, R.; Raciti, G.; Puglisi, G. In Vitro Evaluation of Idebenone-Loaded Solid Lipid Nanoparticles for Drug Delivery to the Brain. *Drug Dev. Ind. Pharm.* **2011**, *37* (6), 737–746.

(141) Yuan, H.; Chen, J.; Du, Y. Z.; Hu, F. Q.; Zeng, S.; Zhao, H. L. Studies on Oral Absorption of Stearic Acid SLN by a Novel Fluorometric Method. *Colloids Surfaces B Biointerfaces* **2007**, *58* (2), 157–164.

(142) Kalam, M. A.; Sultana, Y.; Ali, A.; Aqil, M.; Mishra, A. K.; Chuttani, K. Preparation, Characterization, and Evaluation of Gatifloxacin Loaded Solid Lipid Nanoparticles as Colloidal Ocular Drug Delivery System. *J. Drug Target.* **2010**, *18* (3), 191–204.

(143) Arana, L.; Salado, C.; Vega, S.; Aizpurua-Olaizola, O.; Arada, I. de la; Suarez, T.; Usobiaga, A.; Arrondo, J. L. R.; Alonso, A.; Goñi, F. M. Solid Lipid Nanoparticles for Delivery of Calendula Officinalis Extract. *Colloids Surfaces B Biointerfaces* **2015**, *135*, 18–26.

(144) Xie, S.; Zhu, L.; Dong, Z.; Wang, Y.; Wang, X.; Zhou, W. Preparation and Evaluation of Ofloxacin-Loaded Palmitic Acid Solid Lipid Nanoparticles. *Int. J. Nanomedicine* **2011**, *6*, 547–

555.

(145) Schöler, N.; Hahn, H.; Müller, R. H.; Liesenfeld, O. Effect of Lipid Matrix and Size of Solid Lipid Nanoparticles (SLN) on the Viability and Cytokine Production of Macrophages. *Int. J. Pharm.* **2002**, *231* (2), 167–176.

(146) Beloqui, A.; Solinís, M. Á.; Rodríguez-Gascón, A.; Almeida, A. J.; Préat, V. Nanostructured Lipid Carriers: Promising Drug Delivery Systems for Future Clinics. *Nanomedicine Nanotechnology, Biol. Med.* **2016**, *12* (1), 143–161.

(147) Bose, S.; Du, Y.; Takhistov, P.; Michniak-Kohn, B. Formulation Optimization and Topical Delivery of Quercetin from Solid Lipid Based Nanosystems. *Int. J. Pharm.* **2013**, *441* (1–2), 56–66.

(148) Becker, K.; Salar-Behzadi, S.; Zimmer, A. Solvent-Free Melting Techniques for the Preparation of Lipid-Based Solid Oral Formulations. *Pharm. Res.* **2015**, *32* (5), 1519–1545.

(149) Azhar Shekoufeh Bahari, L.; Hamishehkar, H. The Impact of Variables on Particle Size of Solid Lipid Nanoparticles and Nanostructured Lipid Carriers; A Comparative Literature Review. *Adv. Pharm. Bull.* **2016**, *6* (2), 143–151.

(150) Gokce, E. H.; Korkmaz, E.; Dellera, E.; Sandri, G.; Bonferoni, M. C.; Ozer, O. Resveratrol-Loaded Solid Lipid Nanoparticles versus Nanostructured Lipid Carriers: Evaluation of Antioxidant Potential for Dermal Applications. *Int. J. Nanomedicine* **2012**, *7*, 1841–1850.

(151) Huang, Z.; Hua, S.; Yang, Y.; Fang, J. Development and Evaluation of Lipid Nanoparticles for Camptothecin Delivery: A Comparison of Solid Lipid Nanoparticles, Nanostructured Lipid Carriers, and Lipid Emulsion. *Acta Pharmacol Sin* **2008**, *29* (9), 1094–1102.

(152) Dragicevic, N.; Maibach, H. I. *Percutaneous Penetration Enhancers Chemical Methods in Penetration Enhancement: Nanocarriers*; Springer Berlin Heidelberg, 2016.

(153) Freitas, C.; Müller, R. H. Correlation between Long-Term Stability of Solid Lipid Nanoparticles (SLN^{TM}) and Crystallinity of the Lipid Phase. *Eur. J. Pharm. Biopharm.* **1999**, *47* (2), 125–132.

(154) Ma, H.; Luo, M.; Sanyal, S.; Rege, K.; Dai, L. L. The One-Step Pickering Emulsion Polymerization Route for Synthesizing Organic-Inorganic Nanocomposite Particles. *Mater.* **2010**, *3* (2), 1186–1202.

(155) Pickering, S. U. CXCVI.-Emulsions. *J. Chem. Soc. Trans.* **1907**, *91* (0), 2001–2021.

(156) Vignati, E.; Piazza, R.; Lockhart, T. P. Pickering Emulsions: Interfacial Tension, Colloidal Layer Morphology, and Trapped-Particle Motion. *Langmuir* **2003**, *19* (17), 6650–6656.

(157) Yang, Y.; Fang, Z.; Chen, X.; Zhang, W.; Xie, Y.; Chen, Y.; Liu, Z.; Yuan, W. An Overview of Pickering Emulsions: Solid-Particle Materials, Classification, Morphology, and Applications. *Front. Pharmacol.* **2017**, *8*, 287.

(158) Smeets, N. M. B. Amphiphilic Hyperbranched Polymers from the Copolymerization of a Vinyl and Divinyl Monomer: The Potential of Catalytic Chain Transfer Polymerization. *Eur. Polym. J.* **2013**, *49* (9), 2528–2544.

(159) Smeets, N. M. B.; Freeman, M. W.; McKenna, T. F. L. Polymer Architecture Control in Emulsion Polymerization via Catalytic Chain Transfer Polymerization. *Macromolecules* **2011**, *44* (17), 6701–6710.

(160) Costello, P. .; Martin, I. .; Slark, A. .; Sherrington, D. .; Titterton, A. Branched Methacrylate Copolymers from Multifunctional Monomers: Chemical Composition and Physical Architecture Distributions. *Polymer* **2002**, *43* (2), 245–254.

(161) O'Brien, N.; McKee, A.; Sherrington, D. C.; Slark, A. T.; Titterton, A. Facile, Versatile and Cost Effective Route to Branched Vinyl Polymers. *Polymer* **2000**, *41* (15), 6027–6031.

(162) Cormack, P. a G.; Sherrington, D. C. Synthesis of Branched Poly (Methyl Methacrylate) S : Effect of the Branching Comonomer Structure Franc. *Macromoleculars* **2004**, No. Dcm, 2096–2105.

(163) Matyjaszewski, K.; Spanswick, J. Controlled/living Radical Polymerization. *Mater. Today* **2005**, *8* (3), 26–33.

(164) Zhang, H. Controlled/"living" Radical Precipitation Polymerization: A Versatile Polymerization Technique for Advanced Functional Polymers. *Eur. Polym. J.* **2013**, *49* (3), 579–600.

(165) Chisholm, M. S.; Martin, I. K.; Slark, A. T. Facile and Cost-Effective Branched Acrylic Copolymers from Multifunctional Comonomers and Multifunctional Chain Transfer Agents. *Polym. Chem.* **2015**, *6* (41), 7333–7341.

(166) Shipp, D. A. Reversible-Deactivation Radical Polymerizations. *Polym. Rev.* **2011**, *51* (2), 99–103.

(167) Moad, G.; Rizzardo, E. Chapter 1 The History of Nitroxide-Mediated Polymerization. In *Nitroxide Mediated Polymerization: From Fundamentals to Applications in Materials Science*; The Royal Society of Chemistry, 2016; pp 1–44.

(168) Grubbs, R. B. Nitroxide-Mediated Radical Polymerization: Limitations and Versatility. *Polym. Rev.* **2011**, *51* (2), 104–137.

(169) Greene, A. C.; Grubbs, R. B. Nitroxide-Mediated Polymerization of Methyl Methacrylate and Styrene with New Alkoxyamines from 4-Nitrophenyl 2-Methylpropionat-2-Yl Radicals. *Macromolecules* **2010**, *43* (24), 10320–10325.

(170) Moad, G.; Chong, Y. K. K.; Postma, A.; Rizzardo, E.; Thang, S. H. Advances in RAFT Polymerization: The Synthesis of Polymers with Defined End-Groups. *Polymer* **2005**, *46* (19), 8458–8468.

(171) Moad, G.; Rizzardo, E.; Thang, S. H. Radical Addition–fragmentation Chemistry in Polymer Synthesis. *Polymer* **2008**, *49* (5), 1079–1131.

(172) Vana, P. Kinetic Aspects of RAFT Polymerization. *Macromol. Symp.* **2007**, *248* (1), 71–81.

(173) Poli, R.; Shaver, M. P. Atom Transfer Radical Polymerization (ATRP) and Organometallic Mediated Radical Polymerization (OMRP) of Styrene Mediated by Diaminobis(phenolato)iron(II) Complexes: A DFT Study. *Inorg. Chem.* **2014**, *53* (14), 7580–7590.

(174) Gao, H.; Min, K.; Matyjaszewski, K. Gelation in ATRP Using Structurally Different Branching Reagents: Comparison of Inimer, Divinyl and Trivinyl Cross-Linkers. *Macromolecules* **2009**, *42* (21), 8039–8043.

(175) Wang, J. S.; Matyjaszewski, K. Controlled/"Living" Radical Polymerization. Halogen Atom Transfer Radical Polymerization Promoted by a Cu(I)/Cu(II) Redox Process. *Macromolecules*

1995, *28* (23), 7901–7910.

(176) Kato, M.; Kamigaito, M.; Sawamoto, M.; Higashimura, T. Polymerization of Methyl Methacrylate with the Carbon Tetrachloride/Dichlorotris-(triphenylphosphine)ruthenium(II)/Methylaluminum Bis(2,6-Di-Tert-Butylphenoxide) Initiating System: Possibility of Living Radical Polymerization. *Macromolecules* **1995**, *28* (5), 1721–1723.

(177) Matyjaszewski, K. Atom Transfer Radical Polymerization (ATRP): Current Status and Future Perspectives. *Macromolecules* **2012**, *45* (10), 4015–4039.

(178) Bao, F.; Feng, L.; Gao, J.; Tan, Z.; Xing, B.; Ma, R.; Yan, C. New Cobalt-Mediated Radical Polymerization (CMRP) of Methyl Methacrylate Initiated by Two Single-Component Dinuclear β-Diketone Cobalt (II) Catalysts. *PLoS One* **2010**, *5* (10), e13629.

(179) Wang, J.-S.; Matyjaszewski, K. Controlled/"living" radical Polymerization. Atom Transfer Radical Polymerization in the Presence of Transition-Metal Complexes. *J. Am. Chem. Soc.* **1995**, *117* (20), 5614–5615.

(180) Patten, T. E.; Matyjaszewski, K. Atom Transfer Radical Polymerization and the Synthesis of Polymeric Materials. *Adv. Mater.* **1998**, *10* (12), 901–915.

(181) Guan, Z. Control of Polymer Topology through Transition-Metal Catalysis: Synthesis of Hyperbranched Polymers by Cobalt-Mediated Free Radical Polymerization. *J. Am. Chem. Soc.* **2002**, *124* (20), 5616–5617.

(182) Matyjaszewski, K.; Wei, M.; Xia, J.; McDermott, N. E. Controlled/"Living" Radical Polymerization of Styrene and Methyl Methacrylate Catalyzed by Iron Complexes. *Macromolecules* **1997**, *30* (26), 8161–8164.

(183) Auty, S. E. R.; Andren, O. C. J.; Y. Hern, F.; Malkoch, M.; Rannard, S. P. "One-Pot" Sequential Deprotection/functionalisation of Linear-Dendritic Hybrid Polymers Using a Xanthate Mediated thiol/Michael Addition. *Polym. Chem.* **2015**, *6* (4), 573–582.

(184) Dwyer, A. B.; Chambon, P.; Town, A.; Hatton, F. L.; Ford, J.; Rannard, S. P. Exploring the Homogeneous Controlled Radical Polymerisation of Hydrophobic Monomers in Anti-Solvents for Their Polymers: RAFT and ATRP of Various Alkyl Methacrylates in Anhydrous Methanol to High Conversion and Low Dispersity. *Polym. Chem.* **2015**, *6* (41), 7286–7296.

(185) Ford, J.; Chambon, P.; North, J.; Hatton, F. L.; Giardiello, M.; Owen, A.; Rannard, S. P. Multiple and Co-Nanoprecipitation Studies of Branched Hydrophobic Copolymers and A–B Amphiphilic Block Copolymers, Allowing Rapid Formation of Sterically Stabilized Nanoparticles in Aqueous Media. *Macromolecules* **2015**, *48* (6), 1883–1893.

(186) He, T.; Adams, D. J.; Butler, M. F.; Yeoh, C. T.; Cooper, A. I.; Rannard, S. P. Direct Synthesis of Anisotropic Polymer Nanoparticles. *Angew. Chemie* **2007**, *119* (48), 9403–9407.

(187) He, T.; Adams, D. J.; Butler, M. F.; Cooper, A. I.; Rannard, S. P. Polymer Nanoparticles: Shape-Directed Monomer-to-Particle Synthesis. *J. Am. Chem. Soc.* **2009**, *131* (4), 1495–1501.

(188) Hatton, F. L.; Chambon, P.; Savage, A. C.; Rannard, S. P. Role of Highly Branched, High Molecular Weight Polymer Structures in Directing Uniform Polymer Particle Formation during Nanoprecipitation. *Chem. Commun.* **2016**, *52* (20), 3915–3918.

(189) Hatton, F. L.; Chambon, P.; McDonald, T. O.; Owen, A.; Rannard, S. P. Hyperbranched

Polydendrons: A New Controlled Macromolecular Architecture with Self-Assembly in Water and Organic Solvents. *Chem. Sci.* **2014**, *5* (5), 1844–1853.

(190) Cauldbeck, H.; Le Hellaye, M.; Long, M.; Kennedy, S. M.; Williams, R. L.; Kearns, V. R.; Rannard, S. P. Controlling Drug Release from Non-Aqueous Environments: Moderating Delivery from Ocular Silicone Oil Drug Reservoirs to Combat Proliferative Vitreoretinopathy. *J. Control. Release* **2016**, *244*, 41–51.

(191) Weaver, J. V. M.; Rannard, S. P.; Cooper, A. I. Polymer-Mediated Hierarchical and Reversible Emulsion Droplet Assembly. *Angew. Chemie Int. Ed.* **2009**, *48* (12), 2131–2134.

(192) Rogers, H. E.; Chambon, P.; Auty, S. E. R.; Hern, F. Y.; Owen, A.; Rannard, S. P. Synthesis, Nanoprecipitation and pH Sensitivity of Amphiphilic Linear-Dendritic Hybrid Polymers and Hyperbranched-Polydendrons Containing Tertiary Amine Functional Dendrons. *Soft Matter* **2015**, *11* (35), 7005–7015.

(193) Dwyer, A. B.; Chambon, P.; Town, A.; He, T.; Owen, A.; Rannard, S. P. Is Methanol Really a Bad Solvent for Poly(n-Butyl Methacrylate)? Low Dispersity and High Molecular Weight Polymers of N-Butyl Methacrylate Synthesised via ATRP in Anhydrous Methanol. *Polym. Chem.* **2014**, *5* (11), 3608–3616.

(194) Dale, M. M.; Rang, H. P.; Dale, M. M. *Rang & Dale's Pharmacology*, 6th ed.; Churchill Livingstone: [Edinburgh], 2007.

(195) Liechty, W. B.; Kryscio, D. R.; Slaughter, B. V; Peppas, N. A. Polymers for Drug Delivery Systems. *Annu. Rev. Chem. Biomol. Eng.* **2010**, *1*, 149–173.

(196) Cederbaum, A. I. Molecular Mechanisms of the Microsomal Mixed Function Oxidases and Biological and Pathological Implications. *Redox Biol.* **2015**, *4*, 60–73.

(197) Weitendorf, F.; Reynolds, K. K. The Pharmacist's Perspective on Pharmacogenetics Implementation. *Clin. Lab. Med.* **2016**, *36* (3), 543–556.

(198) Frederiks, C. N.; Lam, S. W.; Guchelaar, H. J.; Boven, E. Genetic Polymorphisms and Paclitaxel- or Docetaxel-Induced Toxicities: A Systematic Review. *Cancer Treat. Rev.* **2015**, *41* (10), 935–950.

(199) Daly, A. K. Polymorphic Variants of Cytochrome P450. In *Cytochrome P450 Function and Pharmacological Roles in Inflammation and Cancer*; Pharmacology, J. P. H. B. T.-A. in, Ed.; Academic Press, 2015; Vol. Volume 74, pp 85–111.

(200) Chakraborty, S.; Shukla, D.; Mishra, B.; Singh, S. Lipid – An Emerging Platform for Oral Delivery of Drugs with Poor Bioavailability. *Eur. J. Pharm. Biopharm.* **2009**, *73* (1), 1–15.

(201) Porter, C. J. H.; Pouton, C. W.; Cuine, J. F.; Charman, W. N. Enhancing Intestinal Drug Solubilisation Using Lipid-Based Delivery Systems. *Adv. Drug Deliv. Rev.* **2008**, *60* (6), 673–691.

(202) Makwana, V.; Jain, R.; Patel, K.; Nivsarkar, M.; Joshi, A. Solid Lipid Nanoparticles (SLN) of Efavirenz as Lymph Targeting Drug Delivery System: Elucidation of Mechanism of Uptake Using Chylomicron Flow Blocking Approach. *Int. J. Pharm.* **2015**, *495* (1), 439–446.

(203) Khan, A. A.; Mudassir, J.; Mohtar, N.; Darwis, Y. Advanced Drug Delivery to the Lymphatic System: Lipid-Based Nanoformulations. *Int. J. Nanomedicine* **2013**, *8*, 2733–2744.

(204) Yu, M.; Yang, Y.; Zhu, C.; Guo, S.; Gan, Y. Advances in the Transepithelial Transport of Nanoparticles. *Drug Discov. Today* **2016**, *21* (7), 1155–1161.

(205) Trevaskis, N. L.; Kaminskas, L. M.; Porter, C. J. H. From Sewer to Saviour — Targeting the Lymphatic System to Promote Drug Exposure and Activity. *Nat. Rev. Drug Discov.* **2015**, *14* (11), 781–803.

(206) Cho, H. J.; Park, J. W.; Yoon, I. S.; Kim, D. D. Surface-Modified Solid Lipid Nanoparticles for Oral Delivery of Docetaxel: Enhanced Intestinal Absorption and Lymphatic Uptake. *Int. J. Nanomedicine* **2014**, *9*, 495–504.

(207) Takatori, T.; Shimono, N.; Higaki, K.; Kimura, T. Evaluation of Sustained Release Suppositories Prepared with Fatty Base Including Solid Fats with High Melting Points. *Int. J. Pharm.* **2004**, *278* (2), 275–282.

(208) Priyanka, K.; Sathali, A. A. H. Preparation and Evaluation of Montelukast Sodium Loaded Solid Lipid Nanoparticles. *J. Young Pharm.* **2012**, *4* (3), 129–137.

(209) Kumar, S.; Randhawa, J. K. High Melting Lipid Based Approach for Drug Delivery: Solid Lipid Nanoparticles. *Mater. Sci. Eng. C* **2013**, *33* (4), 1842–1852.

(210) Liptrott, N. J.; Giardiello, M.; McDonald, T. O.; Rannard, S. P.; Owen, A. Lack of Interaction of Lopinavir Solid Drug Nanoparticles with Cells of the Immune System. *Nanomedicine* **2017**, *12* (17), 2043–2054.

(211) Siccardi, M.; Martin, P.; Smith, D.; Curley, P.; McDonald, T.; Giardiello, M.; Liptrott, N.; Rannard, S.; Owen, A. Towards a Rational Design of Solid Drug Nanoparticles with Optimised Pharmacological Properties. *J. Interdiscip. Nanomedicine* **2016**, *1* (3), 110–123.

(212) Jiang, Y.; Cao, S.; Bright, D. K.; Bever, A. M.; Blakney, A. K.; Suydam, I. T.; Woodrow, K. A. Nanoparticle-Based ARV Drug Combinations for Synergistic Inhibition of Cell-Free and Cell–Cell HIV Transmission. *Mol. Pharm.* **2015**, *12* (12), 4363–4374.

(213) Ramanathan, R.; Jiang, Y.; Read, B.; Golan Paz, S.; Woodrow, K. A. A. Biophysical Characterization of Small Molecule Antiviral-Loaded Nanolipogels for HIV-1 Chemoprophylaxis and Topical Mucosal Application. *Acta Biomater.* **2016**, *36*, 122–131.

(214) Gaur, P. K.; Mishra, S.; Bajpai, M.; Mishra, A. Enhanced Oral Bioavailability of Efavirenz by Solid Lipid Nanoparticles: In Vitro Drug Release and Pharmacokinetics Studies. *Biomed Res. Int.* **2014**, *2014*, 1–9.

(215) Desai, J.; Thakkar, H. Effect of Particle Size on Oral Bioavailability of Darunavir-Loaded Solid Lipid Nanoparticles. *J. Microencapsul.* **2016**, *33* (7), 669–678.

(216) Bhalekar, M. R.; Upadhaya, P. G.; Madgulkar, A. R.; Kshirsagar, S. J.; Dube, A.; Bartakke, U. S. In-Vivo Bioavailability and Lymphatic Uptake Evaluation of Lipid Nanoparticulates of Darunavir. *Drug Deliv.* **2016**, *23* (7), 2581–2586.

(217) Alukda, D.; Sturgis, T.; Youan, B. C. Formulation of Tenofovir Loaded Functionalized Solid Lipid Nanoparticles Intended for HIV Prevention. *J. Pharm. Sci.* **2016**, *100* (8), 3345–3356.

(218) Neves, A. R.; Queiroz, J. F.; Reis, S. Brain-Targeted Delivery of Resveratrol Using Solid Lipid Nanoparticles Functionalized with Apolipoprotein E. *J. Nanobiotechnology* **2016**, *14* (1), 27.

(219) Miller, R.; Aksenenko, E. V; Fainerman, V. B. Dynamic Interfacial Tension of Surfactant

Solutions. *Adv. Colloid Interface Sci.* **2016**.

(220) Goibier, L.; Lecomte, S.; Leal-Calderon, F.; Faure, C. The Effect of Surfactant Crystallization on Partial Coalescence in O/W Emulsions. *J. Colloid Interface Sci.* **2017**, *500*, 304–314.

(221) Tadros, T. Colloid and Interface Aspects of Pharmaceutical Science. In *Colloid and Interface Science in Pharmaceutical Research and Development*; Elsevier, 2014; pp 29–54.

(222) Quintanilla-Carvajal, M. X.; Matiacevich, S. Role of Surfactants and Their Applications in Structured Nanosized Systems BT - Food Nanoscience and Nanotechnology. In *Food Nanoscience and Nanotechnology*; Hernández-Sánchez, H., Gutiérrez-López, G. F., Eds.; Springer International Publishing: Cham, 2015; pp 177–186.

(223) Tadros, T. F. Introduction. In *Applied Surfactants*; Wiley-VCH Verlag GmbH & Co. KGaA: Weinheim, FRG, 2005; pp 1–17.

(224) Ikeuchi-Takahashi, Y.; Ishihara, C.; Onishi, H. Formulation and Evaluation of Morin-Loaded Solid Lipid Nanoparticles. *Biol. Pharm. Bull.* **2016**, *39* (9), 1514–1522.

(225) Geszke-Moritz, M.; Moritz, M. Solid Lipid Nanoparticles as Attractive Drug Vehicles: Composition, Properties and Therapeutic Strategies. *Mater. Sci. Eng. C* **2016**, *68*, 982–994.

(226) Hao, J.; Wang, X.; Bi, Y.; Teng, Y.; Wang, J.; Li, F.; Li, Q.; Zhang, J.; Guo, F.; Liu, J. Fabrication of a Composite System Combining Solid Lipid Nanoparticles and Thermosensitive Hydrogel for Challenging Ophthalmic Drug Delivery. *Colloids Surfaces B Biointerfaces* **2014**, *114*, 111–120.

(227) Shubhra, Q. T. H.; Tóth, J.; Gyenis, J.; Feczkó, T. Poloxamers for Surface Modification of Hydrophobic Drug Carriers and Their Effects on Drug Delivery. *Polym. Rev.* **2014**, *54* (1), 112–138.

(228) Ekambaram, P.; Abdul, H. S. A. Formulation and Evaluation of Solid Lipid Nanoparticles of Ramipril. *J. Young Pharm.* **2011**, *3* (3), 216–220.

(229) Sanjula, B.; Shah, F. M.; Javed, A.; Alka, A. Effect of Poloxamer 188 on Lymphatic Uptake of Carvedilol-Loaded Solid Lipid Nanoparticles for Bioavailability Enhancement. *J. Drug Target.* **2009**, *17* (3), 249–256.

(230) Mohtar, N.; A. K. Khan, N.; Darwis, Y. Solid Lipid Nanoparticles of Atovaquone Based on 2(4) Full-Factorial Design. *Iran. J. Pharm. Res. IJPR* **2015**, *14* (4), 989–1000.

(231) Emanuele, M.; Balasubramaniam, B. Differential Effects of Commercial-Grade and Purified Poloxamer 188 on Renal Function. *Drugs R. D.* **2014**, *14* (2), 73–83.

(232) Batrakova, E. V; Kabanov, A. V. Pluronic Block Copolymers: Evolution of Drug Delivery Concept from Inert Nanocarriers to Biological Response Modifiers. *J. Control. Release* **2008**, *130* (2), 98–106.

(233) de Araújo, D. R.; Oshiro, A.; da Silva, D. C.; Akkari, A. C. S.; de Mello, J. C.; Rodrigues, T. Poloxamers as Drug-Delivery Systems: Physicochemical, Pharmaceutical, and Toxicological Aspects. In *Nanotoxicology: Materials, Methodologies, and Assessments*; Durán, N., Guterres, S. S., Alves, O. L., Eds.; Springer New York: New York, NY, NY, 2014; pp 281–298.

(234) Lee, R. C.; Hannig, J.; Matthews, K. L.; Myerov, A.; Chen, C. T. Pharmaceutical Therapies for Sealing of Permeabilized Cell Membranes in Electrical Injuriesa. *Ann. N. Y. Acad. Sci.* **1999**, *888* (1), 266–273.

(235) Miller, D. W.; Batrakova, E. V; Kabanov, A. V. Inhibition of Multidrug Resistance-Associated Protein (MRP) Functional Activity with Pluronic Block Copolymers. *Pharm. Res.* **1999**, *16* (3), 396–401.

(236) Chu, Y.; Yu, H.; Zhang, Y.; Zhang, G.; Ma, Y.; Zhuo, R.; Jiang, X. Synthesis and Characterization of Biodegradable Amphiphilic ABC Y-Shaped Miktoarm Terpolymer by Click Chemistry for Drug Delivery. *J. Polym. Sci. Part A Polym. Chem.* **2014**, *52* (23), 3346–3355.

(237) Guan, H.; Xie, Z.; Zhang, P.; Deng, C.; Chen, X.; Jing, X. Synthesis and Characterization of Biodegradable Amphiphilic Triblock Copolymers Containing L-Glutamic Acid Units. *Biomacromolecules* **2005**, *6* (4), 1954–1960.

(238) Macon, A. L. B.; Rehman, S. U.; Bell, R. V; Weaver, J. V. M. Reversible Assembly of pH Responsive Branched Copolymer-Stabilised Emulsion via Electrostatic Forces. *Chem. Commun.* **2016**, *52* (1), 136–139.

(239) Wei, W.; Wang, T.; Yi, C.; Liu, J.; Liu, X. Self-Assembled Micelles Based on Branched Poly (Styrene-Alt-Maleic Anhydride) as Particulate Emulsifiers. *RSC Adv.* **2015**, *5* (2), 1564–1570.

(240) Moghimi, S. M.; Hunter, A. C. Poloxamers and Poloxamines in Nanoparticle Engineering and Experimental Medicine. *Trends Biotechnol.* **2000**, *18* (10), 412–420.

(241) Pasquali, R. C.; Taurozzi, M. P.; Bregni, C. Some Considerations about the Hydrophilic–lipophilic Balance System. *Int. J. Pharm.* **2008**, *356* (1–2), 44–51.

(242) Venishetty, V. K.; Chede, R.; Komuravelli, R.; Adepu, L.; Sistla, R.; Diwan, P. V. Design and Evaluation of Polymer Coated Carvedilol Loaded Solid Lipid Nanoparticles to Improve the Oral Bioavailability: A Novel Strategy to Avoid Intraduodenal Administration. *Colloids Surf. B. Biointerfaces* **2012**, *95*, 1–9.

(243) Hou, C.; Lin, S.; Liu, F.; Hu, J.; Zhang, G.; Liu, G.; Tu, Y.; Zou, H.; Luo, H. Synthesis of poly(2-Hydroxyethyl Methacrylate) End-Capped with Asymmetric Functional Groups via Atom Transfer Radical Polymerization. *New J. Chem.* **2014**, *38* (6), 2538–2547.

(244) Gottlieb, H. E.; Kotlyar, V.; Nudelman, A. NMR Chemical Shifts of Common Laboratory Solvents as Trace Impurities. *J. Org. Chem.* **1997**, *62* (21), 7512–7515.

(245) Bannister, I.; Billingham, N. C.; Armes, S. P.; Rannard, S. P.; Findlay, P. Development of Branching in Living Radical Copolymerization of Vinyl and Divinyl Monomers. *Macromolecules* **2006**, *39* (22), 7483–7492.

(246) Odian, G. Step Polymerization. In *Principles of Polymerization*; John Wiley & Sons, Inc.: Hoboken, NJ, USA, 2004; pp 39–197.

(247) Jafari, S. M. *Nanoencapsulation of Food Bioactive Ingredients: Principles and Applications*; Elsevier Science, 2017.

(248) Malvern. Mastersizer 2000 user manual https://www.malvern.com/en/support/resource-center/user-manuals/MAN0384EN (accessed Feb 22, 2018).

(249) Chan, L. W.; Tan, L. H.; Heng, P. W. S. Process Analytical Technology: Application to Particle Sizing in Spray Drying. *AAPS PharmSciTech* **2008**, *9* (1), 259–266.

(250) Taylor, P. Ostwald Ripening in Emulsions. *Adv. Colloid Interface Sci.* **1998**, *75* (2), 107–163.

(251) Hu, K.; Bard, A. J. Characterization of Adsorption of Sodium Dodecyl Sulfate on Charge-

Regulated Substrates by Atomic Force Microscopy Force Measurements. *Langmuir* **1997**, *13* (20), 5418–5425.

(252) Koda, Y.; Terashima, T.; Sawamoto, M. LCST-Type Phase Separation of Poly[poly(ethylene Glycol) Methyl Ether Methacrylate]s in Hydrofluorocarbon. *ACS Macro Lett.* **2015**, *4* (12), 1366–1369.

(253) Luzon, M.; Boyer, C.; Peinado, C.; Corrales, T.; Whittaker, M.; Tao, L.; Davis, T. P. Water-Soluble, Thermoresponsive, Hyperbranched Copolymers Based on PEG-Methacrylates: Synthesis, Characterization, and LCST Behavior. *J. Polym. Sci. Part A Polym. Chem.* **2010**, *48* (13), 2783–2792.

(254) Phillips, D. J.; Gibson, M. I. Towards Being Genuinely Smart: "Isothermally-Responsive" Polymers as Versatile, Programmable Scaffolds for Biologically-Adaptable Materials. *Polym. Chem.* **2015**, *6* (7), 1033–1043.

(255) OptiMelt. Melting Point Apparatus http://www.optimelt.co.uk/pdfs/OptiMelt.pdf (accessed Feb 18, 2018).

(256) Lee, H. N.; Lodge, T. P. Lower Critical Solution Temperature (LCST) Phase Behavior of Poly(ethylene Oxide) in Ionic Liquids. *J. Phys. Chem. Lett.* **2010**, *1* (13), 1962–1966.

(257) Rodríguez-Ropero, F.; Hajari, T.; van der Vegt, N. F. A. Mechanism of Polymer Collapse in Miscible Good Solvents. *J. Phys. Chem. B* **2015**, *119* (51), 15780–15788.

(258) Ju, B.; Cao, S.; Zhang, S. Effect of Additives on the Cloud Point Temperature of 2-Hydroxy-3-Isopropoxypropyl Starch Solutions. *J. Phys. Chem. B* **2013**, *117* (39), 11830–11835.

(259) zur Mühlen, A.; Schwarz, C.; Mehnert, W. Solid Lipid Nanoparticles (SLN) for Controlled Drug Delivery--Drug Release and Release Mechanism. *Eur. J. Pharm. Biopharm.* **1998**, *45* (2), 149–155.

(260) Lasa-Saracibar, B.; Estella-Hermoso de Mendoza, A.; Guada, M.; Dios-Vieitez, C.; Blanco-Prieto, M. J. Lipid Nanoparticles for Cancer Therapy: State of the Art and Future Prospects. *Expert Opin. Drug Deliv.* **2012**, *9* (10), 1245–1261.

(261) Lai, F.; Sinico, C.; De Logu, A.; Zaru, M.; Müller, R. H.; Fadda, A. M. SLN as a Topical Delivery System for Artemisia Arborescens Essential Oil: In Vitro Antiviral Activity and Skin Permeation Study. *Int. J. Nanomedicine* **2007**, *2* (3), 419–425.

(262) Müller, R.; Maaben, S.; Weyhers, H.; Mehnert, W. Phagocytic Uptake and Cytotoxicity of Solid Lipid Nanoparticles (SLN) Sterically Stabilized with Poloxamine 908 and Poloxamer 407. *J. Drug Target.* **1996**, *4* (3), 161–170.

(263) Mosallaei, N.; Jaafari, M. R.; Hanafi Bojd, M. Y.; Golmohammadzadeh, S.; Malaekeh Nikouei, B. Docetaxel-Loaded Solid Lipid Nanoparticles: Preparation, Characterization, In Vitro, and In Vivo Evaluations. *J. Pharm. Sci.* **2017**, *102* (6), 1994–2004.

(264) Mosallaei, N.; Mahmoudi, A.; Ghandehari, H.; Yellepeddi, V. K.; Jaafari, M. R.; Malaekeh-Nikouei, B. Solid Lipid Nanoparticles Containing 7-Ethyl-10-Hydroxycamptothecin (SN38): Preparation, Characterization, in Vitro, and in Vivo Evaluations. *Eur. J. Pharm. Biopharm.* **2016**, *104*, 42–50.

(265) Lingling, G.; Yuan, Z.; Weigen, L. Preparation, Optimization, Characterization and in Vivo Pharmacokinetic Study of Asiatic Acid Tromethamine Salt-Loaded Solid Lipid Nanoparticles.

Drug Dev. Ind. Pharm. **2016**, *42* (8), 1325–1333.

(266) Shah, M.; Chuttani, K.; Mishra, A. K.; Pathak, K. Oral Solid Compritol 888 ATO Nanosuspension of Simvastatin: Optimization and Biodistribution Studies. *Drug Dev. Ind. Pharm.* **2011**, *37* (5), 526–537.

(267) Lebouille, J. G. J. L.; Stepanyan, R.; Slot, J. J. M.; Cohen Stuart, M. A.; Tuinier, R. Nanoprecipitation of Polymers in a Bad Solvent. *Colloids Surfaces A Physicochem. Eng. Asp.* **2014**, *460*, 225–235.

(268) Gavini, E.; Sanna, V.; Sharma, R.; Juliano, C.; Usai, M.; Marchetti, M.; Karlsen, J.; Giunchedi, P. Solid Lipid Microparticles (SLM) Containing Juniper Oil as Anti-Acne Topical Carriers: Preliminary Studies. *Pharm Dev Technol* **2005**, *10* (4), 479–487.

(269) Wang, T.; Wang, N.; Zhang, Y.; Shen, W.; Gao, X.; Li, T. Solvent Injection-Lyophilization of Tert-Butyl Alcohol/water Cosolvent Systems for the Preparation of Drug-Loaded Solid Lipid Nanoparticles. *Colloids Surfaces B Biointerfaces* **2010**, *79* (1), 254–261.

(270) Dorraj, G.; Moghimi, H. R. Preparation of SLN-Containing Thermoresponsive In-Situ Forming Gel as a Controlled Nanoparticle Delivery System and Investigating Its Rheological, Thermal and Erosion Behavior. *Iran. J. Pharm. Res.* **2015**, *14* (2), 347–358.

(271) Negi, J. S.; Chattopadhyay, P.; Sharma, A. K.; Ram, V. Development of Solid Lipid Nanoparticles (SLNs) of Lopinavir Using Hot Self Nano-Emulsification (SNE) Technique. *Eur. J. Pharm. Sci.* **2013**, *48* (1–2), 231–239.

(272) Slater, R. A.; Mcdonald, T. O.; Adams, D. J.; Draper, E. R.; Weaver, V. M.; Rannard, S. P. Architecture-Driven Aqueous Stability of Hydrophobic , Branched Polymer Nanoparticles Prepared by Rapid Nanoprecipitation. **2012**, 9816–9827.

(273) Deng, H.; Liu, J.; Zhao, X.; Zhang, Y.; Liu, J.; Xu, S.; Deng, L.; Dong, A.; Zhang, J. PEG-B-PCL Copolymer Micelles with the Ability of pH-Controlled Negative-to-Positive Charge Reversal for Intracellular Delivery of Doxorubicin. *Biomacromolecules* **2014**, *15* (11), 4281–4292.

(274) Nobbmann, U. Derived count rate – what is it? http://www.materials-talks.com/blog/2015/06/11/derived-count-rate-what-is-it/ (accessed Feb 22, 2018).

(275) Lorenzen, T. Profile of Maraviroc: A CCR5 Antagonist in the Management of Treatment-Experienced HIV Patients. *HIV/AIDS - Res. Palliat. Care* **2010**, *2*, 151.

(276) MacArthur, R. D.; Novak, R. M. Maraviroc: The First of a New Class of Antiretroviral Agents. *Clin. Infect. Dis.* **2008**, *47* (2), 236–241.

(277) Dumond, J. B.; Patterson, K. B.; Pecha, A. L.; Werner, R. E.; Andrews, E.; Damle, B.; Tressler, R.; Worsley, J.; Kashuba, A. D. M. Maraviroc Concentrates in the Cervicovaginal Fluid and Vaginal Tissue of HIV-Negative Women. *J. Acquir. Immune Defic. Syndr.* **2009**, *51* (5), 546.

(278) Parboosing, R.; Maguire, G. E. M.; Govender, P.; Kruger, H. G. Nanotechnology and the Treatment of HIV Infection. *Viruses* **2012**, *4* (4), 488–520.

(279) Severino, P.; Andreani, T.; Macedo, A. S.; Fangueiro, J. F.; Santana, M. H. A.; Silva, A. M.; Souto, E. B. Current State-of-Art and New Trends on Lipid Nanoparticles (SLN and NLC) for Oral Drug Delivery. *J. Drug Deliv.* **2012**, *2012*, 750891.

(280) Helgason, T.; Awad, T. S.; Kristbergsson, K.; McClements, D. J.; Weiss, J. Effect of Surfactant

Surface Coverage on Formation of Solid Lipid Nanoparticles (SLN). *J. Colloid Interface Sci.* **2009**, *334* (1), 75–81.

(281) Shi, F.; Zhao, J. H.; Liu, Y.; Wang, Z.; Zhang, Y. T.; Feng, N. P. Preparation and Characterization of Solid Lipid Nanoparticles Loaded with Frankincense and Myrrh Oil. *Int. J. Nanomedicine* **2012**, *7*, 2033–2043.

(282) Nair, R.; Kumar, A. C. K.; Priya, V. K.; Yadav, C. M.; Raju, P. Y. Formulation and Evaluation of Chitosan Solid Lipid Nanoparticles of Carbamazepine. *Lipids Health Dis.* **2012**, *11*, 72.

(283) Hatziantoniou, S.; Deli, G.; Nikas, Y.; Demetzos, C.; Papaioannou, G. T. Scanning Electron Microscopy Study on Nanoemulsions and Solid Lipid Nanoparticles Containing High Amounts of Ceramides. *Micron* **2007**, *38* (8), 819–823.

(284) Dudhipala, N.; Janga, K. Y. Lipid Nanoparticles of Zaleplon for Improved Oral Delivery by Box–Behnken Design: Optimization, in Vitro and in Vivo Evaluation. *Drug Dev. Ind. Pharm.* **2017**, *43* (7), 1205–1214.

(285) Gaspar, D. P.; Serra, C.; Lino, P. R.; Gonçalves, L.; Taboada, P.; Remuñán-López, C.; Almeida, A. J. Microencapsulated SLN: An Innovative Strategy for Pulmonary Protein Delivery. *Int. J. Pharm.* **2017**, *516* (1), 231–246.

(286) Aboutaleb, E.; Atyabi, F.; Khoshayand, M. R.; Vatanara, A. R.; Ostad, S. N.; Kobarfard, F.; Dinarvand, R. Improved Brain Delivery of Vincristine Using Dextran Sulfate Complex Solid Lipid Nanoparticles: Optimization and in Vivo Evaluation. *J. Biomed. Mater. Res. Part A* **2014**, *102* (7), 2125–2136.

(287) Pandita, D.; Kumar, S.; Poonia, N.; Lather, V. Solid Lipid Nanoparticles Enhance Oral Bioavailability of Resveratrol, a Natural Polyphenol. *Food Res. Int.* **2014**, *62*, 1165–1174.

(288) Küchler, S.; Radowski, M. R.; Blaschke, T.; Dathe, M.; Plendl, J.; Haag, R.; Schäfer-Korting, M.; Kramer, K. D. Nanoparticles for Skin Penetration Enhancement – A Comparison of a Dendritic Core-Multishell-Nanotransporter and Solid Lipid Nanoparticles. *Eur. J. Pharm. Biopharm.* **2009**, *71* (2), 243–250.

(289) Chirio, D.; Gallarate, M.; Peira, E.; Battaglia, L.; Serpe, L.; Trotta, M. Formulation of Curcumin-Loaded Solid Lipid Nanoparticles Produced by Fatty Acids Coacervation Technique. *J. Microencapsul.* **2011**, *28* (6), 537–548.

(290) Velmurugan, S.; Mohamed Ashraf, A. Analytical Method Development and Validation of Miraviroc in Bulk and Pharmaceutical Formulation by UV Spectroscopy. *Int. J. Pharm. Sci. Res.* **2013**, *4* (11), 4366–4370.

(291) Zhang, C.; Zhang, T.; Oyler, N. A.; Youan, B. B. C. Direct and Real-Time Quantification of Tenofovir Release from pH-Sensitive Microparticles into Simulated Biological Fluids Using (1)H-NMR. *J. Pharm. Sci.* **2014**, *103* (4), 1170–1177.

(292) Hansraj, G. P.; Singh, S. K.; Kumar, P. Sumatriptan Succinate Loaded Chitosan Solid Lipid Nanoparticles for Enhanced Anti-Migraine Potential. *Int. J. Biol. Macromol.* **2015**, *81*, 467–476.

(293) Shah, M.; Pathak, K. Development and Statistical Optimization of Solid Lipid Nanoparticles of Simvastatin by Using 2(3) Full-Factorial Design. *AAPS PharmSciTech* **2010**, *11* (2), 489–496.

(294) Lapresta-Fernández, A.; García-García, J. M.; París, R.; Huertas-Roa, R.; Salinas-Castillo, A.; de

la Llana, S. A.; Huertas-Pérez, J. F.; Guarrotxena, N.; Capitán-Vallvey, L. F.; Quijada-Garrido, I. Thermoresponsive Gold Polymer Nanohybrids with a Tunable Cross-Linked MEO2MA Polymer Shell. *Part. Part. Syst. Charact.* **2014**, *31* (11), 1183–1191.

(295) Price, D. A.; Gayton, S.; Selby, M. D.; Ahman, J.; Haycock-Lewandowski, S.; Stammen, B. L.; Warren, A. Initial Synthesis of UK-427,857 (Maraviroc). *Tetrahedron Lett.* **2005**, *46* (30), 5005–5007.

(296) Fulmer, G. R.; Miller, A. J. M.; Sherden, N. H.; Gottlieb, H. E.; Nudelman, A.; Stoltz, B. M.; Bercaw, J. E.; Goldberg, K. I. NMR Chemical Shifts of Trace Impurities: Common Laboratory Solvents, Organics, and Gases in Deuterated Solvents Relevant to the Organometallic Chemist. *Organometallics* **2010**, *29* (9), 2176–2179.

(297) Zhang, D.; Liu, Q.; Shi, X.; Li, Y. Tetrabutylammonium Hexafluorophosphate and 1-Ethyl-3-Methyl Imidazolium Hexafluorophosphate Ionic Liquids as Supporting Electrolytes for Non-Aqueous Vanadium Redox Flow Batteries. *J. Power Sources* **2012**, *203*, 201–205.

(298) Lee, M. K.; Kim, M. Y.; Kim, S.; Lee, J. Cryoprotectants for Freeze Drying of Drug Nano-Suspensions: Effect of Freezing Rate. *J. Pharm. Sci.* **2009**, *98* (12), 4808–4817.

(299) Schwarz, C.; Mehnert, W. Freeze-Drying of Drug-Free and Drug-Loaded Solid Lipid Nanoparticles (SLN). *Int. J. Pharm.* **1997**, *157* (2), 171–179.

(300) Vighi, E.; Ruozi, B.; Montanari, M.; Battini, R.; Leo, E. Re-Dispersible Cationic Solid Lipid Nanoparticles (SLNs) Freeze-Dried without Cryoprotectors: Characterization and Ability to Bind the pEGFP-Plasmid. *Eur. J. Pharm. Biopharm.* **2007**, *67* (2), 320–328.

(301) Doktorovova, S.; Shegokar, R.; Fernandes, L.; Martins-Lopes, P.; Silva, A. M.; Müller, R. H.; Souto, E. B. Trehalose Is Not a Universal Solution for Solid Lipid Nanoparticles Freeze-Drying. *Pharm. Dev. Technol.* **2014**, *19* (8), 922–929.

(302) Soares, S.; Fonte, P.; Costa, A.; Andrade, J.; Seabra, V.; Ferreira, D.; Reis, S.; Sarmento, B. Effect of Freeze-Drying, Cryoprotectants and Storage Conditions on the Stability of Secondary Structure of Insulin-Loaded Solid Lipid Nanoparticles. *Int. J. Pharm.* **2013**, *456* (2), 370–381.

(303) Howard, M. D.; Lu, X.; Jay, M.; Dziubla, T. D. Optimization of the Lyophilization Process for Long-Term Stability of Solid–lipid Nanoparticles. *Drug Dev. Ind. Pharm.* **2012**, *38* (10), 1270–1279.

(304) Moretton, M. A.; Chiappetta, D. A.; Sosnik, A. Cryoprotection-Lyophilization and Physical Stabilization of Rifampicin-Loaded Flower-like Polymeric Micelles. *J. R. Soc. Interface* **2012**, *9* (68), 487–502.

(305) Jourghanian, P.; Ghaffari, S.; Ardjmand, M.; Haghighat, S.; Mohammadnejad, M. Sustained Release Curcumin Loaded Solid Lipid Nanoparticles. *Adv. Pharm. Bull.* **2016**, *6* (1), 17–21.

(306) Shah, M.; Agrawal, Y. K.; Garala, K.; Ramkishan, A. Solid Lipid Nanoparticles of a Water Soluble Drug, Ciprofloxacin Hydrochloride. *Indian J. Pharm. Sci.* **2012**, *74* (5), 434–442.

(307) Harivardhan Reddy, L.; Vivek, K.; Bakshi, N.; Murthy, R. S. R. Tamoxifen Citrate Loaded Solid Lipid Nanoparticles (SLN^{TM}): Preparation, Characterization, In Vitro Drug Release, and Pharmacokinetic Evaluation. *Pharm. Dev. Technol.* **2006**, *11* (2), 167–177.

(308) Riddick, T. M. *Control of Colloid Stability through Zeta Potential: With a Closing Chapter on Its Relationship to Cardiovascular Disease*; Published for Zeta-Meter, inc., by Livingston Pub. Co.,

1968.

(309) Walker, D. K.; Bowers, S. J.; Mitchell, R. J.; Potchoiba, M. J.; Schroeder, C. M.; Small, H. F. Preclinical Assessment of the Distribution of Maraviroc to Potential Human Immunodeficiency Virus (HIV) Sanctuary Sites in the Central Nervous System (CNS) and Gut-Associated Lymphoid Tissue (GALT). *Xenobiotica* **2008**, *38* (10), 1330–1339.

(310) Walker, D. K. Species Differences in Dispersion of the CCR5 Antagonist, UK-427,857, A New Potential Treatment for HIV. *Drug Metab. Dispos.* **2005**, *33* (4), 587–595.

(311) Bukowski, T. R.; Moffett, T. C.; Revkin, J. H.; Ploger, J. D.; Bassingthwaighte, J. B. Triple-Label β Liquid Scintillation Counting. *Anal. Biochem.* **1992**, *204* (1), 171–180.

(312) PerkinElmer. Liquid Scintillation Counting http://www.perkinelmer.com/lab-products-and-services/application-support-knowledgebase/radiometric/liquid-scintillation-counting.html (accessed Feb 20, 2018).

(313) Garcia-Perez, J.; Rueda, P.; Staropoli, I.; Kellenberger, E.; Alcami, J.; Arenzana-Seisdedos, F.; Lagane, B. New Insights into the Mechanisms Whereby Low Molecular Weight CCR5 Ligands Inhibit HIV-1 Infection. *J. Biol. Chem.* **2011**, *286* (7), 4978–4990.

(314) Abel, S.; van der Ryst, E.; Rosario, M. C.; Ridgway, C. E.; Medhurst, C. G.; Taylor-Worth, R. J.; Muirhead, G. J. Assessment of the Pharmacokinetics, Safety and Tolerability of Maraviroc, a Novel CCR5 Antagonist, in Healthy Volunteers. *Br J Clin Pharmacol* **2008**, *65*.

(315) Johnson, C. S. Diffusion Ordered Nuclear Magnetic Resonance Spectroscopy: Principles and Applications. *Prog. Nucl. Magn. Reson. Spectrosc.* **1999**, *34* (3–4), 203–256.

(316) Mallol, R.; Rodriguez, M. A.; Brezmes, J.; Masana, L.; Correig, X. Human Serum/plasma Lipoprotein Analysis by NMR: Application to the Study of Diabetic Dyslipidemia. *Prog. Nucl. Magn. Reson. Spectrosc.* **2013**, *70*, 1–24.

(317) Mora, S.; Otvos, J. D.; Rifai, N.; Rosenson, R. S.; Buring, J. E.; Ridker, P. M. Lipoprotein Particle Profiles by Nuclear Magnetic Resonance Compared with Standard Lipids and Apolipoproteins in Predicting Incident Cardiovascular Disease in Women. *Circulation* **2009**, *119* (7), 931–939.

(318) Lounila, J.; Ala-Korpela, M.; Jokisaari, J.; Savolainen, M. J.; Kesäniemi, Y. A. Effects of Orientational Order and Particle Size on the NMR Line Positions of Lipoproteins. *Phys. Rev. Lett.* **1994**, *72* (25), 4049–4052.

Appendix

Chapter 2 – Synthesis and characterisation of branched oligo ethylene glycol methacrylate (OEGMA) based polymers utilisation ATRP and testing of these polymers in *n*-dodecane model oil studies

Right angular light scattering (RALS) and low-angle light scattering (LALS) obtained for DBiB-(OEGMA) based polymers.

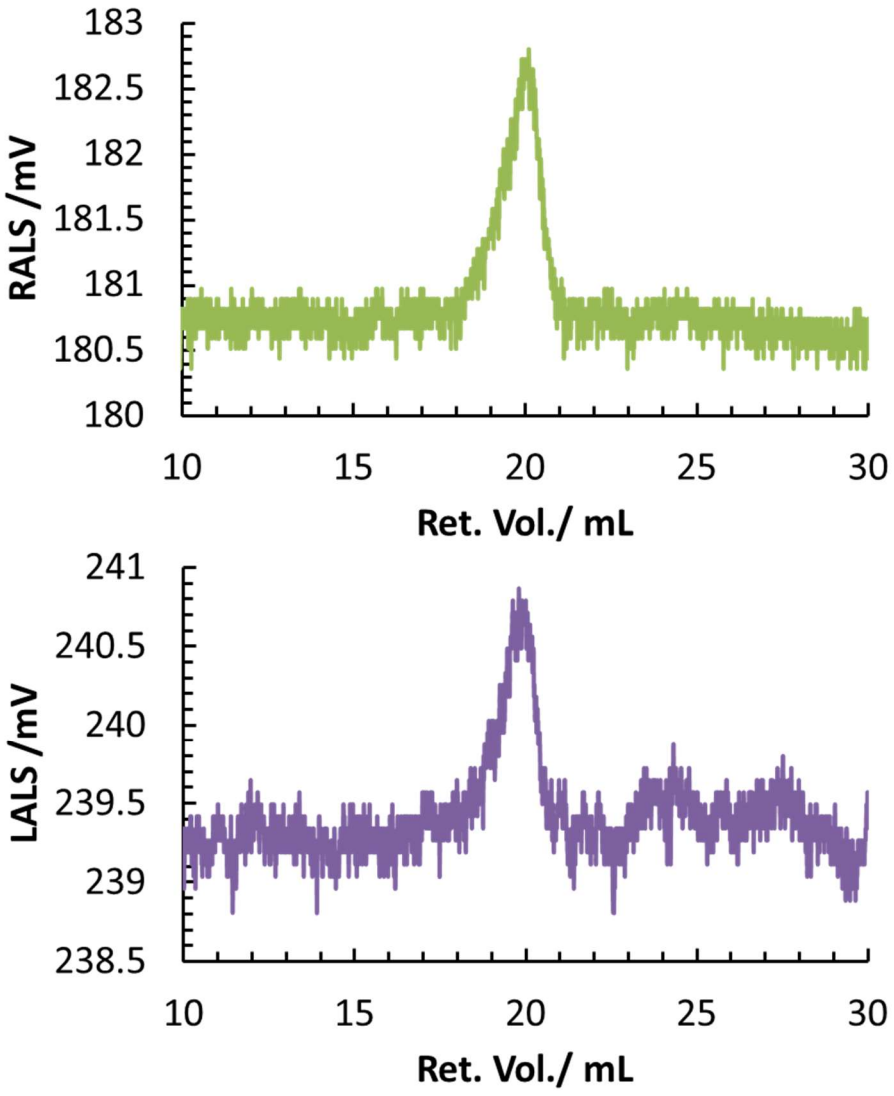

Fig. A1. Raw chromatograms of RALS (green) and LALS (purple) traces of DBiB-p(OEGMA)$_{10}$ from obtained. Analysis performed by GPC with mobile phase of DMF (+ 0.01M) at 1mL/min 60 ˚C. Ret.; retention. Vol.; volume.

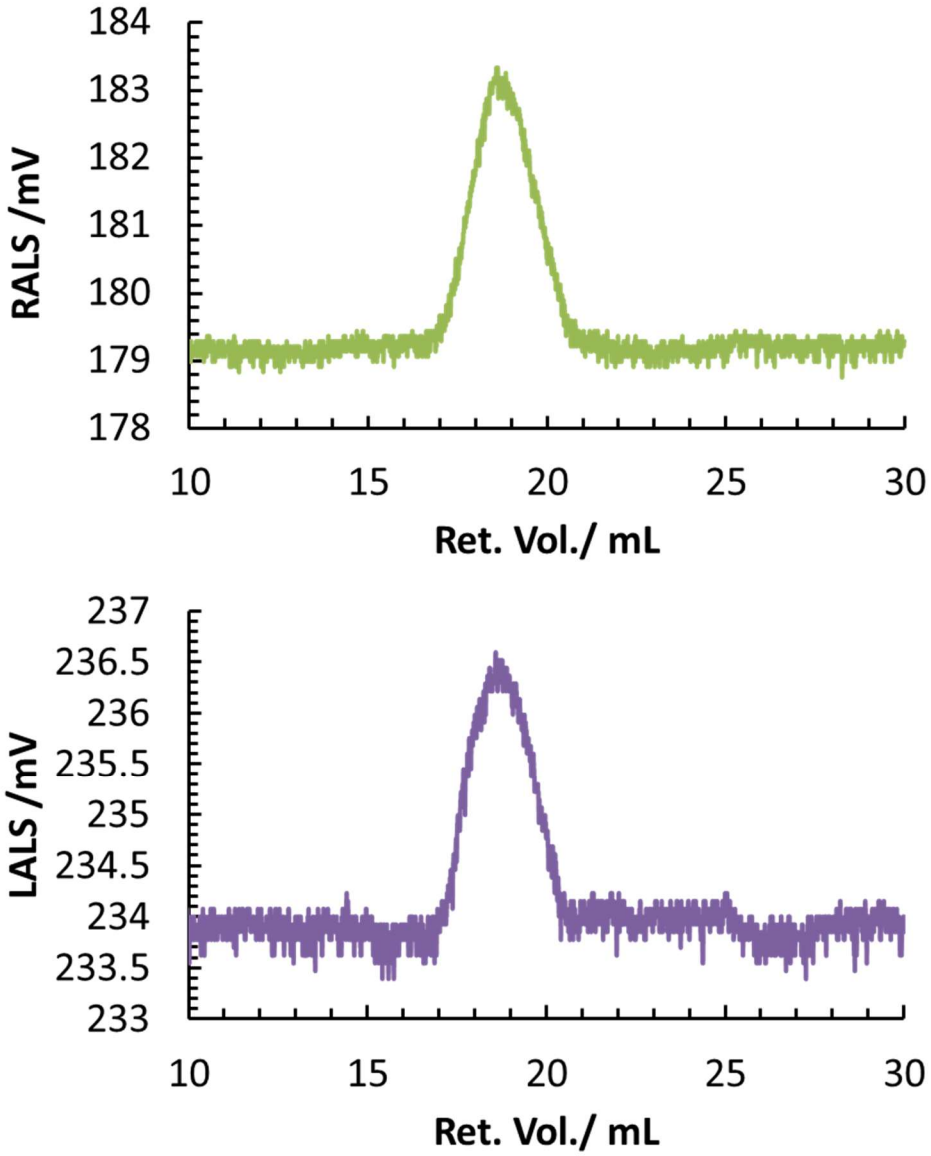

Fig. A2. Raw chromatograms of RALS(green) and LALS (purple) traces of DBiB-p(OEGMA)$_{10}$-co-(EGDMA)$_{0.5}$. Analysis performed by GPC with mobile phase of DMF (+ 0.01M) at 1mL/min 60 ˚C. Ret.; retention. Vol.; volume.

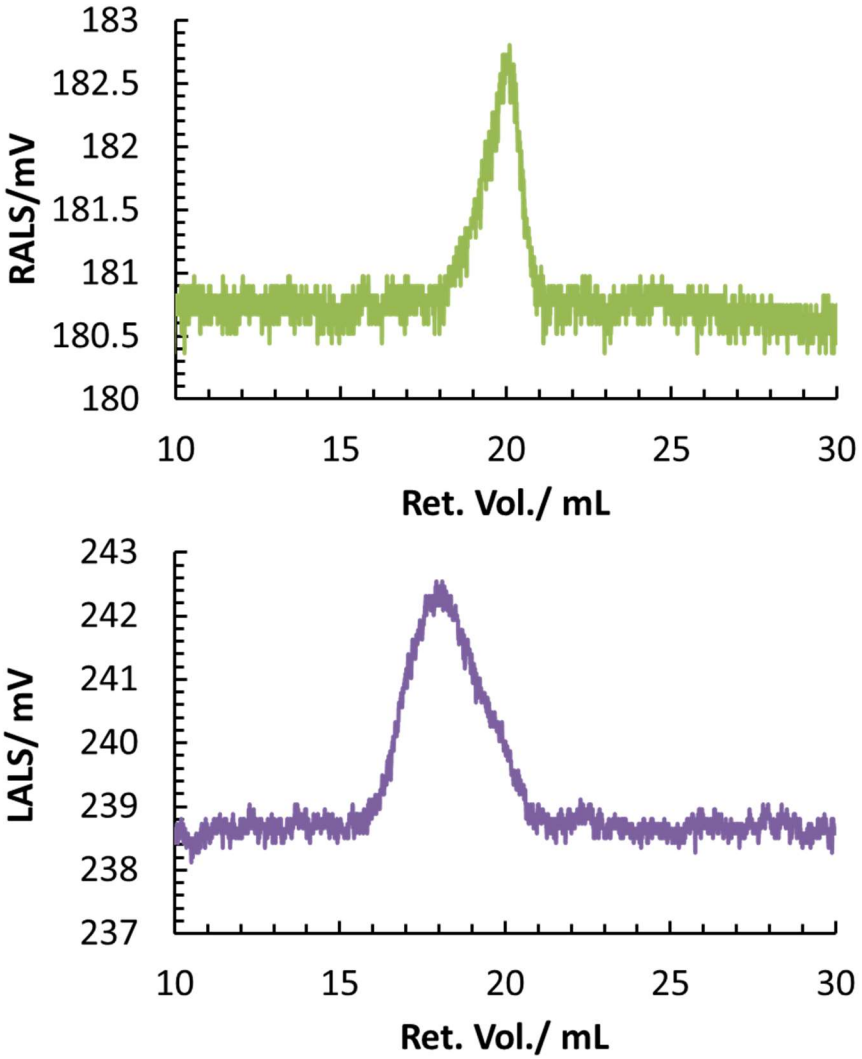

Fig. A3. Raw chromatograms of RALS and LALS traces of DBiB-p(OEGMA)$_{10}$-co-(EGDMA)$_{0.8}$. Analysis performed by GPC with mobile phase of DMF (+ 0.01M) at 1mL/min 60 ˚C. Ret.; retention. Vol.; volume.

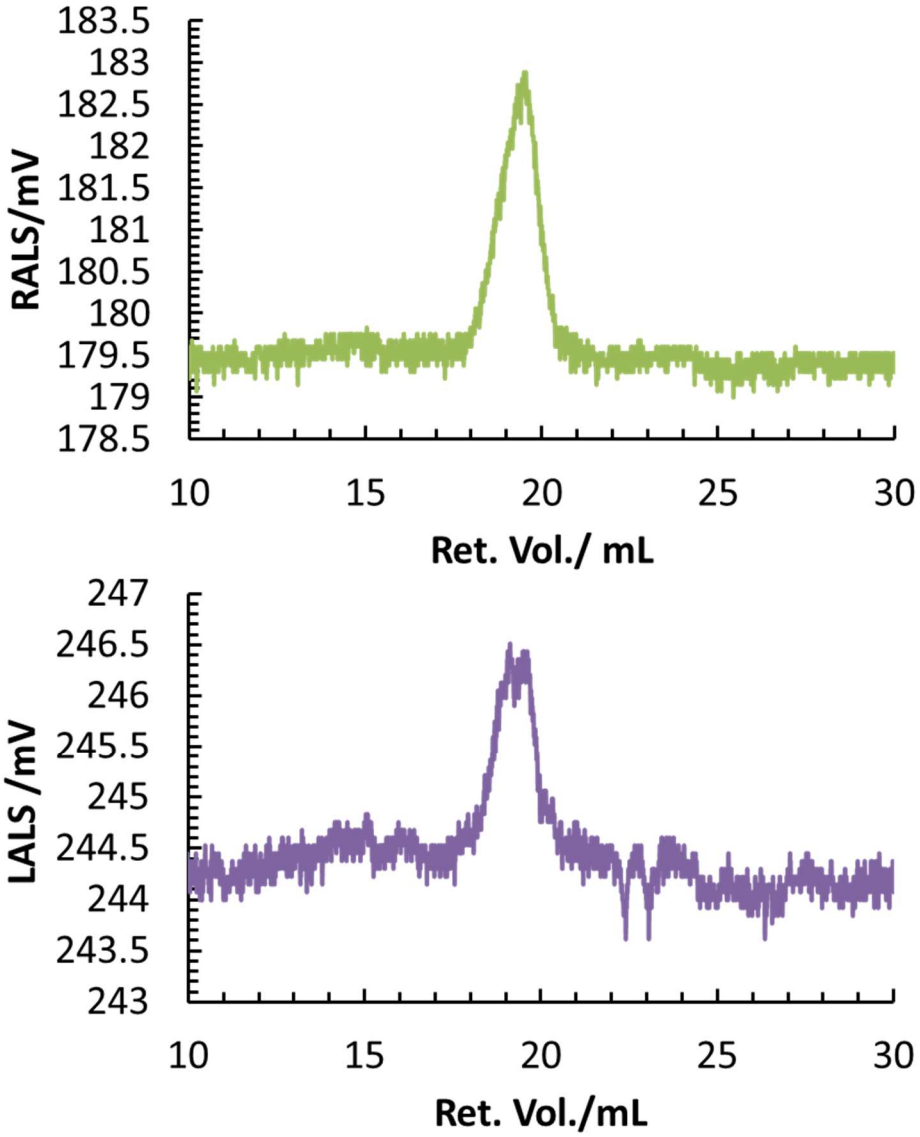

Fig. A4. Raw chromatograms of RALS (green) and LALS (purple) traces of DBiB-p(OEGMA)$_{20}$. Analysis performed by GPC with mobile phase of DMF (+ 0.01M) at 1mL/min 60 ˚C. Ret.; retention. Vol.; volume.

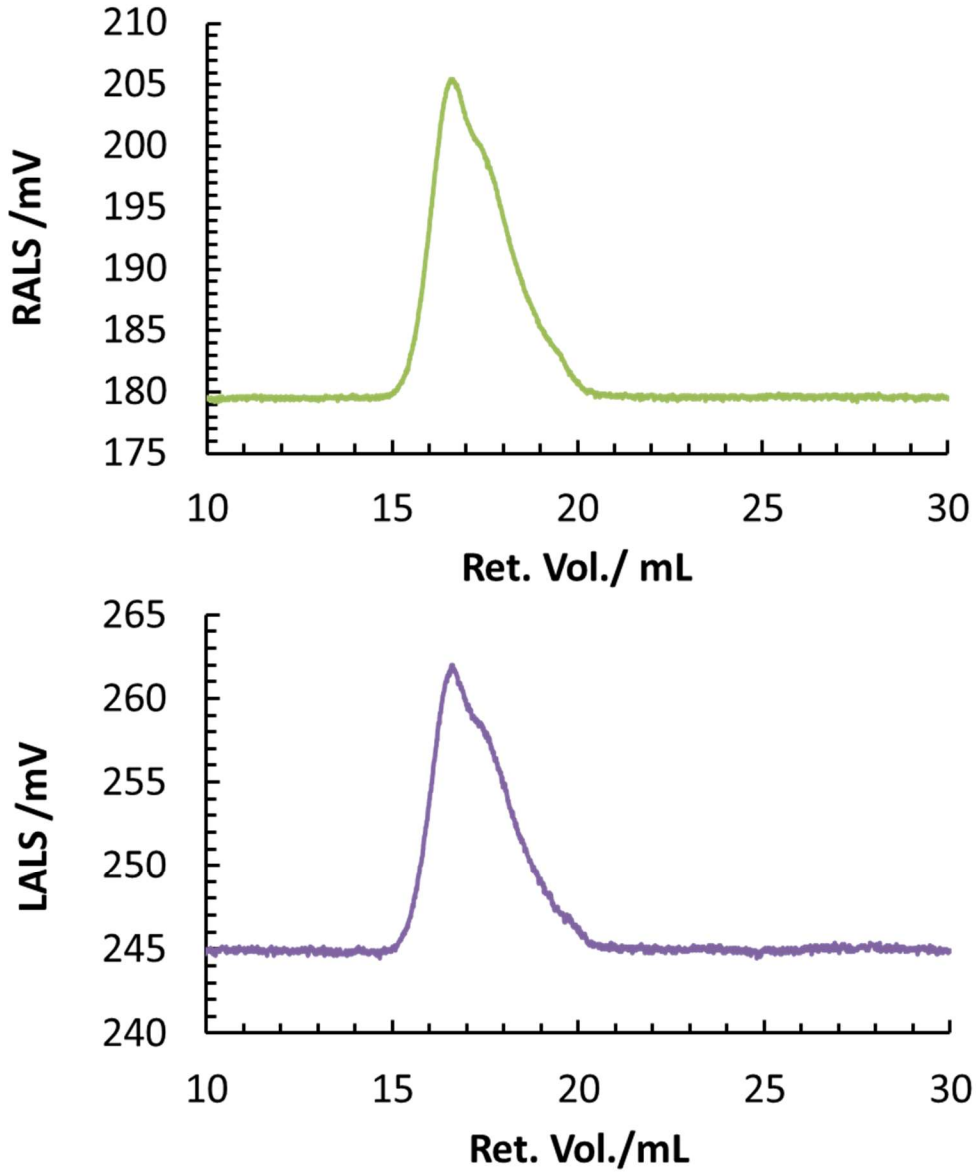

Fig. A5. Raw chromatograms of RALS (green) and LALS (purple) traces of DBiB-p(OEGMA)$_{20}$-co-(EGDMA)$_{0.5}$. Analysis performed by GPC with mobile phase of DMF (+ 0.01M) at 1mL/min 60 ˚C. Ret.; retention. Vol.; volume.

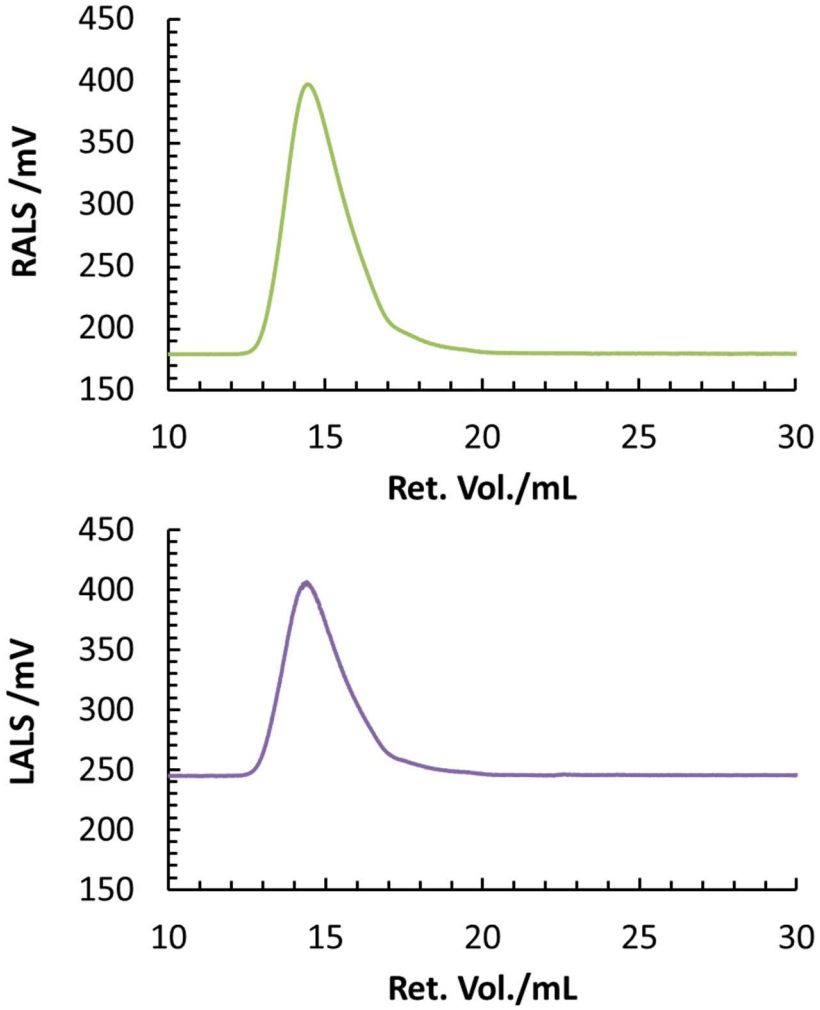

Fig. A6. Raw GPC chromatograms of RALS (green) and LALS (purple) traces of DBiB-p(OEGMA)$_{20}$-co-(EGDMA)$_{0.8}$. Analysis performed by GPC with mobile phase of DMF (+ 0.01M) at 1mL/min 60 ˚C. Ret.; retention. Vol.; volume.

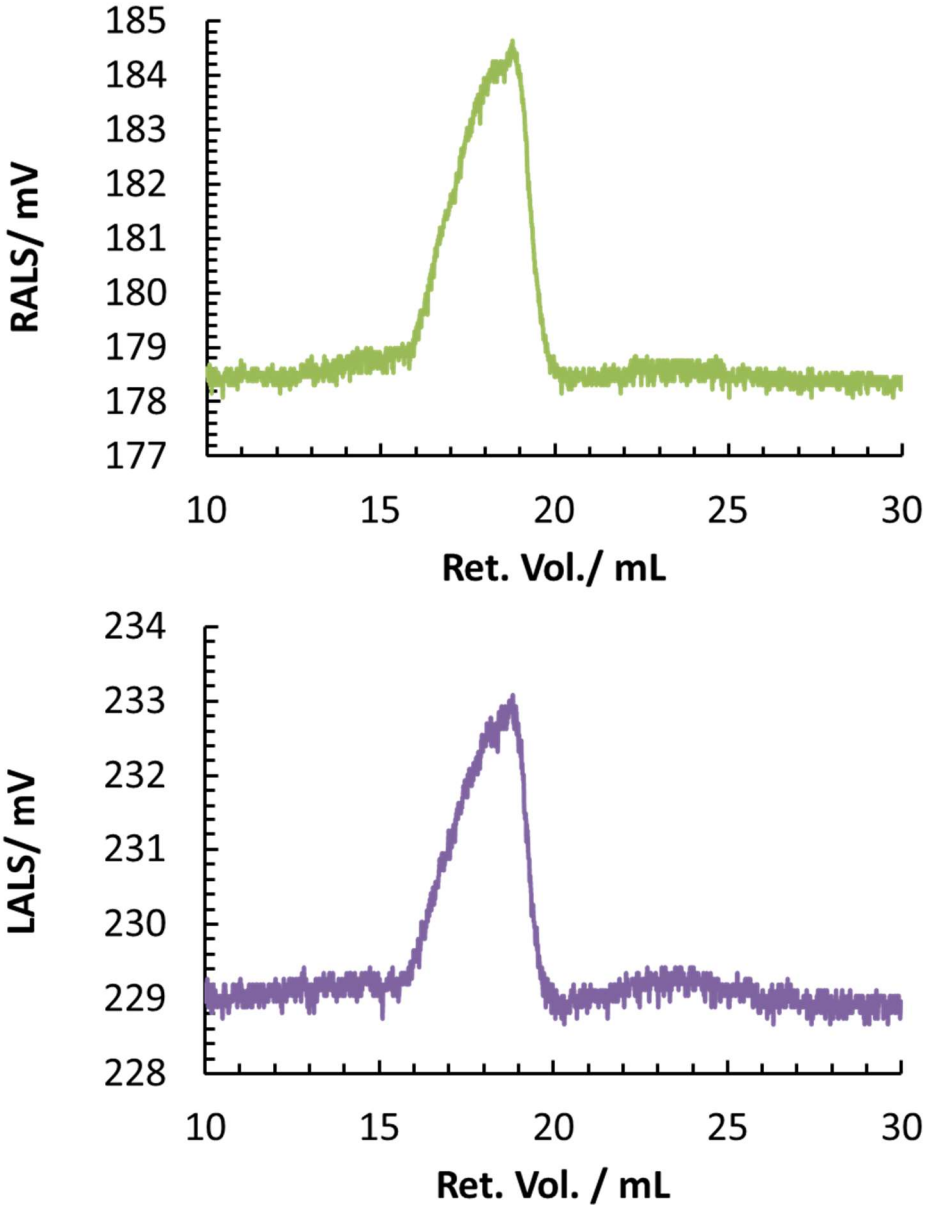

Fig. A7. Raw GPC chromatogram of RALS (green) and LALS (purple) traces of DBiB-p(OEGMA)$_{50}$. Analysis performed by GPC with mobile phase of DMF (+ 0.01M) at 1mL/min 60 ˚C. Ret.; retention. Vol.; volume.

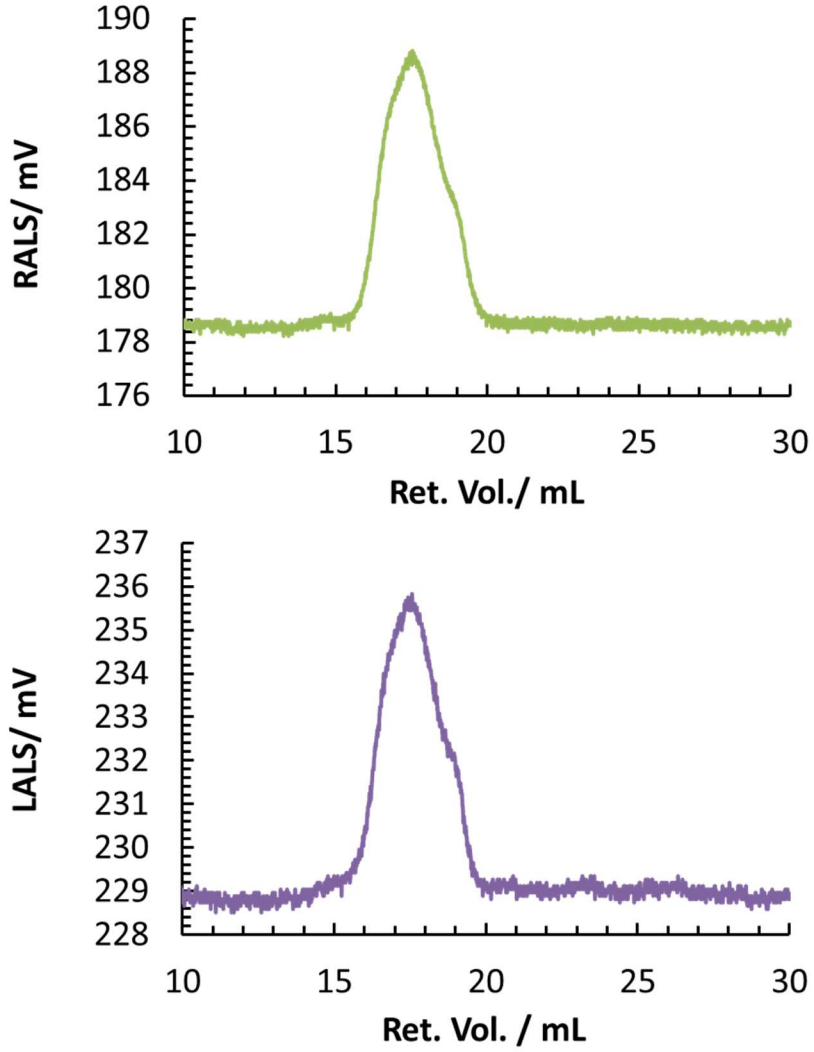

Fig. A8. Raw GPC chromatograms of RALS (green) and LALS (purple) traces of DBiB-p(OEGMA)$_{50}$ – co-(EGMDA)$_{0.5}$. Analysis performed by GPC with mobile phase of DMF (+ 0.01M) at 1mL/min 60 ˚C. Ret.; retention. Vol.; volume.

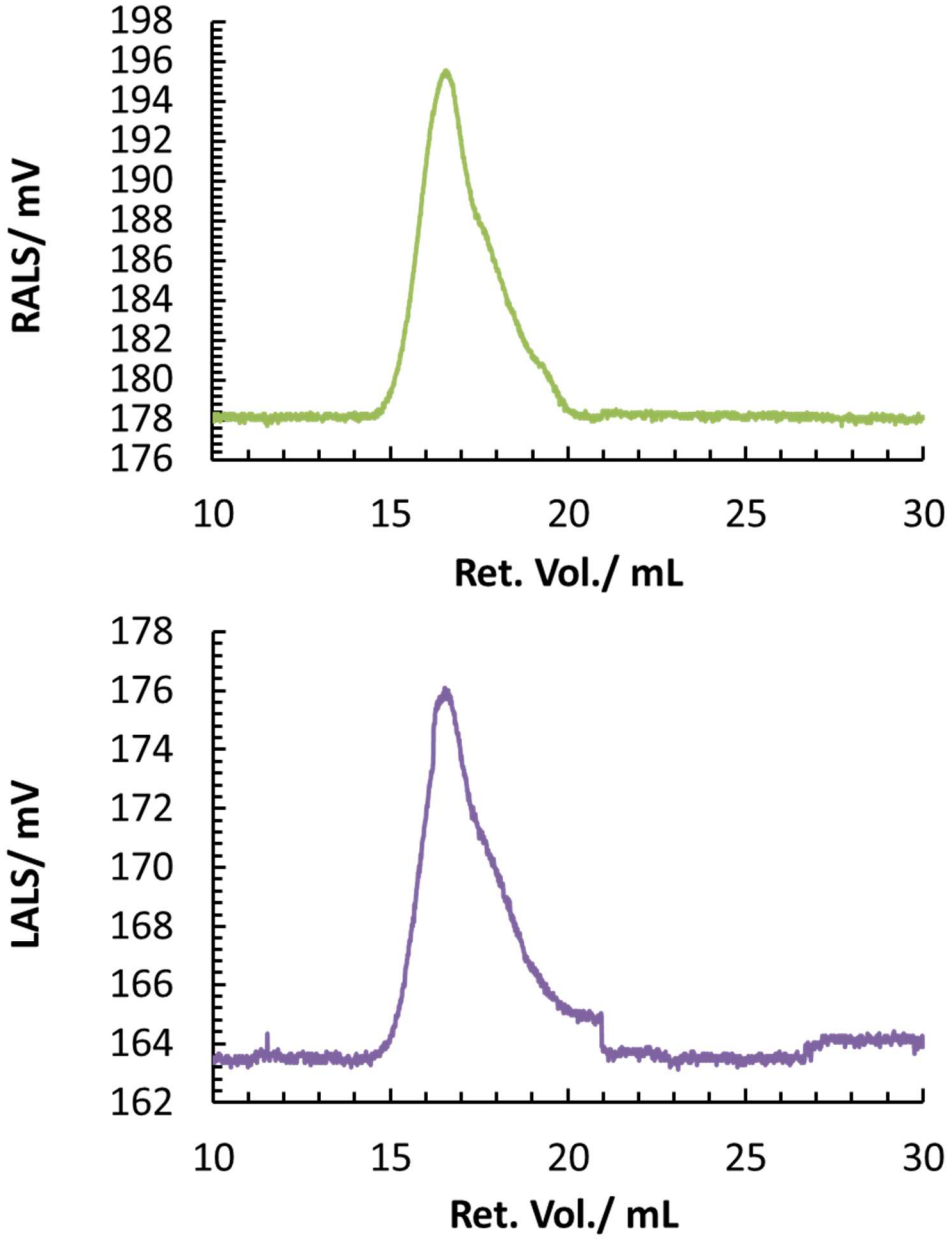

Fig. A9. Raw GPC chromatogram of RALS (green) and LALS (purple) traces of DBiB-p(OEGMA)$_{50}$-co-(EGDMA)$_{0.95}$. Analysis performed by GPC with mobile phase of DMF (+ 0.01M) at 1mL/min 60 ˚C. Ret.; retention. Vol.; volume.

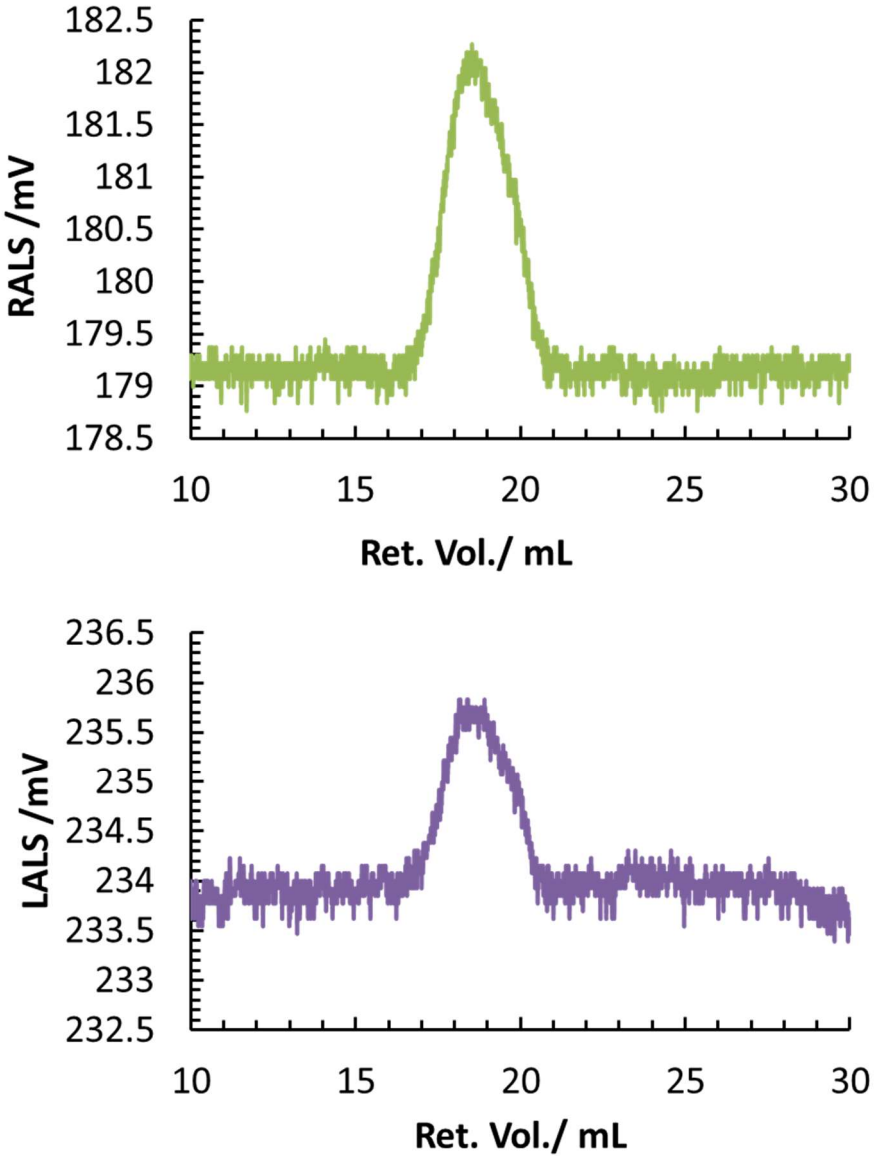

Fig. A10. Raw GPC chromatograms of RALS (green) and LALS (purple) traces of DBiB-p(OEGMA)$_{10}$-co-(PEGDMA)$_{0.2}$. Analysis performed by GPC with mobile phase of DMF (+ 0.01M) at 1mL/min 60 ˚C. Ret.; retention. Vol.; volume.

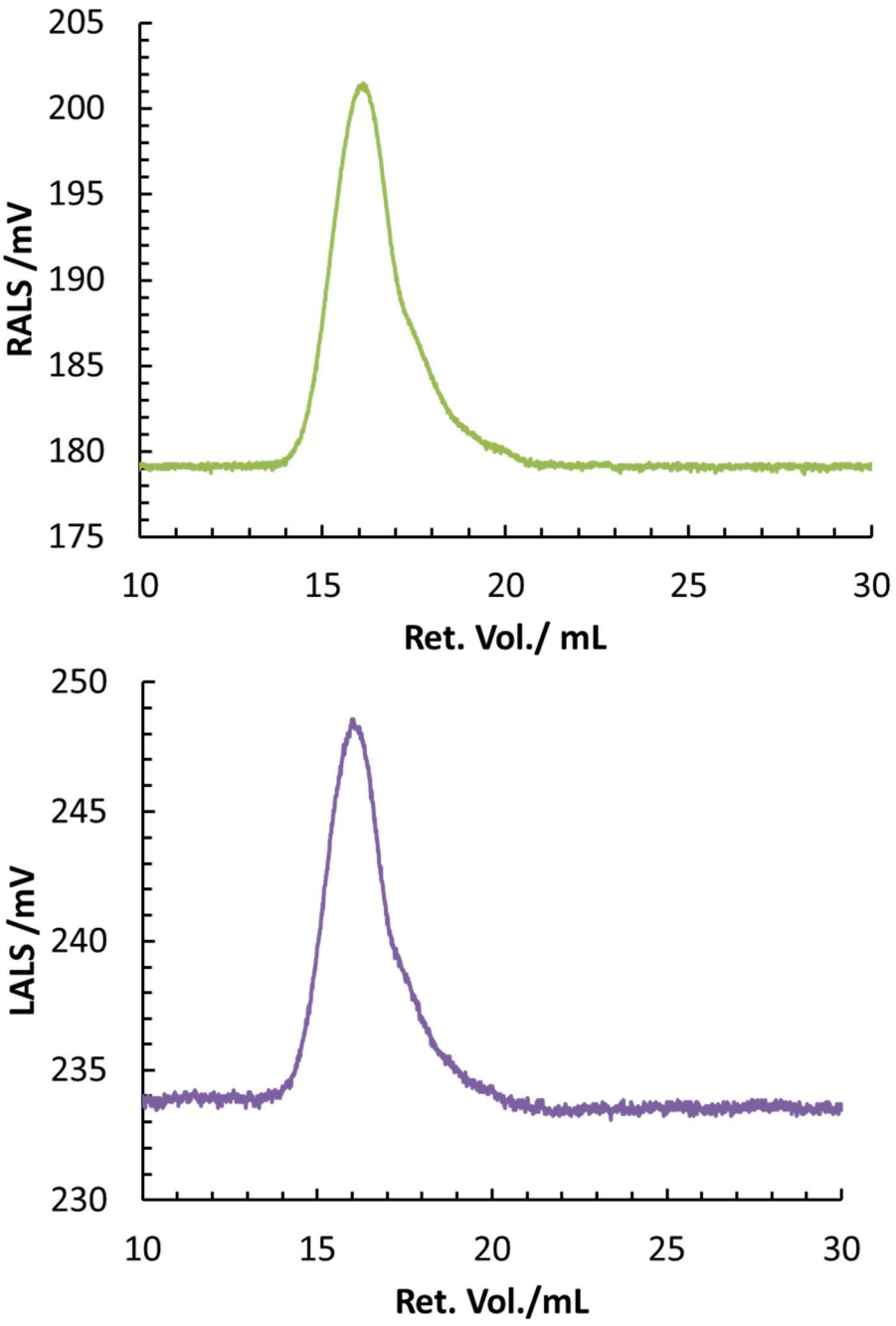

Fig. A11. Raw GPC chromatogramsa **of** RALS (green) and LALS (purple) traces of DBiB-p(OEGMA)$_{10}$-co-(PEGDMA)$_{0.5}$. Analysis performed by GPC with mobile phase of DMF (+ 0.01M) at 1mL/min 60 ˚C. Ret.; retention. Vol.; volume.

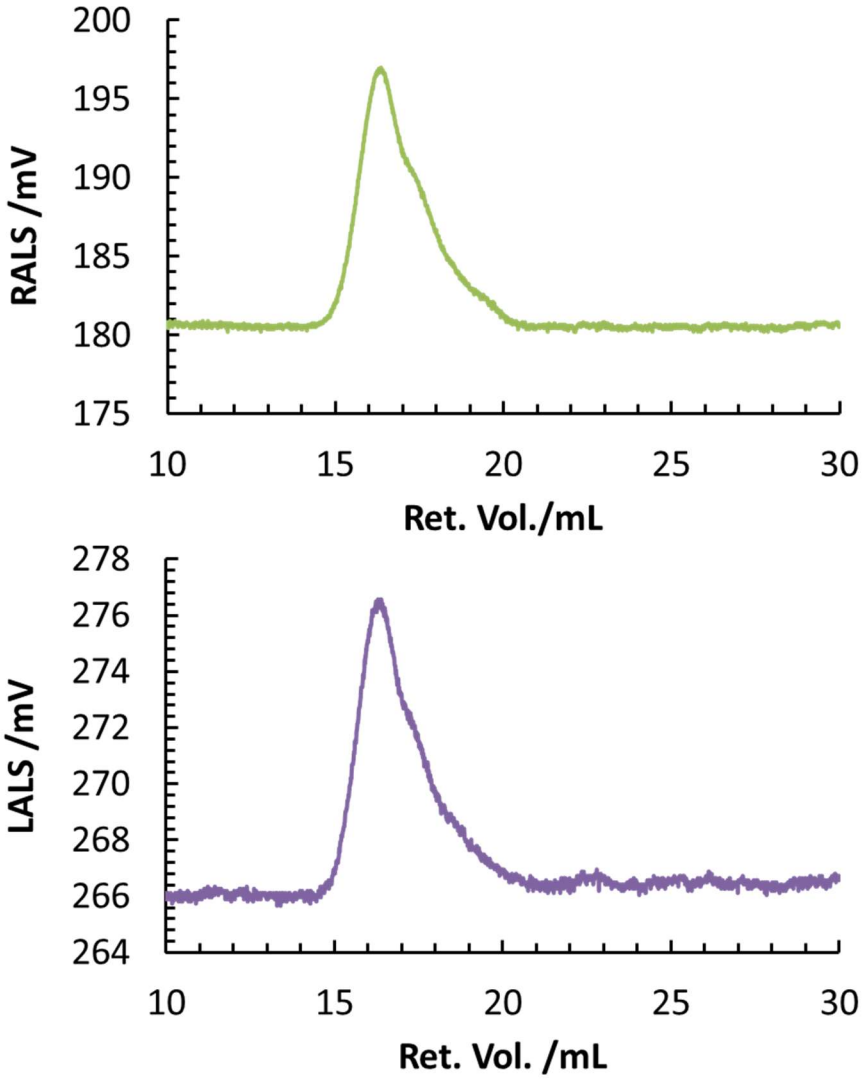

Fig. A12. Raw GPC chromatograms of RALS (green) and LALS (purple) traces of DBiB-p(OEGMA)$_{20}$-co-(PEGDMA)$_{0.5}$ from GPC. Analysis performed by GPC with mobile phase of DMF (+ 0.01M) at 1mL/min 60 ˚C. Ret.; retention. Vol.; volume.

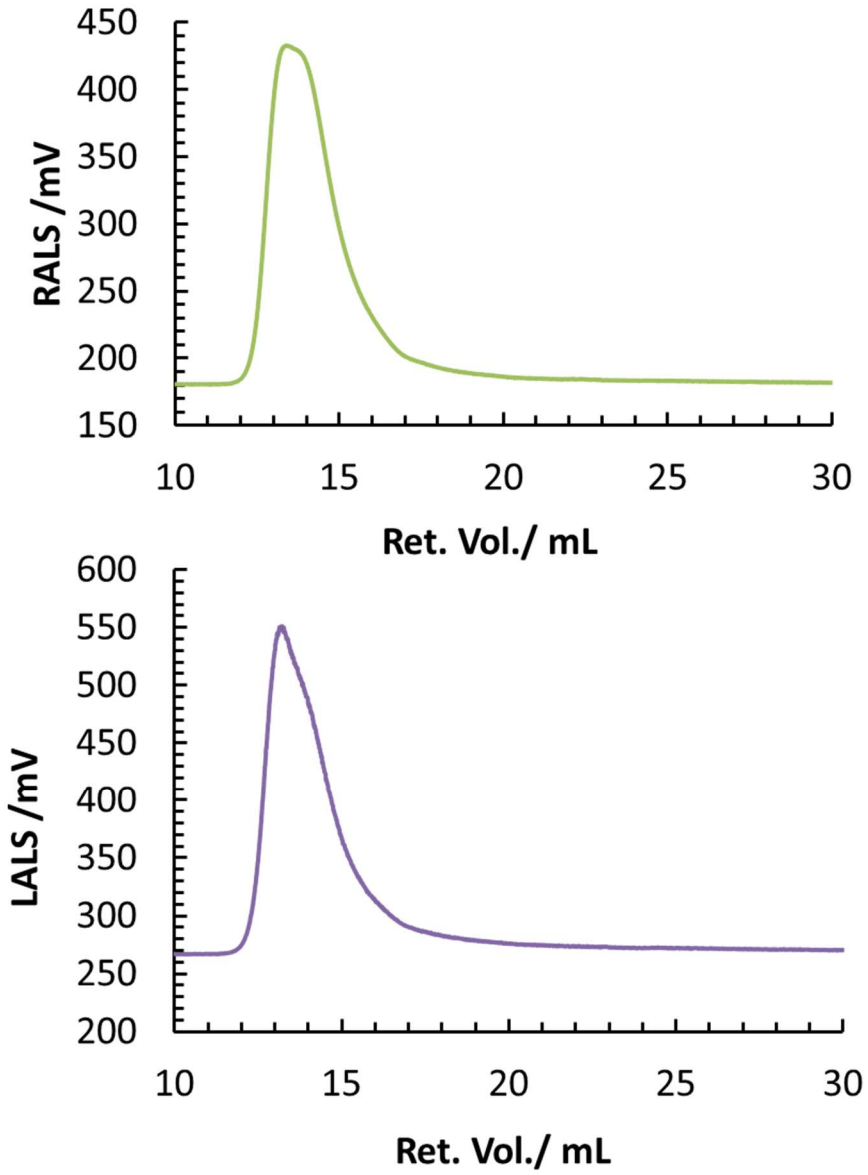

Fig. A13. Raw GPC chromatograms of RALS (green) and LALS (purple) traces of DBiB-p(OEGMA)$_{20}$-co-(PEGDMA)$_{0.7}$. Analysis performed by GPC with mobile phase of DMF (+ 0.01M) at 1mL/min 60 ˚C. Ret.; retention. Vol.; volume.

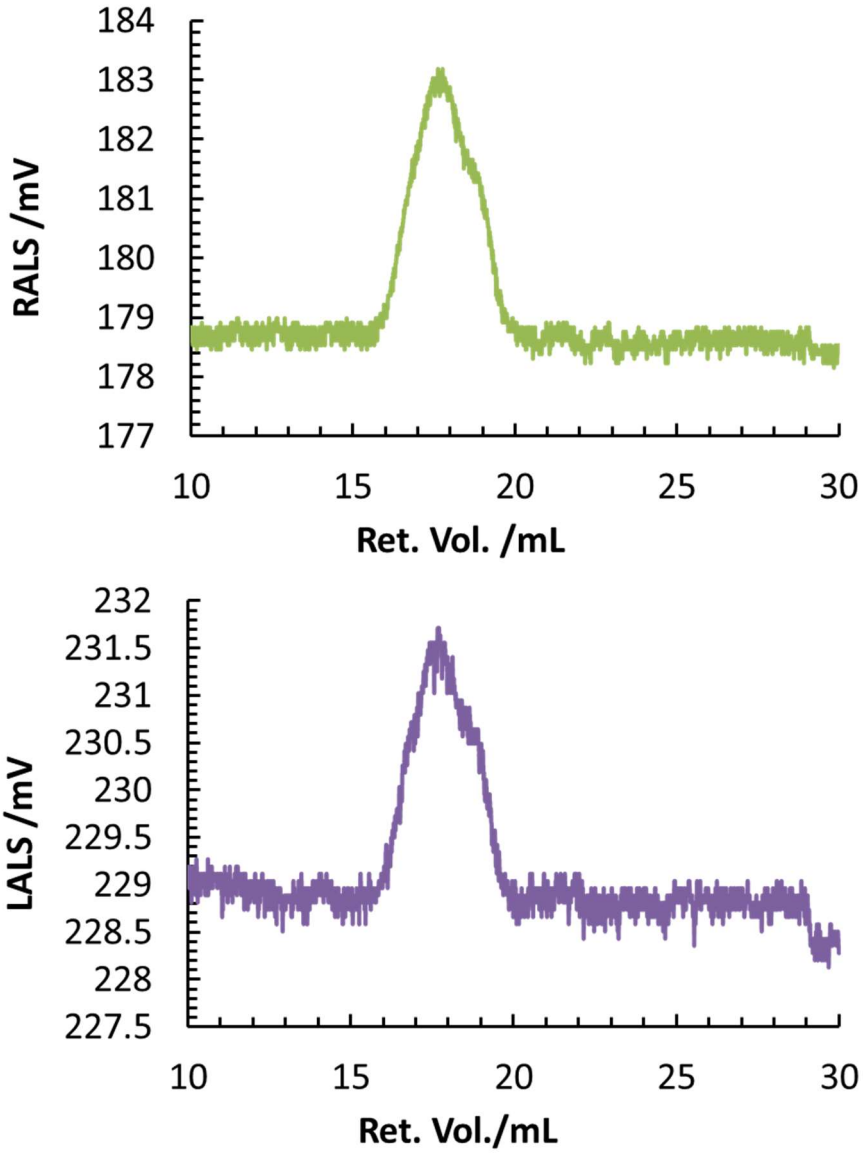

Fig. A14. Raw GPC chromatograms of RALS (green) and LALS (purple) traces of DBiB-p(OEGMA)$_{50}$-co-(PEGDMA)$_{0.2}$. Analysis performed by GPC with mobile phase of DMF (+ 0.01M) at 1mL/min 60 ˚C. Ret.; retention. Vol.; volume.

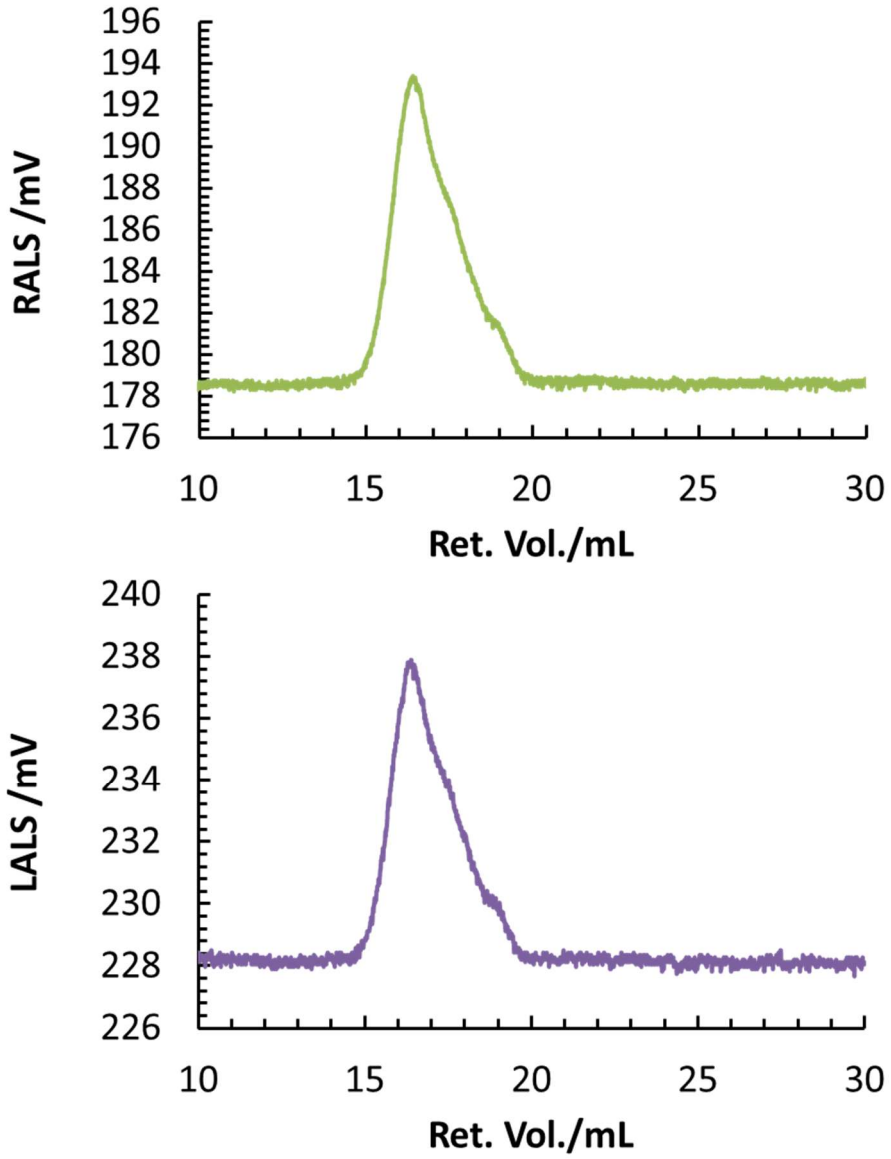

Fig. A15. Raw GPC chromatograms of RALS (green) and LALS (purple) traces of DBiB-p(OEGMA)$_{50}$-co-(PEGDMA)$_{0.5}$. Analysis performed by GPC with mobile phase of DMF (+ 0.01M) at 1mL/min 60 ˚C. Ret.; retention. Vol.; volume.

Laser diffraction results obtained for DBiB-(OEGMA) based polymers obtained on Mastersizer 2000.

Day	Span	D[4,3]	D[3,2]	d(0.1)	d(0.5)	d(0.9)
0	1.20	2.61	2.15	1.31	2.40	4.19
1	0.91	2.36	2.09	1.39	1.51	3.46
3	1.26	2.09	1.72	1.07	1.85	3.39
5	1.18	2.99	2.46	1.51	2.77	4.78
7	1.43	2.62	2.06	1.20	2.31	4.51
11	1.14	3.49	2.85	1.79	3.26	5.52

Fig. A16. Laser diffraction data obtained for *n*-dodecane emulsion droplet stabilised with DBiB-p(OEGMA)$_{10}$ on day 0,1,3,5,7 and 11. Span, D[4,3], D[3,2], d(0.1), d(0.5) and d(0.9) are given in μm. d(0.1) = D(10 %), d(0.5) = D(50 %) and d(0.9) = D(90 %).

Day 0

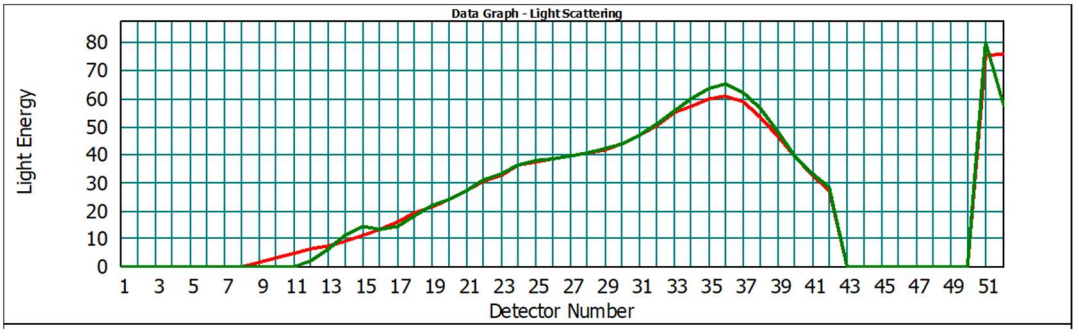

Day 11

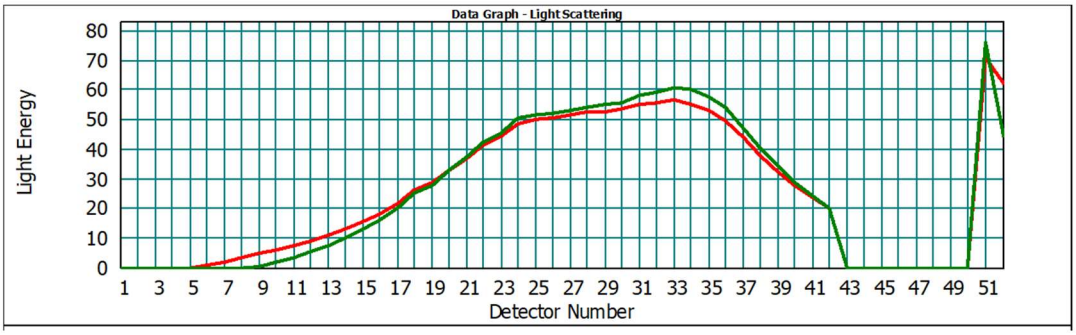

Fig. A17. Laser diffraction graph obtained for *n*-dodecane emulsion droplet stabilised with DBiB-p(OEGMA)$_{10}$ on day 0 and 11.

Day	Span	D[4,3]	D[3,2]	d(0.1)	d(0.5)	d(0.9)
0	1.75	1.33	0.37	0.11	1.32	2.41
1	1.05	1.84	1.59	1.03	1.71	2.83
3	1.02	2.23	1.94	1.25	2.11	3.39
5	0.98	2.78	2.41	1.58	2.63	4.17
7	0.97	2.79	2.42	1.60	2.65	4.17
11	0.79	3.14	2.86	2.04	3.02	4.42

Fig. A18. Laser diffraction data obtained for n-dodecane emulsion droplet stabilised with DBiB-p(OEGMA)$_{20}$ on day 0,1,3,5,7 and 11. Span, D[4,3], D[3,2], d(0.1), d(0.5) and d(0.9) are given in μm. d(0.1) = D(10 %), d(0.5) = D(50 %) and d(0.9) = D(90 %).

Day 0

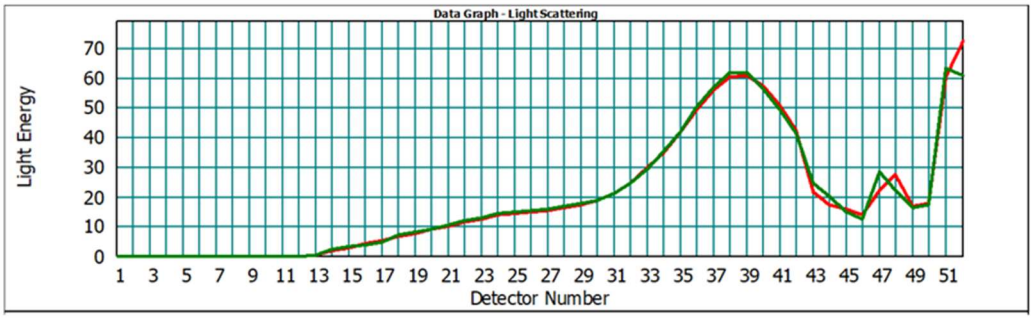

Day 11

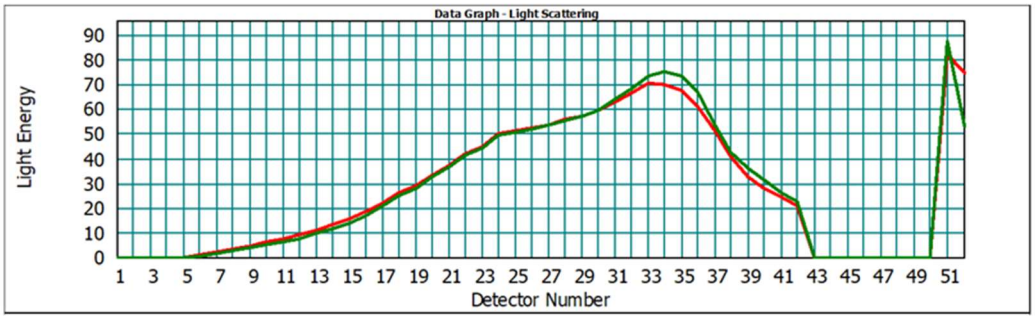

Fig. A19. Laser diffraction graph obtained for *n*-dodecane emulsion droplet stabilised with DBiB-p(OEGMA)$_{20}$ on day 0 and 11.

Day	Span	D[4,3]	D[3,2]	d(0.1)	d(0.5)	d(0.9)
0	1.17	3.09	2.52	1.54	2.88	4.92
1	1.18	3.43	2.78	1.71	3.20	5.48
3	1.12	3.13	2.61	1.64	2.93	4.93

Fig. A20. Laser diffraction data obtained for *n*-dodecane emulsion droplet stabilised with DBiB-p(OEGMA)$_{50}$ on day 0,1 and 3. Span, D[4,3], D[3,2], d(0.1), d(0.5) and d(0.9) are given in μm. d(0.1) = D(10 %), d(0.5) = D(50 %) and d(0.9) = D(90 %).

Day 0

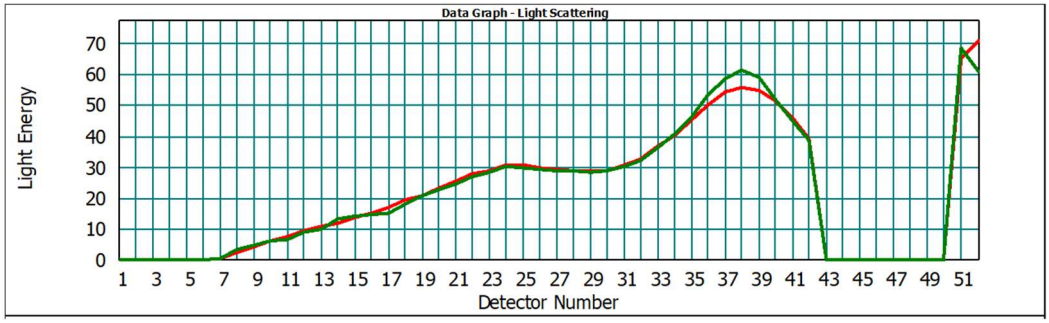

Day 3

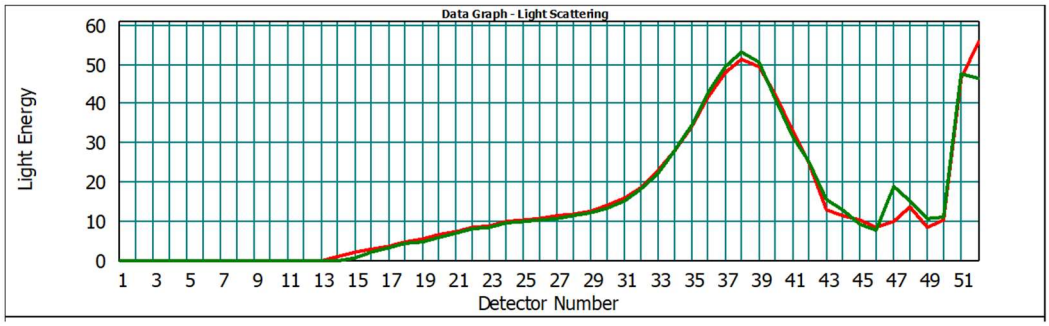

Fig. A21. Laser diffraction graph obtained for *n*-dodecane emulsion droplet stabilised with DBiB-p(OEGMA)$_{50}$ on day 0 and 3.

EGDMA WA# 3 - 4

Day	Span	D[4,3]	D[3,2]	d(0.1)	d(0.5)	d(0.9)
0	1.15	3.57	2.90	1.81	3.34	5.67
1	1.01	3.35	2.80	1.84	3.20	5.09
3	1.01	4.01	3.40	2.31	3.77	6.13
5	1.13	3.75	3.04	1.94	3.52	5.93
7	1.09	4.09	3.36	2.21	3.83	6.39
13	1.08	4.44	3.61	2.42	4.17	6.92
21	1.03	4.73	3.96	2.69	4.42	7.27

Fig. A22. Laser diffraction data obtained for *n*-dodecane emulsion droplet stabilised with DBiB-p(OEGMA)$_{10}$-*co*-(EGDMA)$_{0.5}$ on day 0,1,3,5,7,13 and 21. Span, D[4,3], D[3,2], d(0.1), d(0.5) and d(0.9) are given in μm. d(0.1) = D(10 %), d(0.5) = D(50 %) and d(0.9) = D(90 %).

Day 0

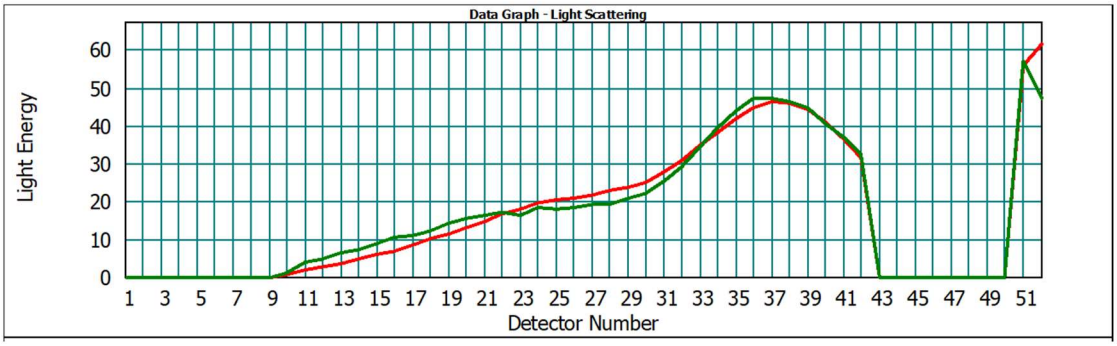

Day 21

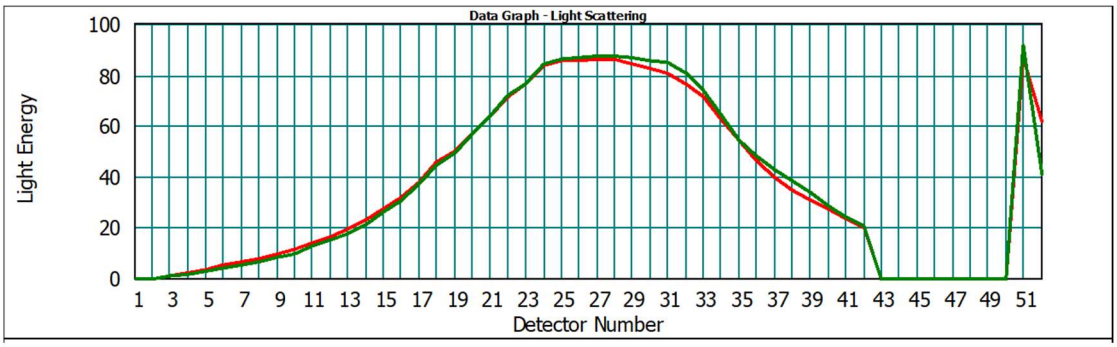

Fig. A23. Laser diffraction graph obtained for *n*-dodecane emulsion droplet stabilised with DBiB-p(OEGMA)$_{10}$-*co*-(EGDMA)$_{0.5}$ on day 0 and 21.

Day	Span	D[4,3]	D[3,2]	d(0.1)	d(0.5)	d(0.9)
0	4.96	4.69	1.69	0.93	1.89	10.82
1	1.20	2.77	2.24	1.32	2.59	4.44
3	1.13	3.19	2.62	1.61	3.01	5.01
5	1.13	3.75	3.04	1.94	3.52	5.92
7	1.03	3.69	3.08	2.04	3.50	5.65
13	1.10	6.96	3.64	2.45	4.06	6.93
21	0.84	4.64	4.21	2.96	4.38	6.65

Fig. A24. Laser diffraction data obtained for *n*-dodecane emulsion droplet stabilised with DBiB-p(OEGMA)$_{20}$-*co*-(EGDMA)$_{0.2}$ on day 0,1,3, 5, 7, 13 and 21. Span, D[4,3], D[3,2], d(0.1), d(0.5) and d(0.9) are given in μm. d(0.1) = D(10 %), d(0.5) = D(50 %) and d(0.9) = D(90 %).

Day 0

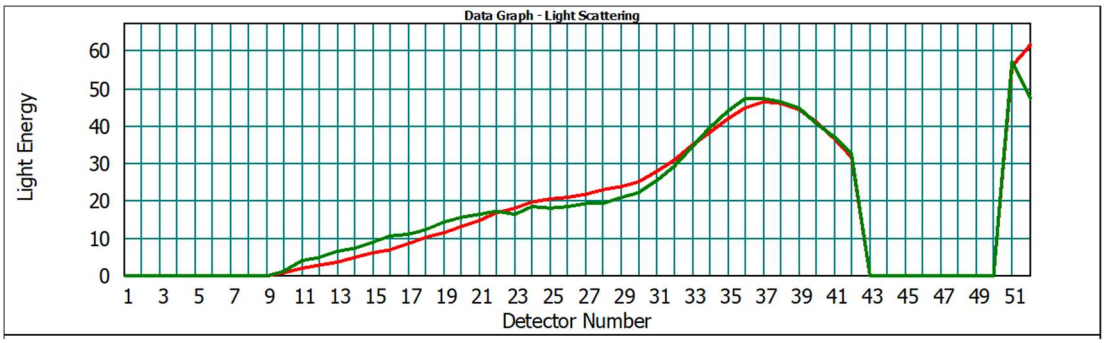

Day 21

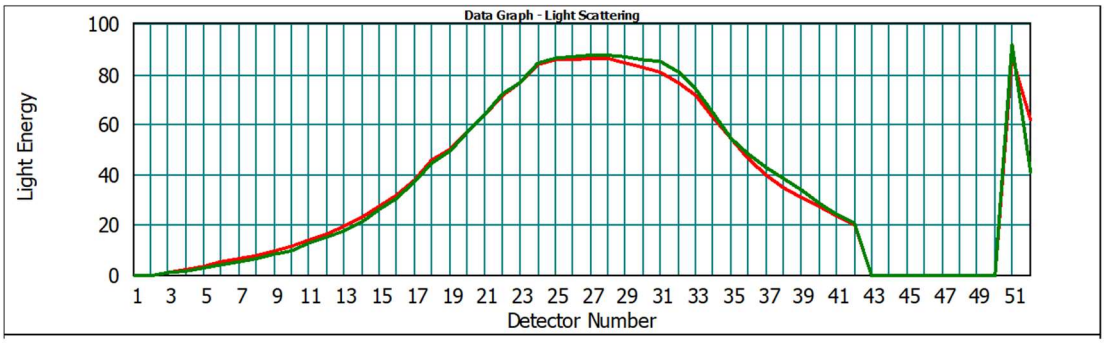

Fig. A25. Laser diffraction graph obtained for *n*-dodecane emulsion droplet stabilised with DBiB-p(OEGMA)$_{20}$-*co*-(EGDMA)$_{0.2}$ on day 0 and 21.

Day	Span	D[4,3]	D[3,2]	d(0.1)	d(0.5)	d(0.9)
0	1.90	0.94	0.40	0.15	0.86	1.78
1	1.58	1.26	0.37	0.11	1.30	2.17
3	0.70	1.81	1.68	1.22	1.75	2.46
5	0.77	2.10	1.92	1.35	2.04	2.92
7	0.76	2.25	2.06	1.46	2.19	3.13
13	0.77	2.60	2.37	1.69	2.52	3.62
21	0.67	3.23	3.02	2.25	3.13	4.37

Fig. A26. Laser diffraction data obtained for *n*-dodecane emulsion droplet stabilised with DBiB-p(OEGMA)$_{50}$-*co*-(EGDMA)$_{0.7}$ on day 0,1,3, 5, 7,13 and 21. Span, D[4,3], D[3,2], d(0.1), d(0.5) and d(0.9) are given in μm. d(0.1) = D(10 %), d(0.5) = D(50 %) and d(0.9) = D(90 %).

Day 0

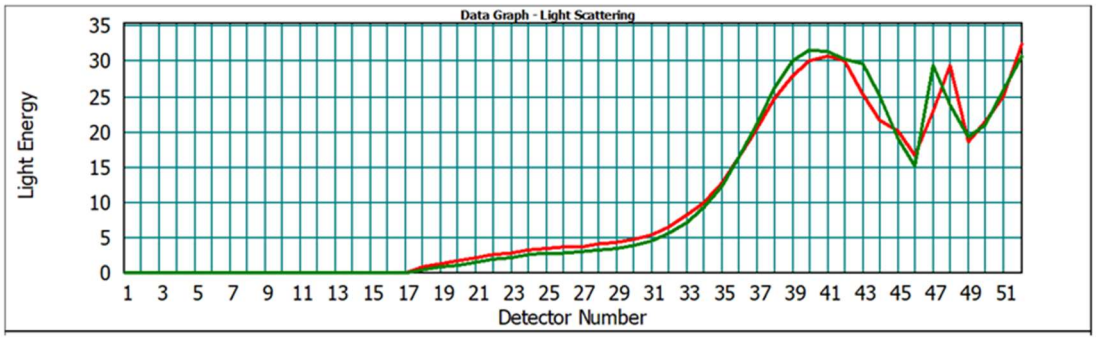

Day 21

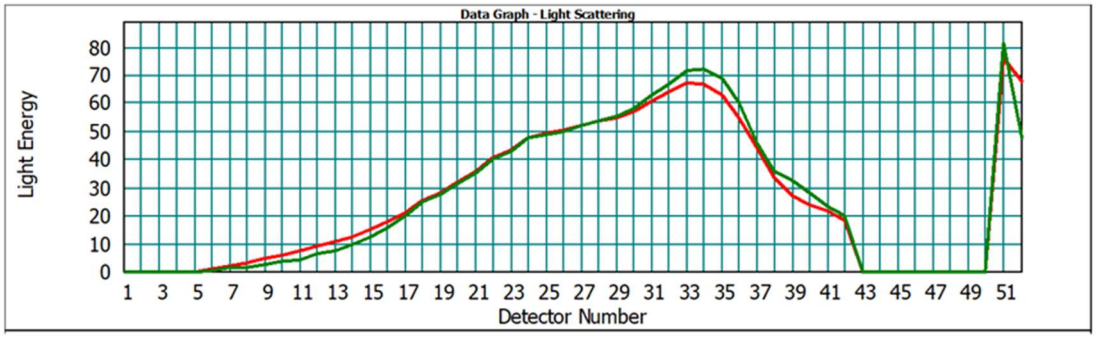

Fig. A27. Laser diffraction graph obtained for *n*-dodecane emulsion droplet stabilised with DBiB-p(OEGMA)$_{50}$-*co*-(EGDMA)$_{0.7}$ on day 0 and 21.

EGDMA WA# 6-9

Day	Span	D[4,3]	D[3,2]	d(0.1)	d(0.5)	d(0.9)
0	0.99	4.37	3.63	2.53	4.13	6.63
1	0.98	4.72	3.96	2.76	4.45	7.13
3	0.97	4.43	3.73	2.60	4.19	6.68
5	0.97	4.57	3.89	2.71	4.31	6.88
7	0.99	4.63	3.91	2.69	4.36	7.02
13	1.01	4.87	4.01	2.81	4.59	7.43
21	0.78	4.85	4.45	3.20	4.60	6.81

Fig. A28. Laser diffraction data obtained for *n*-dodecane emulsion droplet stabilised with DBiB-p(OEGMA)$_{10}$-*co*-(EGDMA)$_{0.6}$ on day 0,1,3, 5, 7, 13 and 21. Span, D[4,3], D[3,2], d(0.1), d(0.5) and d(0.9) are given in μm. d(0.1) = D(10 %), d(0.5) = D(50 %) and d(0.9) = D(90 %).

Day 0

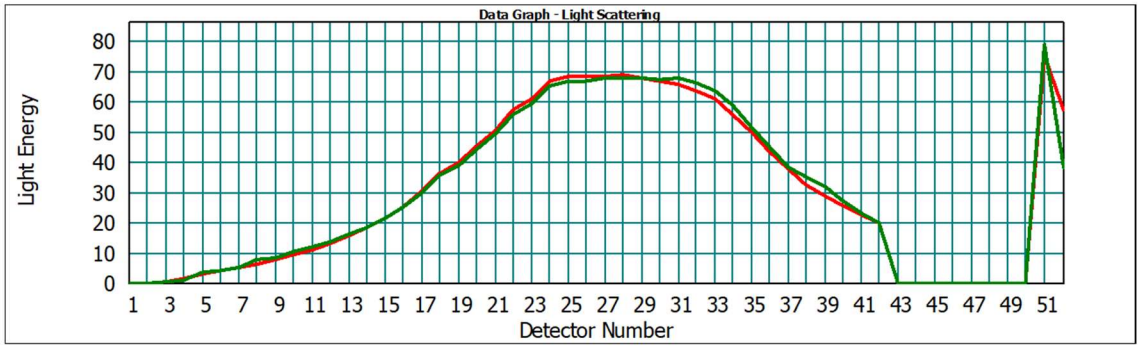

Day 21

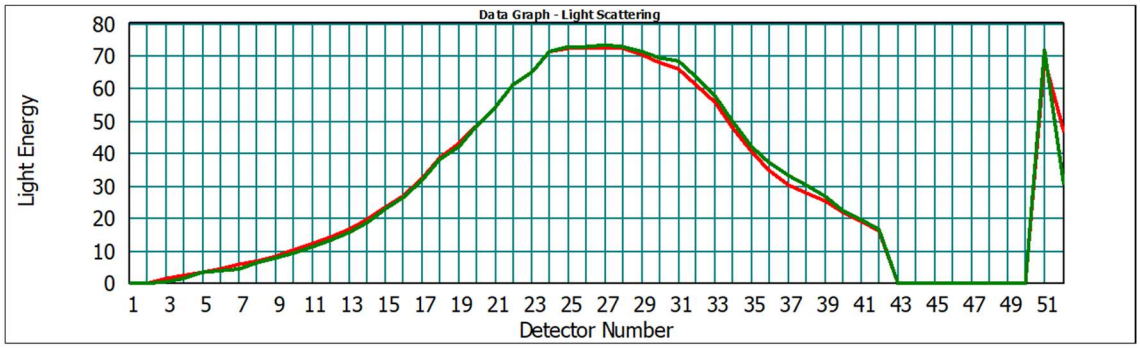

Fig. A29. Laser diffraction graph obtained for *n*-dodecane emulsion droplet stabilised with DBiB-p(OEGMA)$_{10}$-*co*-(EGDMA)$_{0.6}$ on day 0 and 21.

Day	Span	D[4,3]	D[3,2]	d(0.1)	d(0.5)	d(0.9)
0	1.22	2.36	1.90	1.10	2.22	3.80
1	1.04	2.59	2.19	1.37	2.47	3.95
3	1.00	2.93	2.51	1.62	2.80	4.44
5	0.92	3.18	2.75	1.84	3.04	4.73
7	0.72	2.10	1.95	1.40	2.03	2.88
13	0.89	2.74	2.40	1.62	2.62	4.02
21	0.87	4.31	3.90	2.71	4.08	6.26

Fig. A30. Laser diffraction data obtained for *n*-dodecane emulsion droplet stabilised with DBiB-p(OEGMA)$_{20}$-*co*-(EGDMA)$_{0.5}$ on day 0,1,3, 5, 7, 13 and 21. Span, D[4,3], D[3,2], d(0.1), d(0.5) and d(0.9) are given in μm. d(0.1) = D(10 %), d(0.5) = D(50 %) and d(0.9) = D(90 %).

Day 0

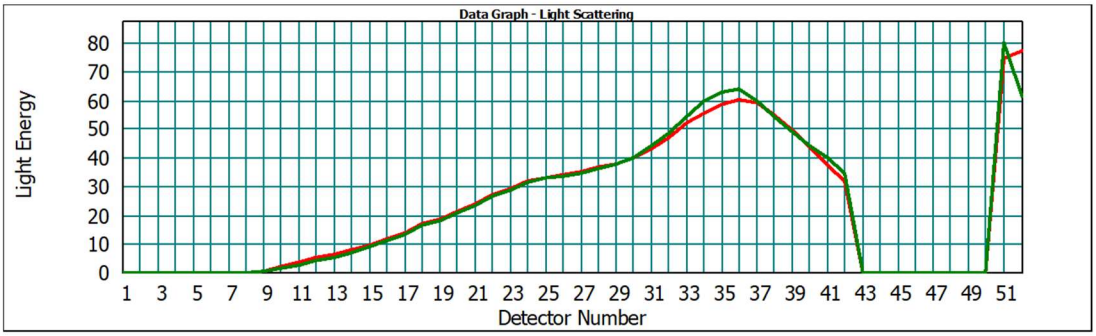

Day 21

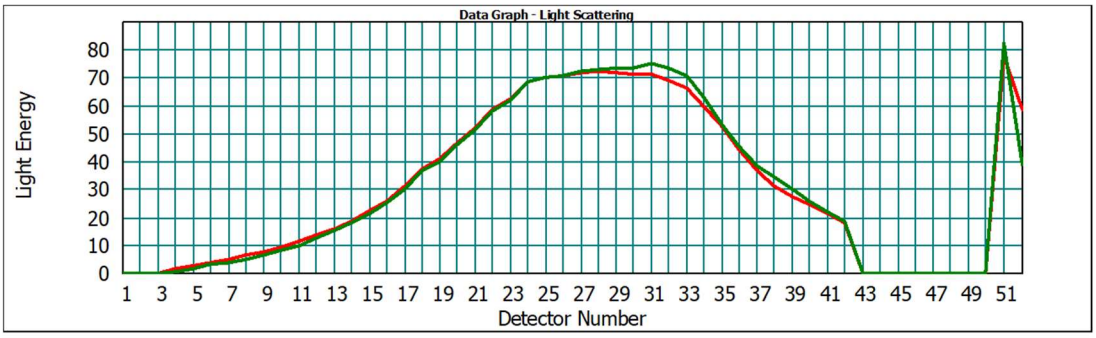

Fig. A31. Laser diffraction graph obtained for *n*-dodecane emulsion droplet stabilised with DBiB-p(OEGMA)$_{20}$-*co*-(EGDMA)$_{0.5}$ on day 0 and 21.

Day	Span	D[4,3]	D[3,2]	d(0.1)	d(0.5)	d(0.9)
0	1.66	1.12	0.38	0.12	1.12	1.98
1	0.72	1.40	1.35	0.98	1.40	1.98
3	0.89	1.82	1.63	1.11	1.73	2.66
5	1.09	1.46	1.12	0.74	1.42	2.21
7	0.84	2.11	1.90	1.31	2.02	3.02
13	0.75	2.45	2.25	1.59	2.38	3.40
21	0.79	2.81	2.55	1.80	2.71	3.94

Fig. A32. Laser diffraction data obtained for *n*-dodecane emulsion droplet stabilised with DBiB-p(OEGMA)$_{50}$-*co*-(EGDMA)$_{0.95}$ on day 0,1,3, 5, 7, 13 and 21. Span, D[4,3], D[3,2], d(0.1), d(0.5) and d(0.9) are given in μm. d(0.1) = D(10 %), d(0.5) = D(50 %) and d(0.9) = D(90 %).

Day 0

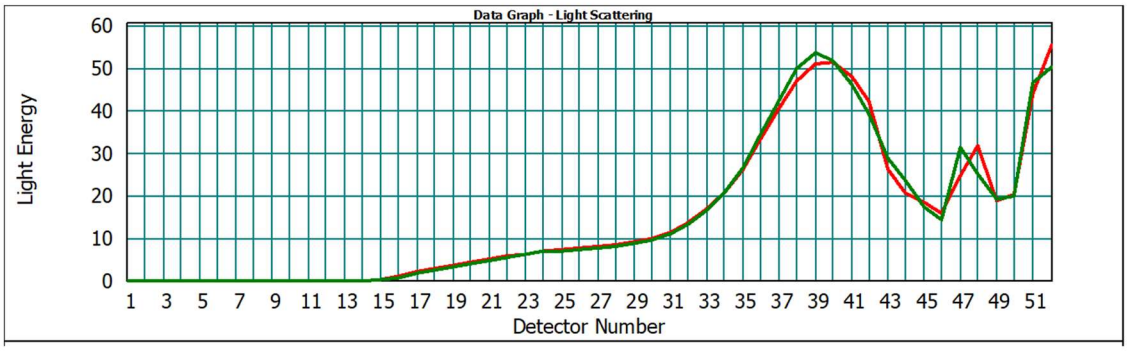

Day 21

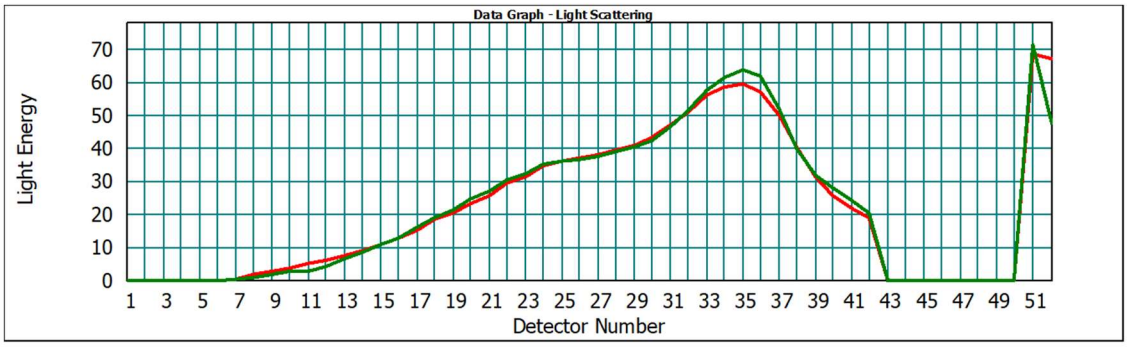

Fig. A33. Laser diffraction graph obtained for *n*-dodecane emulsion droplet stabilised with DBiB-p(OEGMA)$_{50}$-*co*-(EGDMA)$_{0.95}$ on day 0 and 21.

PEGDMA #WA=3

Day	Span	D[4,3]	D[3,2]	d(0.1)	d(0.5)	d(0.9)
0	1.17	3.09	2.52	1.54	2.88	4.92
1	1.18	3.43	2.78	1.72	3.20	5.48
3	1.12	3.13	2.61	1.64	2.93	4.92

Fig. A34. Laser diffraction data obtained for *n*-dodecane emulsion droplet stabilised with DBiB-p(OEGMA)$_{10}$-*co*-(PEGDMA)$_{0.2}$ on day 0,1 and 3. Span, D[4,3], D[3,2], d(0.1), d(0.5) and d(0.9) are given in μm. d(0.1) = D(10 %), d(0.5) = D(50 %) and d(0.9) = D(90 %).

Day 0

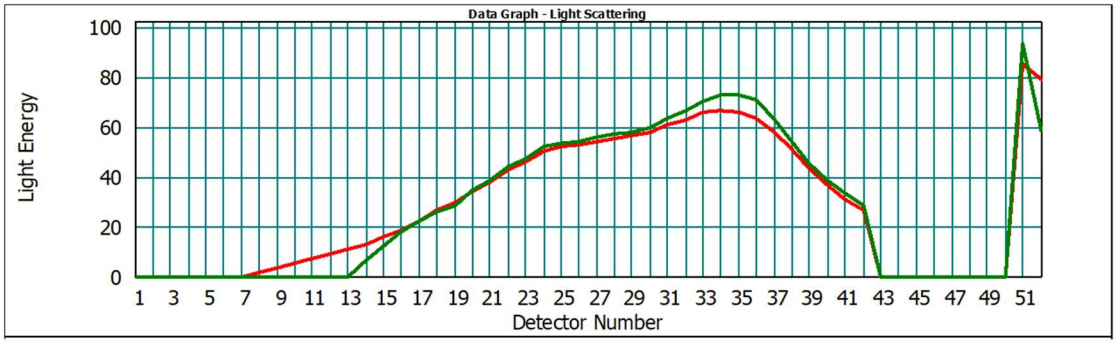

Day 3

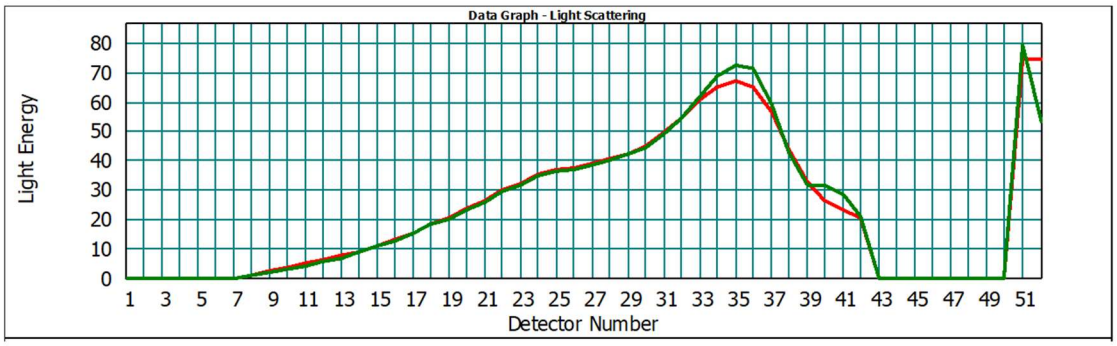

Fig. A35. Laser diffraction graph obtained for *n*-dodecane emulsion droplet stabilised with DBiB-p(OEGMA)$_{10}$-*co*-(PEGDMA)$_{0.2}$ on day 0 and 3.

Day	Span	D[4,3]	D[3,2]	d(0.1)	d(0.5)	d(0.9)
0	1.15	2.21	1.84	1.12	2.06	3.49
1	1.11	2.57	2.15	1.32	2.42	4.02
3	0.96	2.89	2.50	1.65	2.76	4.31
5	0.93	3.05	2.66	1.79	2.91	4.50
7	0.89	3.21	2.83	1.94	3.07	4.69
11	0.87	3.37	3.00	2.09	3.21	4.88

Fig. A36. Laser diffraction data obtained for *n*-dodecane emulsion droplet stabilised with DBiB-p(OEGMA)$_{20}$-*co*-(PEGDMA)$_{0.3}$ on day 0,1,3,5, 7 and 11. Span, D[4,3], D[3,2], d(0.1), d(0.5) and d(0.9) are given in μm. d(0.1) = D(10 %), d(0.5) = D(50 %) and d(0.9) = D(90 %).

Day 0

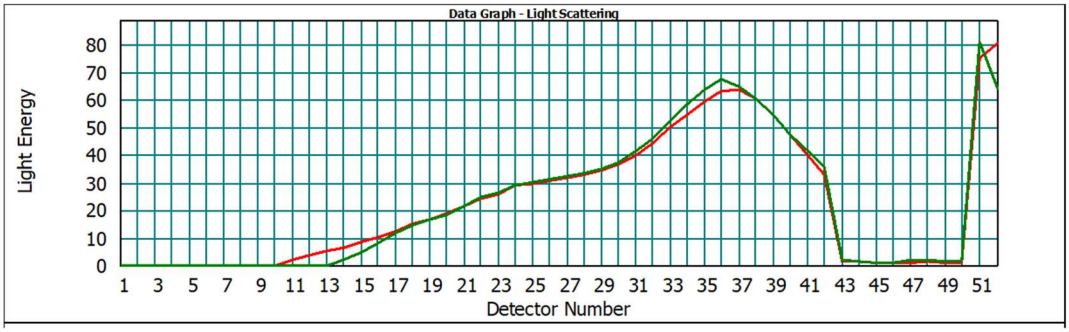

Day 11

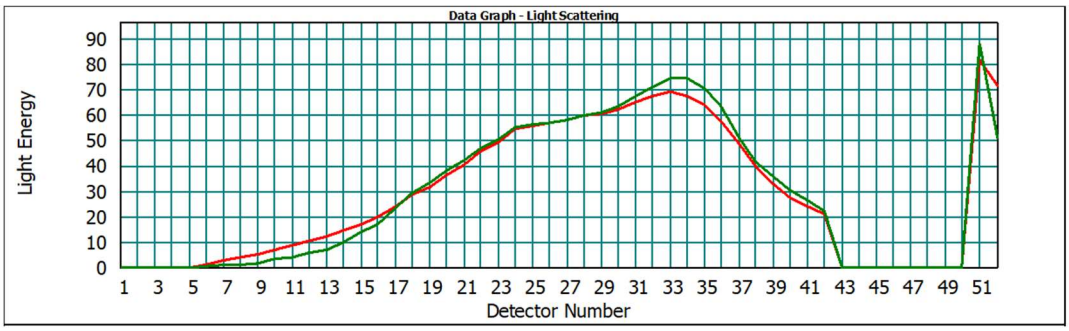

Fig. A37. Laser diffraction graph obtained for *n*-dodecane emulsion droplet stabilised with DBiB-p(OEGMA)$_{20}$-*co*-(PEGDMA)$_{0.3}$ on day 0 and 11.

Day	Span	D[4,3]	D[3,2]	d(0.1)	d(0.5)	d(0.9)
0	1.75	1.10	0.40	0.13	1.07	2.01
1	1.29	1.32	0.69	0.37	1.34	2.08
3	0.76	1.69	1.56	1.11	1.63	2.36
5	0.74	1.89	1.74	1.26	1.82	2.60
7	0.72	1.98	1.83	1.33	1.92	2.71
11	0.75	2.31	2.12	1.51	2.24	3.19

Fig. A38. Laser diffraction data obtained for *n*-dodecane emulsion droplet stabilised with DBiB-p(OEGMA)$_{50}$-*co*-(PEGDMA)$_{0.5}$ on day 0,1,3,5, 7 and 11. Span, D[4,3], D[3,2], d(0.1), d(0.5) and d(0.9) are given in μm. d(0.1) = D(10 %), d(0.5) = D(50 %) and d(0.9) = D(90 %).

Day 0

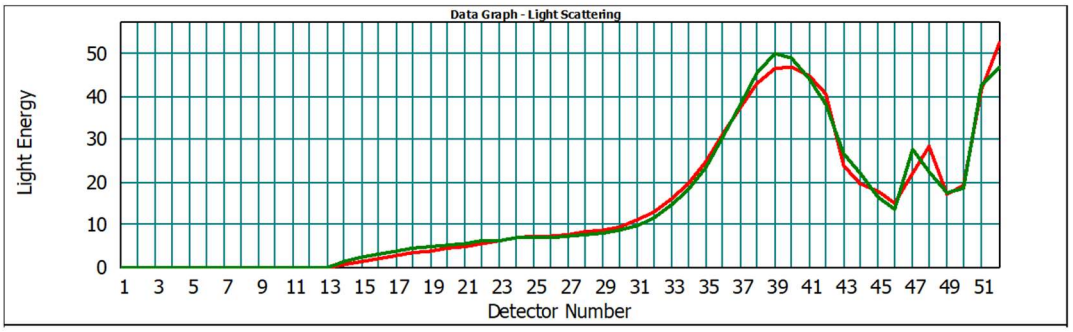

Day 11

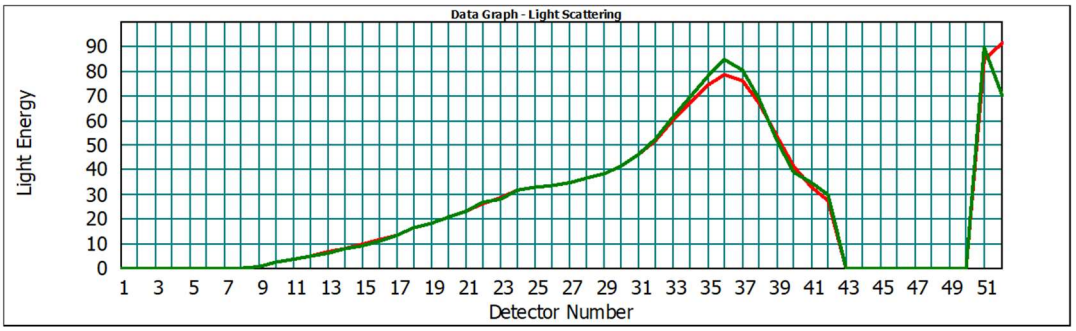

Fig. A39. Laser diffraction graph obtained for *n*-dodecane emulsion droplet stabilised with DBiB-p(OEGMA)$_{50}$-*co*-(PEGDMA)$_{0.5}$ on day 0 and 11.

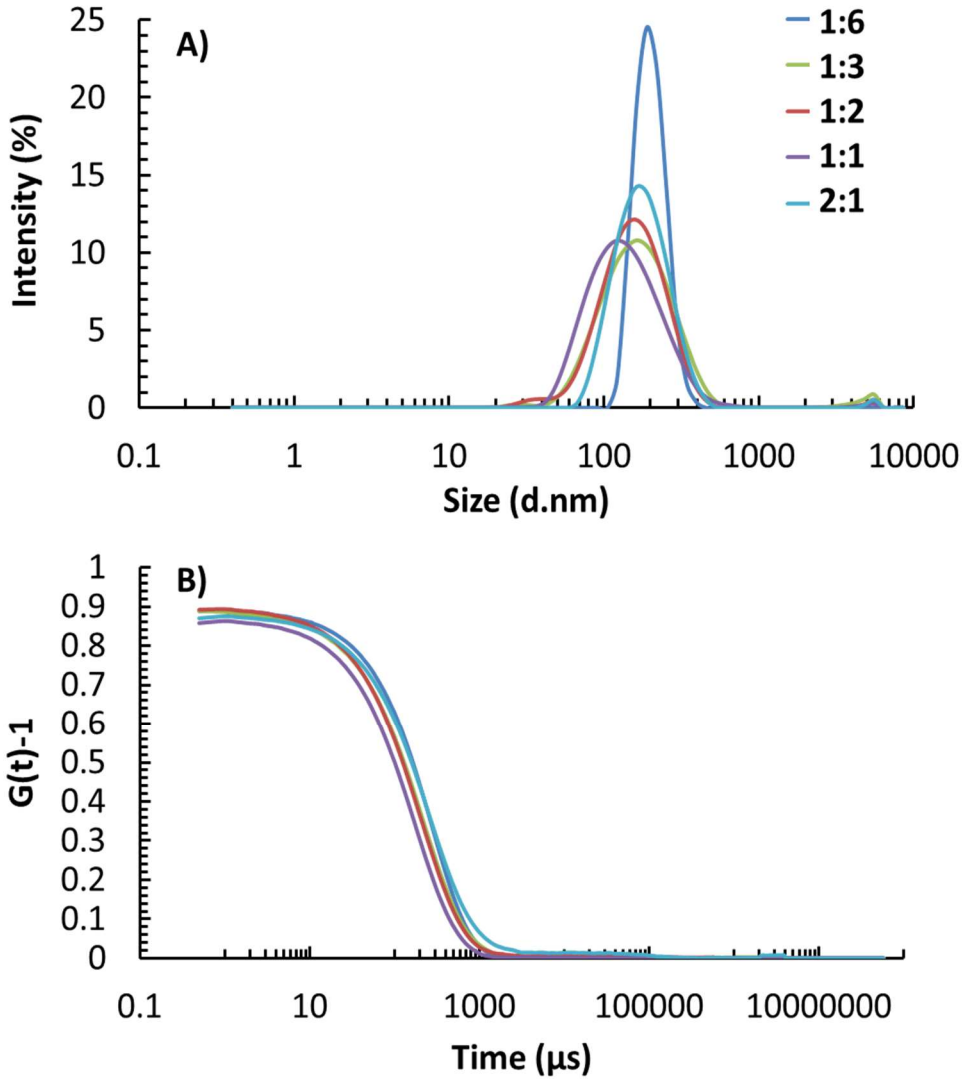

Fig. A40. A) DLS traces and **B)** corresponding correlogram of initial experiments day 0/1 with different compositions. Solvent injection method was performed with 1:6, 1:3, 1:2, 1:1 and 2:1 DBiB-$(OEGMA)_{10}$-*co*-$(EGDMA)_{0.6}$ to Compritol ATO w/w ratio – Related to **Fig. 3.6**

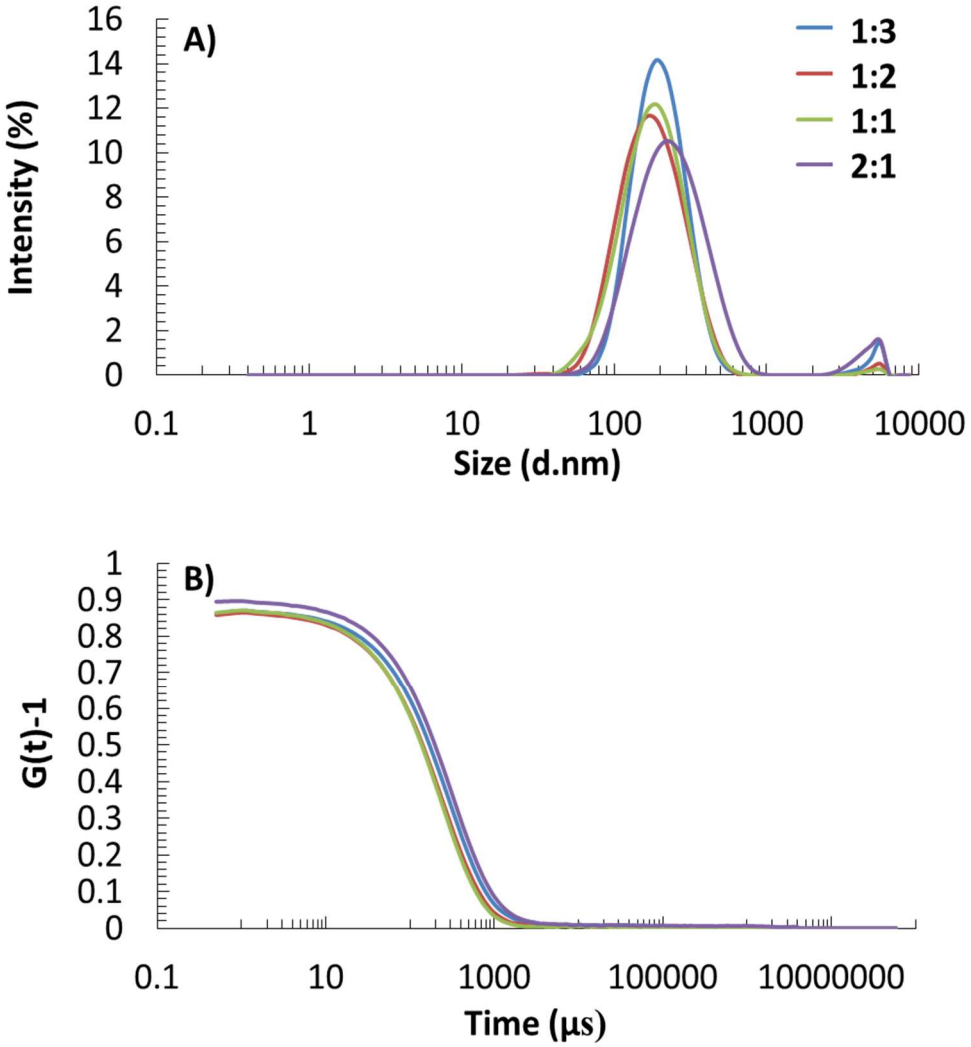

Fig. A41. A) DLS traces and **B)** corresponding correlogram of initial experiments day 5 with different compositions. Solvent injection method was performed with 1:3, 1:2, 1:1 and 2:1 DBiB-$(OEGMA)_{10}$-*co*-$(EGDMA)_{0.6}$ to Compritol ATO w/w ratio – Related to **Fig. 3.6**

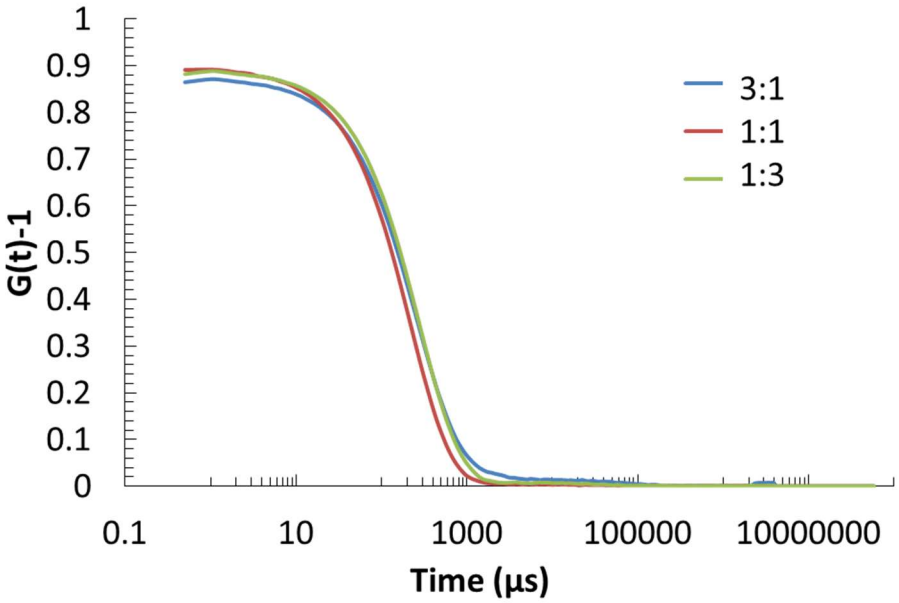

Fig. A42. Correlogram of DBiB-p(OEGMA)$_{10}$ stabilised SLN studies. SLNs were prepared with a Compritol ATO 888 to DBiB-p(OEGMA)10 w/w ratio of 1:3, 1:1 and 3:1 – Related to **Fig. 3.8**

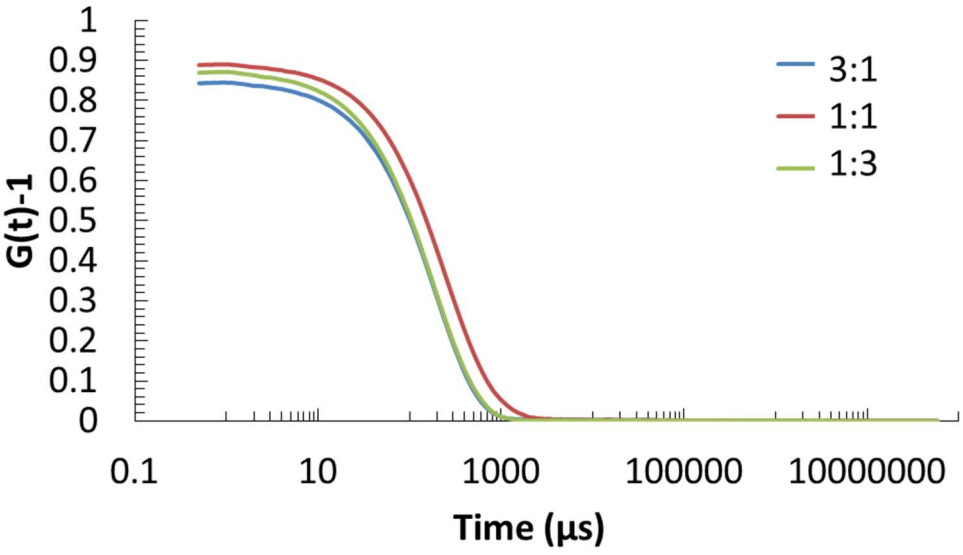

Fig. A43. Correlogram of DBiB-p(OEGMA)$_{10}$-*co*-(EGDMA)$_{0.6}$ stabilised SLN studies. SLNs were prepared with a Compritol ATO 888 to DBiB-p(OEGMA)$_{10}$-*co*-(EGDMA)$_{0.6}$ w/w ratio of 1:3, 1:1 and 3:1 – Related to **Fig. 3.9**

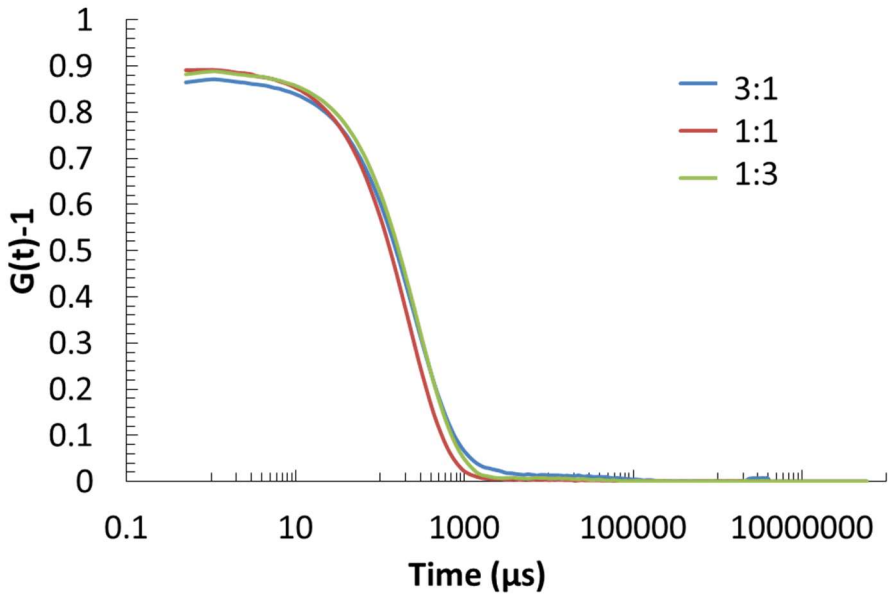

Fig. A44. Correlogram of poloxamer 188 stabilised SLN studies. SLNs were prepared with a Compritol ATO 888 to poloxamer 188 w/w ratio of 1:3, 1:1 and 3:1 – Related to **Fig. 3.10**

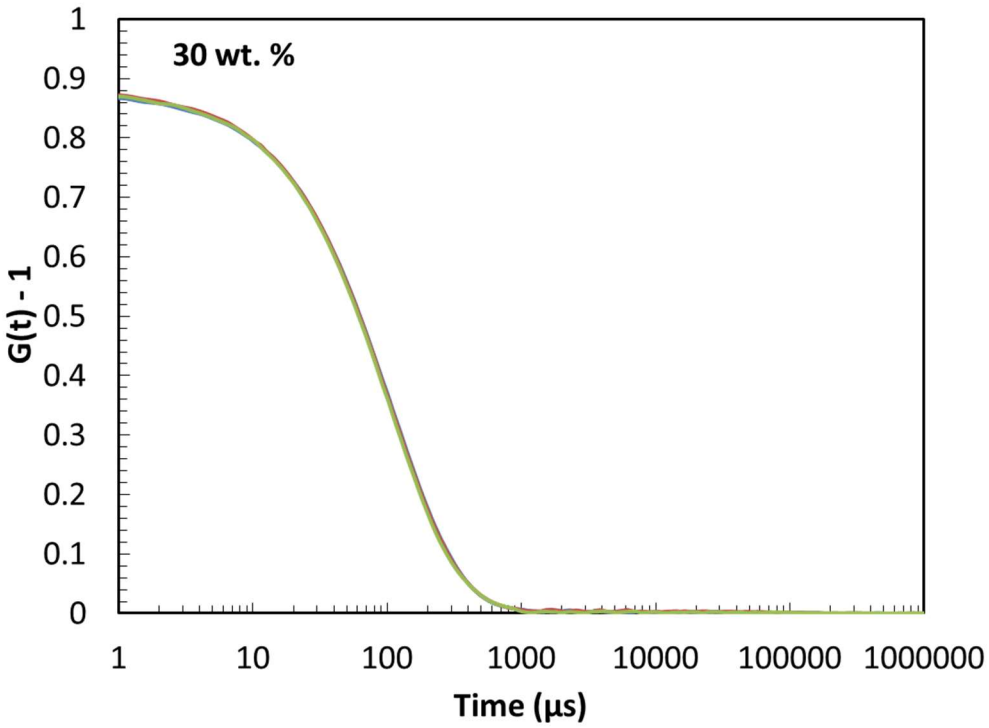

Fig. A45. Correlogram of DLS analysed sample on day 3 containing 1 mL DBiB-p(OEGMA)$_{10}$-*co*-(EGDMA)$_{0.6}$ stabilised SLNs loaded with 30 wt. % MVC. SLNs were prepared with a Compritol ATO 888 to DBiB-p(OEGMA)$_{10}$-*co*-(EGDMA)$_{0.6}$ w/w ratio 3:1 and a solid content of 1.2 mg/mL – Related to **Fig. 4.3**

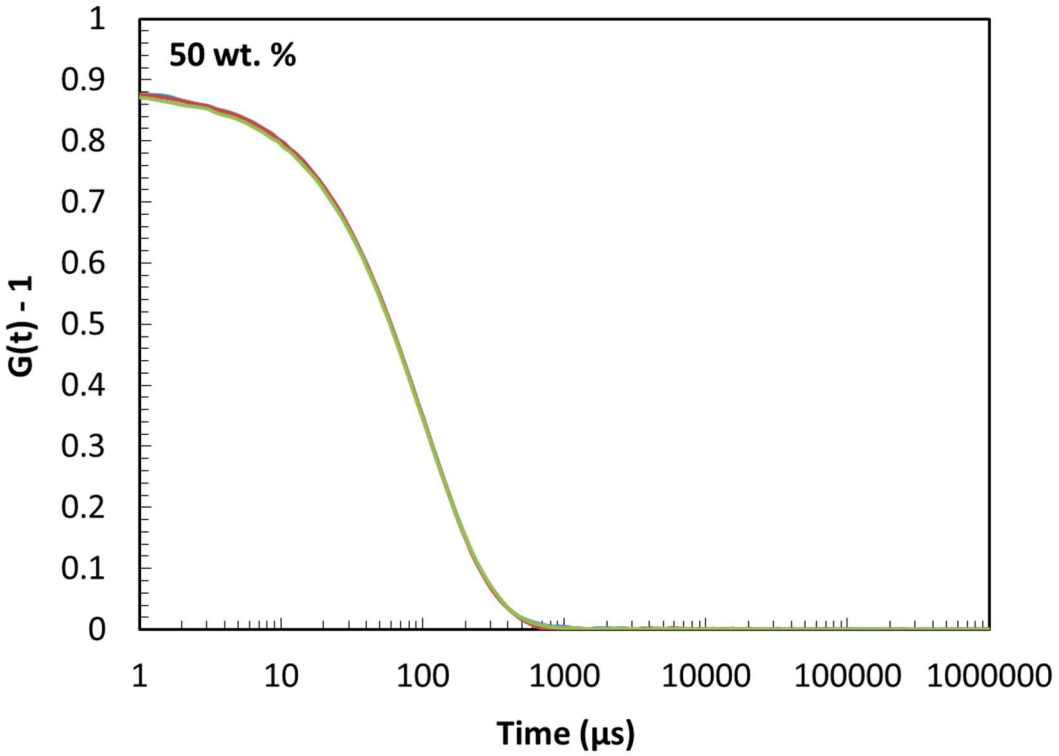

Fig. A46. Correlogram of DLS analysed sample on day 3 containing 1 mL DBiB-p(OEGMA)$_{10}$-*co*-(EGDMA)$_{0.6}$ stabilised SLNs loaded with 50 wt. % MVC. SLNs were prepared with a Compritol ATO 888 to DBiB-p(OEGMA)$_{10}$-*co*-(EGDMA)$_{0.6}$ w/w ratio 3:1 and a solid content of 1.2 mg/mL – Related to **Fig. 4.3**

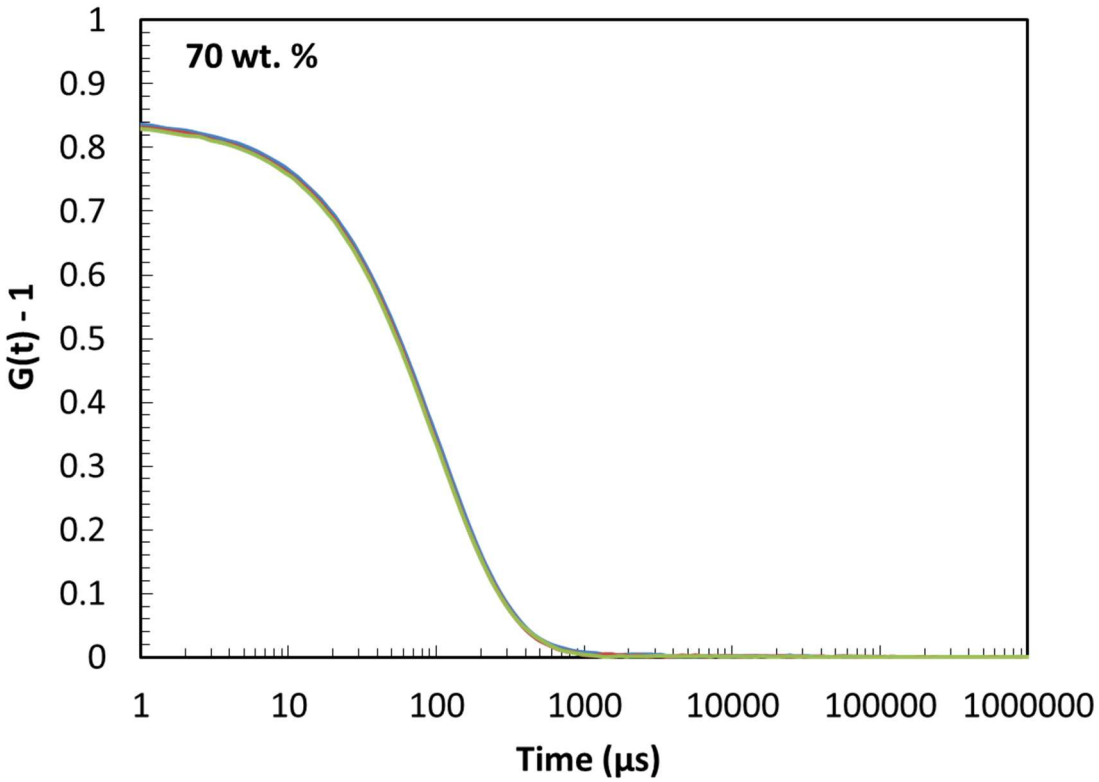

Fig. A47. Correlogram of DLS analysed sample on day 3 containing 1 mL DBiB-p(OEGMA)$_{10}$-*co*-(EGDMA)$_{0.6}$ stabilised SLNs loaded with 70 wt. % MVC. SLNs were prepared with a Compritol ATO 888 to DBiB-p(OEGMA)$_{10}$-*co*-(EGDMA)$_{0.6}$ w/w ratio 3:1 and a solid content of 1.2 mg/mL – Related to **Fig. 4.3**

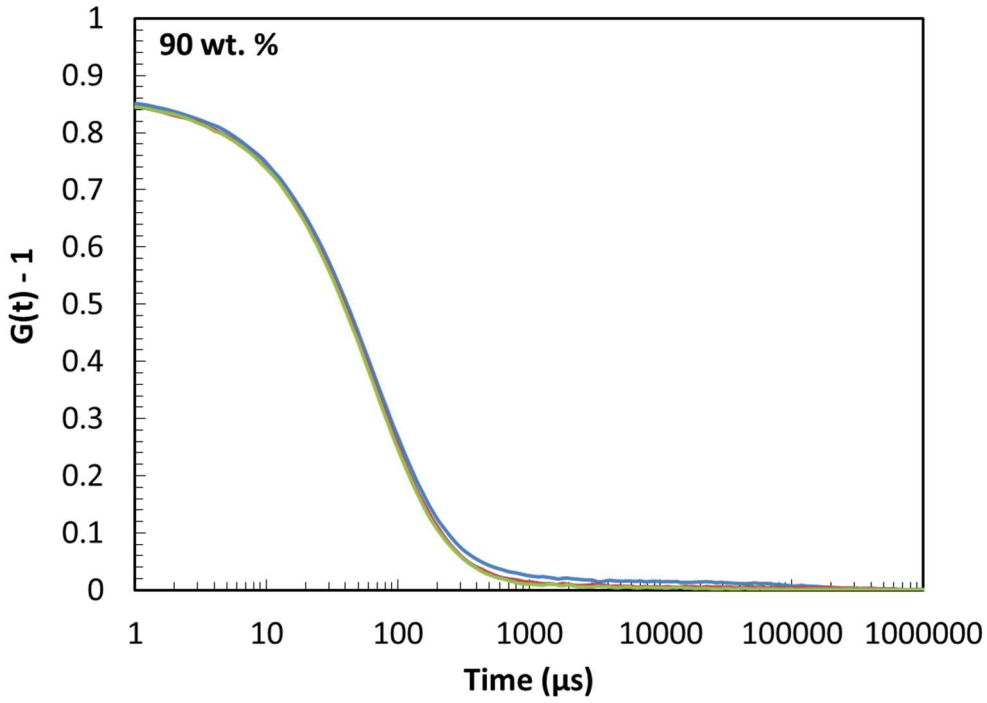

Fig. A48. Correlogram of DLS analysed sample on day 3 containing 1 mL DBiB-p(OEGMA)$_{10}$-*co*-(EGDMA)$_{0.6}$ stabilised SLNs loaded with 90 wt. % MVC. SLNs were prepared with a Compritol ATO 888 to DBiB-p(OEGMA)$_{10}$-*co*-(EGDMA)$_{0.6}$ w/w ratio 3:1 and a solid content of 1.2 mg/mL – Related to **Fig. 4.3**

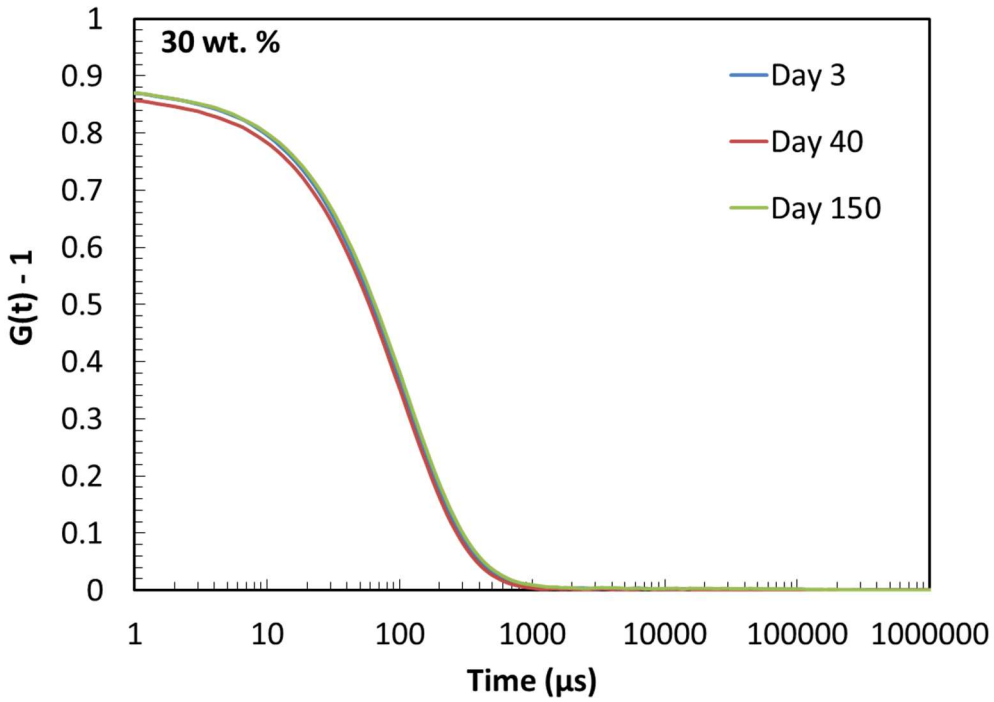

Fig. A49. Correlogram of DLS analysed samples on day 3, 40 and 150 overlayed. Samples contain 1 mL of DBiB-p(OEGMA)$_{10}$-*co*-(EGDMA)$_{0.6}$ stabilised SLNs loaded with 30 wt. % MVC. SLNs were prepared with a Compritol ATO 888 to DBiB-p(OEGMA)$_{10}$-*co*-(EGDMA)$_{0.6}$ w/w ratio 3:1 and a solid content of 1.2 mg/mL – Related to **Fig. 4.7**

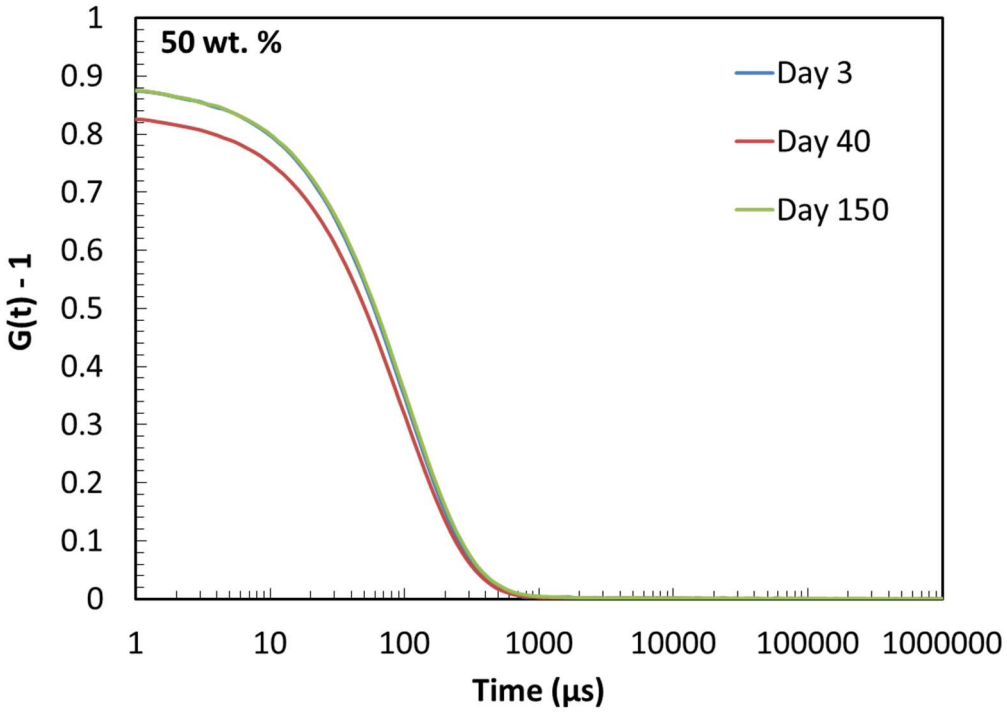

Fig. A50. Correlogram of DLS analysed samples on day 3, 40 and 150 overlaid. Samples contain 1 mL of DBiB-p(OEGMA)$_{10}$-*co*-(EGDMA)$_{0.6}$ stabilised SLNs loaded with 50 wt. % MVC. SLNs were prepared with a Compritol ATO 888 to DBiB-p(OEGMA)$_{10}$-*co*-(EGDMA)$_{0.6}$ w/w ratio 3:1 and a solid content of 1.2 mg/mL – Related to **Fig. 4.7**

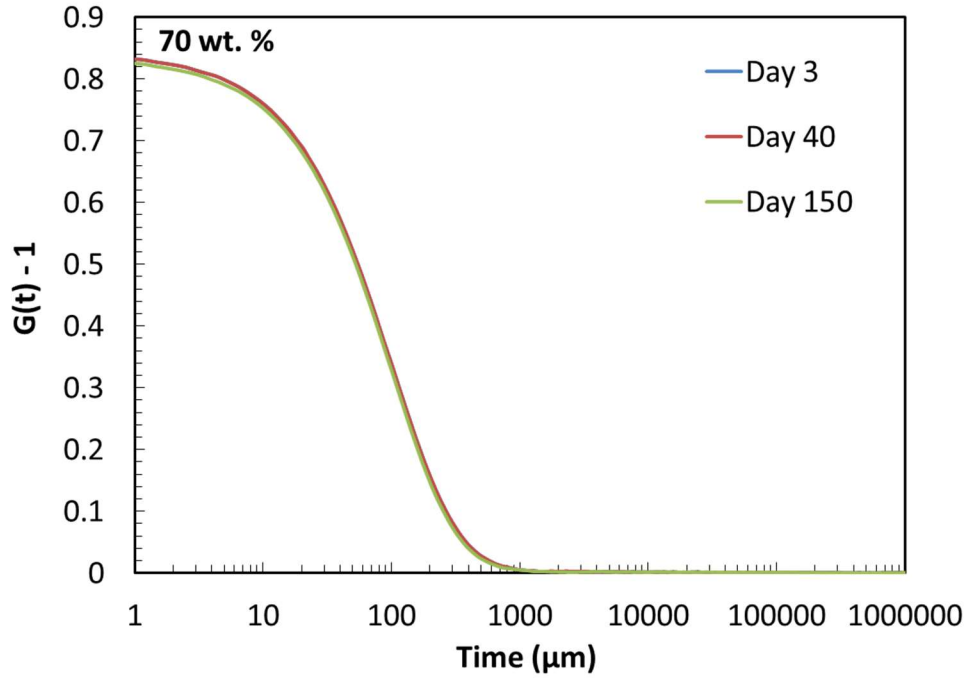

Fig. A51. Correlogram of DLS analysed samples on day 3, 40 and 150 overlaid. Samples contain 1 mL of DBiB-p(OEGMA)$_{10}$-*co*-(EGDMA)$_{0.6}$ stabilised SLNs loaded with 70 wt. % MVC. SLNs were prepared with a Compritol ATO 888 to DBiB-p(OEGMA)$_{10}$-*co*-(EGDMA)$_{0.6}$ w/w ratio 3:1 and a solid content of 1.2 mg/mL – Related to **Fig. 4.7**

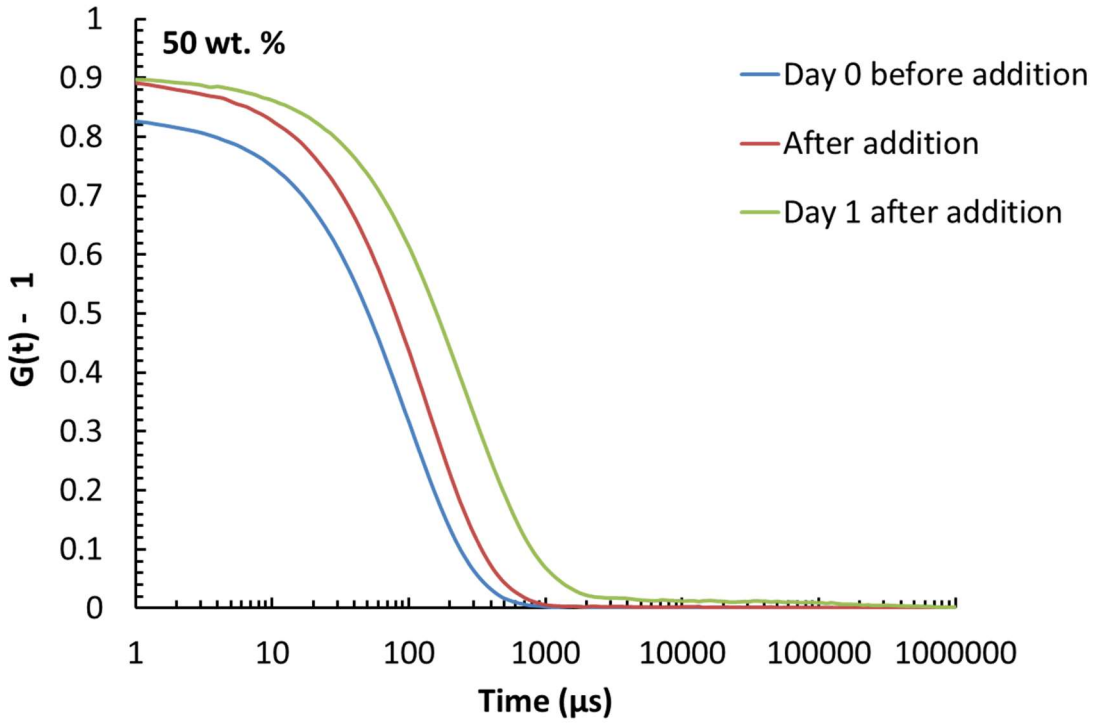

Fig. A52. Correlogram of DLS analysed samples on on day 0, 1 and 2 before and after addition of PBS. The correlograms were overlaid with different colours as shown in the figure. Samples contain 1 mL of PBS treated DBiB-p(OEGMA)$_{10}$-*co*-(EGDMA)$_{0.6}$ stabilised SLNs loaded with 50 wt. % MVC. SLNs were prepared with a Compritol ATO 888 to DBiB-p(OEGMA)$_{10}$-*co*-(EGDMA)$_{0.6}$ w/w ratio 3:1 and a solid content of 1.2 mg of MVC SLN/mL deionised water – Related to **Fig. 4.8**

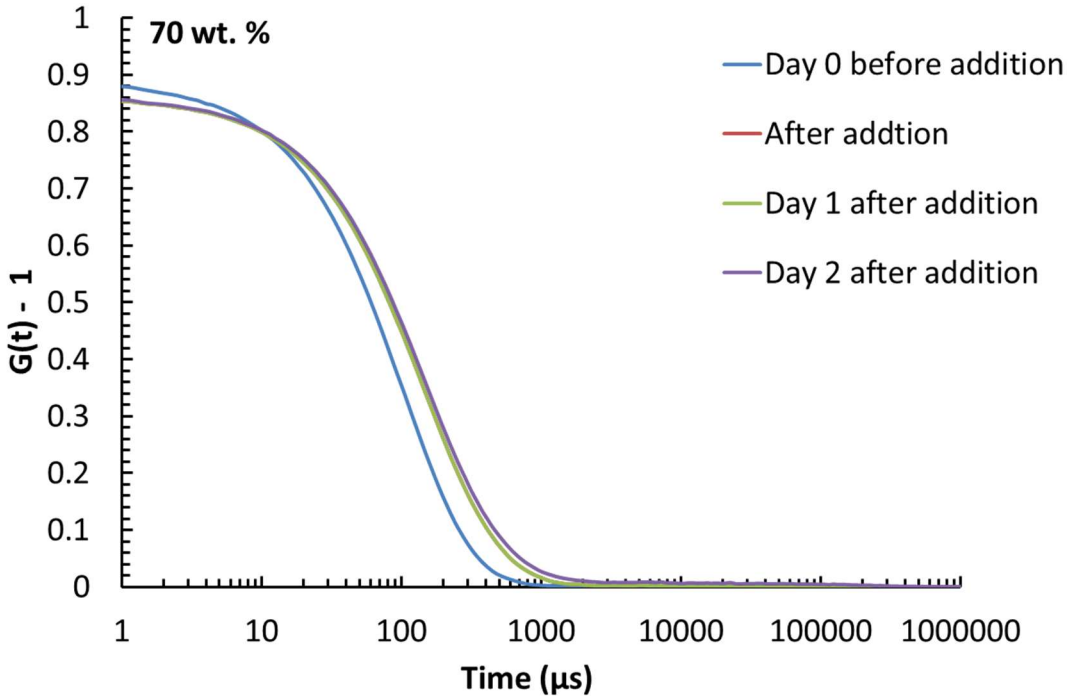

Fig. A53. Correlogram of DLS analysed samples on day 0, 1 and 2 before and after addition of PBS. The correlograms were overlaid with different colours as shown in the figure. Samples contain 1 mL of PBS treated DBiB-p(OEGMA)$_{10}$-*co*-(EGDMA)$_{0.6}$ stabilised SLNs loaded with 70 wt. % MVC. SLNs were prepared with a Compritol ATO 888 to DBiB-p(OEGMA)$_{10}$-*co*-(EGDMA)$_{0.6}$ w/w ratio 3:1 and a solid content of 1.2 mg of MVC SLN/mL deionised water – Related to **Fig. 4.8**

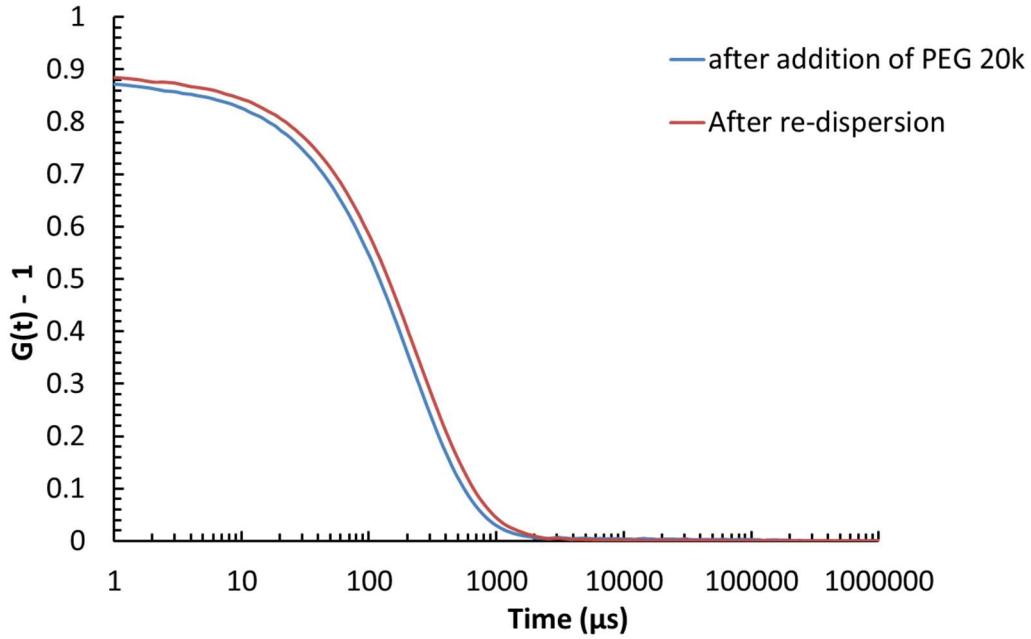

Fig. A54. Correlogram of DLS analysed samples before and after freeze drying and redispersion of 50 wt. % MVC loaded SLN samples freeze dried with 15 mg/mL of PEG 20k – Related to **Fig. 5.1**

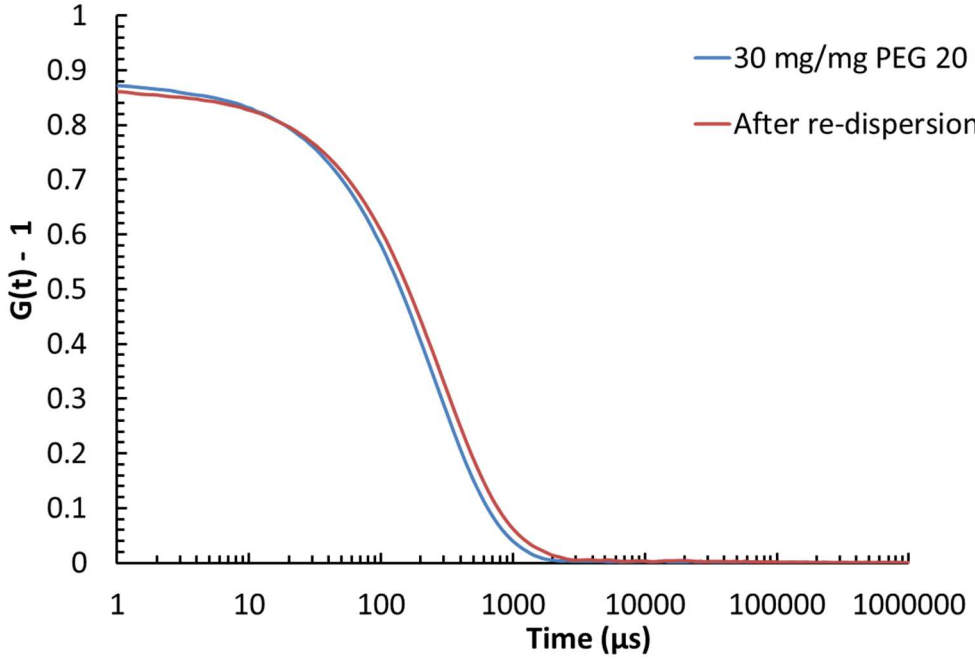

Fig. A55. Correlogram of DLS analysed samples before and after freeze drying and redispersion of 50 wt. % MVC loaded SLN samples freeze dried with 30 mg/mL of PEG 20k – Related to **Fig. 5.1**

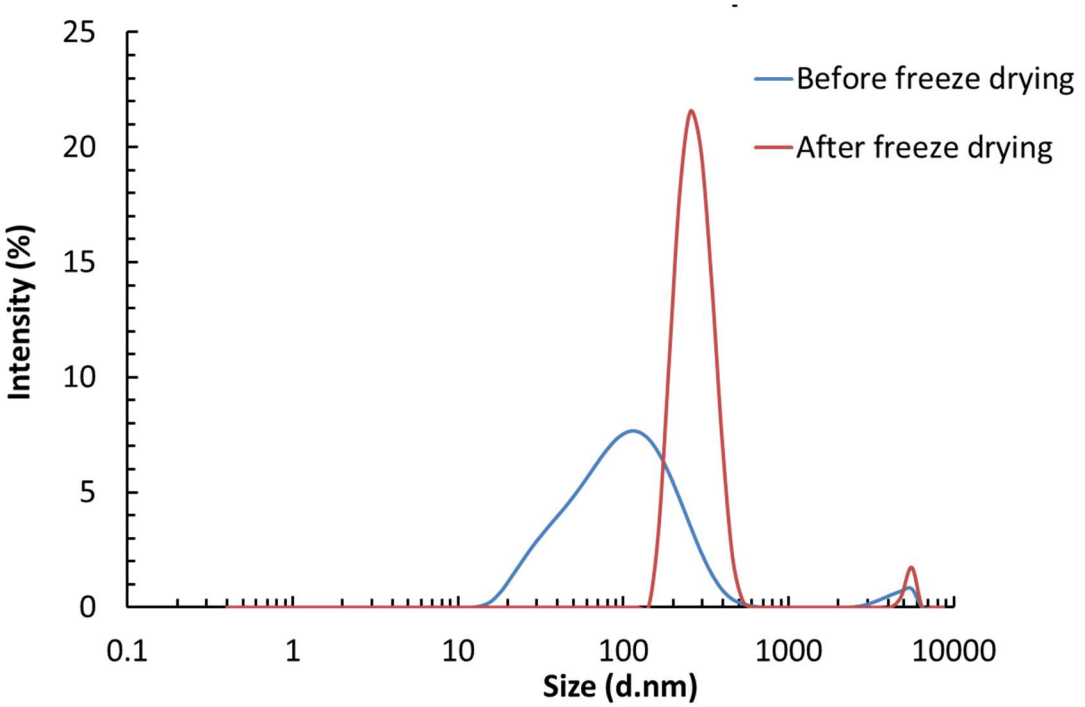

Fig. A56. Traces of DLS analysed sample of 50 wt. % MVC-SLN before and after freeze drying and redispersion. The experiment was performed without cryoprotectant.

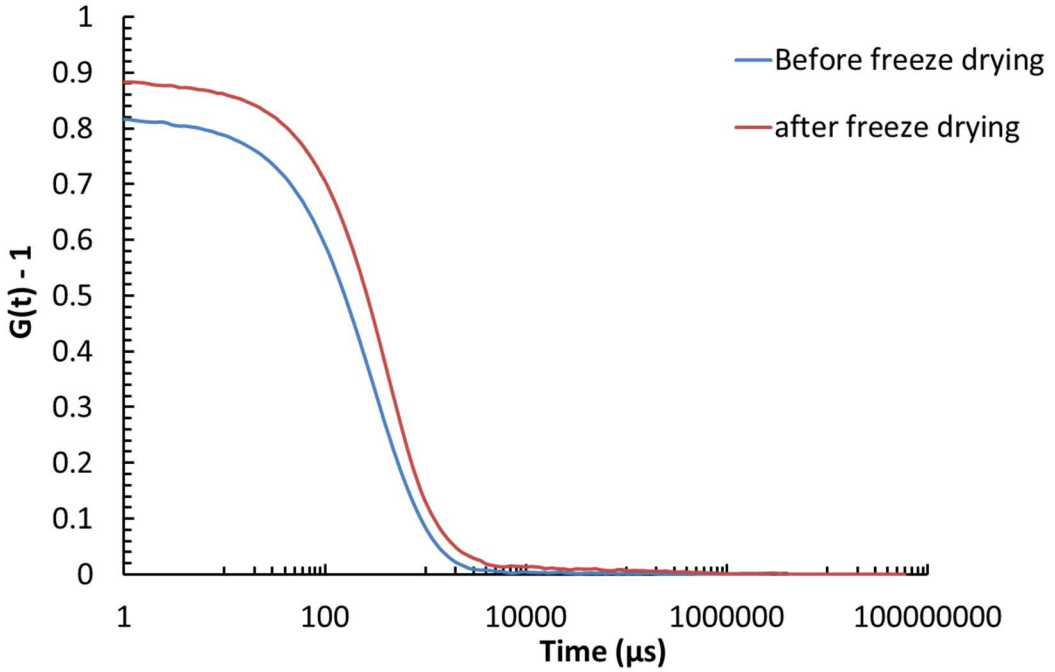

Fig. A57. Overlay of correlogram of DLS analysed sample of 50 wt. % MVC-SLN before and after freeze drying and redispersion. The experiment was performed without cryoprotectant– Related to

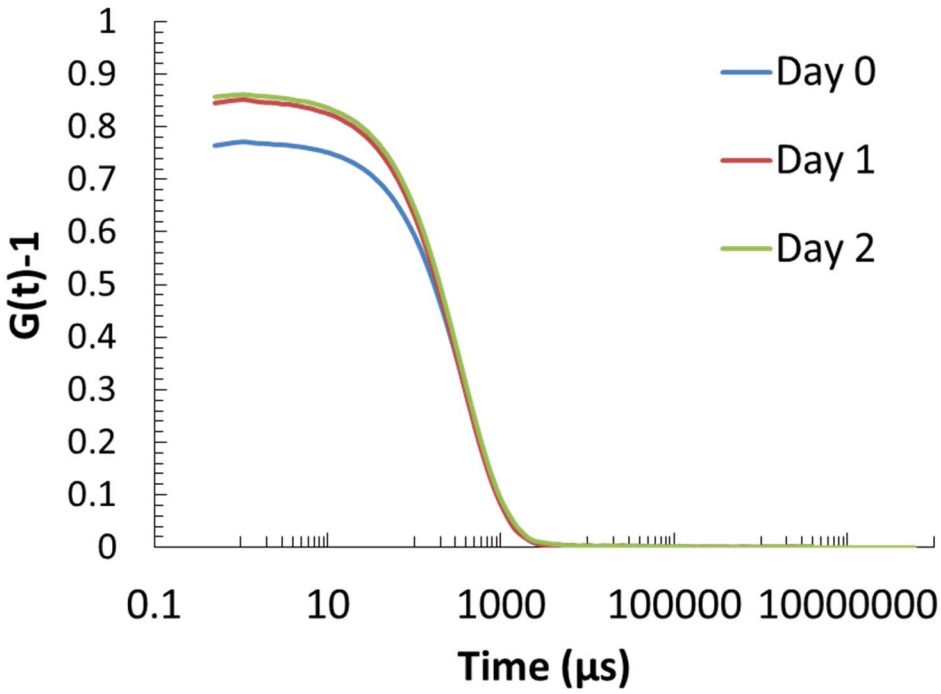

Fig. A58. Correlogram of DLS analysed sample of 80 wt. % MVC-SLN with a concentration of 3.4 mg MVC/mL deionised water. Sample was freeze dried and redispersed using ultra sonication. Day 0, 1 and 2 are measured after freeze drying and redispersion – Related to **Fig. 5.10B**

Fig. A59. Certificate analysis of tritiated MVC.

Moravek | Inc.
Quality Radiochemicals & Labeled Compounds

2108

Certificate of Analysis

MT-1997

Maraviroc, [^{3}H]-

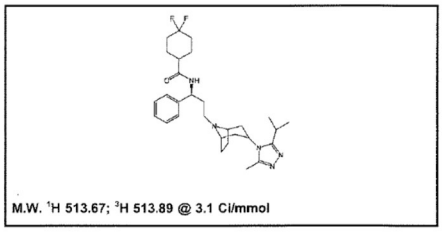

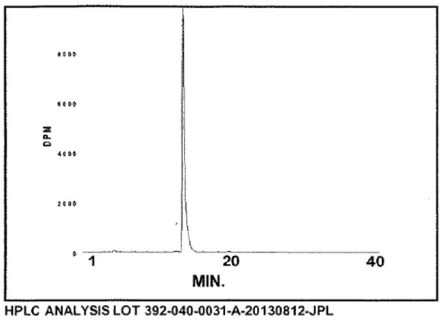

HPLC ANALYSIS LOT 392-040-0031-A-20130812-JPL
File Name: INTJ6599 Date and Time: 10/12/2016 3:17:32 P
Unit 19 Radio

Peak #	Area %	Time	Area
1	0.45	4.41670	101.36712
2	0.27	12.65330	61.05733
3	98.69	13.64330	22303.11215
4	0.22	14.25670	49.30353
5	0.15	14.79000	33.94949
6	0.07	15.09000	15.49375
7	0.01	15.98670	2.34723
8	0.05	16.30000	12.18700
9	0.01	18.28670	2.21568
10	0.08	19.83670	18.48012
Totals	100.00		22599.51340

Lot #: 392-040-0031-A-20130812-JPL

Specific Activity: 3.1 Ci/mmol

Concentration: 1.0 mCi/ml; 165.77 μg/ml

Packaged in: Ethanol solution

Date of Analysis: October 12, 2016

Radiochemical Purity: 98.7%

Column: Phenomenex Prodigy ODS(2) 4.6 x 250mm, 5μm

Flow Rate: 1 ml/min.

Mobile Phase: A: Water with 0.1% Formic Acid
B: Acetonitrile with 0.1% Formic Acid
0-30 min. 0-100% B
Hold to 40 min.

Storage Recommendation: Store at -20°C.

Product Warranty: Stated on the reverse side of this CoA.

Caution: Not For Use In Humans Or Clinical Diagnosis. This product is intended for investigational or manufacturing use only. It is pharmaceutically unrefined and is not intended for use in humans. Responsibility for its use in humans, as a diagnostic reagent, and compliance with federal laws rests solely with the purchaser.

Moravek, Inc. 577 Mercury Lane, Brea, California 92821 www.moravek.com info@moravek.com Phone (714) 990-2018 Fax (714) 990-1824